AD-A128 382 INVESTIGATION OF LITHIUM-THIONYL CHLORIDE BATTERY SAFETY HAZARDS(U) GOULD RESEARCH CENTER ROLLING MEADOWS IL MATERIALS LAB A I ATTIA ET AL. JAN 83 838-012

UNCLASSIFIED N60921-81-C-0363 F/G 10/3 NL

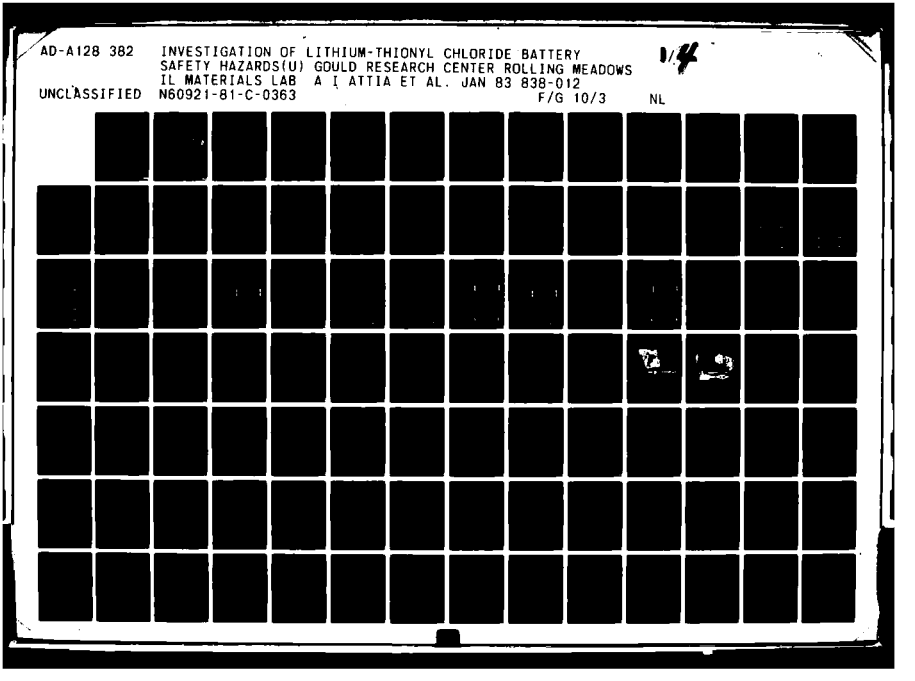

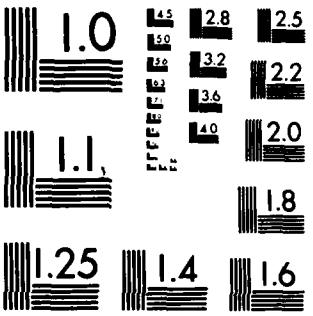

(12)

Report Number: 838-012

Contract No. 60921-81-C-0363 O/K

Investigation of Lithium-Thionyl Chloride Battery Safety Hazards

Alan I. Attia
Gould Research Center, Materials Laboratory
40 Gould Center
Rolling Meadows, Illinois 60008

Kenneth A. Gabriel and Richard P. Burns
Department of Chemistry
University of Illinois at Chicago
Chicago, Illinois 60680

January 1983

Final Report for the Period 28 September 1981 to 31 December 1982

Approved for Public Release: Distribution Unlimited

Prepared for:
NAVAL SURFACE WEAPONS CENTER

Approved by: B. W. Burrows.
B. W. Burrows, Director
Materials Laboratory
Gould Research Center

UNCLASSIFIED

SECURITY CLASSIFICATION OF THIS PAGE (When Data Entered)

REPORT DOCUMENTATION PAGE		READ INSTRUCTIONS BEFORE COMPLETING FORM
1. REPORT NUMBER 838-012	2. GOVT ACCESSION NO.	3. RECIPIENT'S CATALOG NUMBER
4. TITLE (and Subtitle) Investigation of Lithium-Thionyl Chloride Battery Safety Hazards		5. TYPE OF REPORT & PERIOD COVERED Final Report 9/28/81 - 12/31/82 6. PERFORMING ORG. REPORT NUMBER
7. AUTHOR(s) Alan I. Attia, Kenneth A. Gabriel and Richard P. Burns		8. CONTRACT OR GRANT NUMBER(s) N60921-81-C-0363
9. PERFORMING ORGANIZATION NAME AND ADDRESS Gould Research Center, Materials Laboratory 40 Gould Center Rolling Meadows, Illinois 60008		10. PROGRAM ELEMENT, PROJECT, TASK AREA & WORK UNIT NUMBERS
11. CONTROLLING OFFICE NAME AND ADDRESS Naval Surface Weapons Center White Oak, Silver Spring, MD 20910		12. REPORT DATE January 1983 13. NUMBER OF PAGES 191
14. MONITORING AGENCY NAME & ADDRESS(if different from Controlling Office)		15. SECURITY CLASS. (of this report) 15a. DECLASSIFICATION/DOWNGRADING SCHEDULE

16. DISTRIBUTION STATEMENT (of this Report)

Approved for Public Release. Distribution Unlimited.

17. DISTRIBUTION STATEMENT (of the abstract entered in Block 20, if different from Report)

18. SUPPLEMENTARY NOTES

19. KEY WORDS (Continue on reverse side if necessary and identify by block number)

Thionyl-Chloride, lithium, primary cells, lithium batteries, Infrared Spectroscopy, Mass Spectrometry, safety.

20. ABSTRACT (Continue on reverse side if necessary and identify by block number)

This report details the investigations carried out in the last two quarters of the program relating to Contract No. 60921-81-C-0363.

The overall aim of the program was to identify the hazards of Li/$SOCl_2$ batteries during low rate discharge and anode limited reversal. The specific objectives were:

DD FORM 1 JAN 73 1473 EDITION OF 1 NOV 65 IS OBSOLETE

UNCLASSIFIED

SECURITY CLASSIFICATION OF THIS PAGE (When Data Entered)

- To identify the reaction products soluble in the electrolyte.
- To perform quantitative infrared absorption measurements of the products formed during normal discharge, reversal and storage following reversal.
- To measure the heat generation rate of a cell during normal discharge and reversal.
- To determine the presence or absence of free radicals during normal discharge and reversal.
- To analyze by mass spectrometry the gas phase above the electrolyte of a $Li/SOCl_2$ cell during normal discharge and reversal.

During the course of the contract we have

- Optimized the cell design with respect to sampling procedure.
- Developed in-situ FTIR, EPR and mass spectrometric methods of analysis and applied them to operating $Li/SOCl_2$ cells.
- Measured the heat generated by anode limited cells during discharge and reversal.

We have obtained the following results:

- The sources of all the absorption bands in the IR absorption spectrum of the electrolyte were identified.
- In-situ quantitative measurements were obtained for SO_2, SO_2Cl_2 and $SOCl^+AlCl_4^-$ during normal discharge and reversal.
- Processes giving rise to free radical formation were detected during anode limited reversal by in-situ EPR spectroscopy.
- The technique of direct-inlet in-situ mass spectrometry was applied for the first time to the $Li/SOCl_2$ system, to identify without any ambiguity, the presence of HCl, SO_2, CS_2, S_2O, SCl_2 and SO_2Cl^+ as well as Cl^+ and CF_2^+ fragments in the gas phase above an operating cell.
- S_2O was not detected in the liquid phase.
- The appearance potentials for SCl_2, $SOCl_2$, SO_2Cl_2 and S_2Cl_2 were measured.
- Evidence for the formation of Cl_2O was refuted.
- Significant effects directly attributable to temperature and current density were identified and quantified.
- No clearly hazardous reactions were identified other than those inherent in the system.

As a result of this work a much clearer understanding of the chemistry of the $Li/SOCl_2$ system has been achieved. Several analytical techniques have been developed and applied for the first time to the $Li/SOCl_2$ system, which could potentially lead to a more complete explanation of the chemistry of the system.

ACKNOWLEDGEMENT

The research described in this publication was carried out by the Materials Laboratory, Gould Research Center, under contract with the Naval Surface Weapons Center - Electrochemical Technology Block Program (Technical Monitor: Dr. William P. Kilroy).

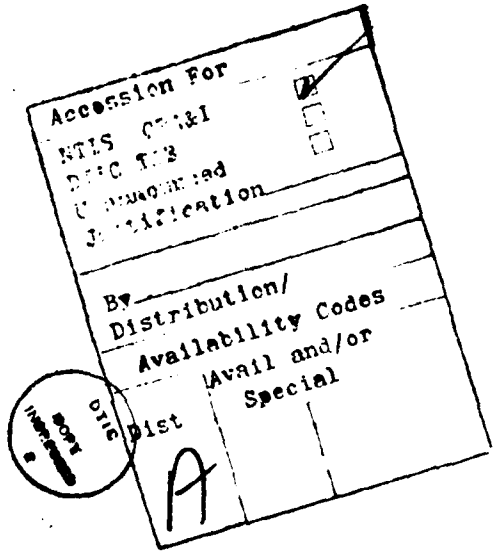

TABLE OF CONTENTS

LIST OF FIGURES

List of Tables

Prepared for Naval Surface Weapons Center
Silver Springs, Maryland
Contract N60921-81-C-0363

Materials Laboratory
Gould Research Center
January 1983

1. Introduction

In the ten years since the feasibility of a lithium-thionyl chloride cell was first recognized (1) remarkable progress has been made in hardware development. Cells as large as 16,000 Ah (2) and batteries of 10.8 MWh (3) have been demonstrated. In a low rate configuration, energy densities of 500 to 600 Wh/kg are easily achieved.

Even in the absence of reported explosions, safety would be a concern for such a dense energetic package; the energy density of a lithium-thionyl chloride cell is approaching that of dynamite (924 Wh/kg). In fact explosions have occurred. In general the hazards associated with lithium-thionyl chloride batteries may be divided into four categories:

- Explosions as a result of an error in battery design. Very large cells were in prototype development prior to a full appreciation of the hazards of the system. It is possible that some of the remaining safety issues are related to cell design.
- Explosions as a result of external physical abuse such as cell incineration and puncture.
- Explosions due to short circuiting which could lead to thermal runaway reactions. These problems appear to have been solved by changes in the battery design (4).
- Explosions due to abnormal electrical operation (i.e., charging (5) and overdischarging (6)) and in partially or fully discharged cells on storage (7 and 8).

This last category is particularly troubling as the explosions are unpredictable and their source only partially characterized. For example EIC reports 3 explosions in evaluating the safety of 10 cells during anode limited

reversal (6). The absence of a definite set of conditions which consistently result in an explosion makes a phenomenological approach to a safe design very costly and time consuming if not impossible. In addition as the evidence for safety will be statistical it can never be completely proven with obvious limitations on cell development.

Complete resolution of the unpredictable safety hazards may only be possible by analytical determination of their causes. In this regard considerable work has been carried out at EIC, GTE, INCO, Union Carbide and Gould on the chemistry of normal discharge and reversal.

The infrared absorption spectrum of lithium-thionyl chloride cell electrolytes has been the subject of several investigations. Istone and Brodd (9) have performed an analysis of the electrolyte, sampling the electrolyte in situ from the electrode surface of a functioning $Li/SOCl_2$ cell and obtaining the infrared absorption spectrum with a Fourier Transform Infrared (FTIR) Spectrometer. They found SO_2Cl_2, SO_2, S_2Cl_2, SCl_2 and HCl as impurities at the beginning of the experiment. Only the intensities of peaks assigned to SO_2 (1335 cm^{-1}) and S_2O (689 cm^{-1}) were observed to change as a function of discharge, and a slight amount of moisture pickup was detected. The S_2O concentration was seen to increase to a maximum and then begin to decay while the SO_2 concentration increased then appeared to level off. Also elemental sulfur was seen to deposit on the cell walls. These observations are consistent with the decomposition reaction of S_2O

$$2\ S_2O \rightarrow 3\ S + SO_2$$

first considered but rejected on the basis of stoichiometry by Schlaikjer, Goebel and Marincic in 1979 (10). The question of the stability of S_2O in a condensed phase was not addressed, and a fairly large shift in the absorption wavelength for S_2O in $SOCl_2$ was left unexplained.

Schlaikjer and co-workers (10) postulated the formation of a sulfur monoxide polymer according to the reaction:

$$2nLi + nSOCl_2 \longrightarrow 2nLiCl + (SO)_n$$

and subsequent decomposition of this polymer to produce elemental sulfur and SO_2.

Spectroelectrochemical studies carried out by Salmon et al at Gould (11) have provided evidence that the principal reaction at the anode current collector on reversal is

$$2\ SOCl_2 \longrightarrow 2\ SOCl^+ + 2e + Cl_2$$

They then speculated that several electrochemical and chemical reactions involving SO_2 were also occurring at the anode

$$SO_2 \xrightarrow{\text{electrochemical}} SO^{++} + O + 2e$$

$$SO_2 + Cl_2 \longrightarrow SO^{++} + 2\ Cl^- + O$$

$$Cl_2 + O \longrightarrow Cl_2O$$

Absorption bands at 1070 cm^{-1} and 690 cm^{-1} in the infrared spectrum of electrolytes from anode limited cells after reversal at 45 mA/cm^2 were assigned respectively to SO^{+2} and Cl_2O.

Abraham and Mank at EIC (12) have also noted the absorption band at 1070 cm^{-1} in anode limited reversal which they assigned to an S-O stretching vibration of a sulfur-oxy compound. Under the same conditions they observed absorption bands at 1415 cm^{-1}, 1110 cm^{-1}, 1335 cm^{-1} and 1150 cm^{-1}. The last two were obviously due to SO_2, and the absorption at 1110 cm^{-1} in the anolyte was assigned to the SO stretching vibration of the complex $SOCl^+AlCl_4^-$, since

a similar absorption was found in the infrared spectra of $AlCl_3$ solutions in $SOCl_2$. The absorption at 1415 cm^{-1} was assigned to SO_2Cl_2. Cl_2 and SCl_2 were identified by cyclic voltammetry. Two other absorption bands observed at 660 cm^{-1} and 790 cm^{-1} in cathode limited reversal, were assigned to Al-S and Al-Cl bond vibration respectively of $LiAlSCl_2$.

Bailey and Blomgren (13) at Union Carbide using IR and ^{27}Al NMR Spectroscopy have identified several oxychloroaluminates in Li_2CO_3 - $AlCl_3/SOCl_2$ electrolyte absorbing at 3200-3400 cm^{-1} ($AlCl_3OH^-$) and 800 cm^{-1} and 695 cm^{-1} ($Li_2(AlCl_3)_2O$), casting strong doubts on the observations of Istone and Brodd and Salmon et al concerning S_2O and Cl_2O.

Although this qualitative work has been useful in elucidating cell chemistry during a potentially hazardous condition, it has not established a causal relationship between these reactions and a potential hazard. Moreover the qualitative evidence itself is still subject to controversy. For example, Cl_2O is an explosively unstable compound; however, the random nature of cell explosions during reversal indicates that its presence is not a sufficient condition for an explosion; moreover, the IR evidence for its presence is tenuous, based on the observation of only one of three possible absorption bands for Cl_2O (14). Similarly the IR evidence for S_2O is not any more solid. S_2O may very well be a reaction intermediate, but its stability in a condensed phase is doubtful (15).

More recently R. McDonald at GTE while investigating the generation of pressure in $Li/SOCl_2$ batteries by mass spectrometry (16) has demonstrated the presence of substantial amounts of hydrogen and nitrogen, pointing to the need for corroboration of results by several techniques.

In view of these considerations the Navy decided that fundamental quantitative studies of lithium-thionyl chloride reactions were required to resolve safety issues. Our overall proposed approach was to conduct quantitative and qualitative studies of reactions occurring during low rate

discharge and during reversal. Specifically we have carried out

- Quantitative and qualitative FTIR spectroscopic studies of $Li/SOCl_2$ cells using both electrolyte samples withdrawn from operating cells and in situ sampling.

- Electron spin resonance spectroscopy experiments at ambient temperature.

- Microcalorimetric measurements of a $Li/SOCl_2$ cell during discharge and reversal.

- In situ low resolution mass spectroscopic studies of the gas phase above the electrolyte of a functioning cell.

This report summarizes the results of these activities for cells discharged at current densities between 1 and 5 mA/cm^2, at room temperature and -20^oC.

2. Summary

Conflicting and irreproducible results which plagued the beginning of this investigation were resolved by resorting to in situ experiments. The extreme sensitivity of the system to moisture made it mandatory to perturb the system as little as possible while sampling for either infrared or mass spectrometric analysis.

For our FTIR studies we have built several circulating electrolyte systems which directly couple the spectroscopic cell to the electrolyte reservoir of the electrochemical cell. Several pumping schemes were tried. In our mass spectrometric investigation, we were able to attach an electrochemical cell to the inlet system of a mass spectrometer thus sampling the gas phase above the electrolyte during discharge. In situ ESR measurements were also more informative than the ESR measurements on electrolyte withdrawn from operating cells.

Although we have not identified every compound formed during discharge or reversal we have developed and applied several analytical techniques to the lithium-thionyl chloride system which have yielded without ambiguity reproducible and quantitative results. We summarize below our most significant findings.

- SO_2 is the only major product of discharge detected by infrared spectroscopy at high and low temperatures; its concentration in solution increases linearly during normal discharge, and at a much slower rate during reversal. The amount of SO_2 produced during normal discharge was always found to be only a fraction of that predicted by

  $$4\ Li + 2\ SOCl_2 \longrightarrow S + SO_2 + LiCl$$

- $SOCl^+$ is formed in substantial quantities during anode limited

reversal, but reaches a steady state concentration which is temperature and current density dependent. At lower temperatures and higher current densities relatively high concentrations of $SOCl^+$ can build up during reversal.

- Chlorine was also detected indirectly in substantial quantities during anode limited reversal. Chlorine may arise either through oxidation of $AlCl_4^-$

$$AlCl_4^- \text{ --- } AlCl_3 + 1/2\ Cl_2 + e$$

or through direct oxidation of $SOCl_2$ as shown below

$$2\ SOCl_2 + 2\ AlCl_4^- \text{ --- } 2\ SOCl^+\ AlCl_4^- + Cl_2 + 2e$$

Infrared evidence obtained during reversal does seem to show that $AlCl_3$ is formed, but both processes could occur. Chlorine, at room temperature, does not accumulate in the cell but reacts to form SO_2Cl_2 and sulfur chlorides.

- SO_2Cl_2 is generated during anode limited reversal. Its concentration increases slowly initially then builds up fairly rapidly to a steady state value which appears to be dependent on the current density. At low current densities very little, if any, SO_2Cl_2 accumulates. Also at low temperatures (-20C) the amount of SO_2Cl_2 produced is not as significant as at higher temperatures (25C).

Following current cutoff after reversal a sharp increase in SO_2Cl_2 concentration always occurs at ambient temperature, but not at -20C. However, upon warming up a cold cell a very large amount of SO_2Cl_2 is produced as the cell reaches ambient temperature. This effect could simply reflect an accelerated rate of reaction between SO_2 and Cl_2. During storage the SO_2Cl_2 concentration slowly decreases.

- Substantial quantities of SCl_2 in the gas phase were detected by mass spectrometry upon anode limited reversal. S_2Cl_2 which has the same mass as SO_2Cl_2 under low resolution but a different fragmentation pattern, was also detected but not in any substantial quantity. Formation of SCL_2 during reversal also gives rise to compounds absorbing in the infrared at 1070 cm^{-1} and 665 cm^{-1}. The exact nature of these compounds cannot be determined by infrared spectroscopy alone, but the absorptions are characteristics of S-O stretching modes (1070 cm^{-1}), and S-O bending or S-S stretching modes (665 cm^{-1}).

- S_2O was detected in the gas phase above an operating cell by high resolution mass spectrometry, but its presence in the electrolyte is doubtful. Several attempts to synthesize S_2O and trap it in thionyl chloride resulted in its decomposition into SO_2 and sulfur.

- No trace of Cl_2O could be detected by mass spectrometry.

- Many of the features of the IR absorption spectrum are simply due to the reaction between $AlCl_3$ or $AlCl_4^-$ and water. The absorption bands generated by these products (aluminum hydroxides and oxochloroaluminates) were identified, but the exact composition of the products is not known at this stage.

- Formation of a free radical was detected during anode limited reversal using in situ EPR spectroscopy, and its half life measured at seven minutes.

- Calorimetric studies of the lithium-thionyl chloride system did not yield any surprises except to confirm the high rate of heat evolution during anode limited reversal.

In conclusion, it appears that we have extracted useful quantitative information with IR spectroscopy. For a more complete identification of the products of discharge, by far the most promising technique is mass spectrometric analysis, especially if it can be refined by coupling a high resolution mass spectrometer with a gas chromatograph.

We have not in the course of this study identified a single clearly hazardous reaction other than those inherent in the system. However, we have noticed significant effects caused by temperature differences or current density differences which may lead to thermal runaway reactions in an improperly designed system.

3. FTIR Spectroscopic Studies

IR studies are presented in this section. The infrared absorption spectrum of electrolyte removed from a lithium-thionyl chloride cell driven into anode limited reversal is presented first to illustrate the main features of the IR spectrum and its evolution as a function of discharge. This experiment provides a basis for comparison with subsequent experiments using in situ sampling of the electrolyte.

We present next the results of various calibration experiments for SO_2, SO_2Cl_2 and $SOCl^+$ as well as IR spectra of known compunds in thionyl chloride which might possibly be reaction products or intermediates in the course of normal discharge or anode limited reversal.

Finally in situ IR spectra from several cells discharged at room temperature or at -20C are presented and discussed.

It is important to note that all spectral frequencies we report here are accurate within $\pm$ 4 cm^{-1}; moreover some shifting of a given absorption band may occur if the base line is sloping, or the band is not fully resolved. All absorbance values we quote are "peak heights" above the baseline.

For badly overlapping bands (i.e., 1070 cm^{-1} and 1115 cm^{-1}) we have used the tangent line technique to obtain reproducible results. We have tried to be consistent in the selection of the prominent minima for drawing our tangents and used difference spectra whenever possible to estimate the peak heights.

All spectra are averages of 100 scans taken with a Nicolet 5-MX FTIR spectrometer. They were all measured accurately to 3 units of absorbance. Frequently we present several spectra together in one figure in which case the absorbance axis is valid only for indicating the absorbance scale; the spectra, drawn to the same scale, were successively shifted to a higher position on the figure.

3.1 Qualitative FTIR Study of Typical Discharge

The cell used for this experiment, SC-68, consists of two concentric electrodes. The thin carbon-Teflon cathode (20 mil thick) is pressed on a nickel grid which is spot welded to the outer wall of the cell body (see Figure 1). The lithium electrode (8 cm^2 x 5 mil) is pressed on a nickel foil substrate which is spot welded around a stainless steel central post. The electrodes are about 0.5 cm apart and separated by a double layer of .005" glass mat. Approximately 14 ml of 1.4 M $LiAlCl_4$ in $SOCl_2$ are added to the cell. Samples can be removed through a Teflon-faced septum.

IR absorption spectra obtained throughout the run are shown in Figures 2-4. Cell SC-68 was taken into anode limited reversal at 5 mA/cm^2. A relatively large amount of SO_2 (1335 and 1144 cm^{-1}) is present initially. After 27.5 hours of discharge, or 20 hours into anode limited reversal (-1.447 V) we notice the formation of a band at 1115 cm^{-1} and one at 1070 cm^{-1}; there is considerable overlap and the band at 1070 cm^{-1} appears as a shoulder on the 1115 cm^{-1} peak.

The current was then reduced to 1 mA/cm^2 (8 mA). After 98.5 hours from the start of discharge (see Figure 2) the only changes in the IR spectrum are an increase in the 1070 cm^{-1} band and an increase at 660-694 cm^{-1}. It appears that two bands absorb in that region, one at 694 cm^{-1} whose presence seems to be related to water contamination, and one at 665 cm^{-1} whose presence is definitely due to anode limited reversal. The band at 1115 cm^{-1} appears to have disappeared indicating an unstable species evident at 5 mA/cm^2 but too unstable to accumulate at 1 mA/cm^2. The current was then readjusted to 5 mA/cm^2 and the cell sampled after 122 hours. The 122 hour spectrum (see Figure 3) shows clearly the presence of absorption bands at 1115 cm^{-1} as well as 1070 cm^{-1}.

Absorptions at 694 cm^{-1} and 822 cm^{-1} are increasing but in this particular case water contamination is evident from the strong absorption at

3200-3600 cm^{-1}. The absorption at 665 cm^{-1} is masked by the stronger absorption at 694 cm^{-1}. A slight increase at 1408 cm^{-1} (SO_2Cl_2) is also noticed. Subsequent spectra after 140 hours (Figure 3) confirm these trends. SO_2Cl_2 (1408 cm^{-1}) increases during reversal along with species absorbing at 1070, 1115, and 665-694 cm^{-1}. Resolution of the 694 cm^{-1} and 665 cm^{-1} bands is difficult and depends on the relative size of the absorptions. Weak absorptions are noticed at 928 cm^{-1} and 822 cm^{-1} but these are also affected by the presence of moisture. Figure 4 shows the IR absorption spectrum for the cell in storage 67, 91, 119, 142 and 254 hours after the current has been turned off. A substantial jump in SO_2Cl_2 concentration is clearly evident. The band at 1115 cm^{-1} has disappeared whereas the one at 1070 cm^{-1} becomes quite evident and remains constant during the storage period. Due to a reduction in the level of contamination the 665 cm^{-1} absorption can clearly be seen while the band at 694 has become a shoulder on the 665 cm^{-1} peak. Absorptions at 2790, 2450, and 1225 cm^{-1} are present throughout the run and are due to HCl and $SOCl_2$. (17)

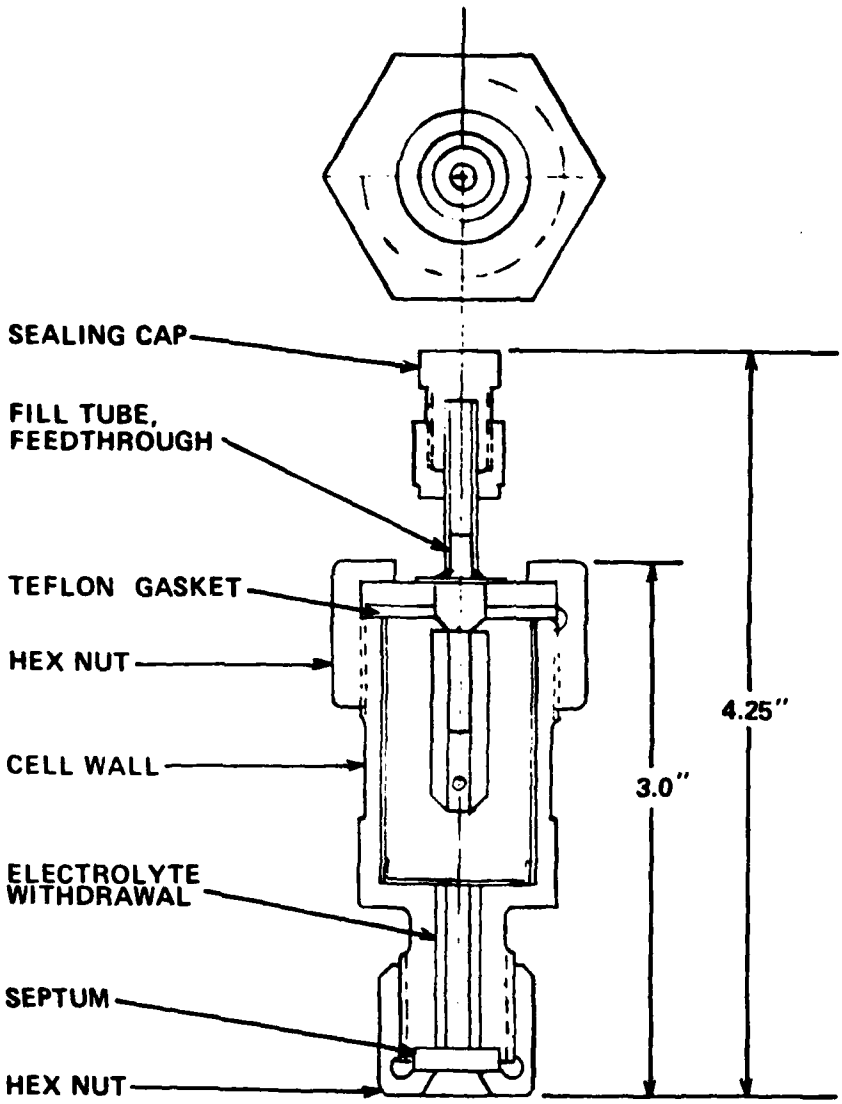

(1951)

Figure 1 **Electrochemical Cell Designed for Electrolyte Withdrawal**

FIGURE 2

SC-68 Anode Limited - RT
i = 40 mA (5mA/cm^2)
Reversal at 5 hrs
IR Absorption Spectra

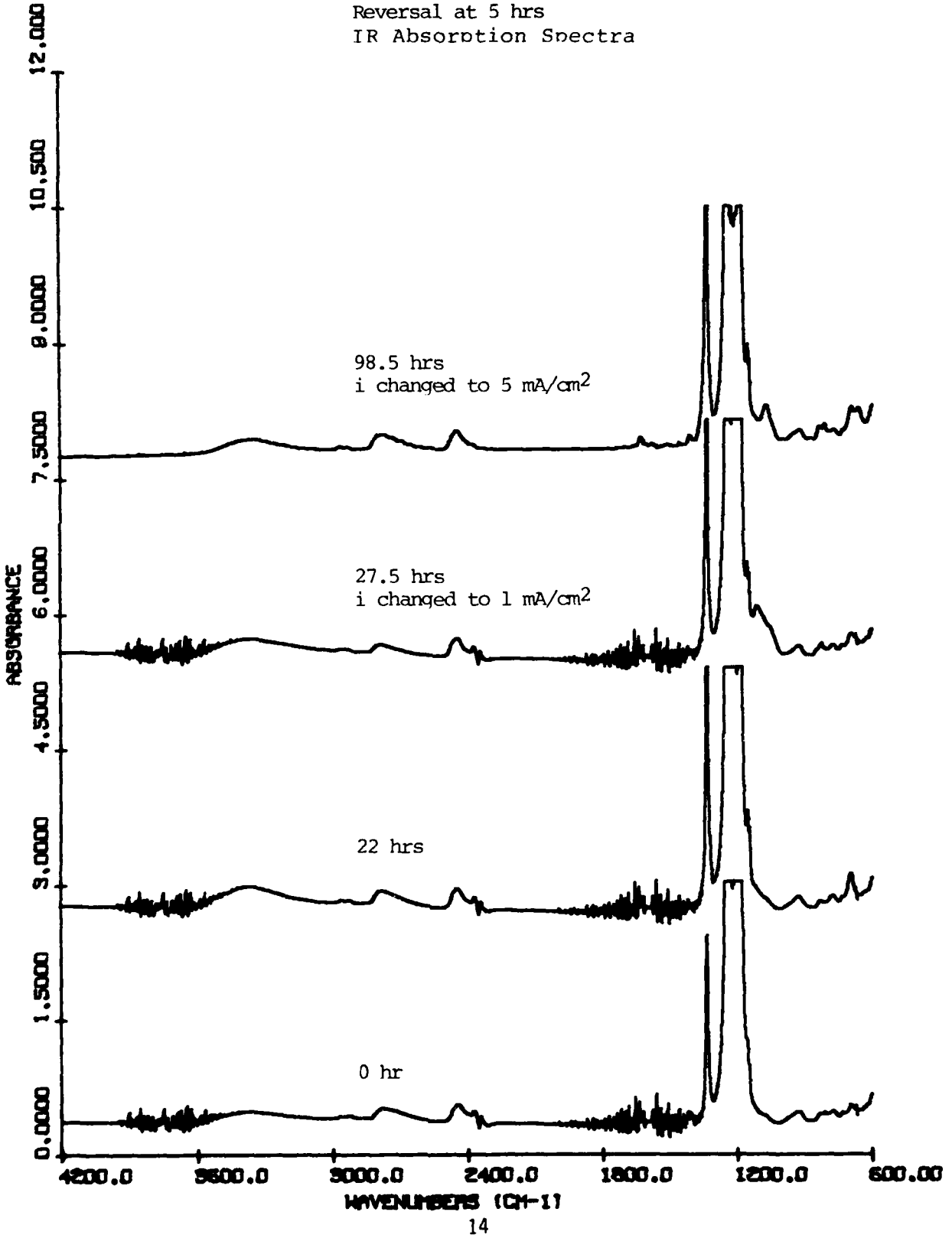

FIGURE 3

SC-68 Anode Limited - RT
i = 40 mA (5mA/cm^2)
Reversal at 5 hrs
IR Absorption Spectra

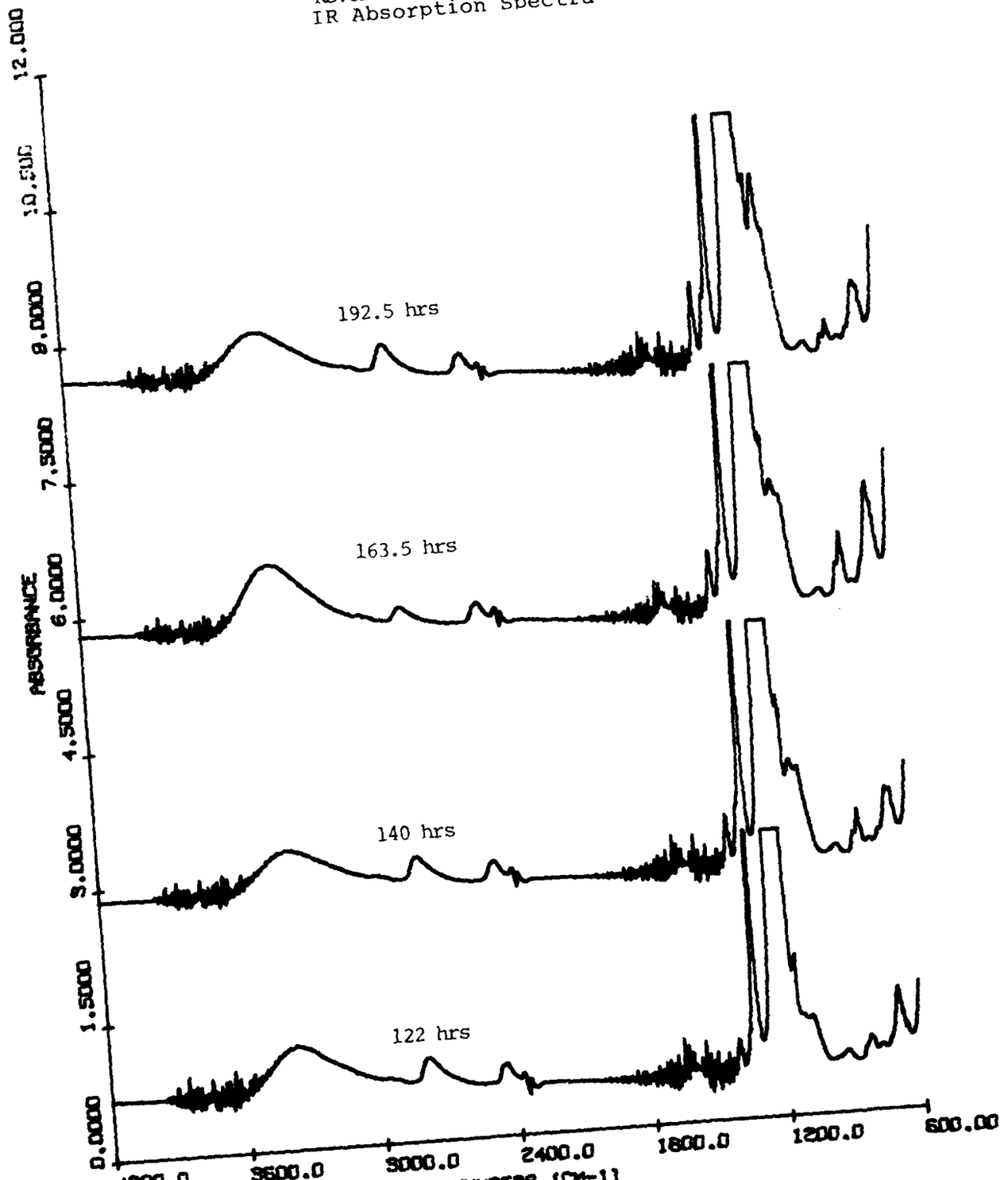

FIGURE 4

SC-68 in Storage after Reversal
i = 0 mA

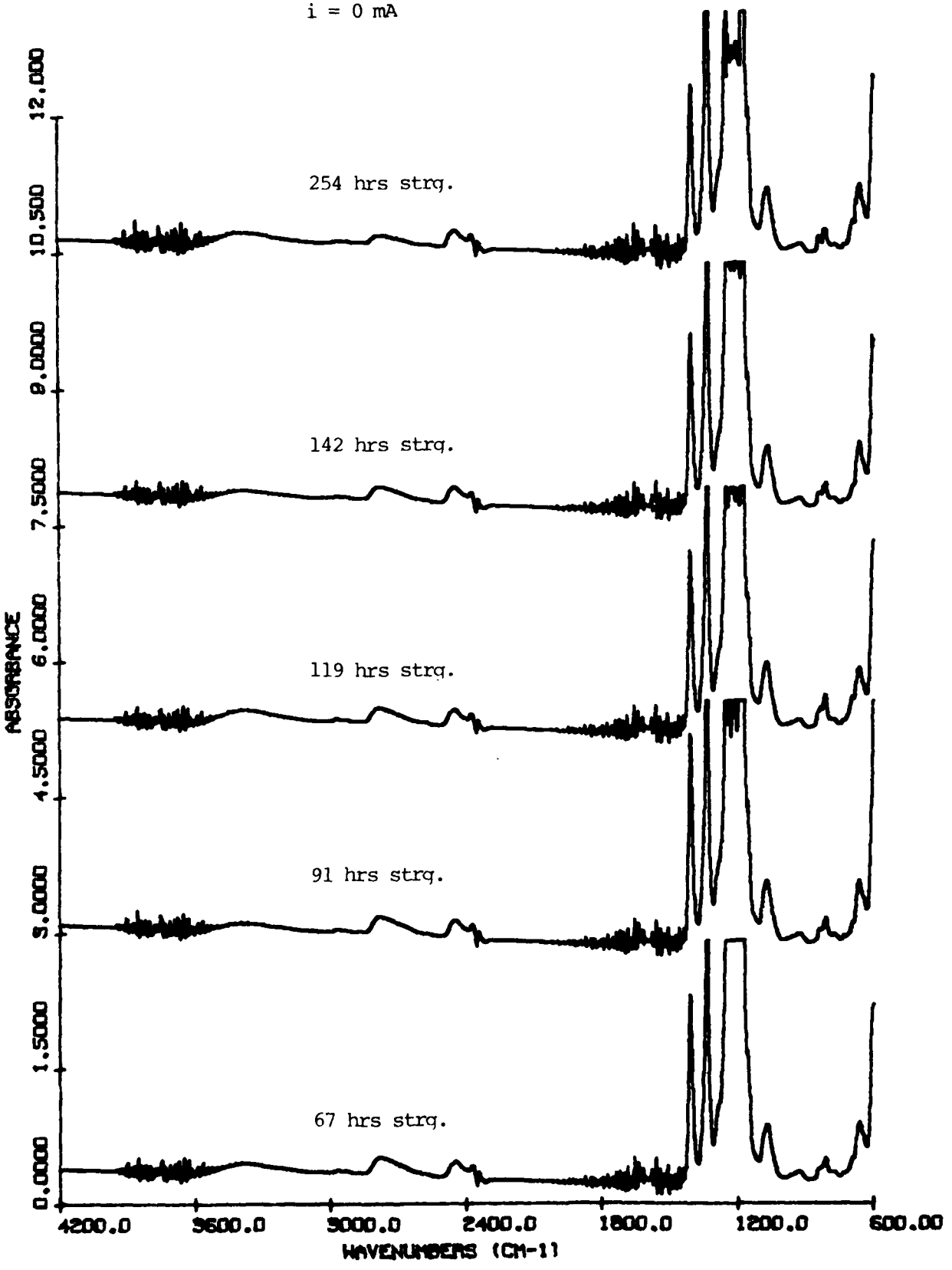

3.2 Identification of Products of Discharge in Solution

On the basis of some of the previous studies which we have summarized in Section 1 we can make the following assignments:

3400 cm^{-1} (broad band)	: $AlCl_3OH^-$
2790 cm^{-1} (broad band)	: HCl
2450 cm^{-1} (broad band)	: $SOCl_2$
1408 cm^{-1}	: SO_2Cl_2
1335 and 1144 cm^{-1}	: SO_2
1225 cm^{-1} (broad band)	: $SOCl_2$
1115 cm^{-1} (broad band)	: $SOCl^+$

To identify the absorption bands at 1070 cm^{-1}, 927, 822, 694 and 665 cm^{-1} we spiked several solutions of electrolyte or pure $SOCl_2$ with known compounds. The IR absorption spectra of H_2O, H_2O with $AlCl_3$, SO_2Cl_2 and $AlCl_3$ in $SOCl_2$ are shown respectively in Figures 5-8. Spectra of H_2O, CO_2, and SCl_2 in electrolyte are shown in Figures 9-11. These spectra are then combined in Figure 12 in an attempt to reconstruct an actual absorption spectrum obtained on reversal.

Addition of water to $SOCl_2$ (Figure 5) results simply in the formation of HCl (2790 cm^{-1}) and SO_2 (1335 and 1144 cm^{-1}). However adding water to either the neutral electrolyte or to a solution of $AlCl_3$ in $SOCl_2$ causes some striking effects. In neutral electrolyte (Figure 9) strong absorptions at 3400 and 694 cm^{-1} appear, whereas in the presence of $AlCl_3$ (Figure 6) bands at 803, 822 as well as 3400 cm^{-1} appear in addition to the $SOCl^+$ band at 1115 cm^{-1}. All these features were observed in Cell SC-68. These results are in agreement with the work of Bailey and Blomgren on the hydroxy- and oxychloroaluminates in Li_2CO_3-$AlCl_3$/$SOCl_2$ electrolytes (13).

SO_2Cl_2 in $SOCl_2$ (Figure 7) simply gives rise to characteristic absorptions at 1408 cm^{-1} and 1171 cm^{-1}. Other absorption bands below 600 cm^{-1}

were not recorded as most of the species generated during discharge and reversal give rise to poorly resolved absorption bands in that region.

The effect of $AlCl_3$ addition to $SOCl_2$ (Figure 8) is quite dramatic giving rise to a strong absorption at 1115 cm^{-1} due to the S-O stretching vibration of the complex $SOCl^+AlCl_4^-$. Both $SOCl^+$ and SO_2Cl_2 were formed during reversal in SC-68.

CO_2 addition (Figure 10) to neutral electrolyte results in some weak absorption bands at 2357, 803, 679 and 656 cm^{-1}. Contamination of an operating cell with CO_2 is possible but occurs to a small extent.

Upon addition of SCl_2 to neutral electrolyte containing SO_2 (Figure 11) a slow increase in the absorption at 1070 cm^{-1} and 665 cm^{-1} is observed, together with increases of SO_2Cl_2 and SO_2. Both the 1070 cm^{-1} and 665 cm^{-1} bands were formed during reversal in SC-68. Although we cannot identify the products giving rise to these absorptions, a reasonable assignment for the band at 1070 cm^{-1} is the S-O stretching vibration. The 665 cm^{-1} band could be due to either S-O bending modes or S-S stretching modes.

At this stage we are confident that the sources of all the peaks in the IR absorption spectrum have been identified. This is demonstrated in the spectral reconstruction shown in Figure 12 where we present a weighted average of the spectra for water in neutral electrolyte, $AlCl_3$ in $SOCl_2$, water in $AlCl_3/SOCl_2$, SO_2 in $SOCl_2$, SO_2Cl_2 in $SOCl_2$, and SCl_2 in neutral electrolyte; this artificially generated IR spectrum is compared to the absorption spectrum of SC-68 during anode limited reversal.

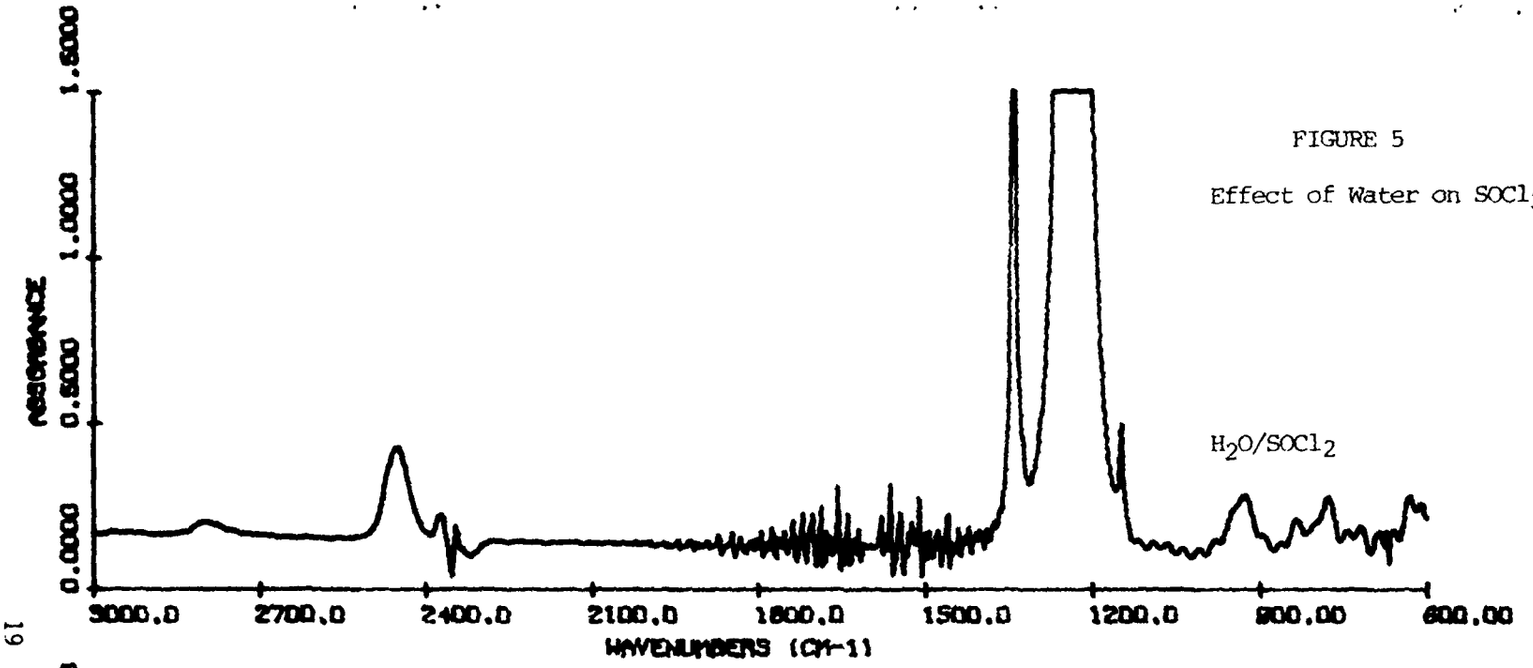

FIGURE 5

Effect of Water on $SOCl_2$ Spectrum

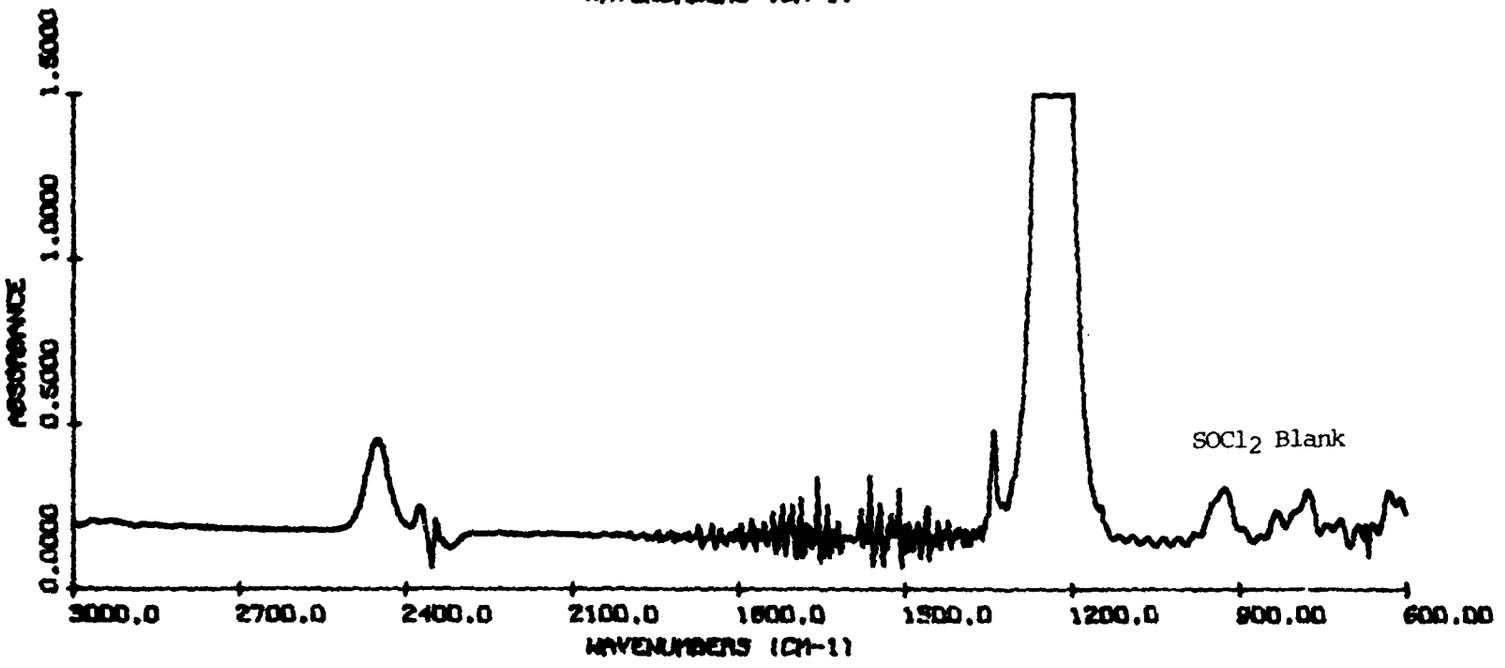

FIGURE 6

Effect of Water and $AlCl_3$ on $SOCl_2$ Spectrum

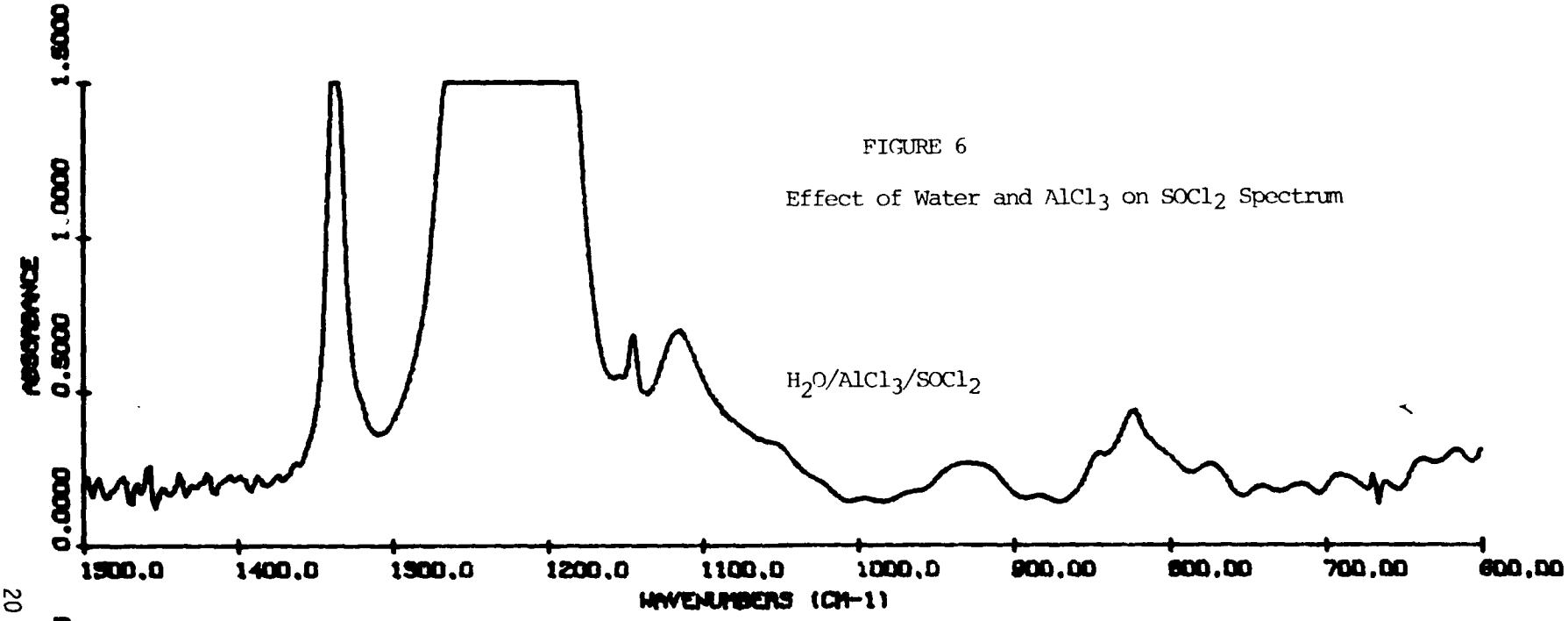

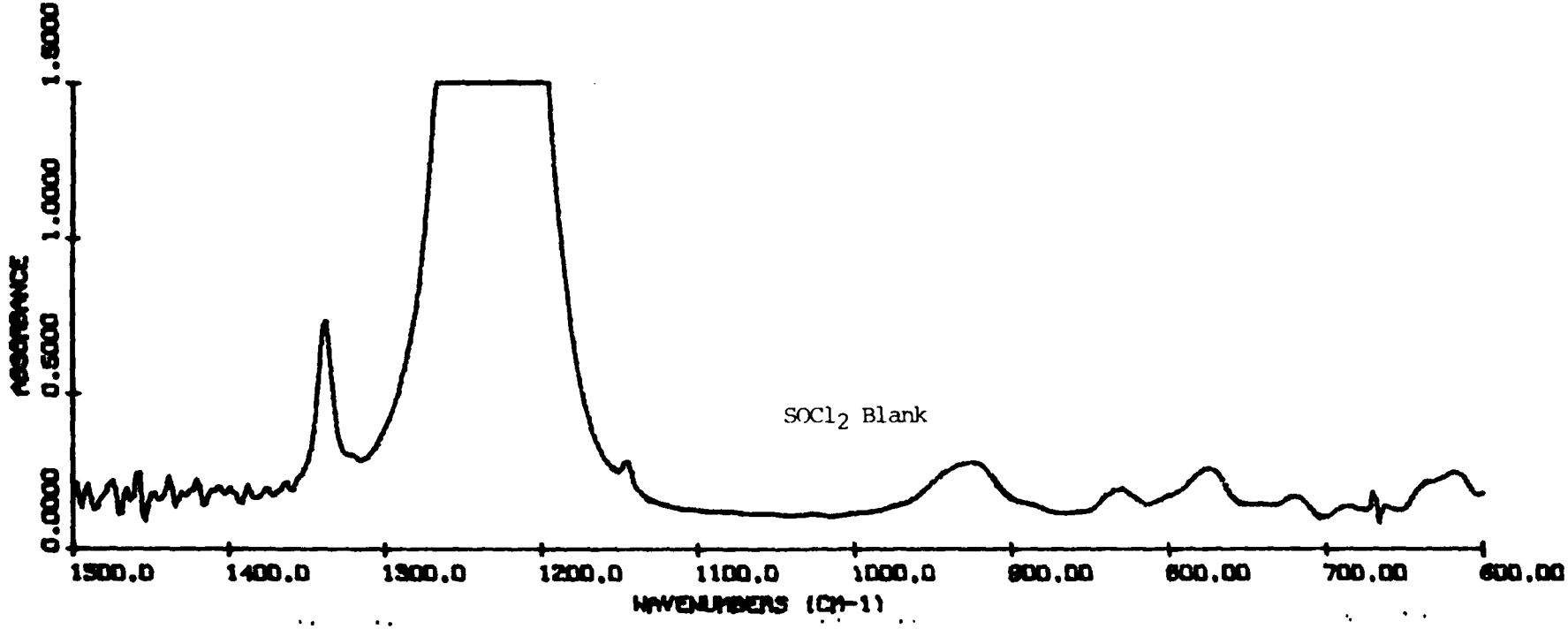

FIGURE 7

Effect of SO_2Cl_2 on $SOCl_2$ Spectrum

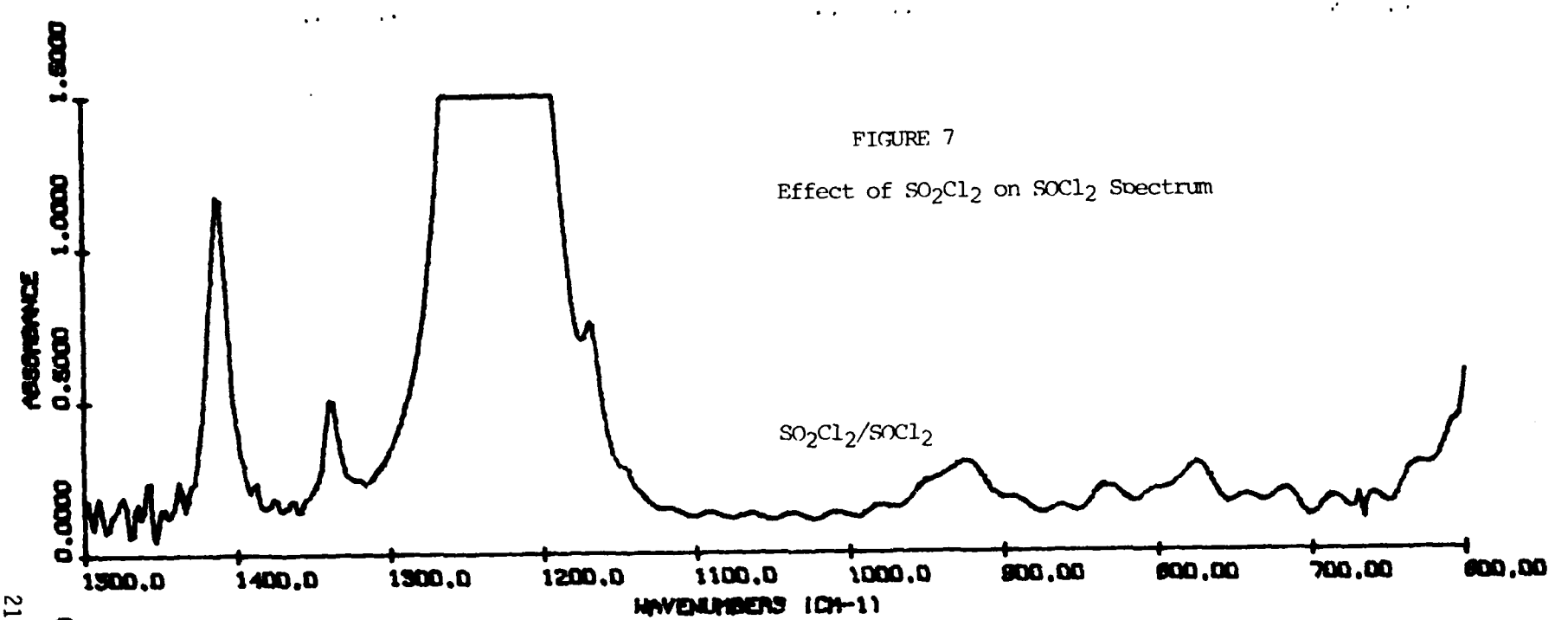

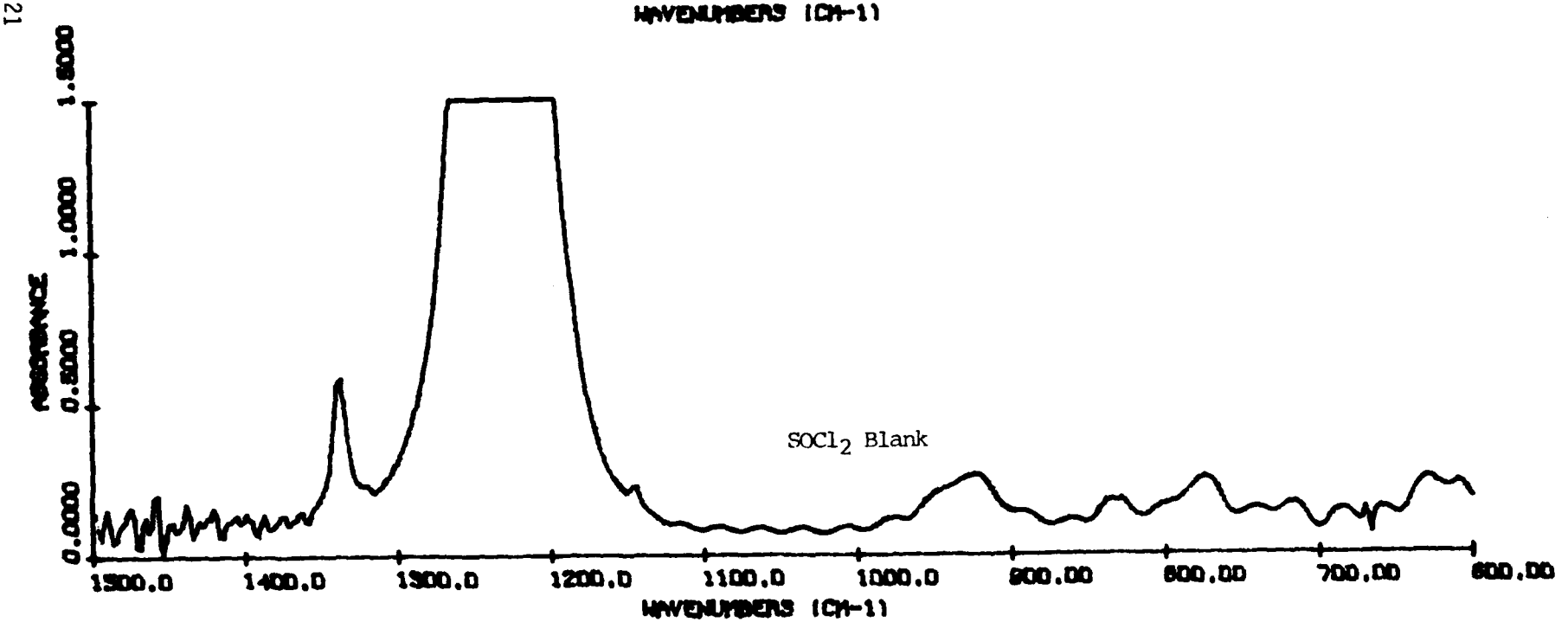

FIGURE 8

Effect of $AlCl_3$ on $SOCl_2$ Spectrum

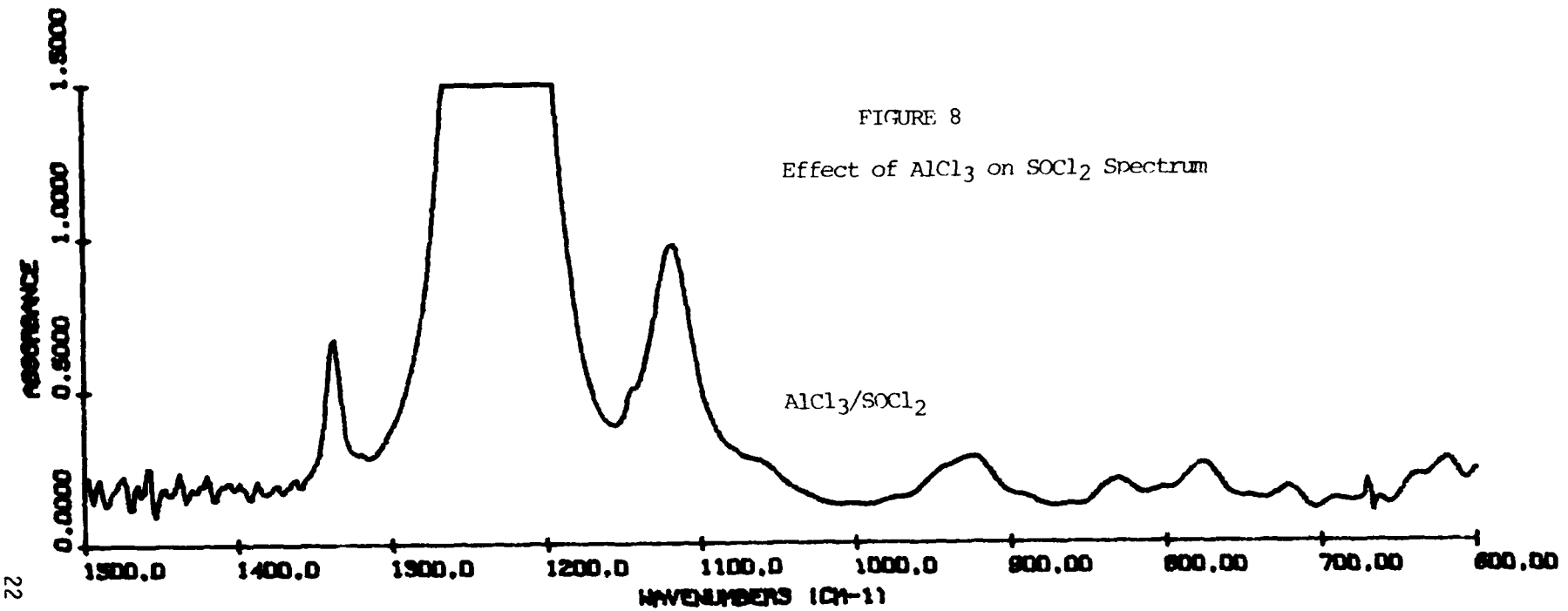

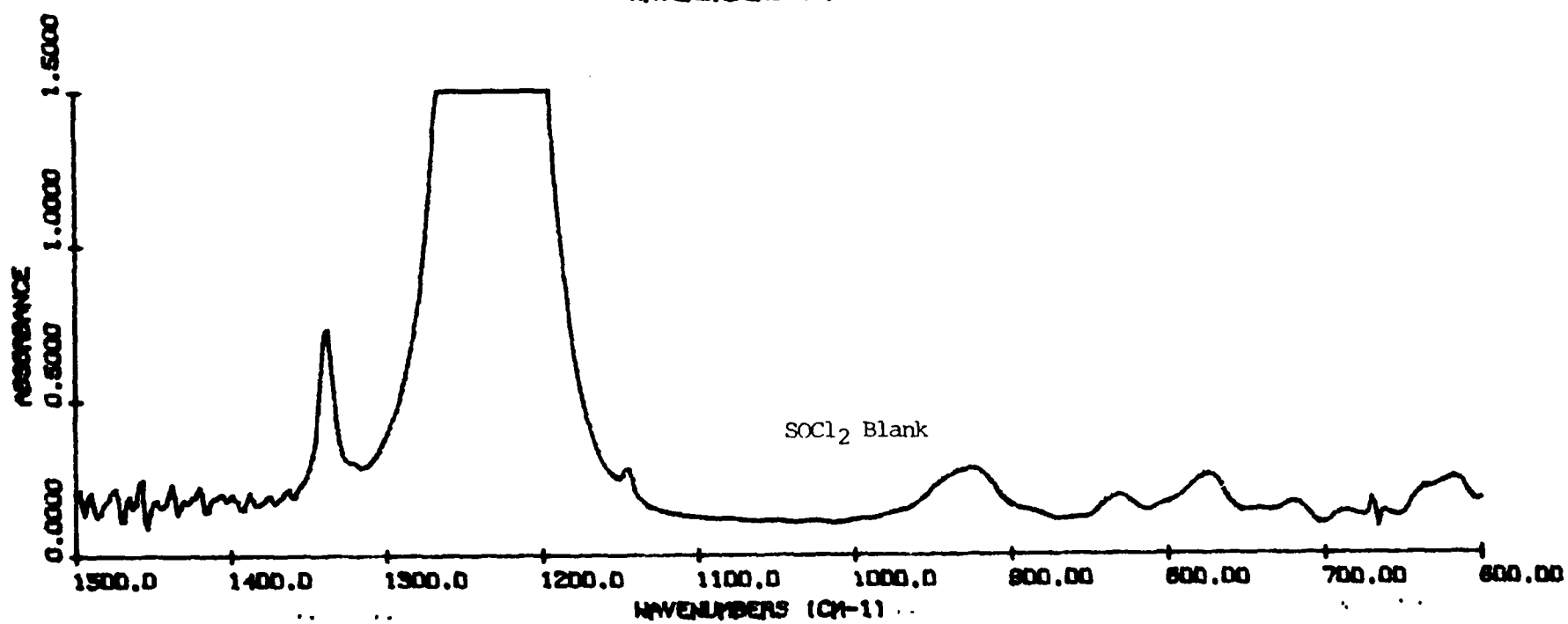

FIGURE 9

Effect of Water on $LiAlCl_4/SOCl_2$ Electrolyte

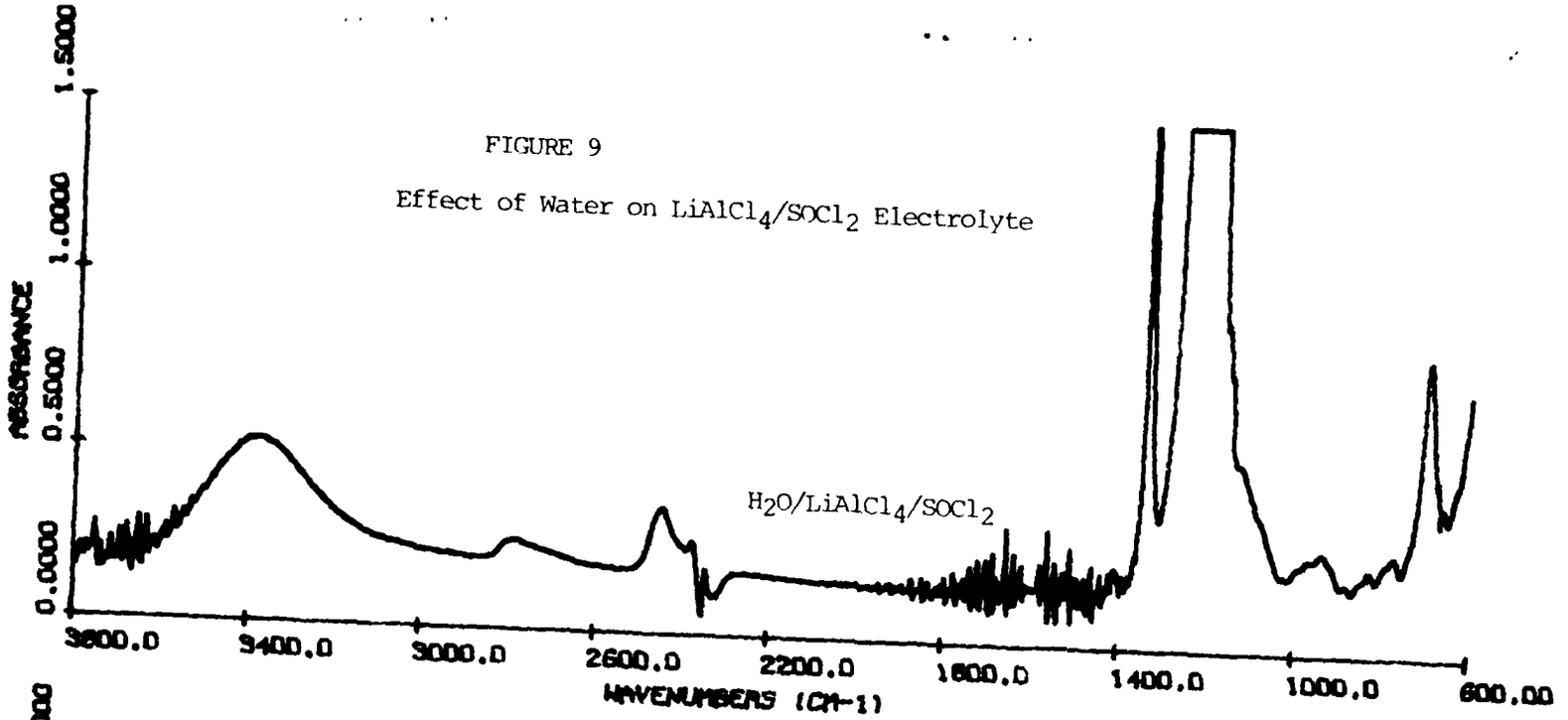

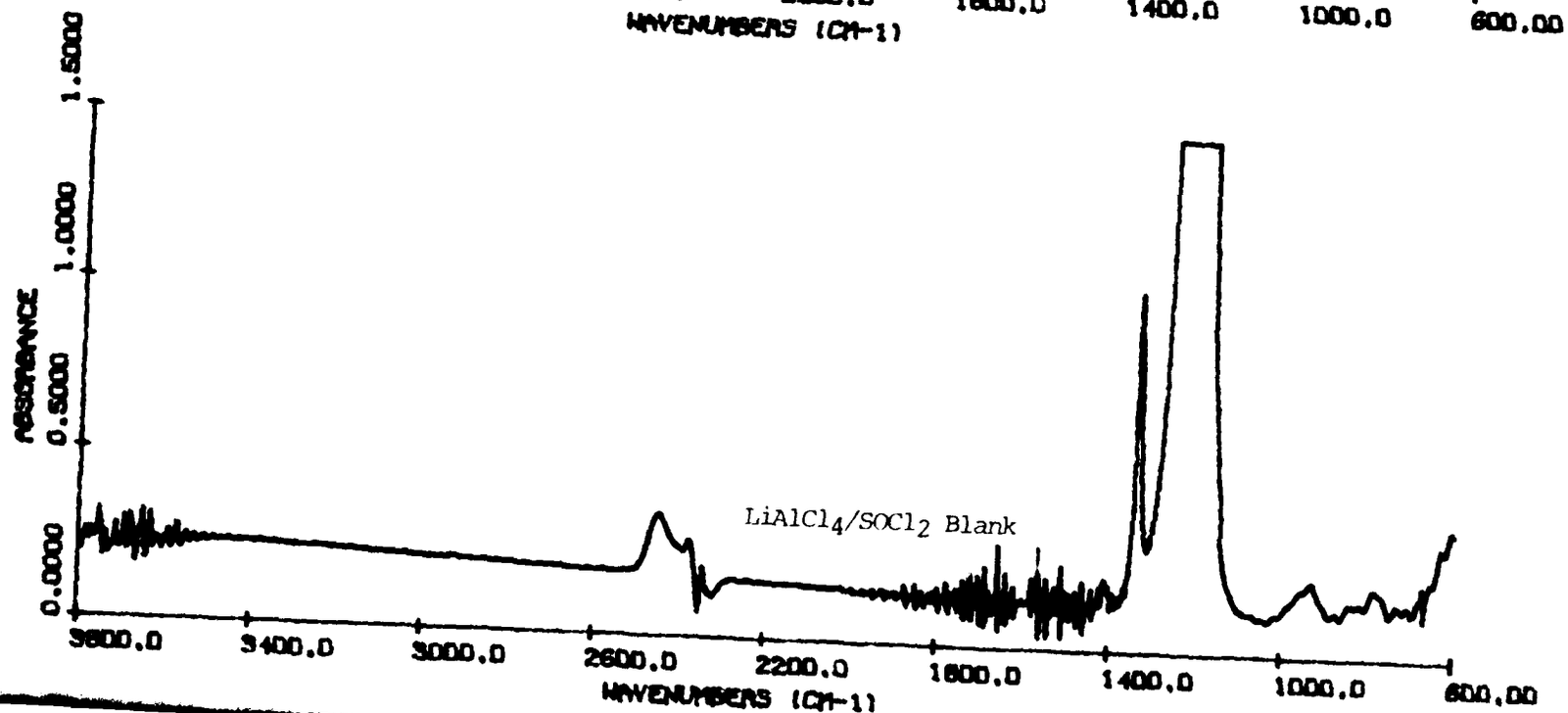

FIGURE 10

Effect of CO_2 on $LiAlCl_4/SOCl_2$ Electrolyte

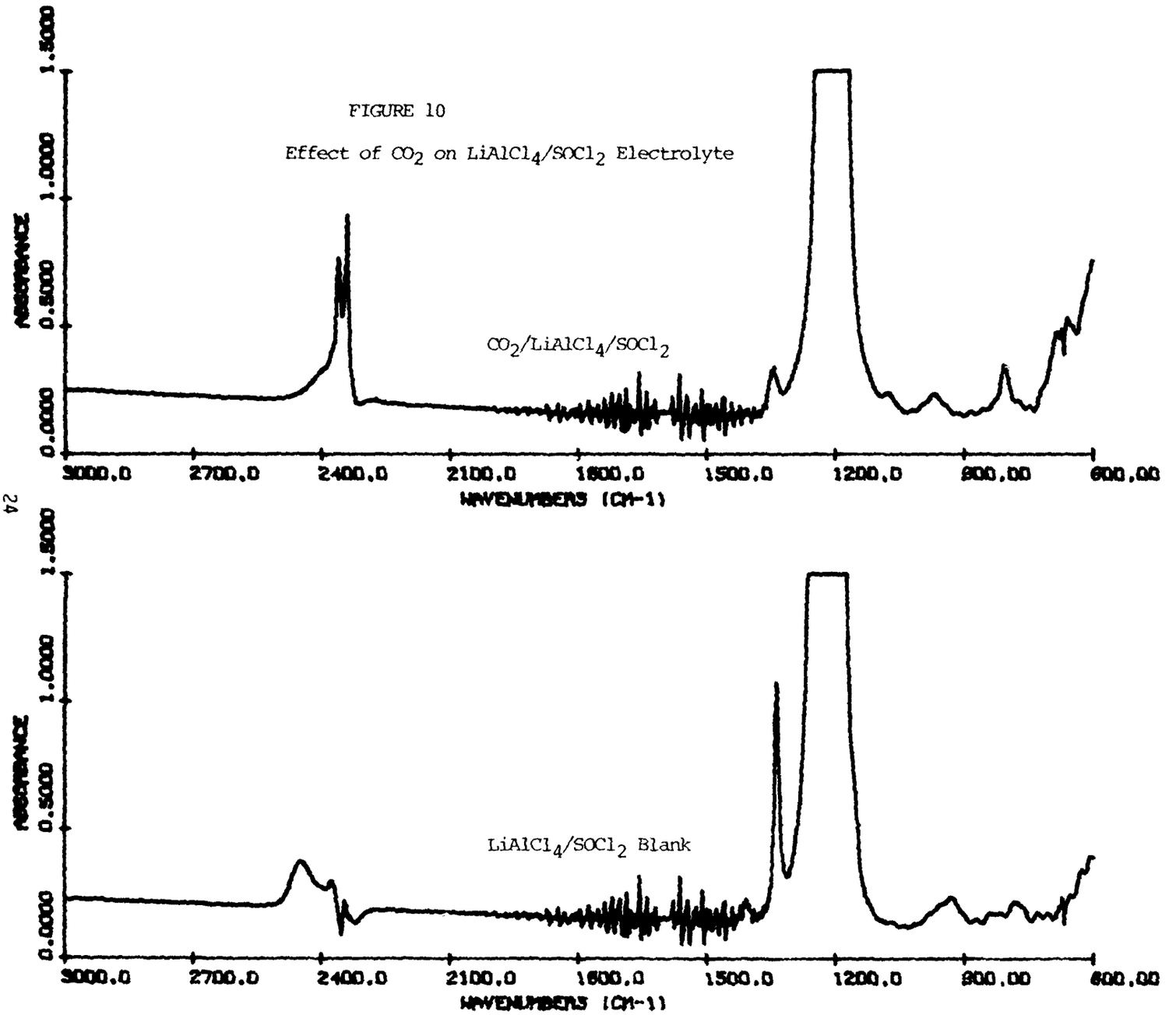

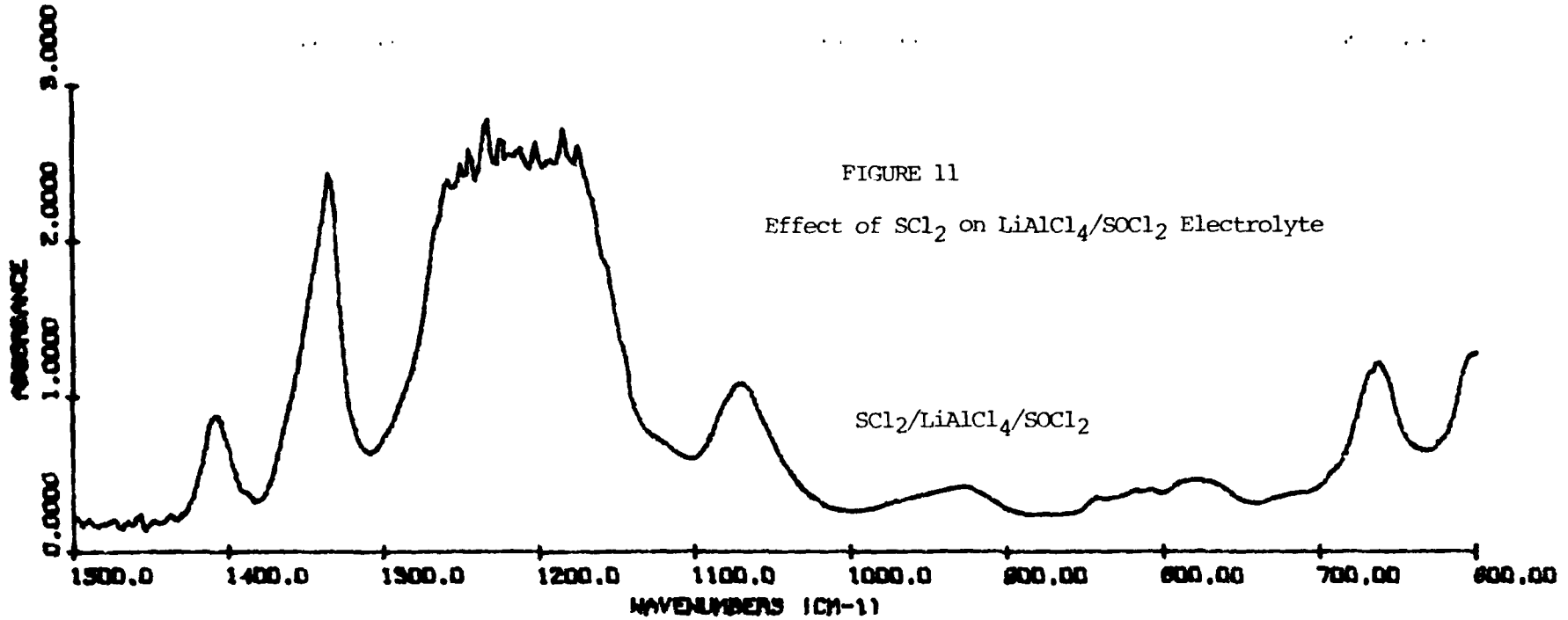

FIGURE 11

Effect of SCl_2 on $LiAlCl_4/SOCl_2$ Electrolyte

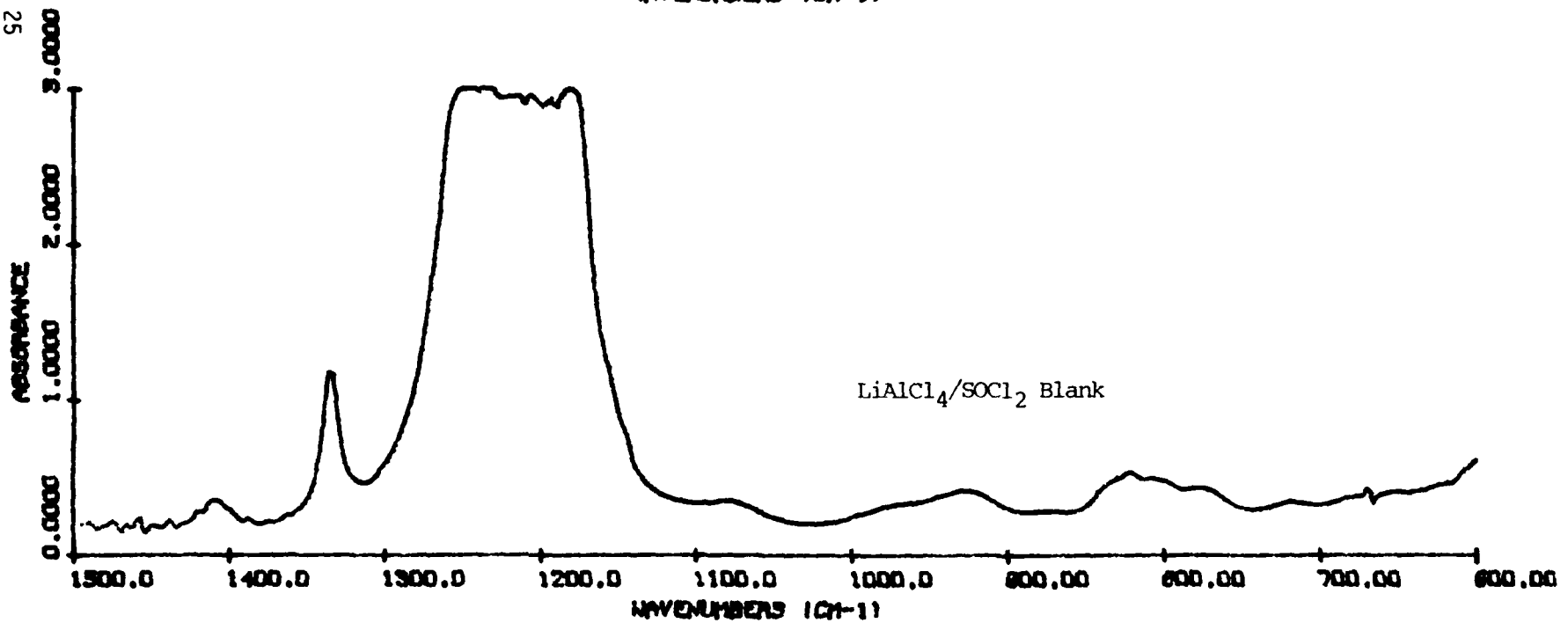

FIGURE 12

IR Absorption Spectrum Reconstructed from
$H_2O/LiAlCl_4/SOCl_2$
$AlCl_3/SOCl_2$
$SO_2/SOCl_2$
$SO_2Cl_2/SOCl_2$
$SCl_2/LiAlCl_4/SOCl_2$

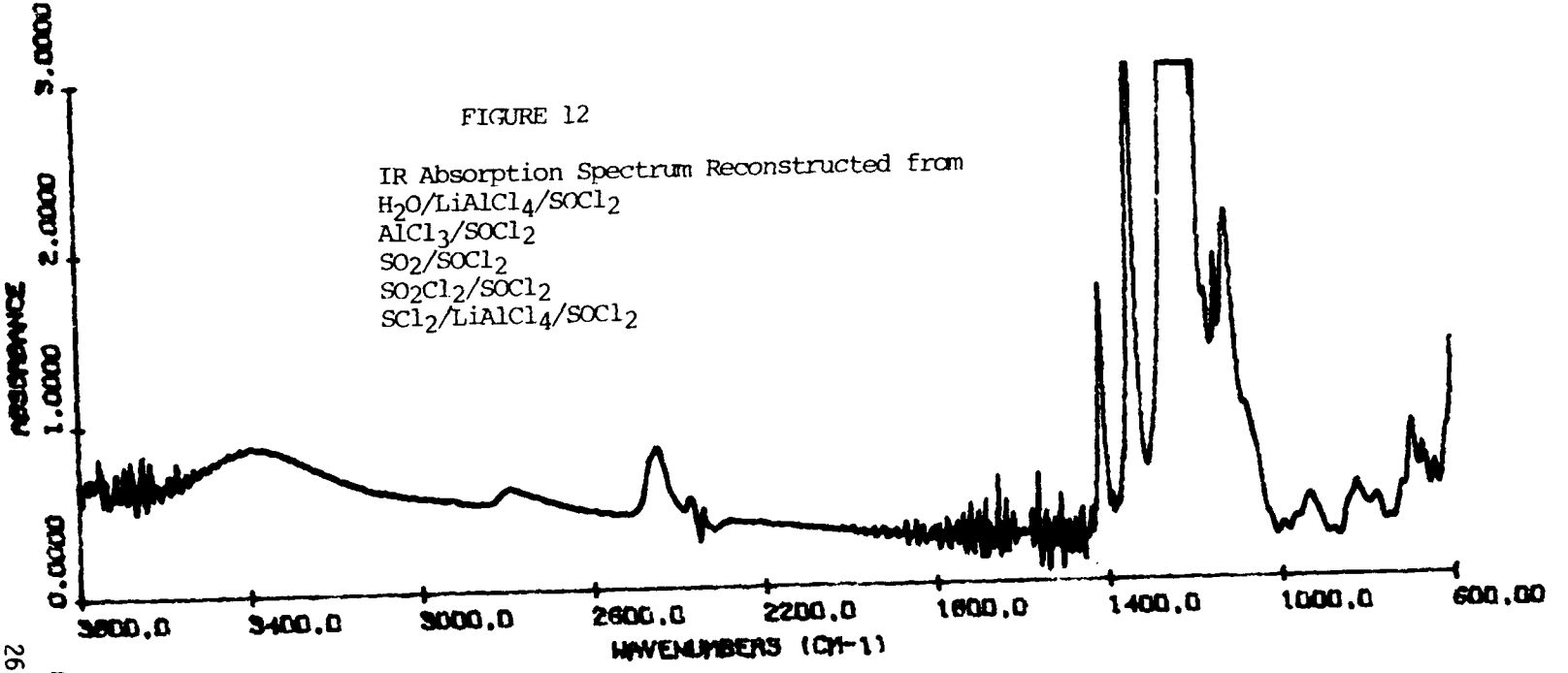

IR Absorption Spectrum from Cell SC-68
During Anode Limited Reversal

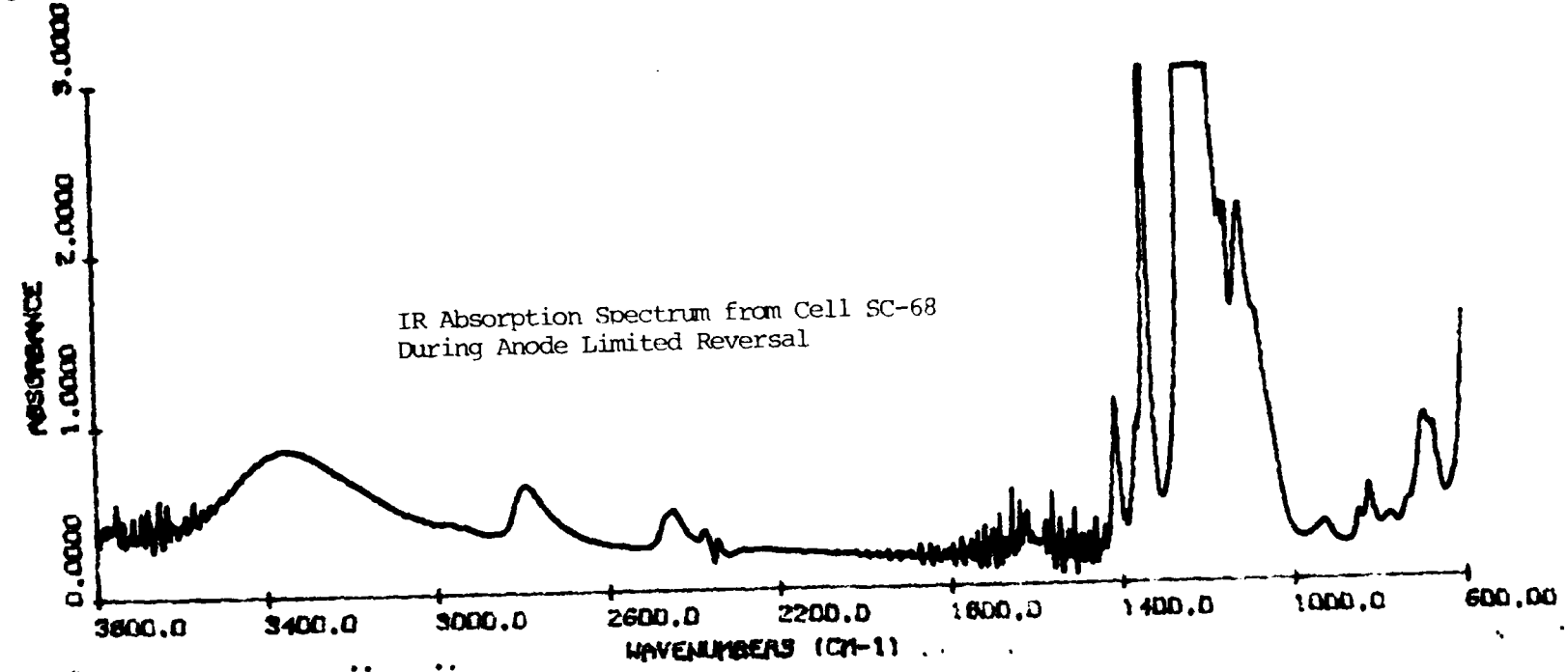

3.3 Synthesis of S_2O

To verify the claim of Isotone and Brodd at INCO (9) that S_2O gives rise to an absorption at 688 cm^{-1}, we have attempted to synthesize S_2O and trap it in $SOCl_2$. For the synthesis we used the reaction between $SOCl_2$ and Ag_2S at 160C (see Figure 13). S_2O in the gas phase has three IR active bands at 1165 cm^{-1}, 679 cm^{-1} and 388 cm^{-1} (15). We were only able to observe a weak band at 1168 cm^{-1} in the gas phase. Attempts to condense S_2O in $SOCl_2$ at 77°K resulted only in the formation of a red polysulfur oxide which decomposed into SO_2 and sulfur upon heating to room temperature. No evidence of S_2O could be observed in the $SOCl_2$ trapping solution.

The absorption band at 688 cm^{-1} which Istone and Brodd assigned to S_2O consists in effect of two absorption bands, one at 694 cm^{-1} due to the interaction of $AlCl_4^-$ and water, the other at 665 cm^{-1} observed only during anode limited reversal. Salmon's assignment of a 690 cm^{-1} absorption to Cl_2O (11) also overlooks the strong interaction of water with the electrolyte. (Later our mass spectrometric analysis will show the presence of S_2O in the gas phase, but no trace of Cl_2O - see Section 4).

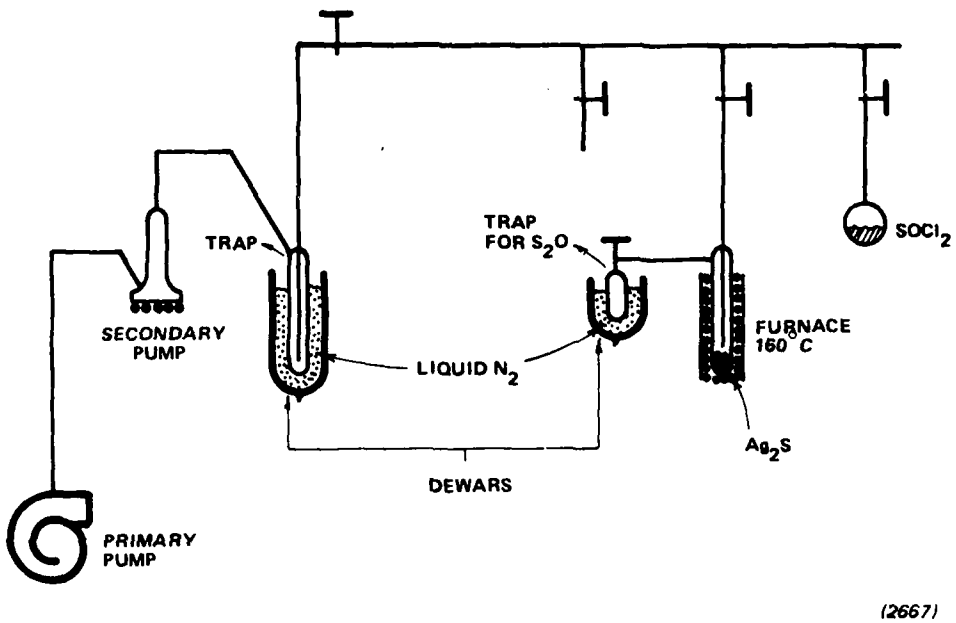

Figure 13 Schematic Diagram of the Vacuum Line used to Synthesize S_2O

$$Ag_2S + SOCl_2 \xrightarrow{160°C} 2AgCl + S_2O$$

3.4 Gas Phase Studies

The gas phase spectra of several compounds such as SO_2, CO_2, $SOCl_2$, SO_2Cl_2, S_2Cl_2 and SCl_2 which might be present during anode limited reversal were measured. These spectra obtained with a 20 cm gas cell equipped with NaCl windows are shown in Figures 14-19. These were compared to the gas phase IR spectrum of a cell driven into anode limited reversal (see Figure 20) at 5 mA/cm^2. SO_2, $SOCl_2$ and SO_2Cl_2 are easily identified. The results for SCl_2 or S_2Cl_2 are inconclusive. S_2Cl_2's strong absorption band at 461-454 cm^{-1} is exactly in the same region as one of the strong absorption bands of $SOCl_2$. SCl_2, if present, would appear as a shoulder on the 502-492 cm^{-1} band of $SOCl_2$ (SCl_2 absorbs at 528-520 cm^{-1}); however, observation of that shoulder would depend on the relative concentrations of $SOCl_2$ and SCl_2. A strong smell points to the presence of at least one of those two sulfur chlorides. Mass spectrometric analysis indicates that substantial amounts of SCl_2 are formed on reversal (see below - Section 4).

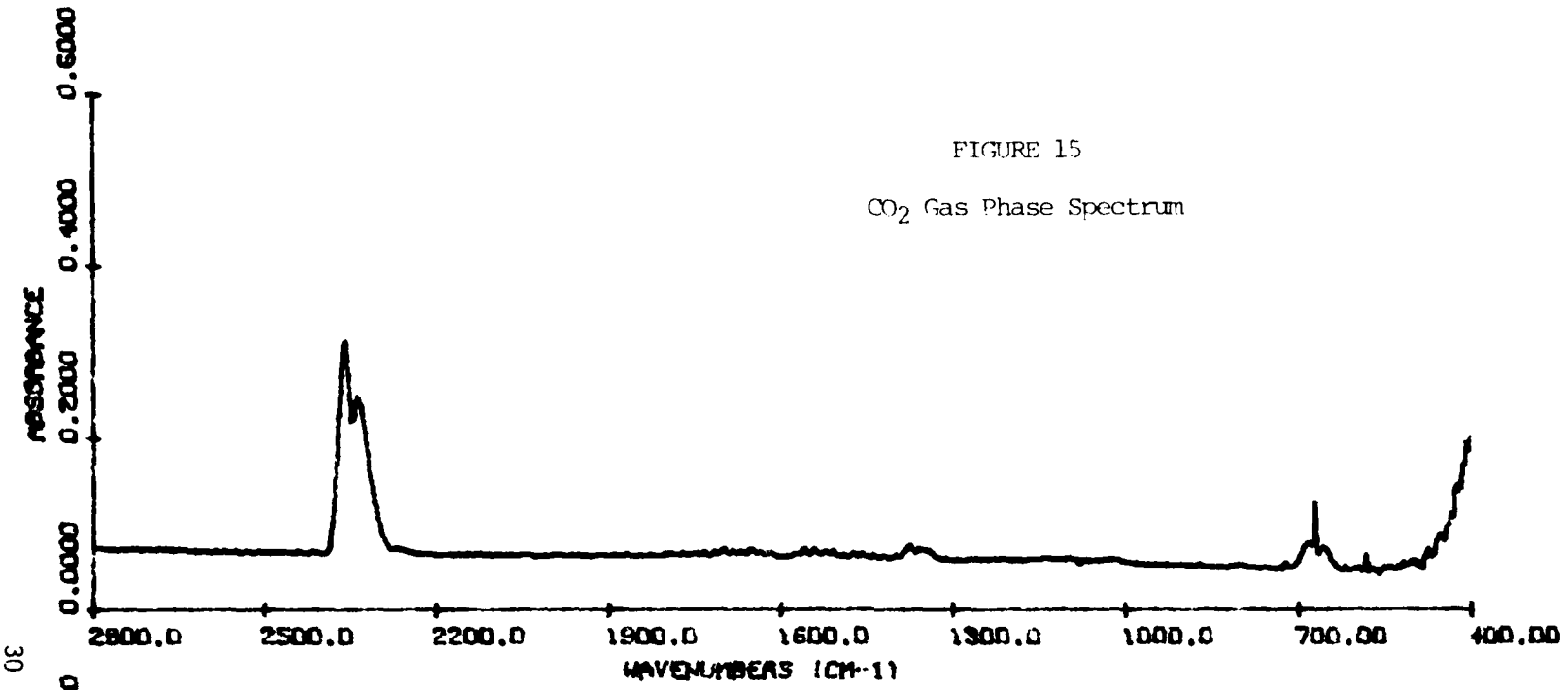

FIGURE 15

CO_2 Gas Phase Spectrum

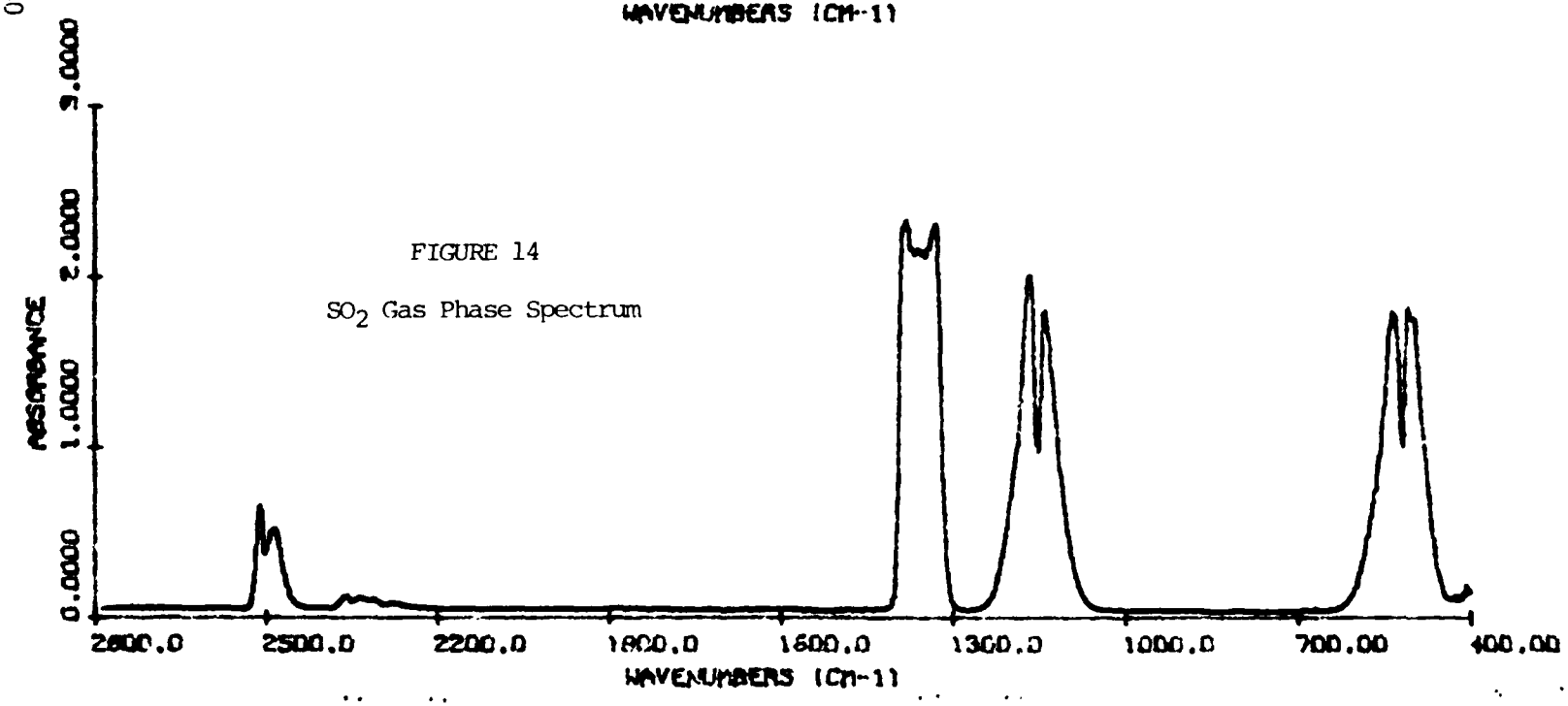

FIGURE 14

SO_2 Gas Phase Spectrum

FIGURE 17

SO_2Cl_2 Gas Phase Spectrum

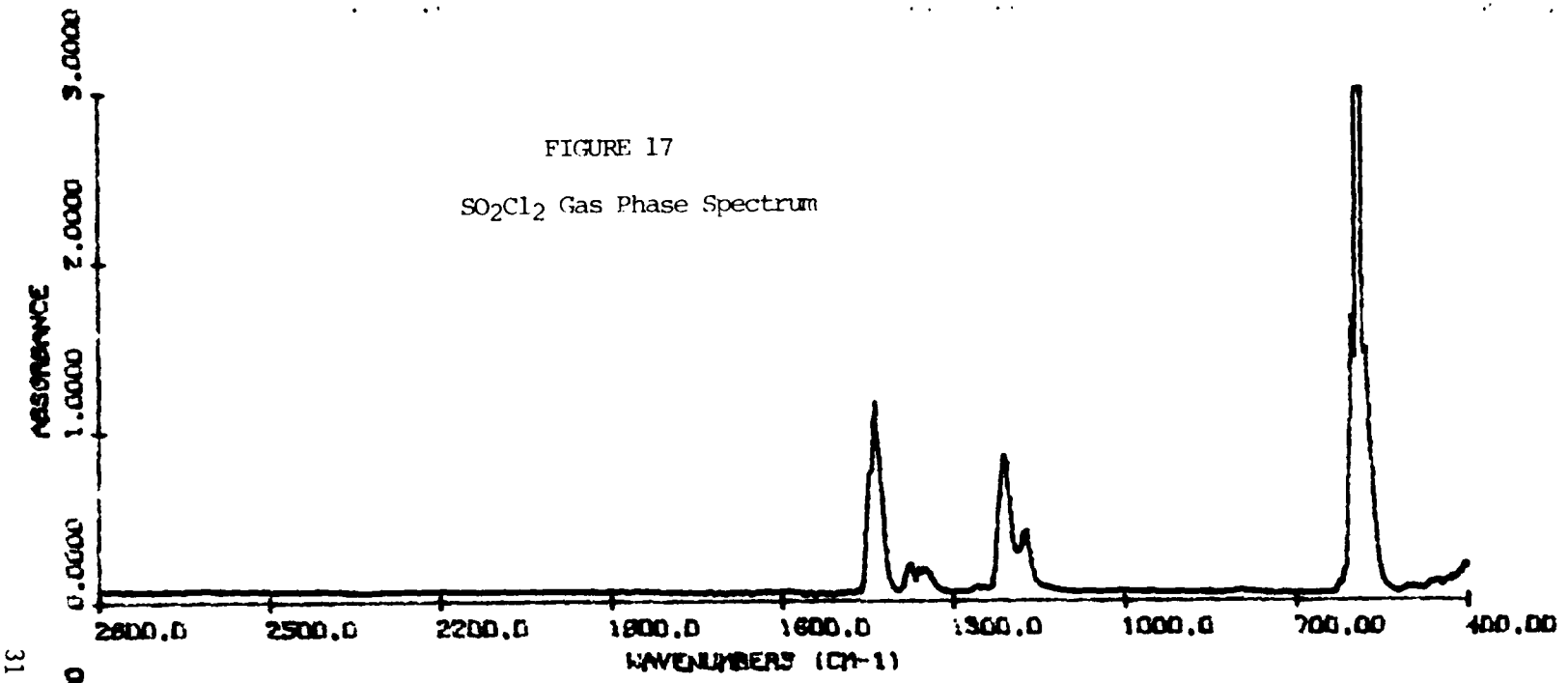

FIGURE 16

$SOCl_2$ Gas Phase Spectrum

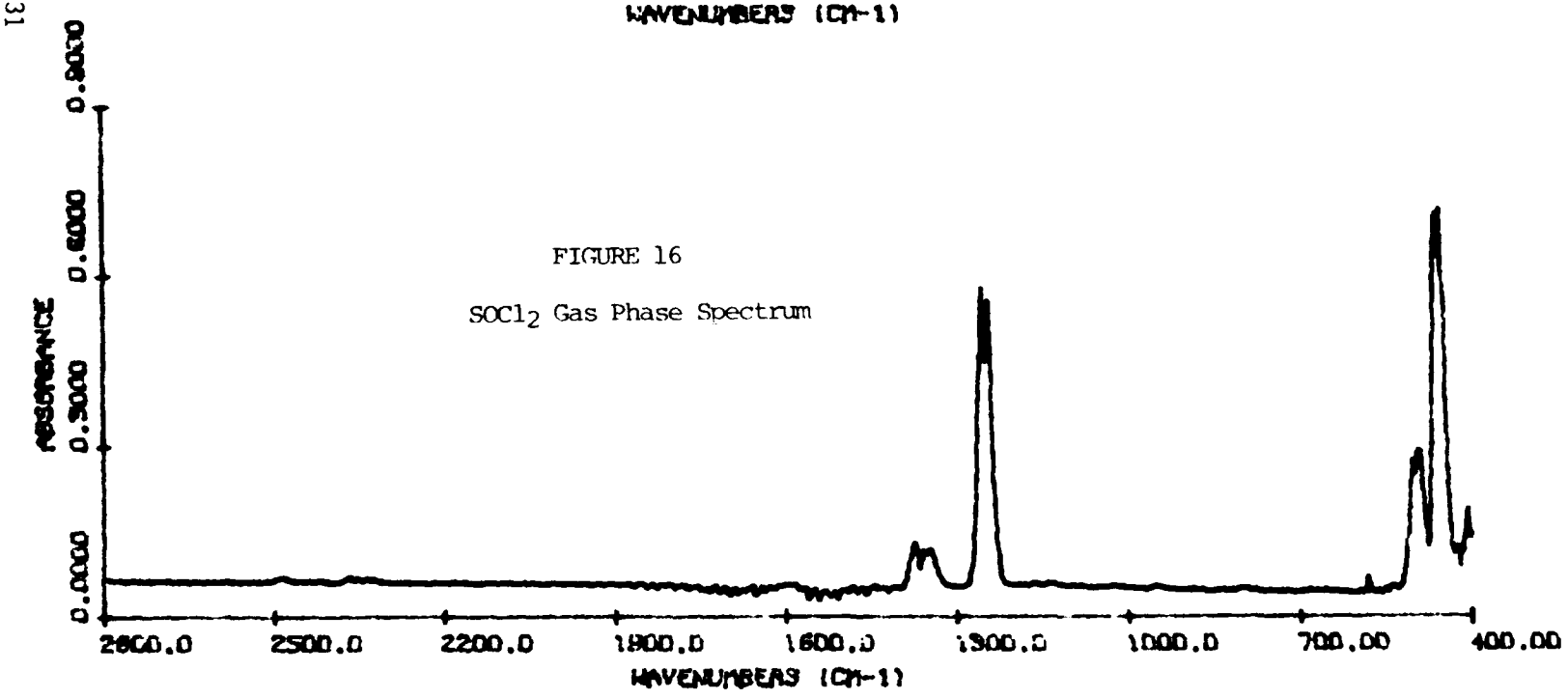

FIGURE 20

Gas Phase Spectrum of Cell in Storage after Anode Limited Reversal

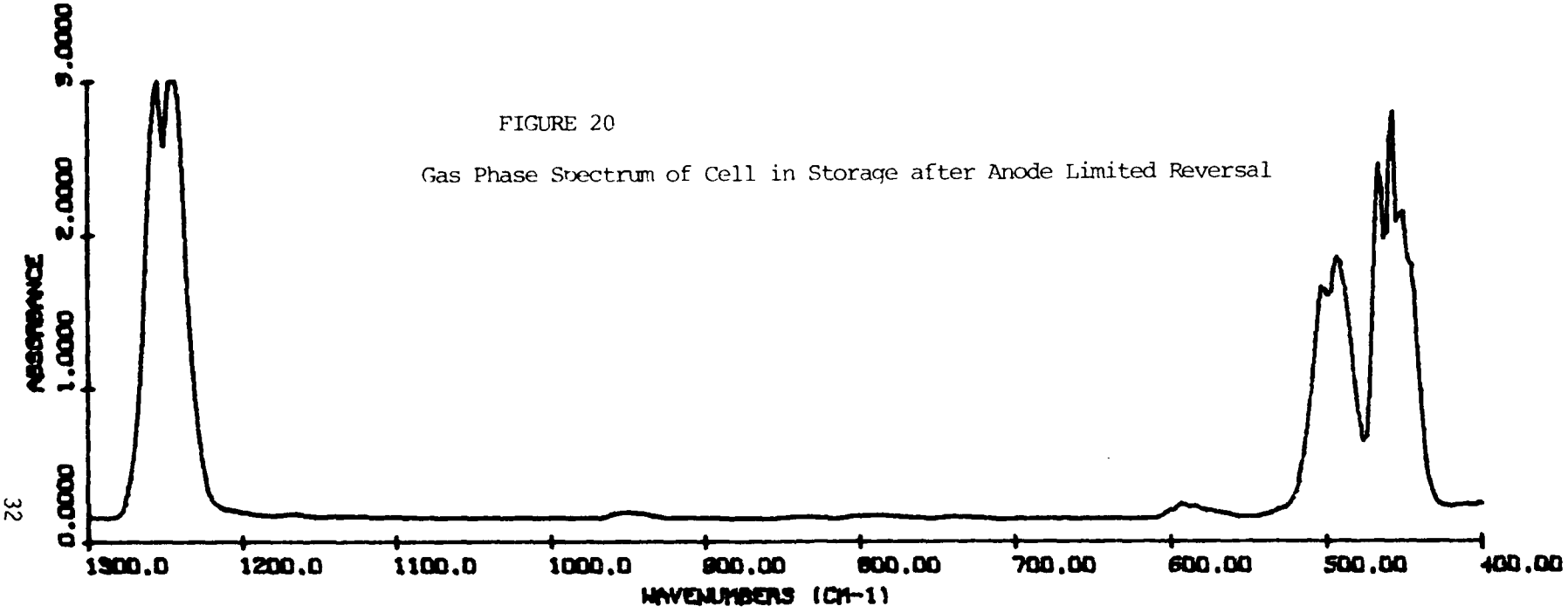

FIGURE 18

S_2Cl_2 Gas Phase Spectrum

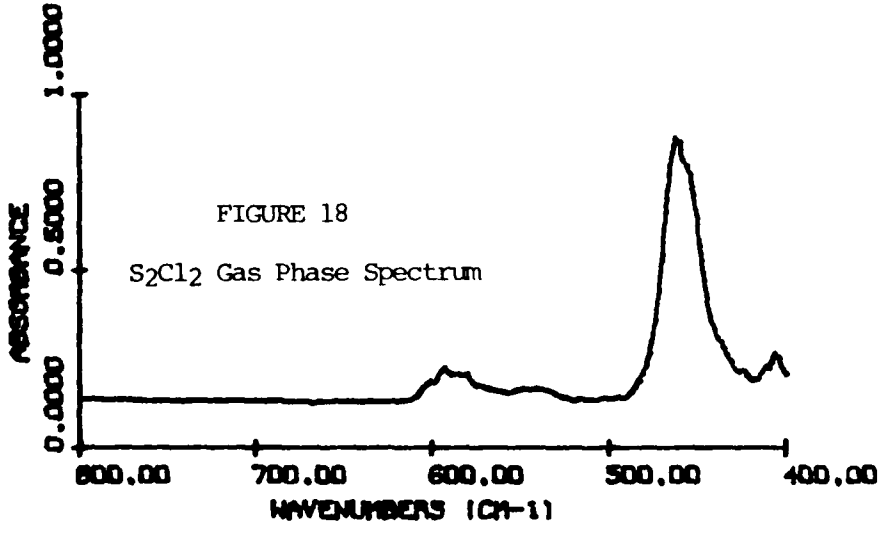

FIGURE 19

SCl_2 Gas Phase Spectrum

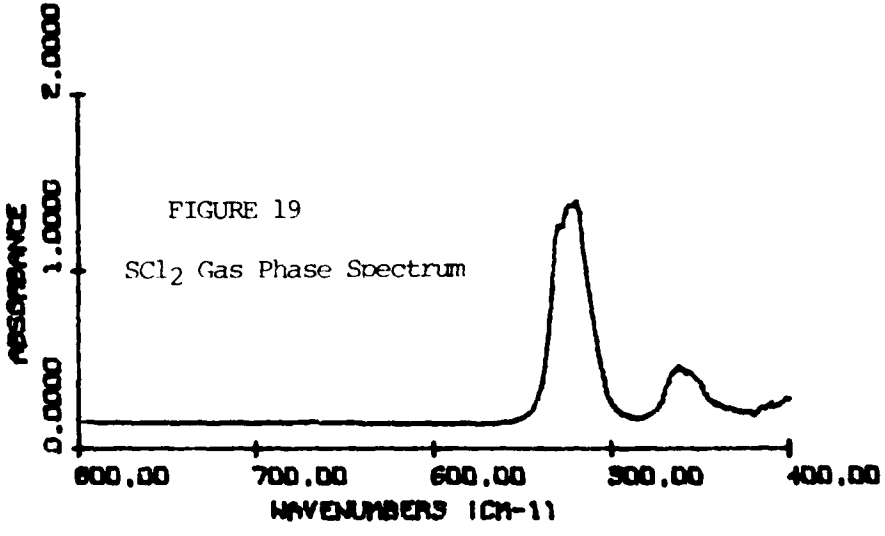

3.5 Calibration Curves

For quantitative analysis of the discharge process we prepared calibration curves for SO_2, SO_2Cl_2 and $SOCl^+$. These are shown respectively in Figures 21, 22 and 23. We have selected the peak height technique as opposed to peak area to assess the concentration of the various species present in our system. The peak area technique although theoretically more correct is more prone to "baseline" errors than the peak height method (18). As most of our absorption peaks are bunched around the very strong absorption bands of $SOCl_2$ we concluded that peak height measurements would be more accurate for our application.

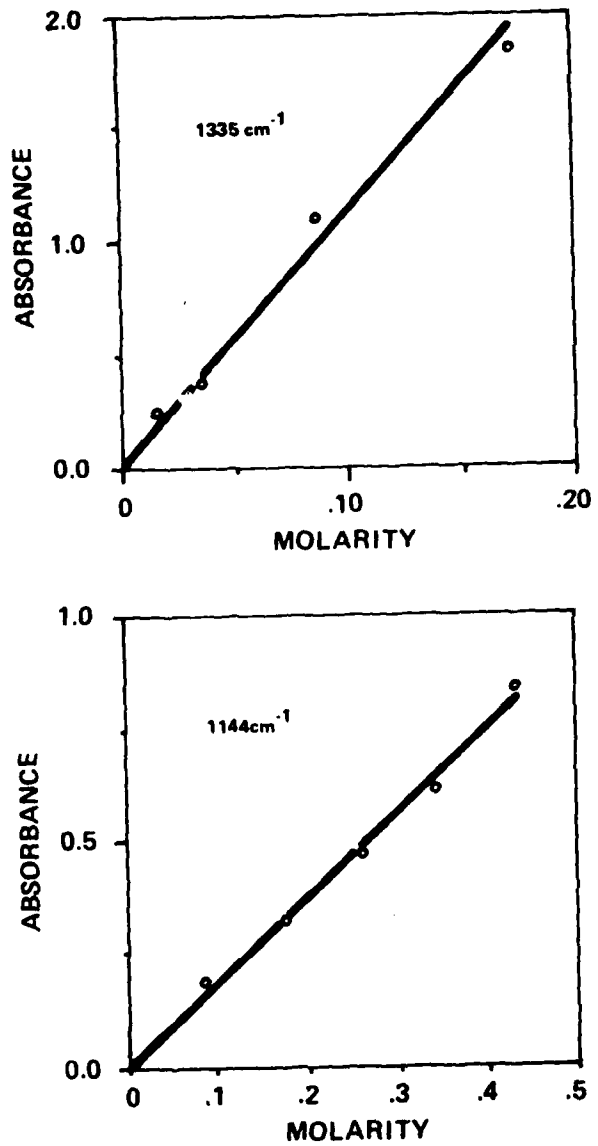

Figure 21 SO_2 Calibration Curves 0.1mm Path Length

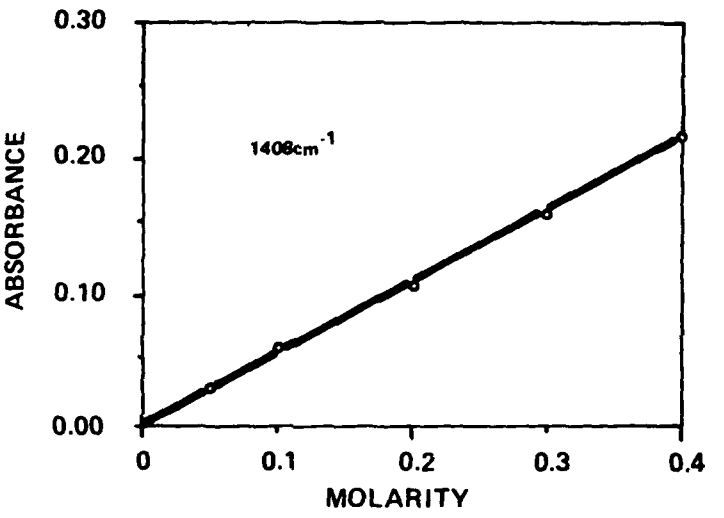

Figure 22 SO_2Cl_2 Calibration Curve 0.1mm Path Length

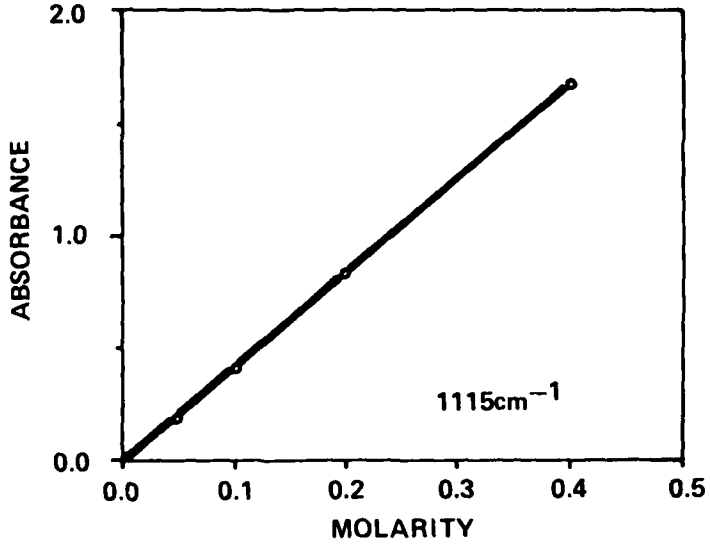

Figure 23 $SOCl^+$ **Calibration Curve**
0.1mm Path Length

3.6 In Situ FTIR Studies

During our early work under this contract, electrolyte from bobbin cells employing carbon for the cathode and equipped with a reservoir above the cathode was sampled at regular intervals and analyzed by FTIR spectroscopy. This method was plagued with difficulties and tended to yield irreproducible results. Going to a thin cathode design (Figure 1) improved the results but it was obvious that better control over the sampling procedure was necessary to prevent contamination with moisture. We settled on a circulating system where we coupled directly a spectroscopic cell to an electrochemical cell using either a manual or automatic pumping method for circulating the electrolyte between the two cells. The electrochemical cell design is shown in Figure 24. A schematic representation of the system incorporating a syringe pump is shown in Figure 25. Photographs of the actual systems used are also included (Figures 26 and 27); the first system utilizes a syringe pump and the second system, a peristaltic pump. The spectroscopic cell incorporates silver chloride windows with a 0.1 mm optical path length though on occasion we have used a 0.05 mm path length. The very first run however, was performed with zinc selenide windows which lasted only seven hours on exposure to the electrolyte.

Eight experiments were performed; these are summarized in Table I.

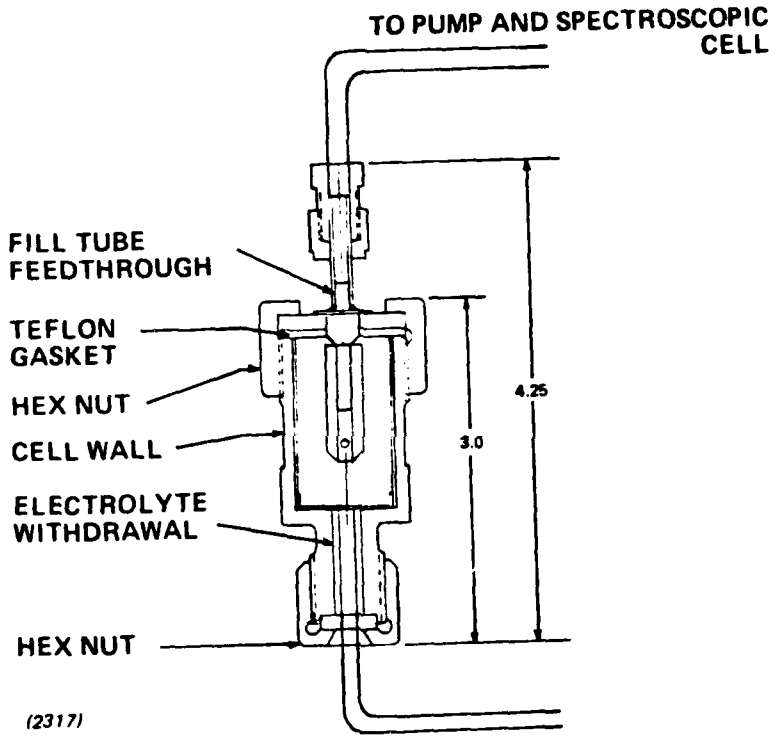

Figure 24 Electrochemical Cell for Flowing Electrolyte System

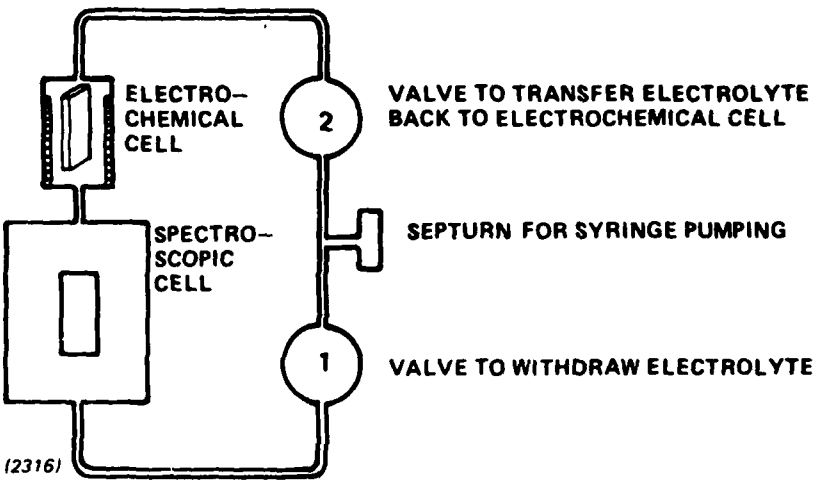

Figure 25 Schematic of a Closed Loop Sampling System

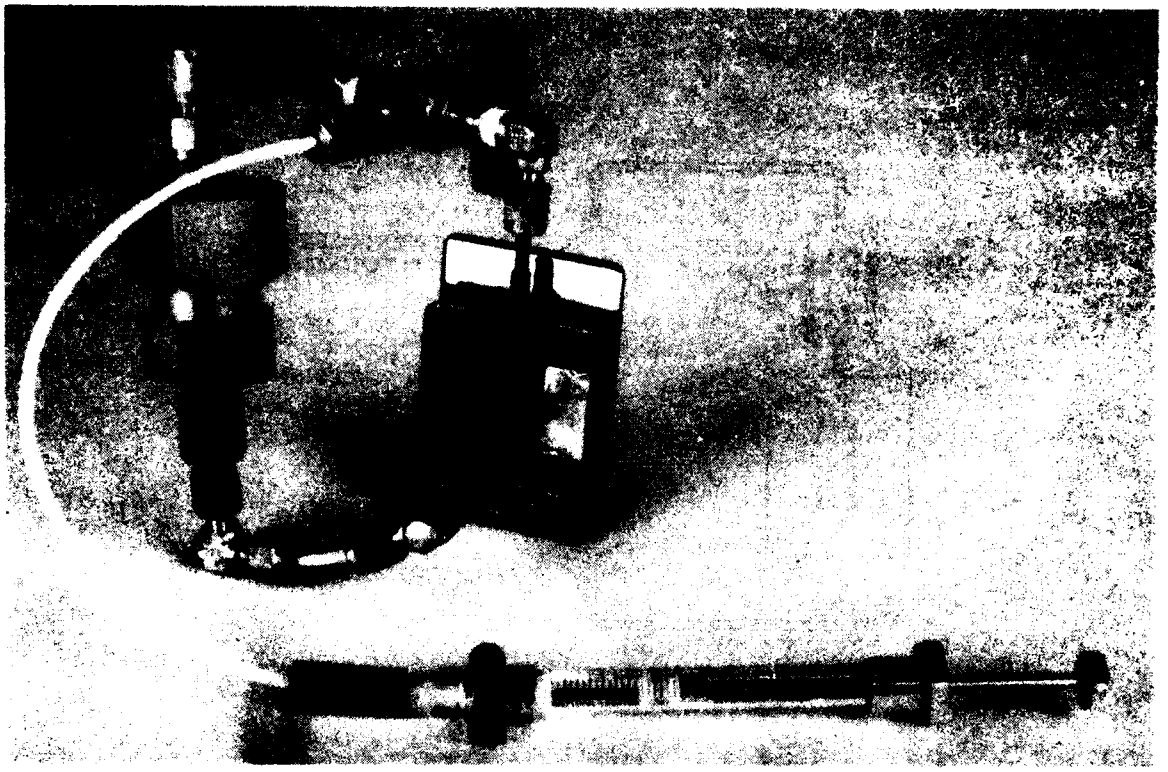

Figure 26

Photograph of Flowing Electrolyte System With Syringe Pump

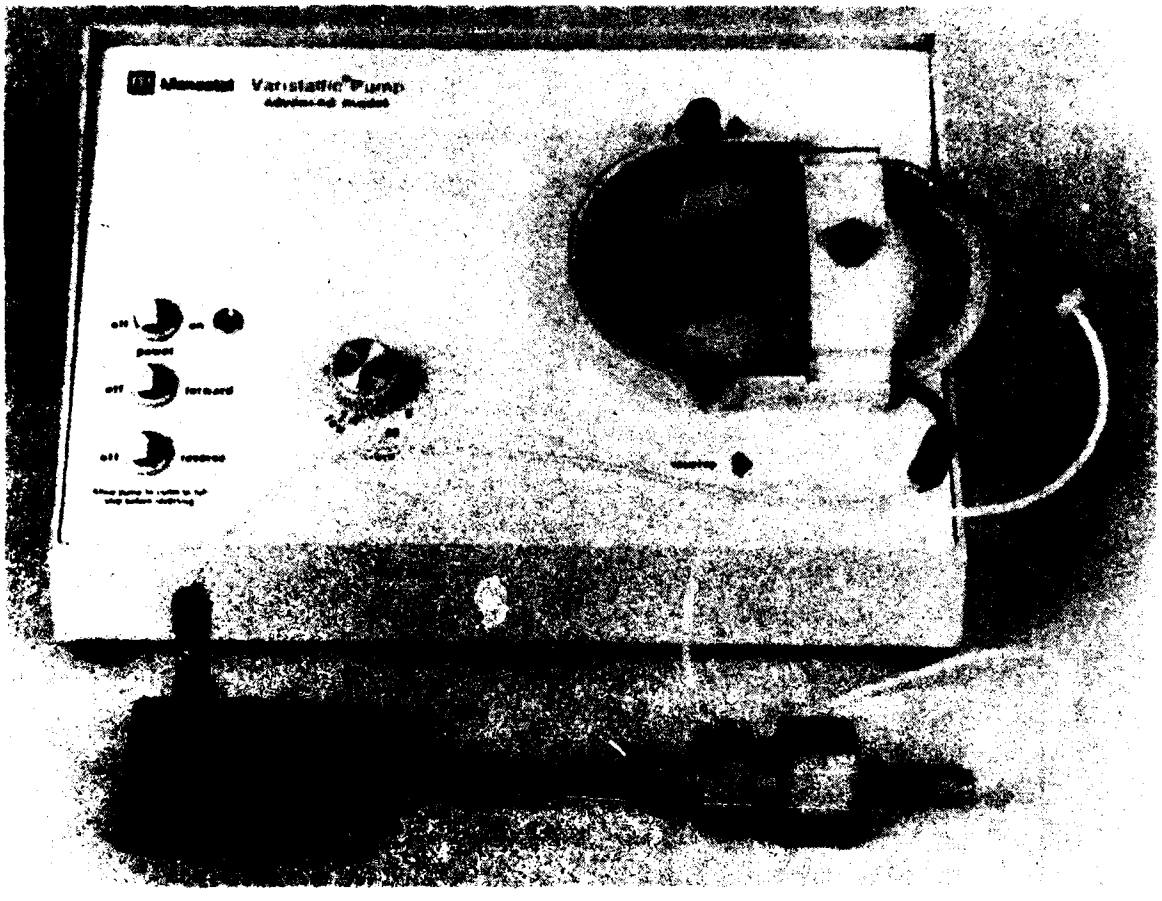

Figure 27

Photograph of Flowing Electrolyte System with Peristaltic Pump

Table I

Cell	Anode	Cathode*	Current and T	Electrolyte 1.4M $LiAlCl_4$	IR Cell	Pumping System
SC-69 Anode Limited	5 mil Li 8 cm^2	20 mil Carbon/10% Teflon 20 cm^2	40 mA RT	16 ml	.10 mm Zinc Selenide	syringe
SC-71 Anode Limited	5 mil Li 8 cm^2	20 mil 20 cm^2	40 mA RT	15 ml	.10 mm AgCl	syringe
SC-73 Anode Limited	20 mil Li 8 cm^2	20 mil 20 cm^2	40 mA RT	15 ml	.1 mm AgCl	syringe
SC-74 Cathode Limited	40 mil Li 20 cm^2	20 mil 10 cm^2	50 mA RT	15 ml	.1 mm AgCl	syringe
SC-75 w/o Lithium	Nickel Foil 10 cm^2	20 mil 20 cm^2	50 mA RT	15 ml	.05 mm AgCl	syringe
SC-77 Anode Limited	5 mil Li 6.9 cm^2	20 mil 20 cm^2	6.9 mA RT	17 ml	.1 mm AgCl	Peristaltic
SC-79 Anode Limited	5 mil 7.4 cm^2	20 mil 20 cm^2	7.4 mA RT	17 ml	.1 mm AgCl	Perstaltic
SC-81 Anode Limited	5 mil 8.1 cm^2	20 mil 20 cm^2	8.1 mA initially then 40.5 on reversal $-20^{\circ}C$	17 ml	.1 mm AgCl	Peristaltic

* The cathode on nickel exmet is spot welded and pressed against the cell housing wall. The anode is pressed on nickel foil which is spot welded on a stainless stell post at the center. In cell SC-74 the positions of the electrodes are reversed.

Cell SC-69

This cell allows periodic circulation of the electrolyte through a zinc selenide spectroscopic cell without exposing the electrolyte to the environment. The cell was constructed with a 20 mil thick cathode using 90% Shawinigan Black/10%PTFE and a 5 mil thick anode. The cell was discharged at 40 mA (5 mA/cm^2 at the anode and 2 mA/cm^2 at the cathode) until fully discharged. After 6 hours the experiment had to be terminated due to fogging of the zinc selenide windows shortly after the onset of reversal. The total electrolyte volume in the system was 16 ml (1.4 M $LiAlCl_4$ in $SOCl_2$) with approximately 15 ml in the electrochemical cell and 1 ml in the balance of the system which includes the tubing leading to the 0.1mm path length spectroscopic cell. The electrolyte was circulated with a manually operated syringe pump every hour until fully discharged. A three way valve allowed withdrawal of electrolyte from the electrochemical cell into the syringe then reinjection of the electrolyte through the spectroscopic cell and back into the electrochemical cell. Approximately 5 ml of electrolyte were pumped twice before every measurement of the IR absorption spectrum.

The absorption spectra are shown in Figure 28. Initially, the SO_2 and $SOCl_2$ absorption bands are the only noticeable features in the IR absorption spectrum, and throughout the discharge SO_2 increases linearly. Difference spectra (Figure 29) show a fairly low level of activity in the region from 600 to 1100 cm^{-1} which could not be evaluated quantitatively. In Figure 30 we have plotted the SO_2 concentration as a function of time into discharge. We also show on the same figure the discharge curve with a well defined knee after 5 hours (200 mAh). The SO_2 concentration increases linearly and corresponds in this case to approximately 7 Faradays/mole SO_2 produced by the end of discharge.

FIGURE 28

SC-69 Anode Limited - RT
i = 40 mA (5mA/cm2)
Reversal at 5.3 hrs
IR Absorption Spectra

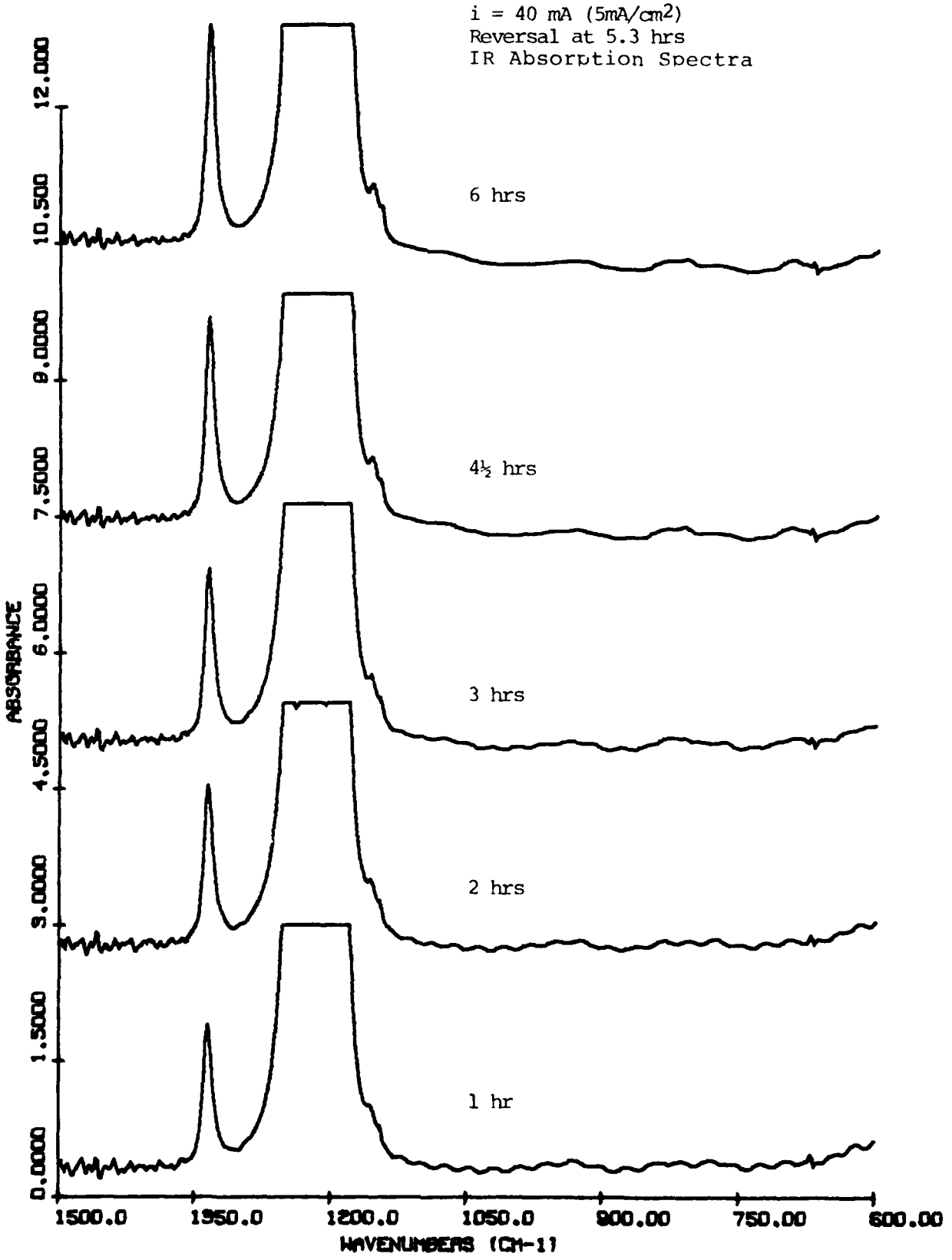

FIGURE 29

SC-69 Anode Limited - RT
Difference Spectra
Reversal at 5.3 hrs
i= 40 mA (5mA/cm^2)

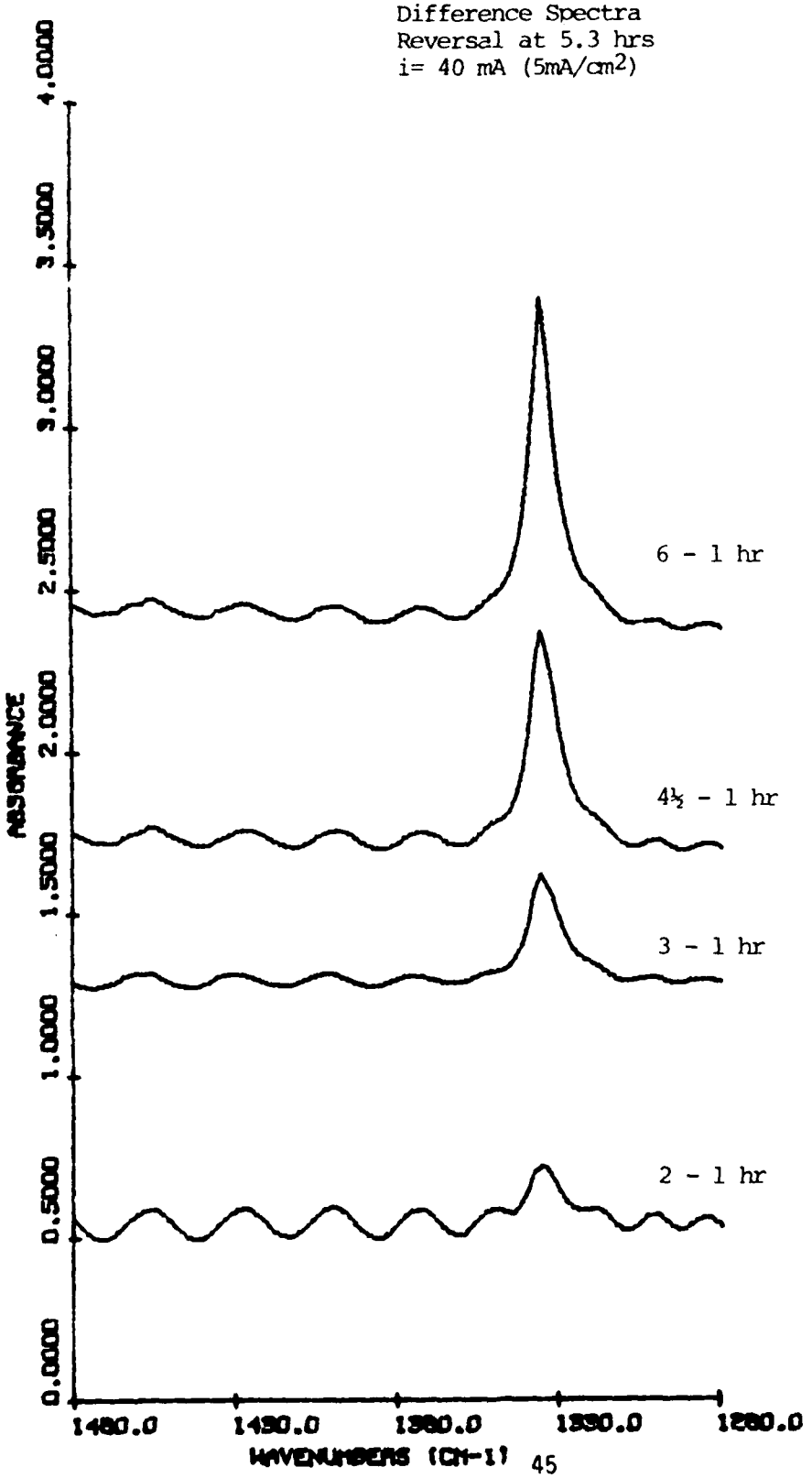

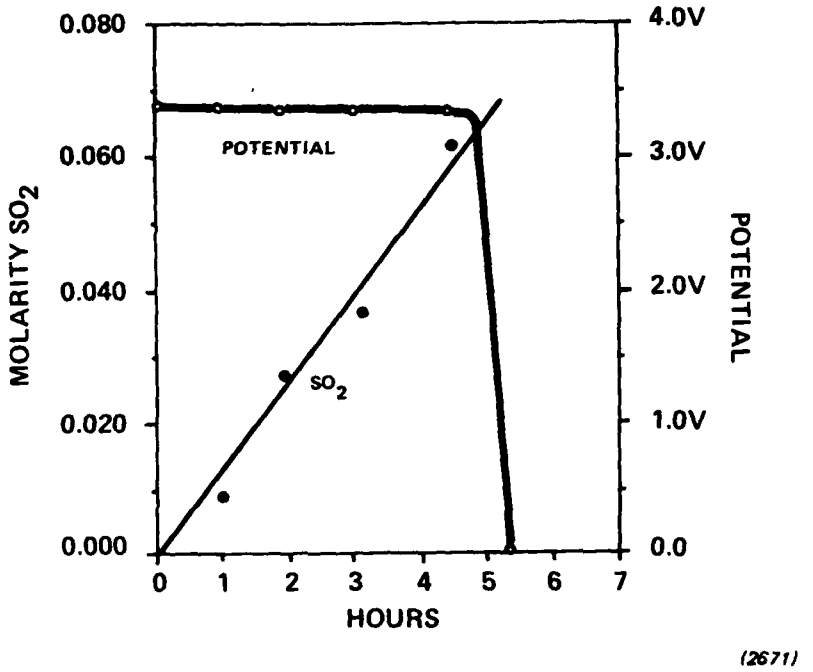

Figure 30 Cell SC-69

SO_2 as a Function of Discharge Anode Limited Cell, i = 40mA(5mA/cm^2)

Cell SC-71

The system is similar to SC-69 except that silver chloride windows were substituted for the zinc selenide windows in the spectroscopic cell. We were able to extract a large amount of information from this cell which discharged in approximately 5 hours at 40 mA before being driven into anode limited reversal for a period of 90 hours. The current was then switched off and the IR absorption spectrum was followed for an additional 50 hours.

The absorption spectra are shown in Figures 31-34.

During discharge the SO_2 concentration increases linearly until the cell is fully discharged then levels off during anode limited reversal (see Figure 35). The results correspond to 6 Faradays per mole of SO_2 produced by the end of discharge. A much slower increase in SO_2 concentration occurs during reversal; we were not able to measure this change after 30 hours due to a steadily growing absorption band at 1115 cm^{-1} which intereferes with the accurate measurement of the SO_2 absorbance at 1144 cm^{-1}. Except for the steady increase in SO_2 concentration, no other change in the absorption spectrum occurs during normal discharge (Figure 36). After the onset of anode limited reversal several significant changes can be noticed, shown in Figures 37-39. The band at 1408 cm^{-1} (SO_2Cl_2) increases steadily, appears to level off after 90 hours in reversal, increases suddenly after the current is switched off then levels off to a steady value 40 hours later (Figure 40).

The absorption band at 1115 cm^{-1} ($SOCl^+$) exhibits an interesting behavior. After the onset of reversal the intensity increases then reaches a steady state value after 40 hours. When the current is turned off the intensity of the absorption decreases to zero in less than 12 hours (see Figure 41).

The 1070 cm^{-1} infrared absorption is poorly resolved even after spectral subtraction, but its presence is quite evident after the current is turned

off. No activity occurs before reversal. After the onset of reversal an increase in the absorption at 1070 cm^{-1} is apparent. This absorption levels off after 25 hours and remains at a steady value after the current is turned off, pointing to a relatively stable product (see Figure 42).

A definite increase in the absorption at 665 cm^{-1} is noticeable after the onset of reversal. This increase continues even after the current has been switched off but appears to approach a steady value (see Figure 43). Again the specie responsible for this absorption is obviously stable in the cell environment; its assignment as Cl_2O or S_2O is in doubt, however, in view of the fact that previous workers overlooked the interaction of water with the electrolyte giving rise to a strong absorption at 694 cm^{-1}.

The complete discharge curve is shown in Figure 44. An important point to be considered is the fact that 5.6 Amp-hour of charge passed through the cell corresponding to approximately 0.2 Faraday. However, the volume of electrolyte did not change by more than 10% during the experiment, indicating recombination of species to form $SOCl_2$ which is then available for further reduction and oxidation.

FIGURE 31

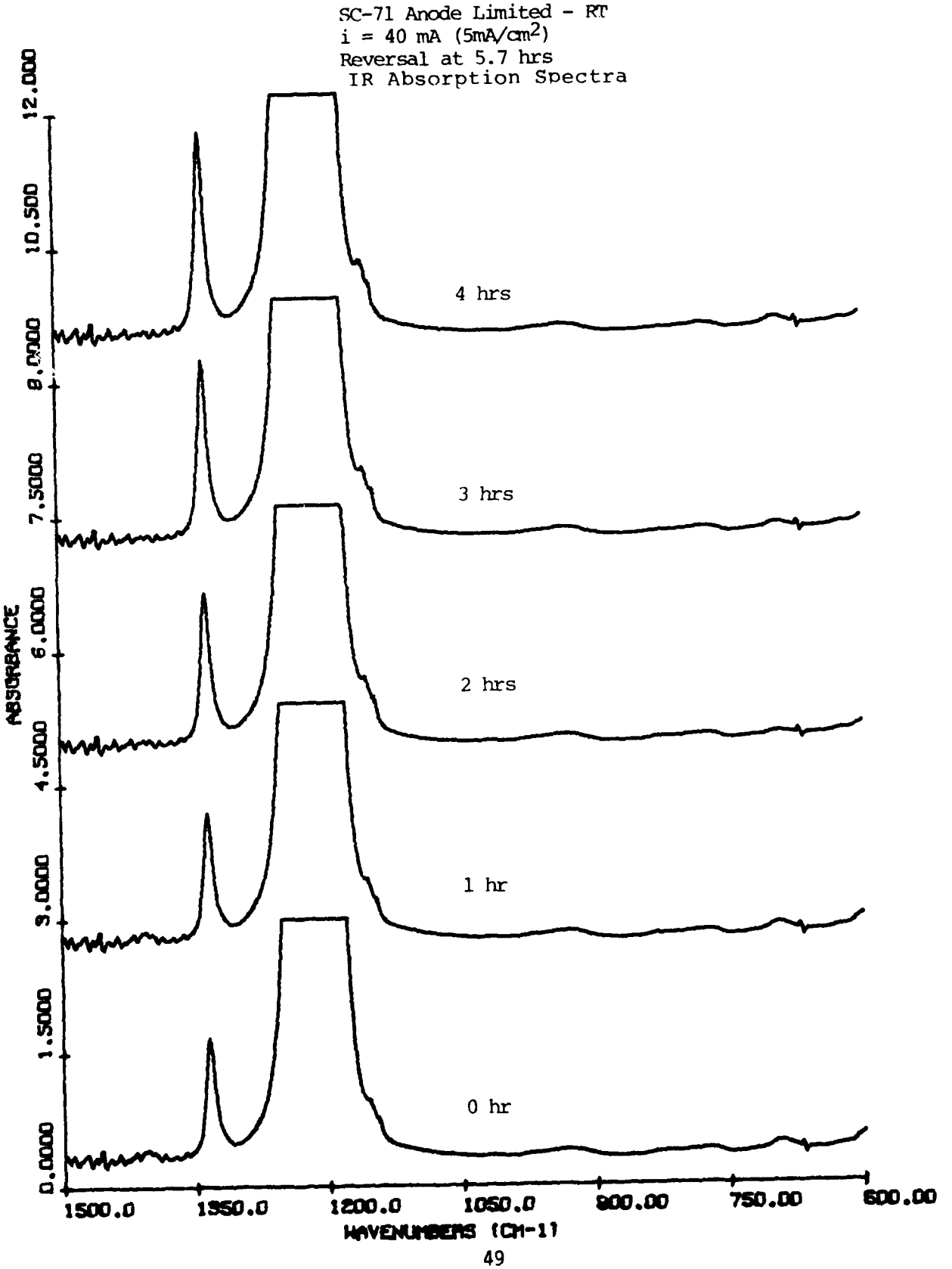
SC-71 Anode Limited - RT
i = 40 mA (5mA/cm2)
Reversal at 5.7 hrs
IR Absorption Spectra
4 hrs
3 hrs
2 hrs
1 hr
0 hr
ABSORBANCE
12.000
10.500
9.0000
7.5000
6.0000
4.5000
3.0000
1.5000
0.0000
1500.0
1350.0
1200.0
1050.0
900.00
750.00
600.00
WAVENUMBERS (CM-1)

FIGURE 32

SC-71 Anode Limited - RT
i = 40 mA (5mA/cm^2)
Reversal at 5.7 hrs
IR Absorption Spectra

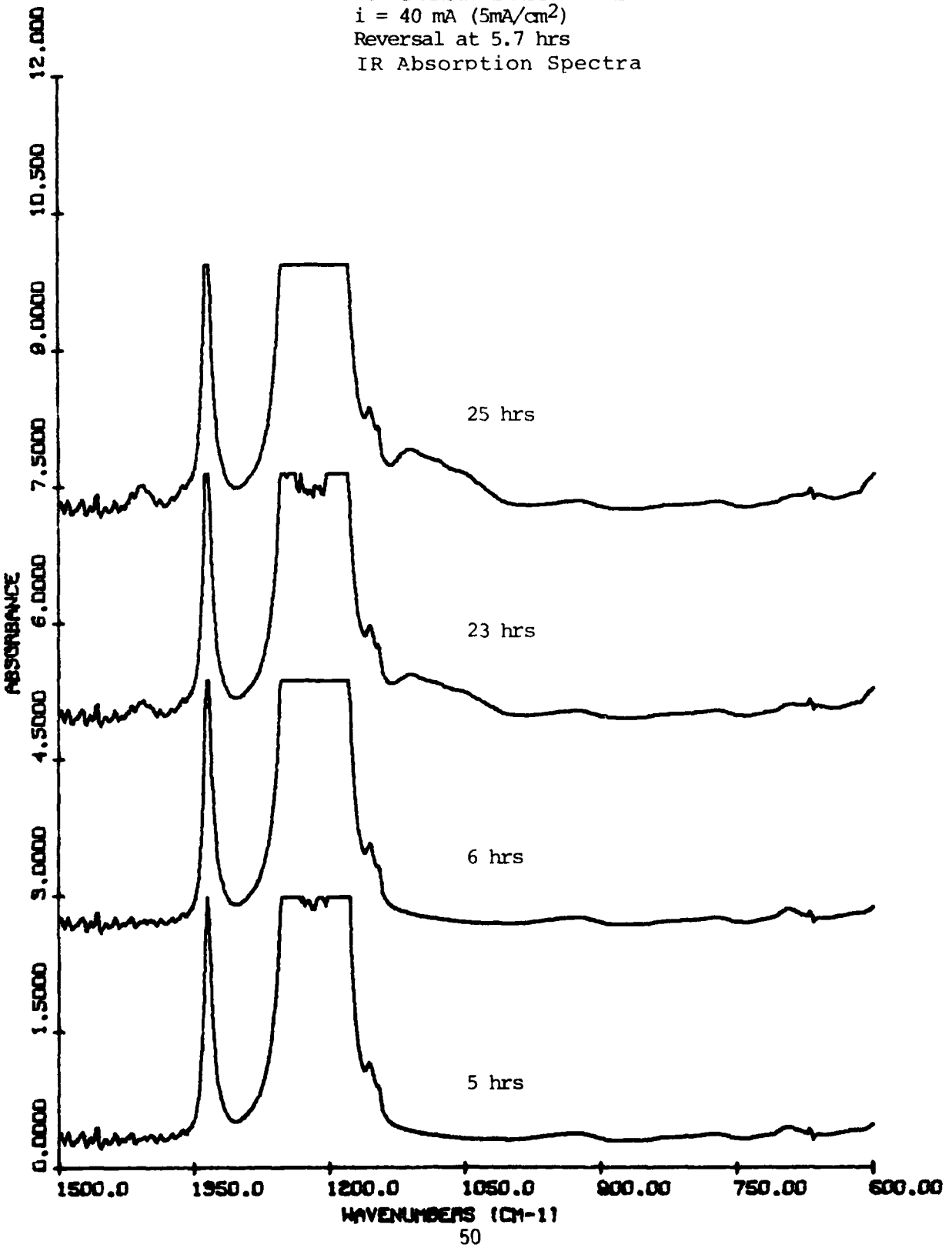

FIGURE 33

SC-71 Anode Limited - RT
i= 40 mA (5mA/cm^2)
Reversal at 5.7 hrs
IR Absorption Spectra

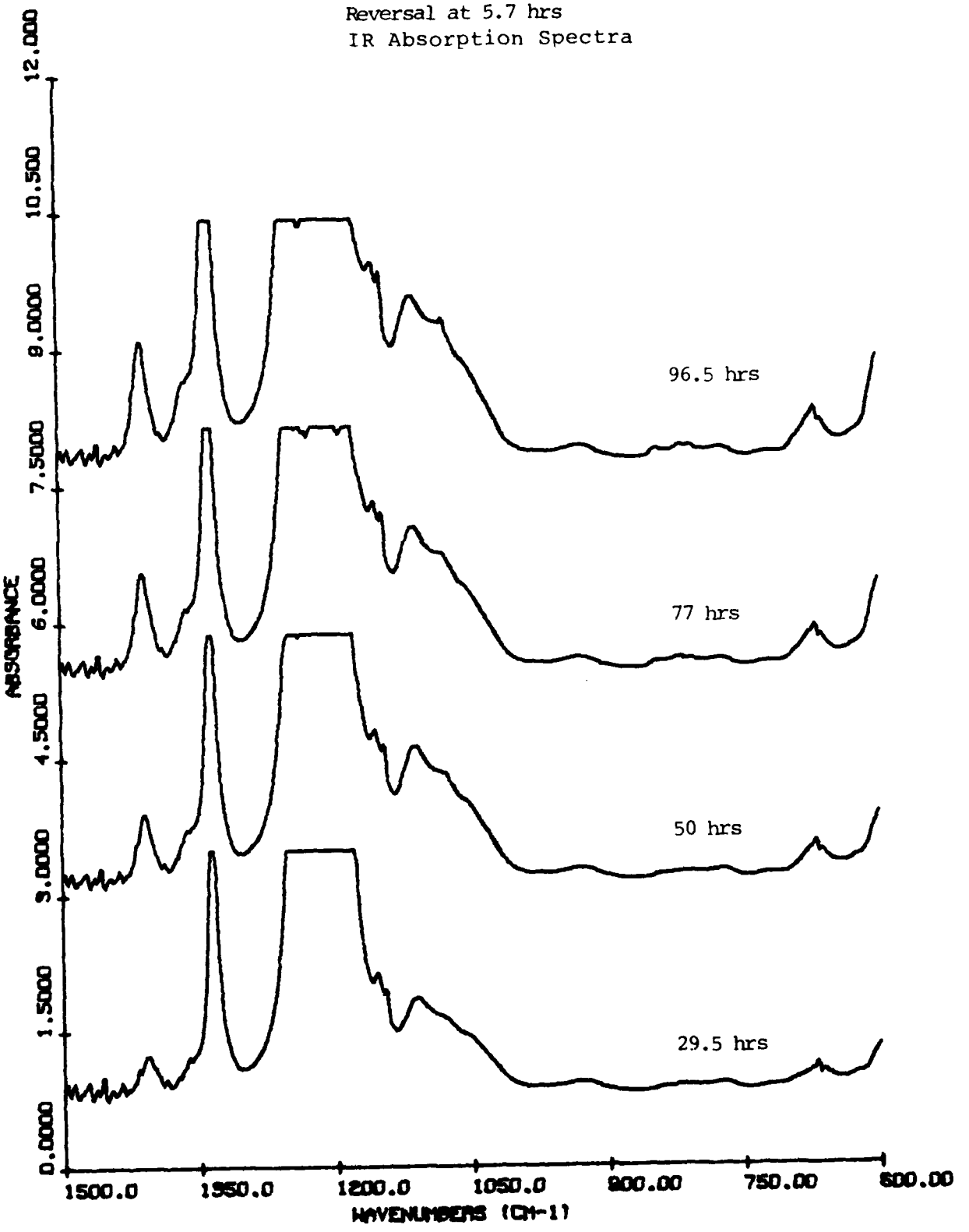

FIGURE 34

SC-71 in Storage after Reversal
i = 0
RT

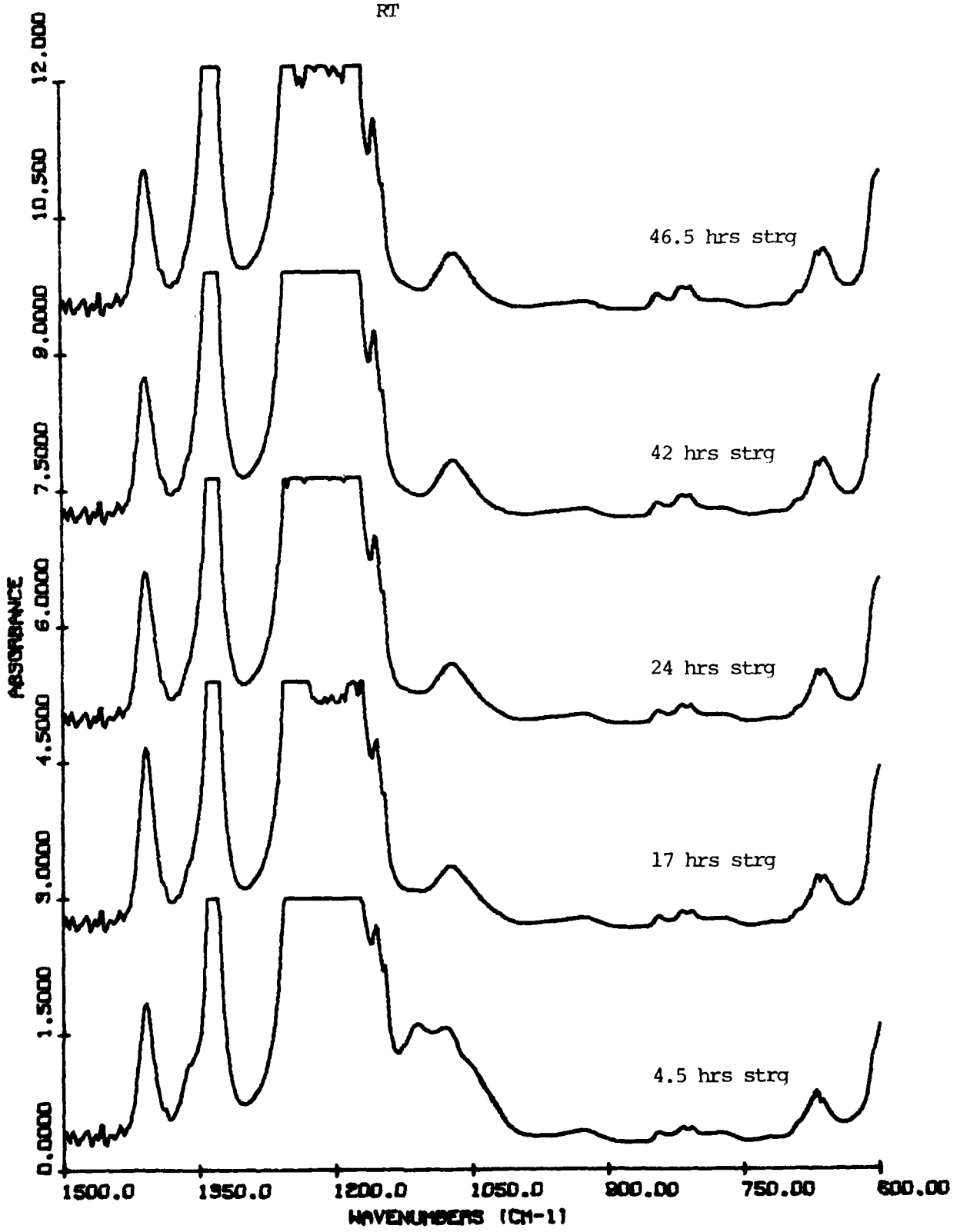

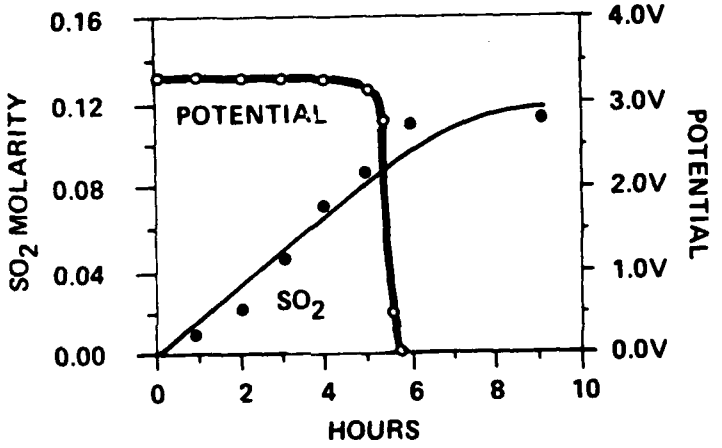

Figure 35 Cell SC-71

SO_2 as a Function of Discharge

Anode Limited Cell, i = 40mA (5mA/cm^2)

FIGURE 36

SC-71 Anode Limited - RT
i = 40 mA ($5mA/cm^2$)
Difference Spectra for SO_2
Reversal at 5.7 hrs

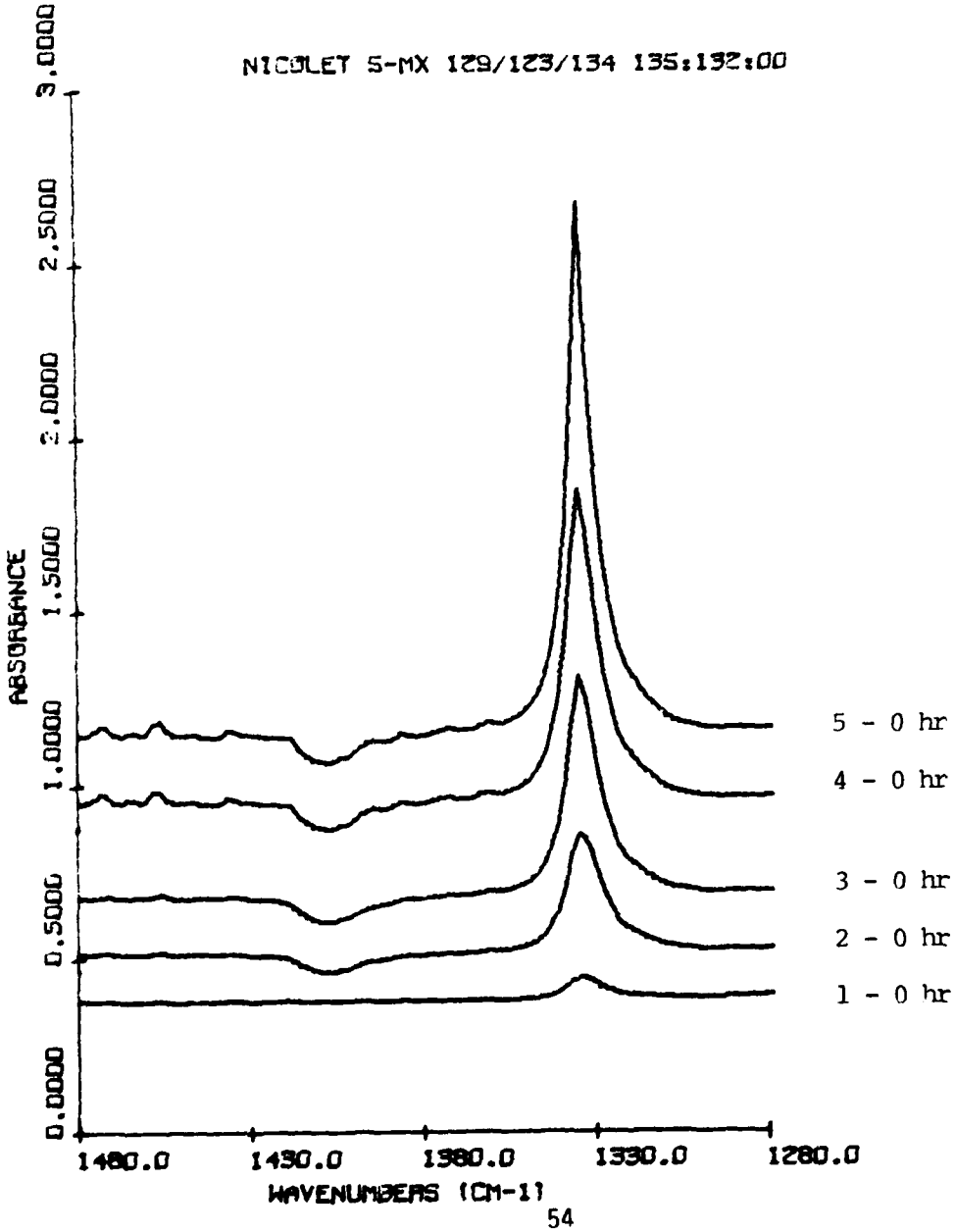

FIGURE 37

SC-71 Anode Limited - RT
Difference Spectra for SO_2Cl_2
Reversal at 5.7 hrs

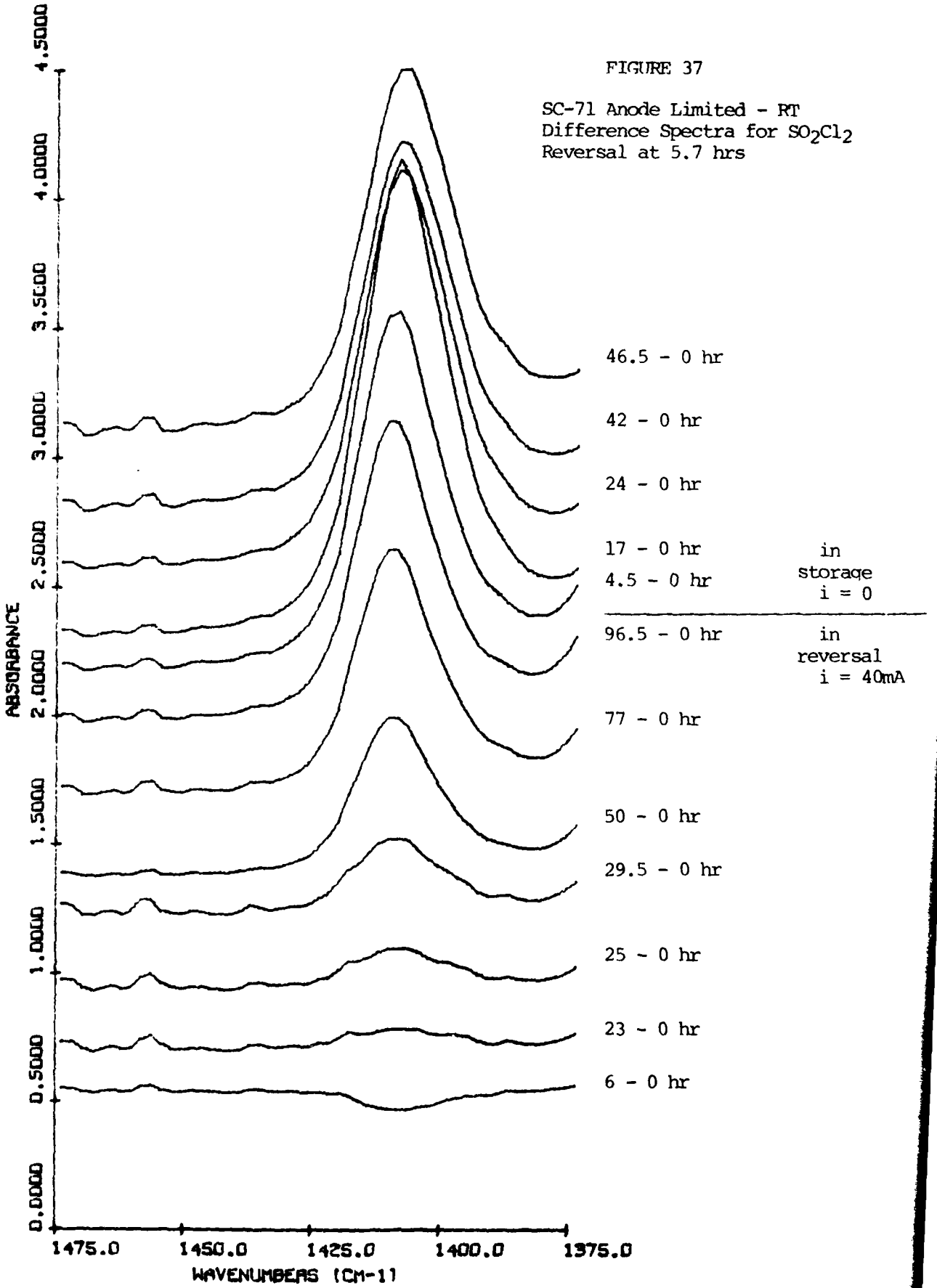

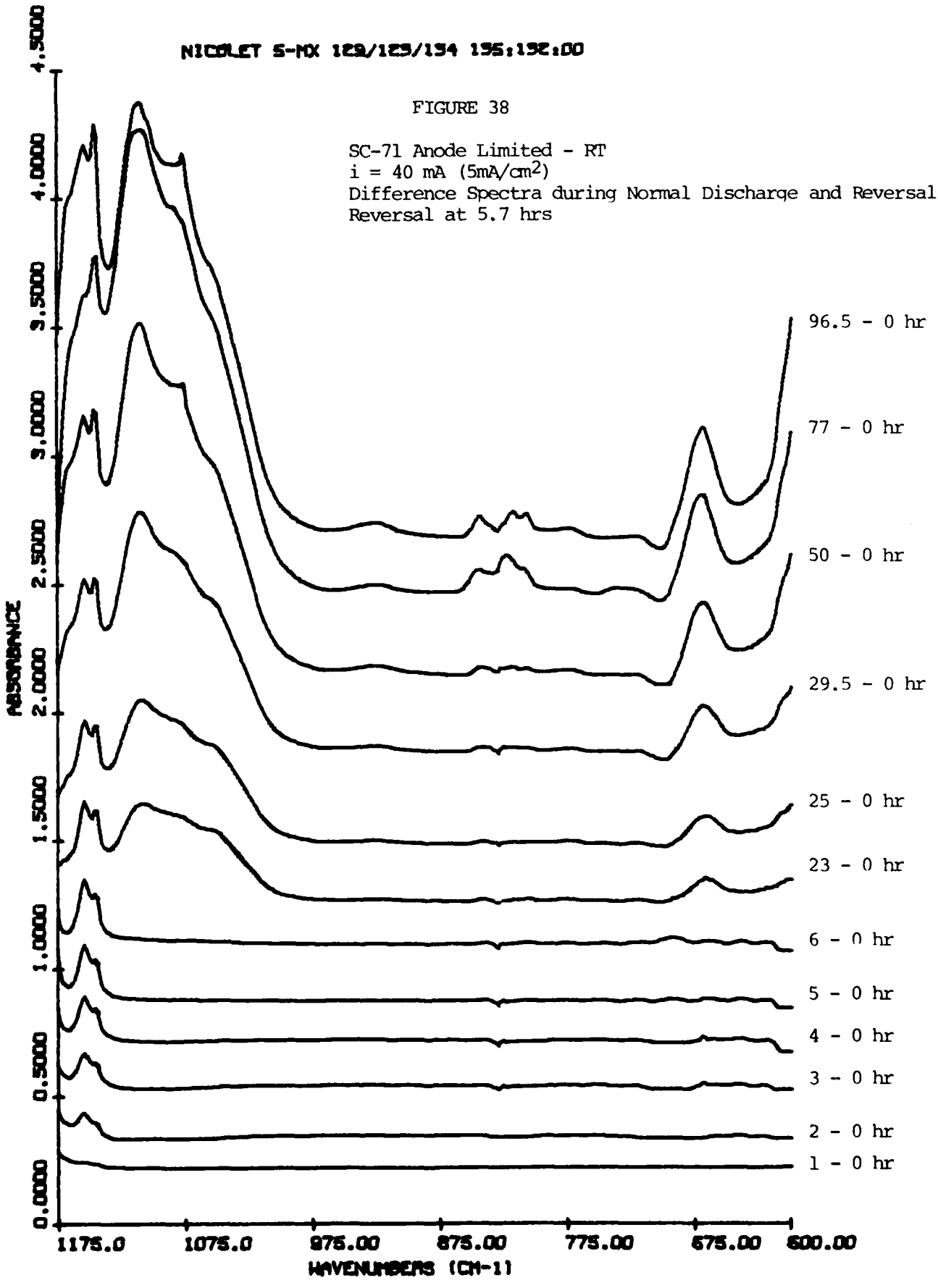

FIGURE 38

SC-71 Anode Limited - RT
i = 40 mA (5mA/cm^2)
Difference Spectra during Normal Discharge and Reversal
Reversal at 5.7 hrs

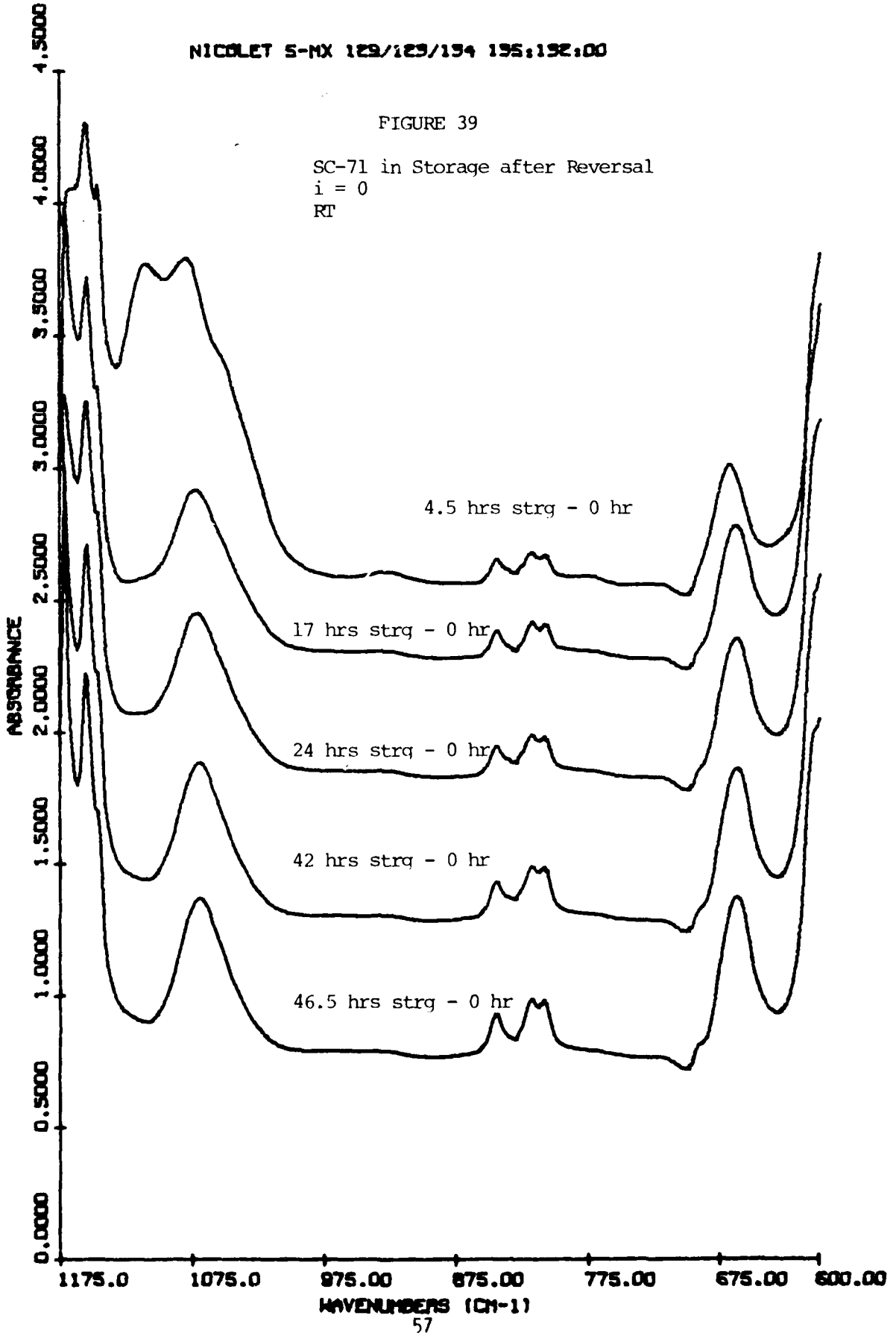

FIGURE 39

SC-71 in Storage after Reversal
i = 0
RT

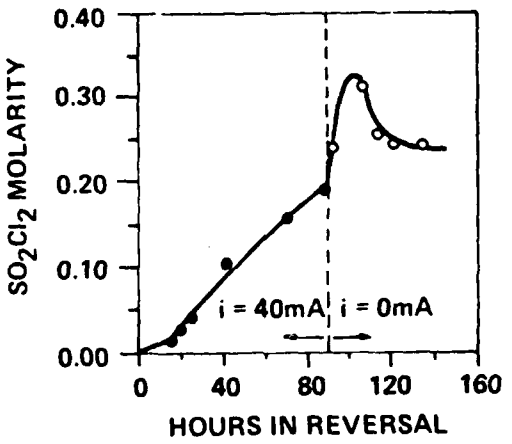

(2322)

Figure 40 Cell SC-71
SO_2Cl_2 Formation during Reversal
Anode Limited Cell, i = 40mA (5mA/cm^2)

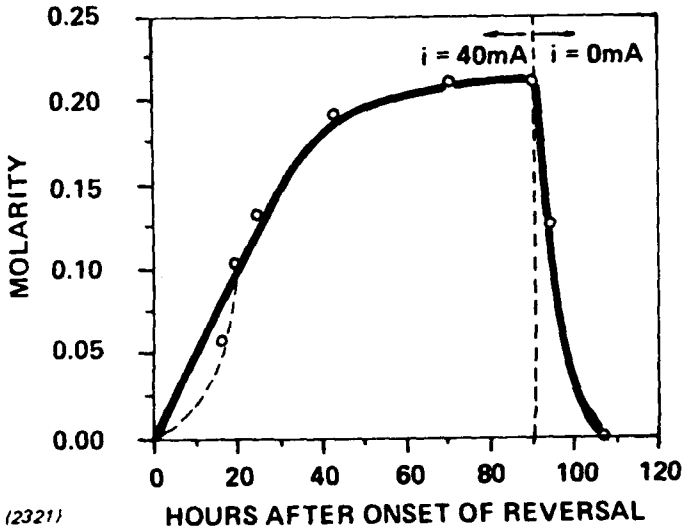

Figure 41 Cell SC-71
$SOCl^+$ Formation during Reversal
Anode Limited Cell, i = 4um A (5mA/cm^2)

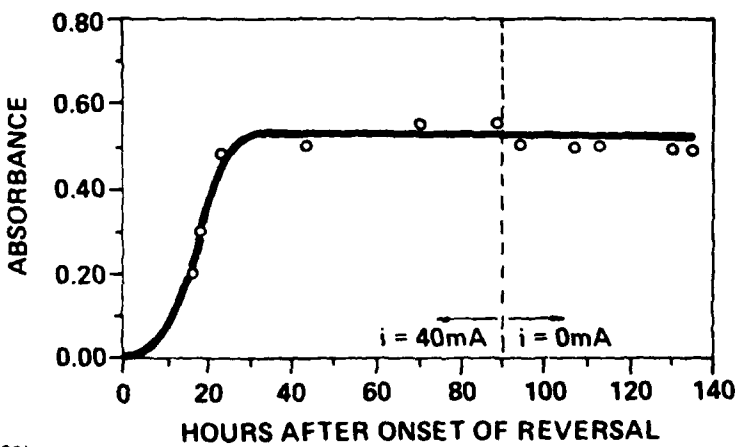

Figure 42 Cell SC-71
Intensity of Infrared Absorption at 1070cm^{-1}
Anode Limited Cell, i = 40mA (5mA/cm^2)

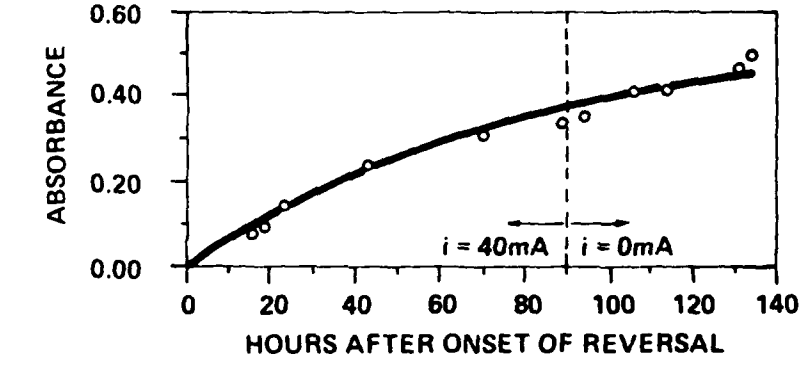

Figure 43 Cell SC-71
Intensity of Infrared Absorption at 665cm^{-1}
Anode Limited Cell, i = 40mA (5mA/cm^2)

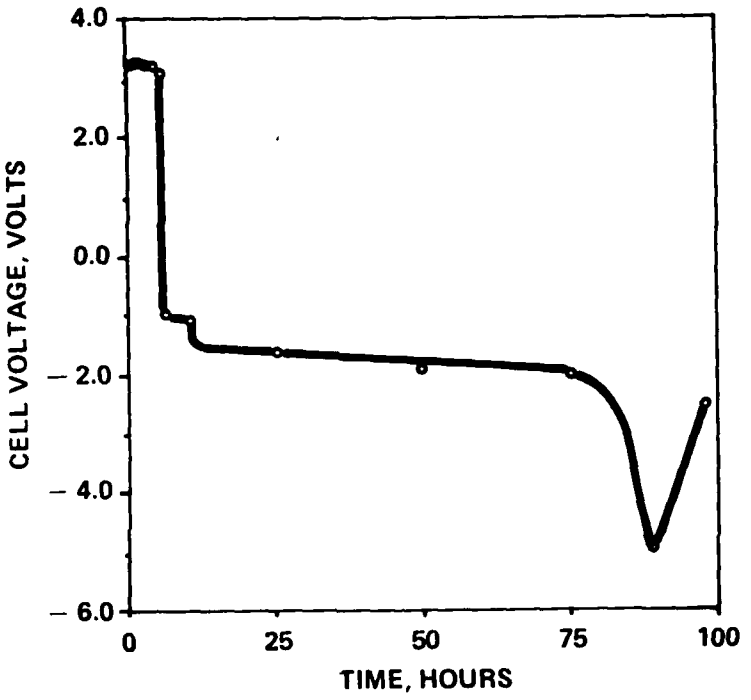

Figure 44 Discharge Curve – Cell SC-71
i = 40mA (5mA/cm^2)
Anode Limited

Cell SC-73

Cell SC-73 is similar to SC-71 except for a greater thickness of lithium at the anode: 20 mils instead of 5 mils. The cell discharged for 22 hours before anode limited reversal. Its behavior parallels that of Cell SC-71 except that a higher rate of SO_2 generation was observed; this may be an artifact due to moisture pickup in the system. Otherwise the trends are the same (Figures 45-46). The SO_2 concentration increases linearly during normal discharge then at a much reduced rate after anode limited reversal (see Figure 47). Sulfuryl chloride increases only after the onset of reversal (see Figure 48). The absorptions at 1070 cm^{-1} and 1115 cm^{-1} show trends similar to SC-71 clearly noticeable in Figure 49. A significant difference, however, is evident in the increased absorption at 694 cm^{-1} during discharge (water pickup). At the end of discharge the 694 absorption band decreases in intensity and another band at 665 cm^{-1} increases until a steady value is obtained (see Figure 50). The test was discontinued after 94 hours of discharge. A complete discharge curve is shown in Figure 51.

FIGURE 45

SC-73 Anode Limited - RT
i = 40 mA (5mA/cm^2)
Reversal at 22 hrs
IR Absorption Spectra

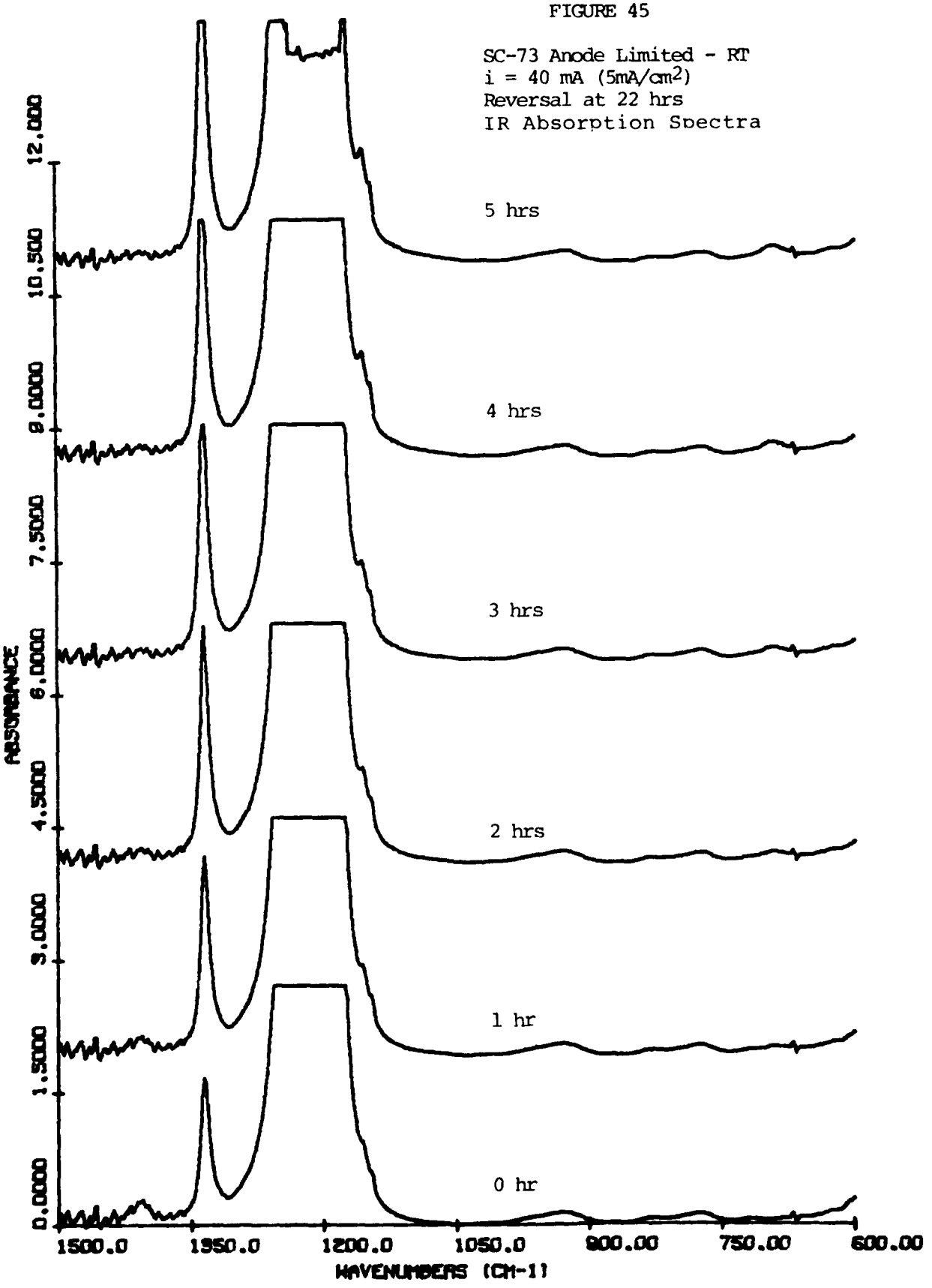

FIGURE 46

SC-73 Anode Limited - RT
i = 40 mA (5mA/cm^2)
Reversal at 22 hrs
IR Absorption Spectra

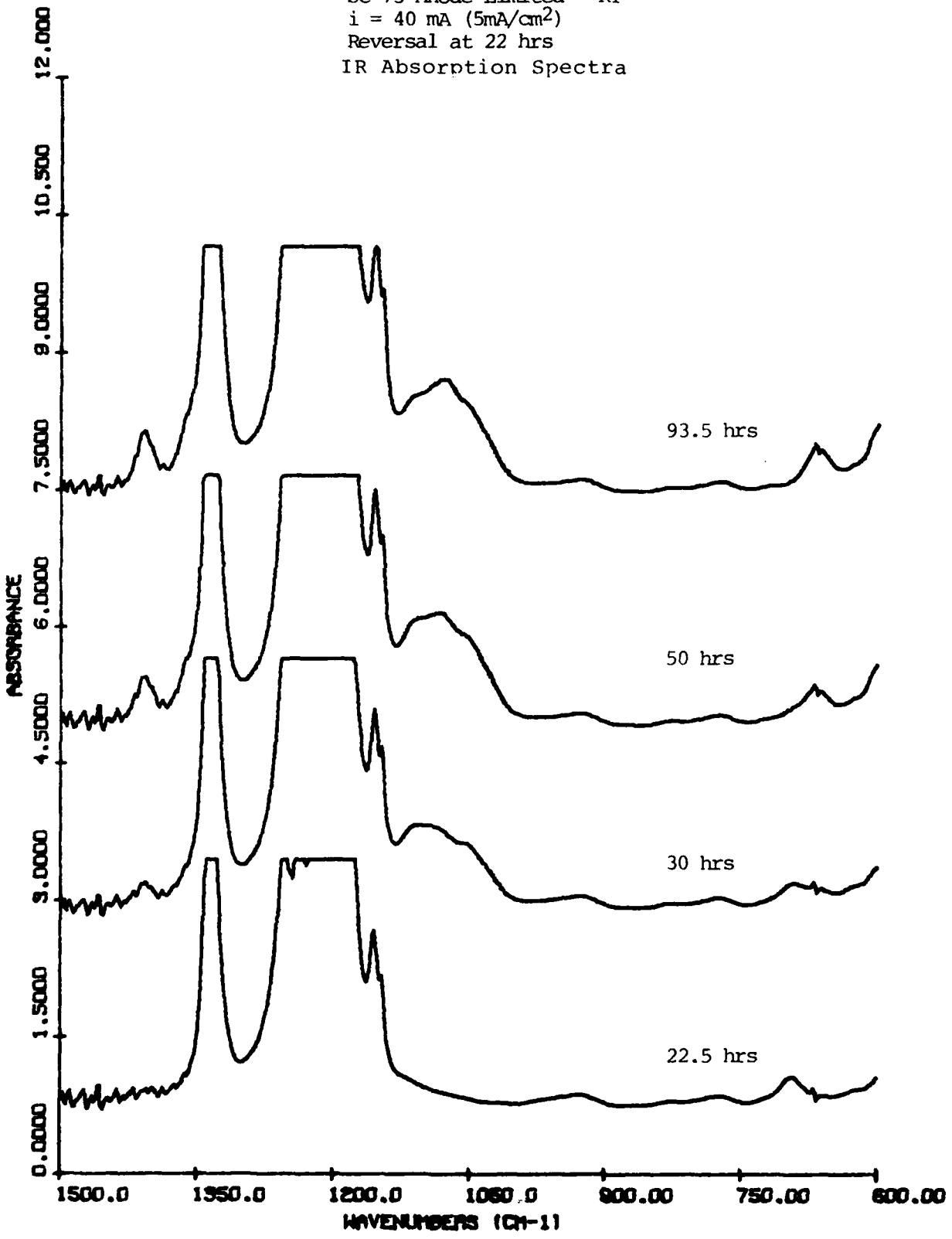

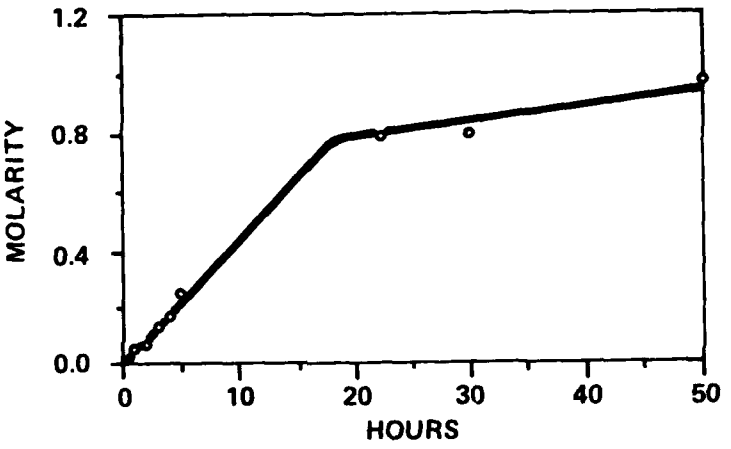

(2673)

Figure 47 Cell SC-73

SO_2 As a Function of Discharge Anode Limited Cell, i = 40mA(5mA/cm^2)

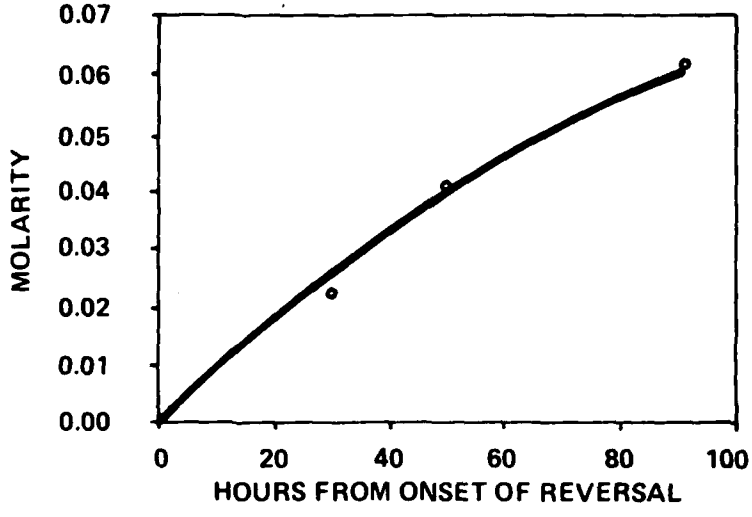

(2674)

Figure 48 Cell SC-73

SO_2Cl_2 as a Function of Discharge Anode Limited Cell, i = 40mA (5mA/cm^2)

FIGURE 49

SC-73 Anode Limited - RT
i = 40 mA (5mA/cm^2)
Difference Spectra during Normal Discharge and Reversal
Reversal at 22 hrs

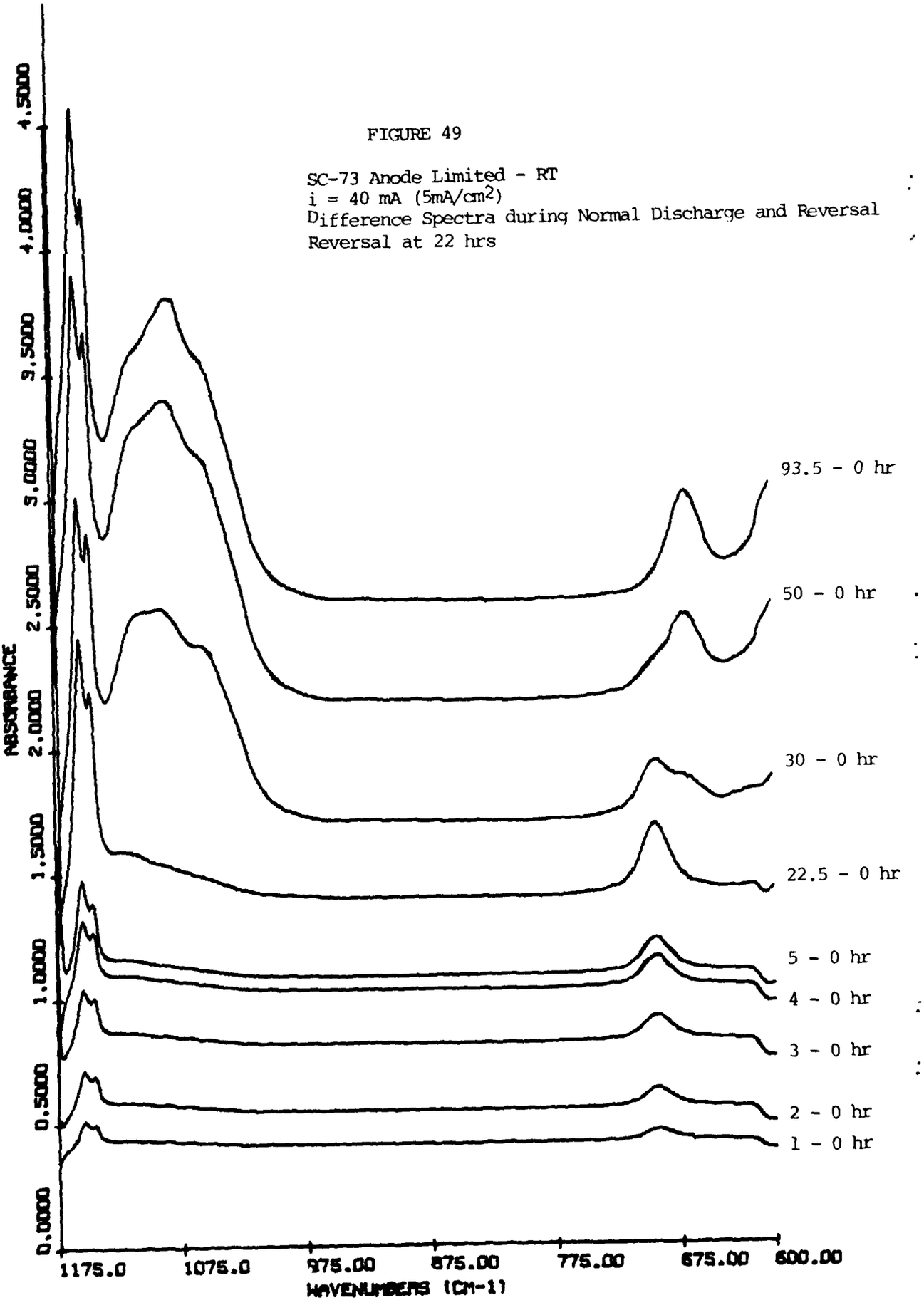

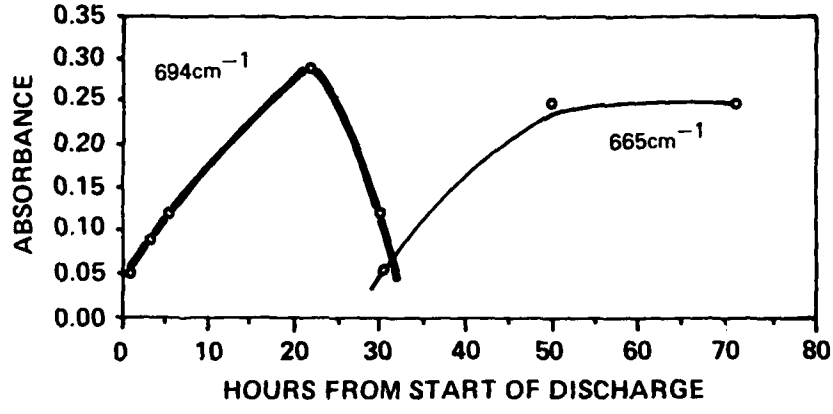

(2675)

Figure 50 Cell SC-73
Relative Intensities of Bands at 694cm^{-1} and 665cm^{-1}
Anode Limited Cell, i = 40mA (5mA/cm^2)

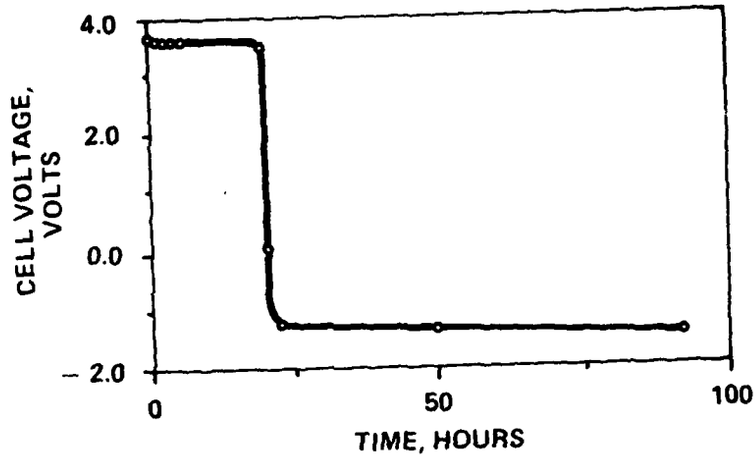

Figure 51 Discharge Curve — Cell SC-73
i = 40mA (5mA/cm^2)
Anode Limited

Cell SC-74

In this cell we reversed the positions of the anode and cathode and increased the lithium thickness to 40 mils to ensure a cathode limited condition. The cell was discharged at 50 mA for about 6 hours before cathode limited reversal occurred. The cell was then driven for an additional 66 hours at 50 mA. Spectra obtained during normal discharge are shown in Figure 52, those during reversal in Figure 53.

The main difference in the spectrum from that of anode limited cells is the absence of a sulfuryl chloride peak at 1408 cm^{-1} and of a peak at 1115 cm^{-1} (Figure 54). During normal discharge a slight increase in absorption at 694 cm^{-1} appears to occur, indicating moisture pick up; this increase levels off during reversal (see Figure 55). During reversal slight increases are observed at 803 cm^{-1}, 980 cm^{-1} and 1070 cm^{-1} (see Figures 56a, b and c). Formation of a slight absorption at 1070 cm^{-1} indicates that SCl_2 is formed in small quantities during cathode limited reversal. The discharge curve is shown in Figure 57.

FIGURE 52

SC-74 Cathode Limited - RT
i = 50 mA (5mA/cm^2)
Reversal at 5.6 hrs

IR Absorption Spectra

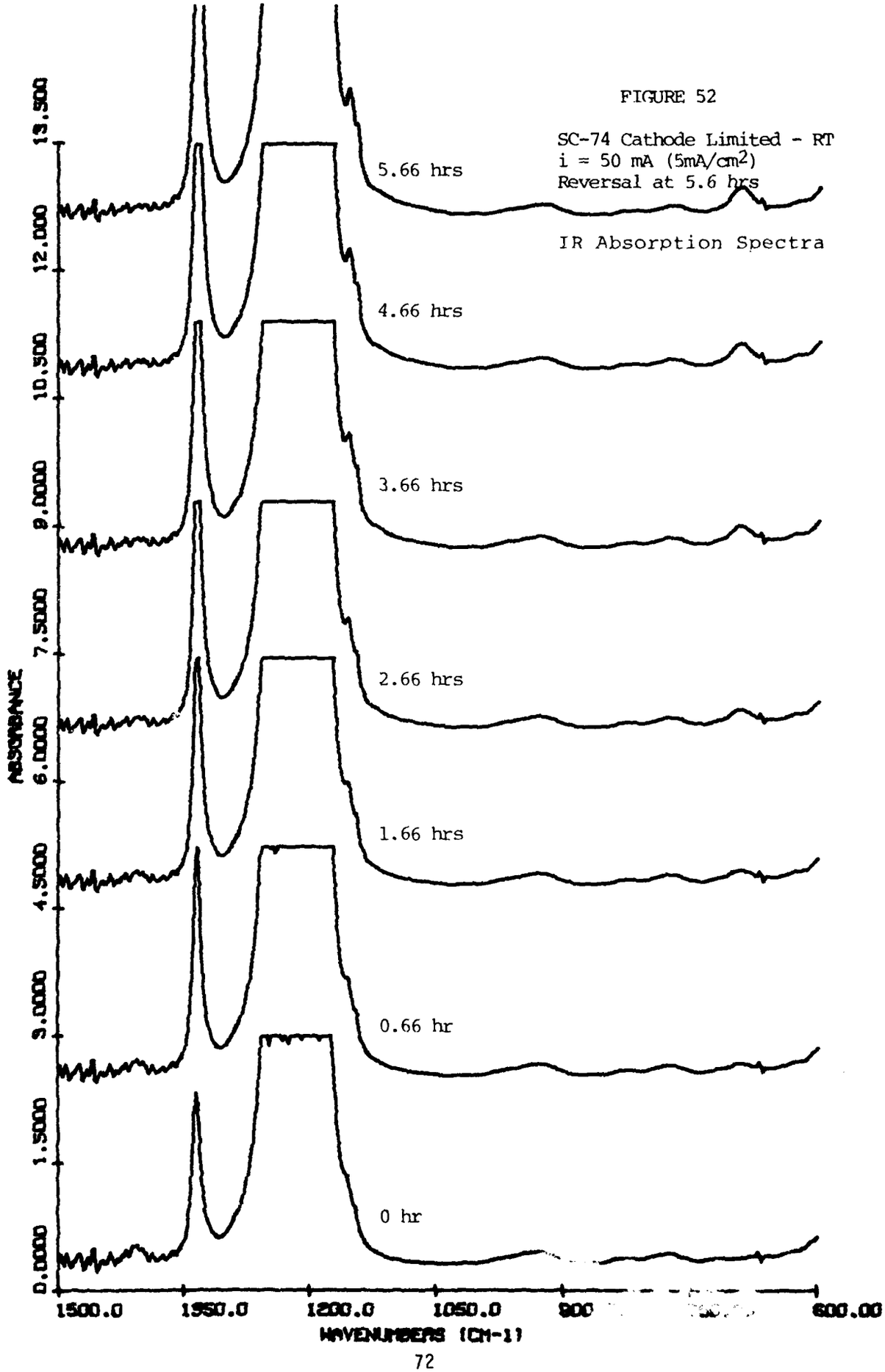

FIGURE 53

SC-74 Cathode Limited - RT
i = 50 mA (5mA/cm^2)
Reversal at 5.6 hrs
IR Absorption Spectra

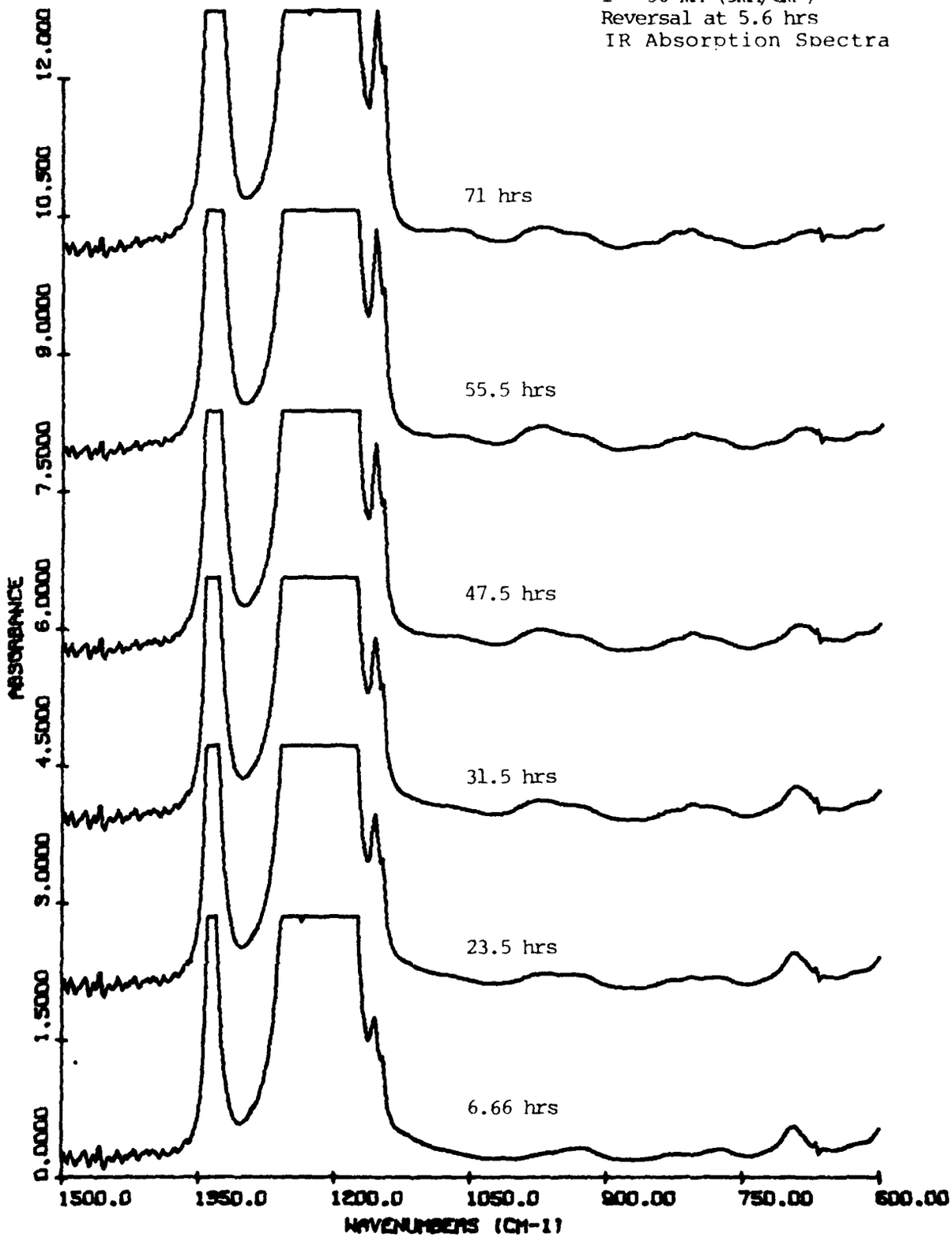

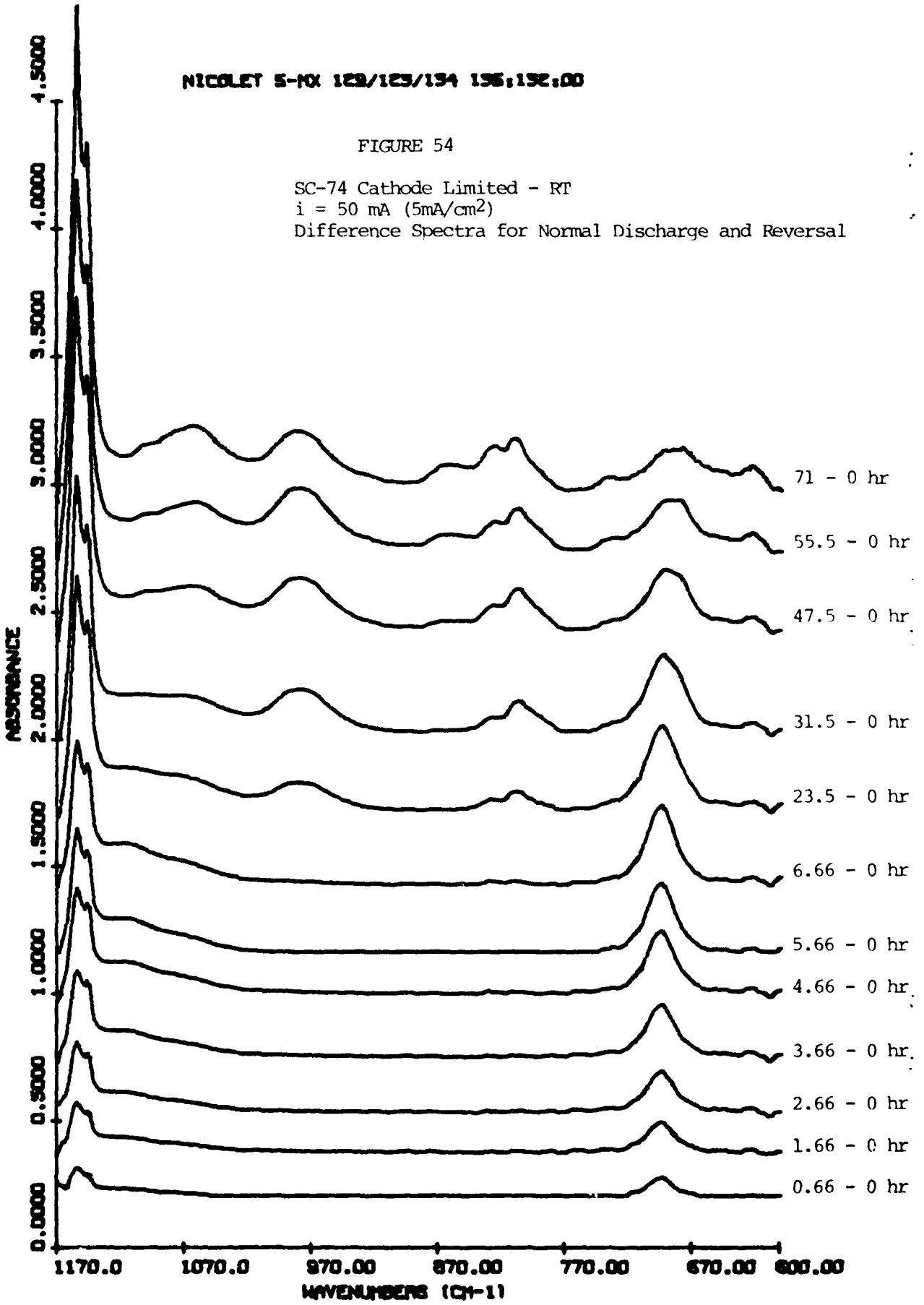

FIGURE 54

SC-74 Cathode Limited - RT
i = 50 mA (5mA/cm^2)
Difference Spectra for Normal Discharge and Reversal

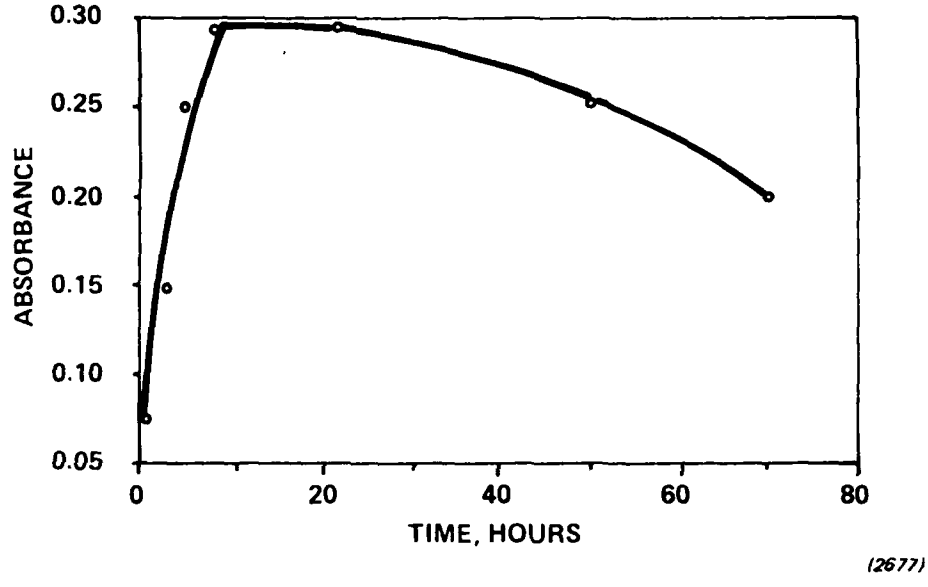

Figure 55 Cell SC-74
Cathode Limited Cell, 50mA
Intensity of 694cm^{-1} Band

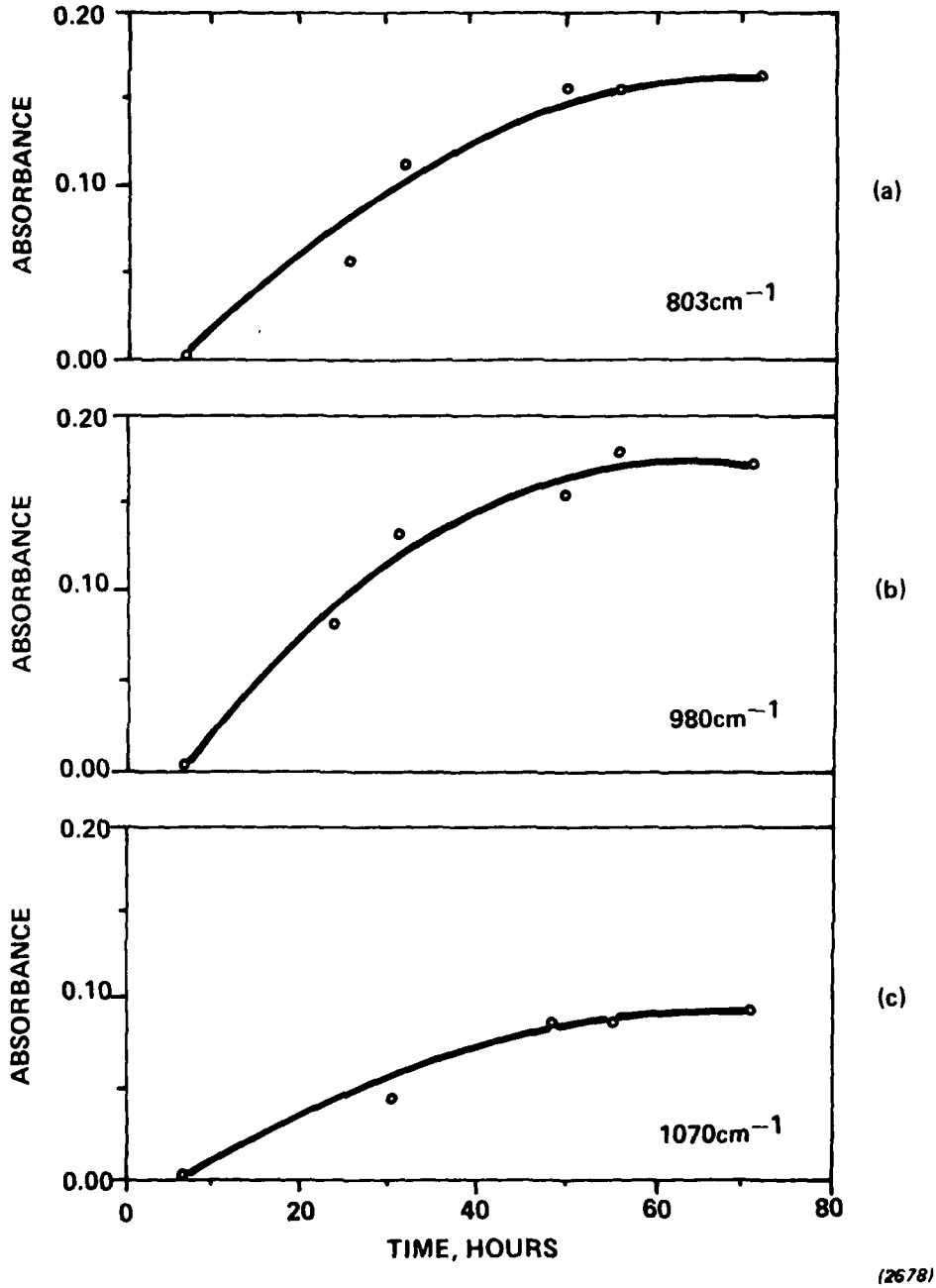

Figure 56 Cell SC-74
Intensity of Absorptions at (a) 803, (b) 980, and (c) 1070 cm^{-1}

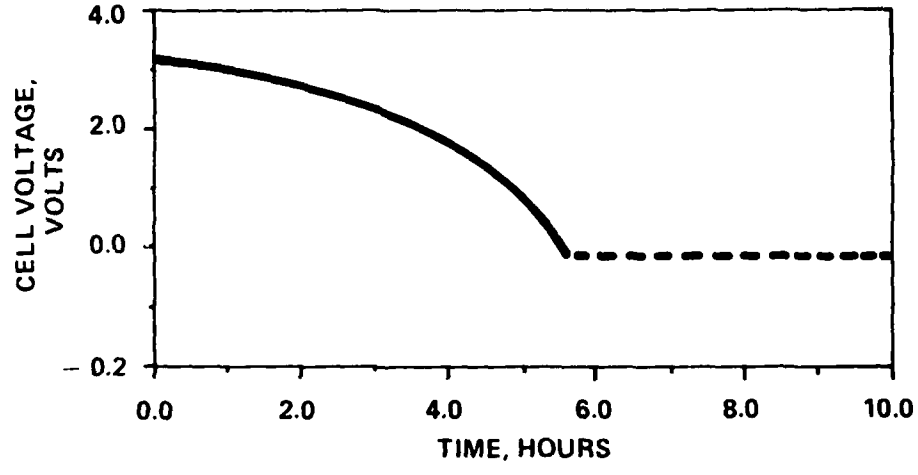

Figure 57 Discharge Curve – Cell SC-74
i = 50mA (5mA/cm^2)
Cathode Limited

Cell SC-75

IR absorption spectra for this run are shown in Figure 58. This particular cell is similar to SC-71 except that no lithium was added to the cell and the path length for the IR spectroscopic cell is only 0.05mm instead of 0.1mm. The cell was driven at 50 mA. We wanted to verify with this experiment the reduced rate of SO_2 formation observed in our previous cells after the onset of reversal. This was confirmed (see Figures 59a and 60). The average rate of formation of SO_2 was about 3 to 4 times less than during normal discharge. In addition we tracked the formation of SO_2Cl_2 (Figures 59b and 60) and observed a very sharp increase at 1115 cm^{-1} (Figure 61). Very slight increases in absorptions at 665 cm^{-1} and 1070 cm^{-1} are also noticeable.

The electrolysis curve for this cell is shown in Figure 62.

FIGURE 58

SC-75 Electrolysis Cell - RT
without Lithium
i = 50 mA (5mA/cm^2)
IR Absorption Spectra

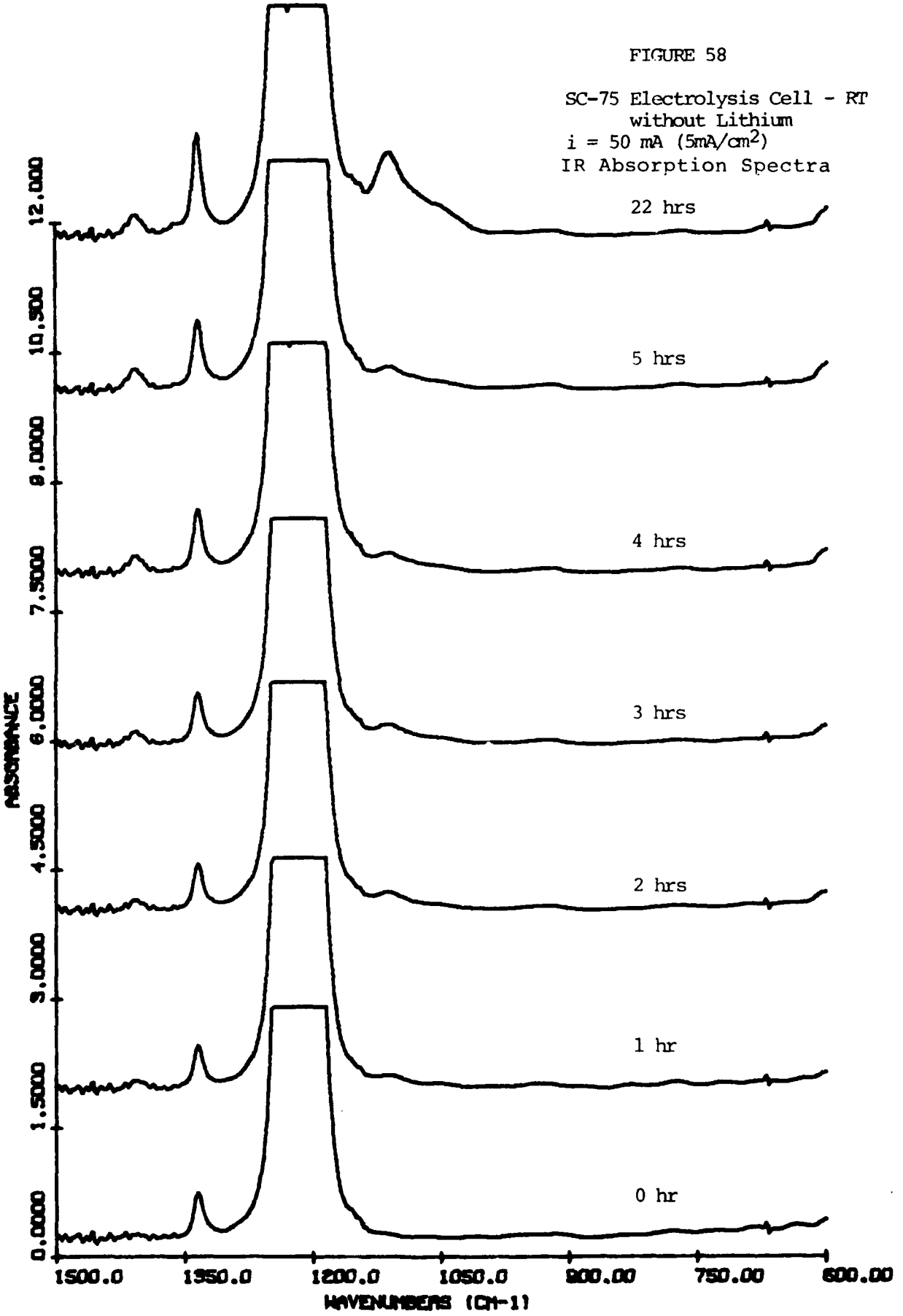

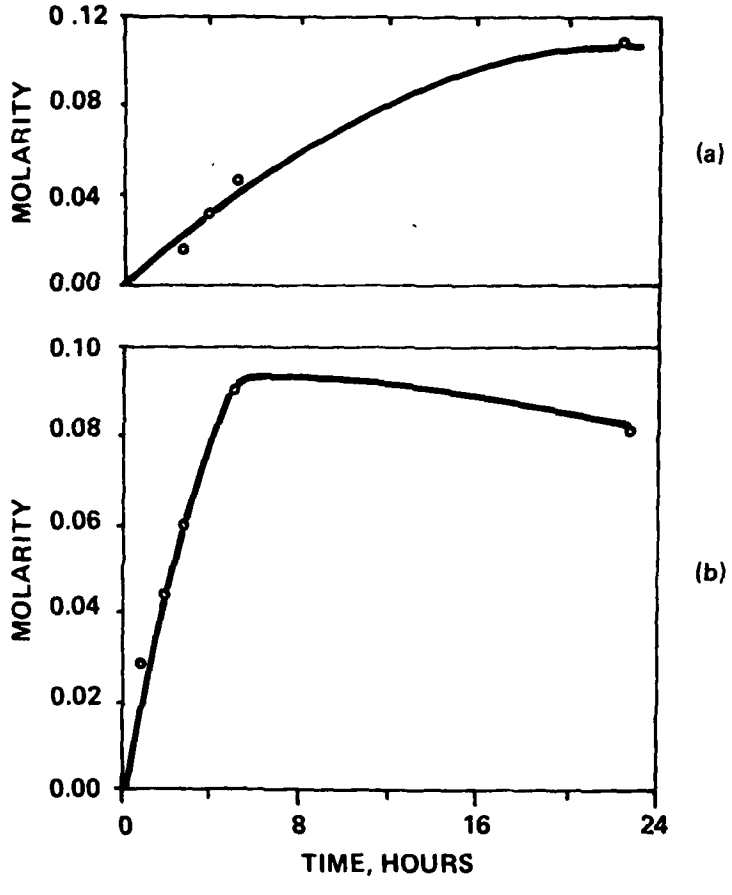

Figure 59 Cell SC-75

(a) SO_2 Formation upon Electrolysis, 50mA

(b) SO_2Cl_2 Formation upon Electrolysis, 50mA

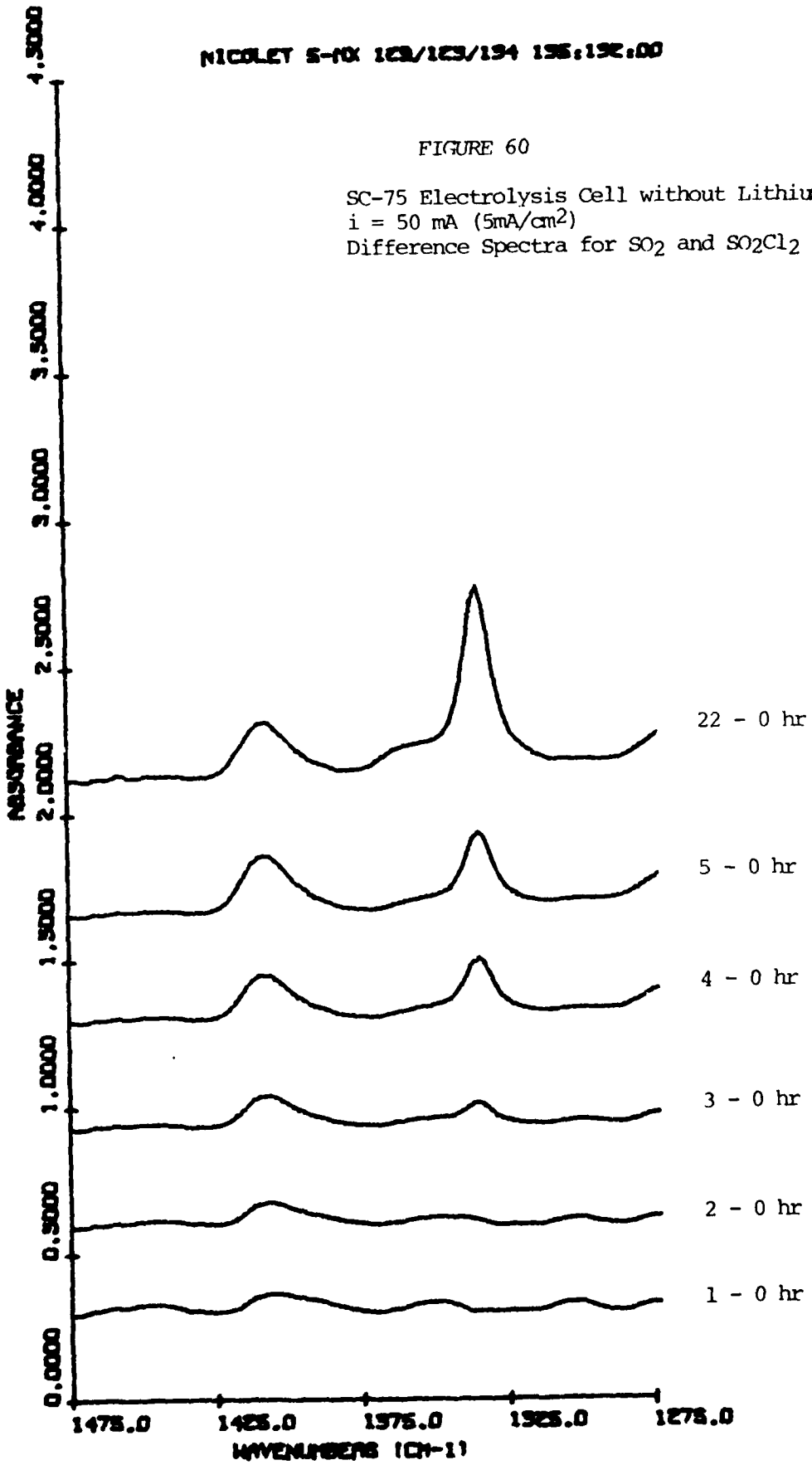

FIGURE 60

SC-75 Electrolysis Cell without Lithium - RT
i = 50 mA ($5mA/cm^2$)
Difference Spectra for SO_2 and SO_2Cl_2

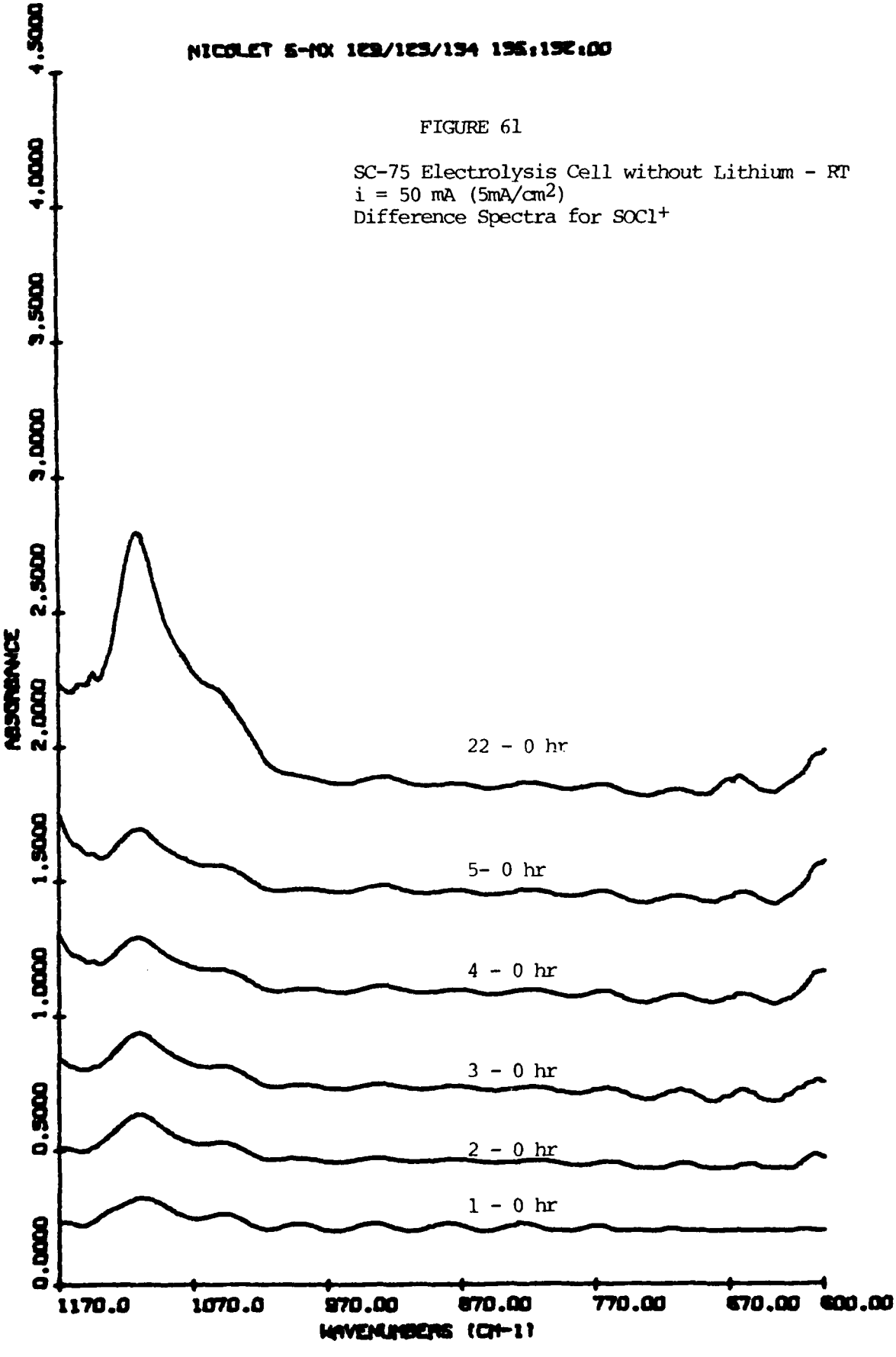

FIGURE 61

SC-75 Electrolysis Cell without Lithium - RT
i = 50 mA (5mA/cm^2)
Difference Spectra for $SOCl^+$

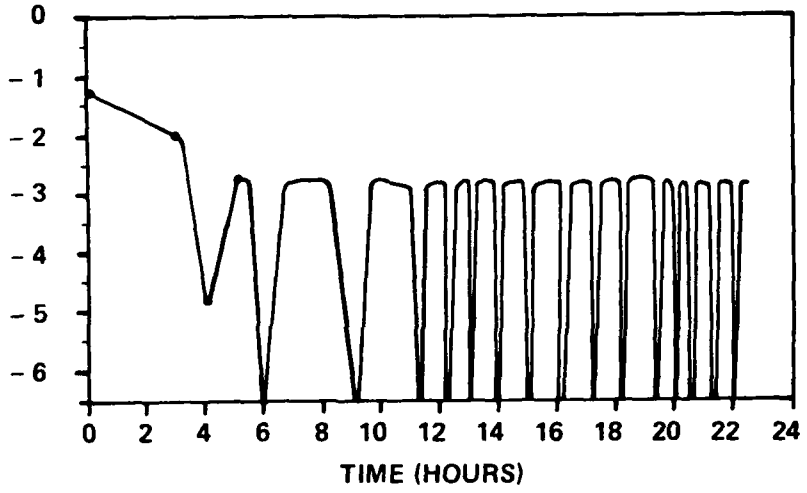

Figure 62 Electrolysis Curve - Cell SC-75 Total Current 50mA(5mA/cm^2)

Cell SC-77

Evolution of the IR absorption spectrum during normal discharge and anode limited reversal is shown in Figures 63 and 64. In this particular case we used a peristaltic pump to circulate the electrolyte around and simplify the sampling. We discharged the cell at 6.9 mA (1 mA/cm^2 at the anode) for 23 hours before reversal and continued at the same rate for an additional 25 hours. The behavior of this cell is reflected in the difference spectra shown in Figures 65 and 66.

The trends are the same as with the higher current cells except for the reduced rate of SO_2 and $SOCl^+$ formation (see Figures 67a and 67b). It is interesting to note that SO_2Cl_2 barely begins to form at this current after 24 hours into reversal. The rate of SO_2 production during discharge corresponds to about 6.0 Faradays/mole of SO_2. The discharge curve is shown in Figure 68.

FIGURE 63

SC-77 Anode Limited - RT
i = 6.9 mA (1mA/cm^2)
Reversal at 23¼ hrs
IR Absorption Spectra

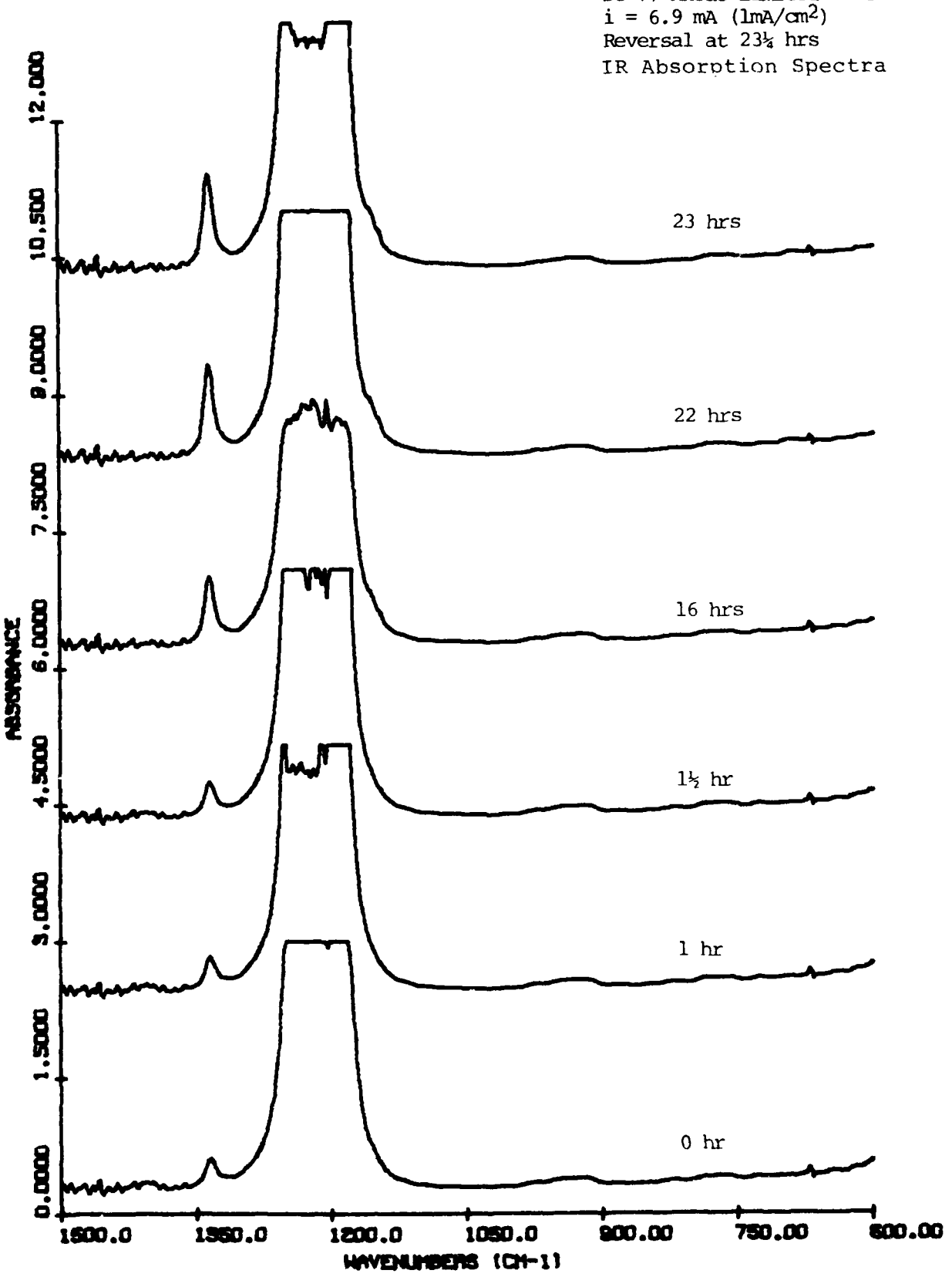

AD-A128 382 INVESTIGATION OF LITHIUM-THIONYL CHLORIDE BATTERY SAFETY HAZARDS(U) GOULD RESEARCH CENTER ROLLING MEADOWS IL MATERIALS LAB A I ATTIA ET AL. JAN 83 838-012

UNCLASSIFIED N60921-81-C-0363 F/G 10/3 NL

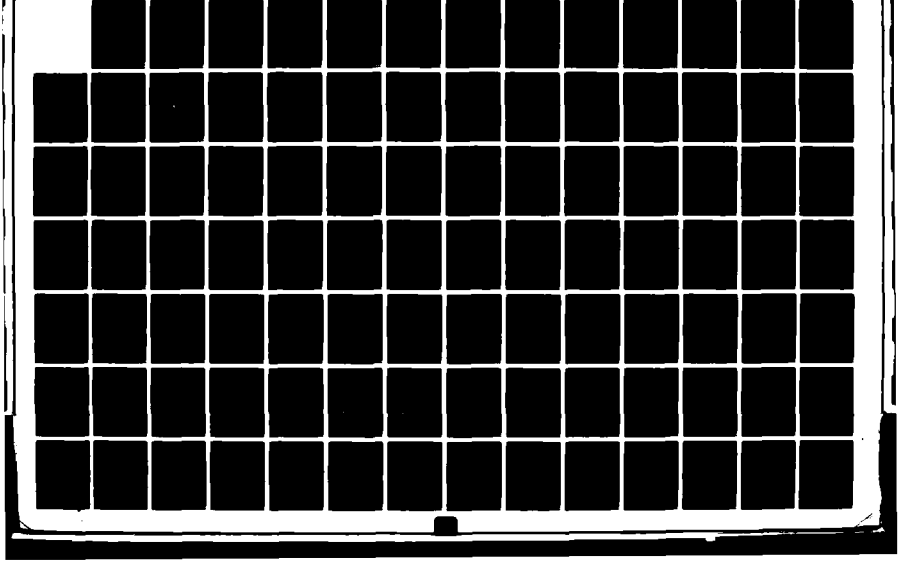

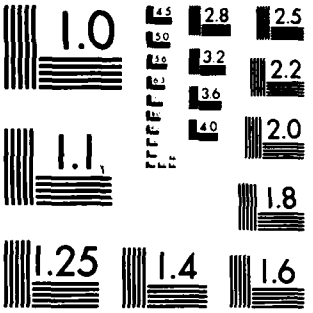

FIGURE 64

SC-77 Anode Limited - RT
i = 6.9 mA (1mA/cm^2)
Reversal at 23¼ hrs
Current Switched off at 47½ hrs
IR Absorption Spectra

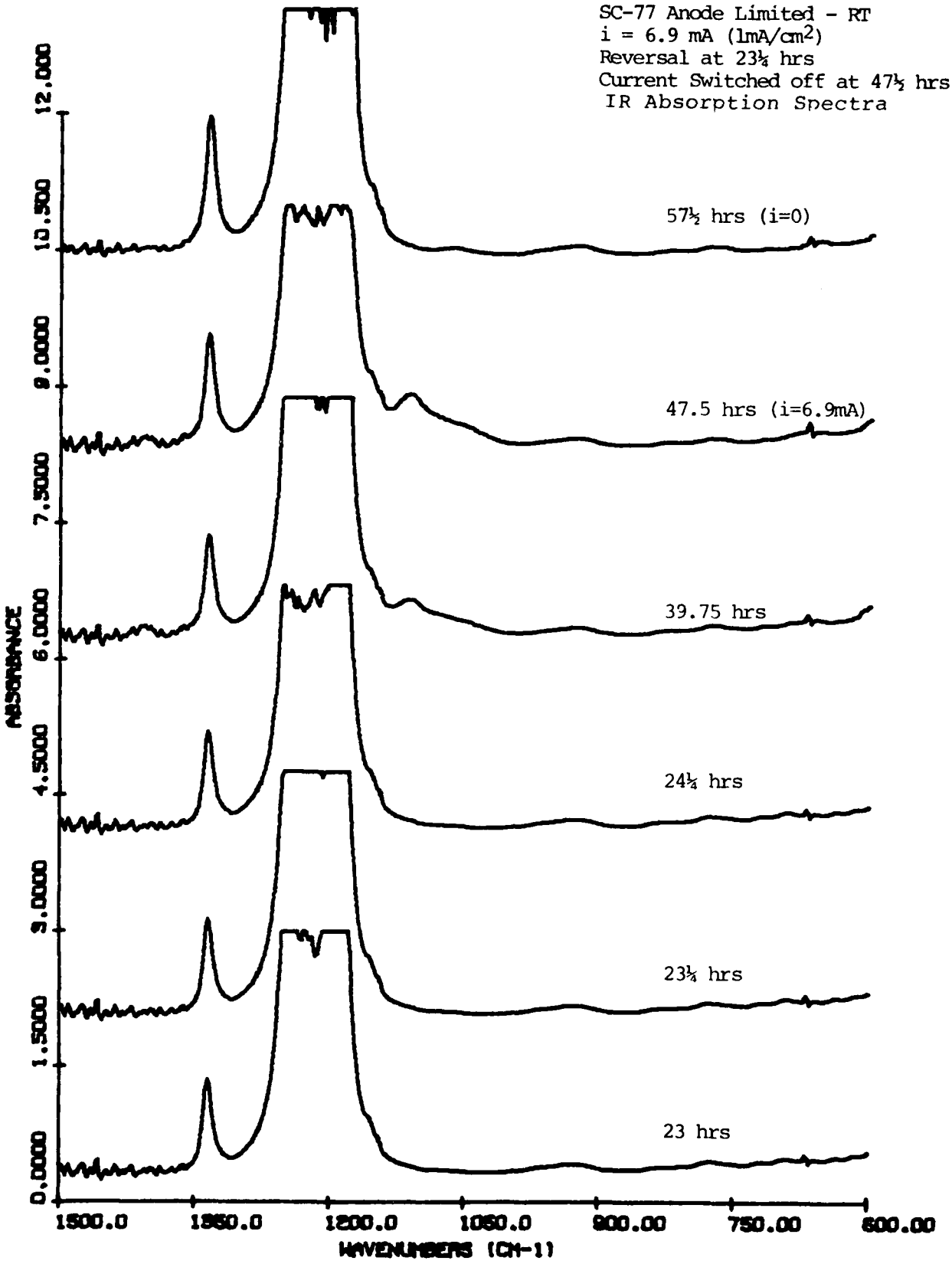

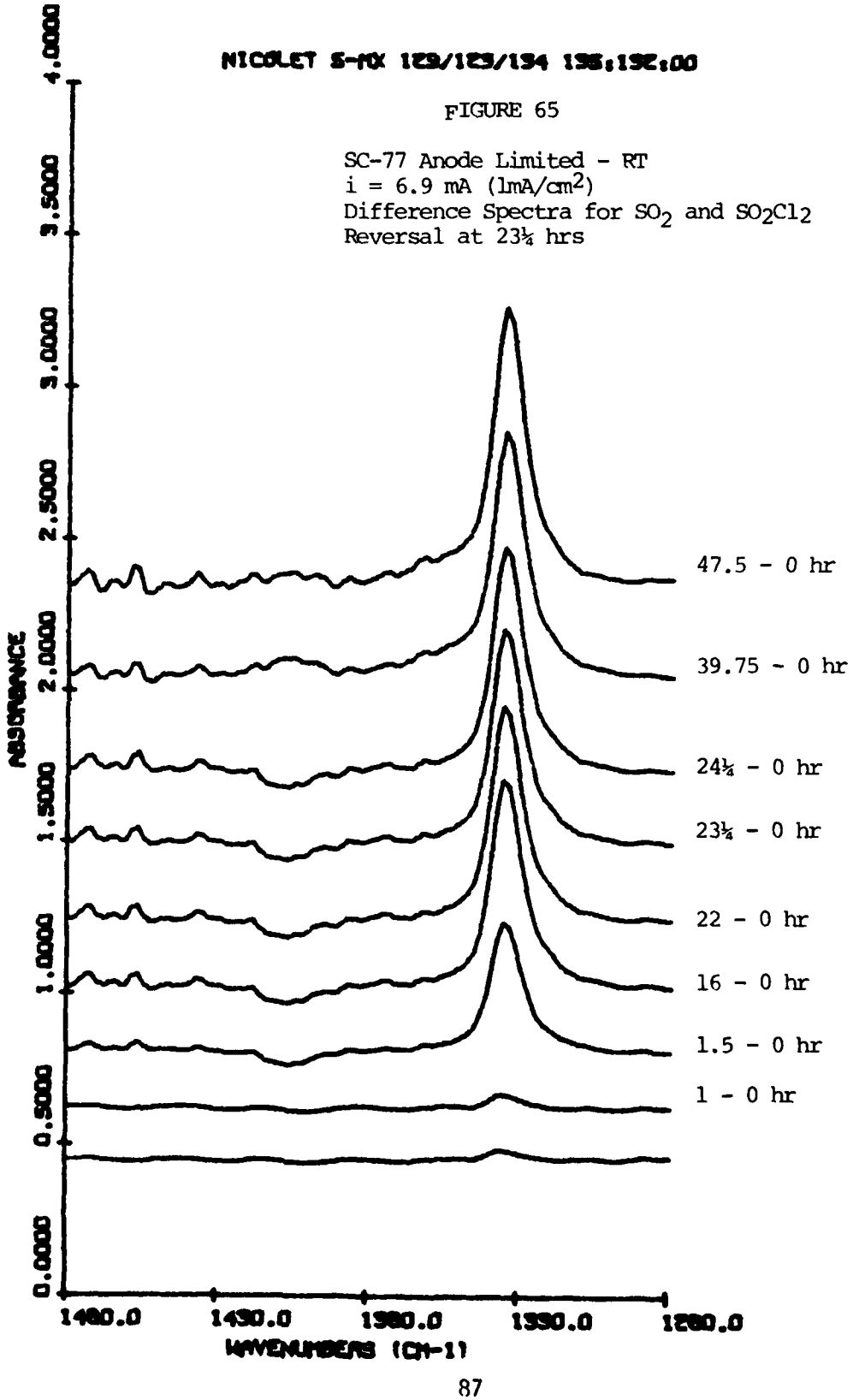

FIGURE 65

SC-77 Anode Limited - RT
i = 6.9 mA (1mA/cm^2)
Difference Spectra for SO_2 and SO_2Cl_2
Reversal at 23¼ hrs

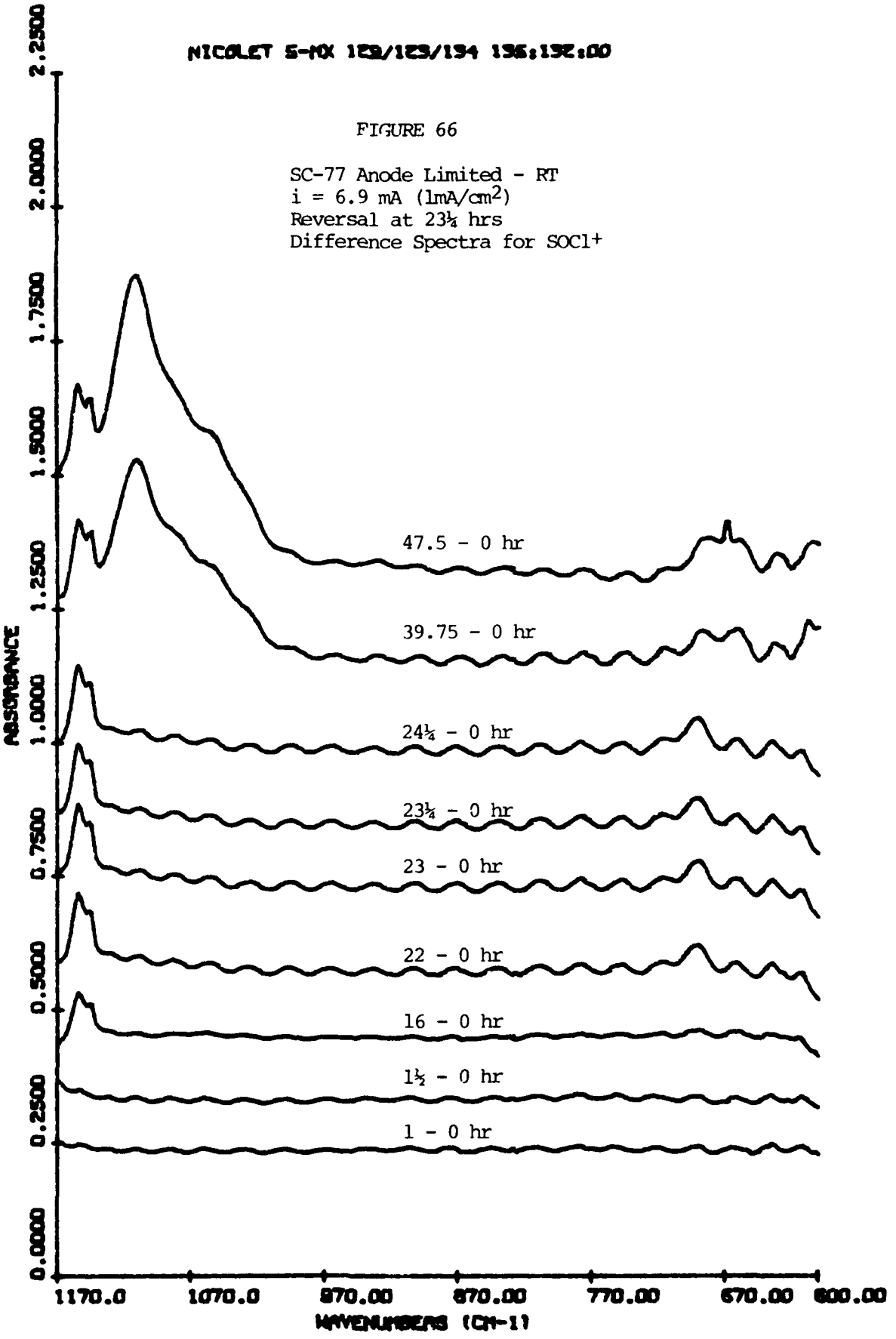

FIGURE 66

SC-77 Anode Limited - RT
i = 6.9 mA (1mA/cm^2)
Reversal at 23¼ hrs
Difference Spectra for $SOCl^+$

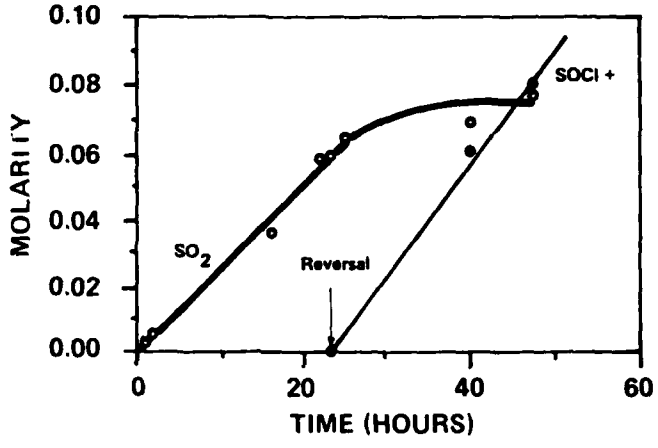

(2682)

Figure 67 Cell SC-77

SO_2 and SOCl + Formation During Reversal
Anode Limited: i = 6.9MA(1mA/cm^2)

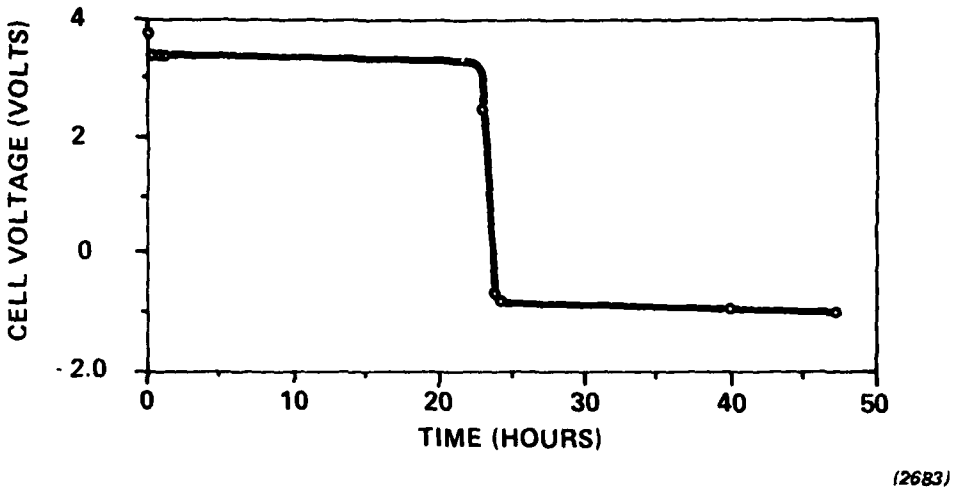

Figure 68 Discharge Curve - Cell SC-77 i = 6.9mA (1mA/cm^2) Anode Limited

Cell SC-79

This experiment is a duplicate of SC-77, but we were able to run it over a longer period of time (see IR spectra in Figures 69-71). The cell discharged at 7.4 mA for about 20 hours then was driven into reversal for about 64 hours; measurements were taken for an additional 8 hours after current cutoff. Difference spectra are shown for the reversal condition in Figure 72. In spite of the prolonged period of reversal very little SO_2Cl_2 accumulates. $SOCl^+$ formed during reversal decays essentially to zero within 8 hours after turning the current off. A significant peak at 665 cm^{-1} appears during reversal; this peak was noticeable in the preceding experiment but had not accumulated to any extent after only 24 hours of reversal. A peak at 1070 cm^{-1} which appears as a shoulder on the 1115 cm^{-1} peak during reversal becomes very evident after the current is turned off and $SOCl^+$ decays. These results are summarized in Figures 73a-d. The results for sulfur dioxide are similar to those for SC-77 but more erratic, indicating a possible leak in the system. Figure 74 shows the discharge curve.

FIGURE 69

SC-79 Anode Limited - RT
i = 7.4 mA (1mA/cm^2)
Reversal at 23 hours
IR Absorption Spectra

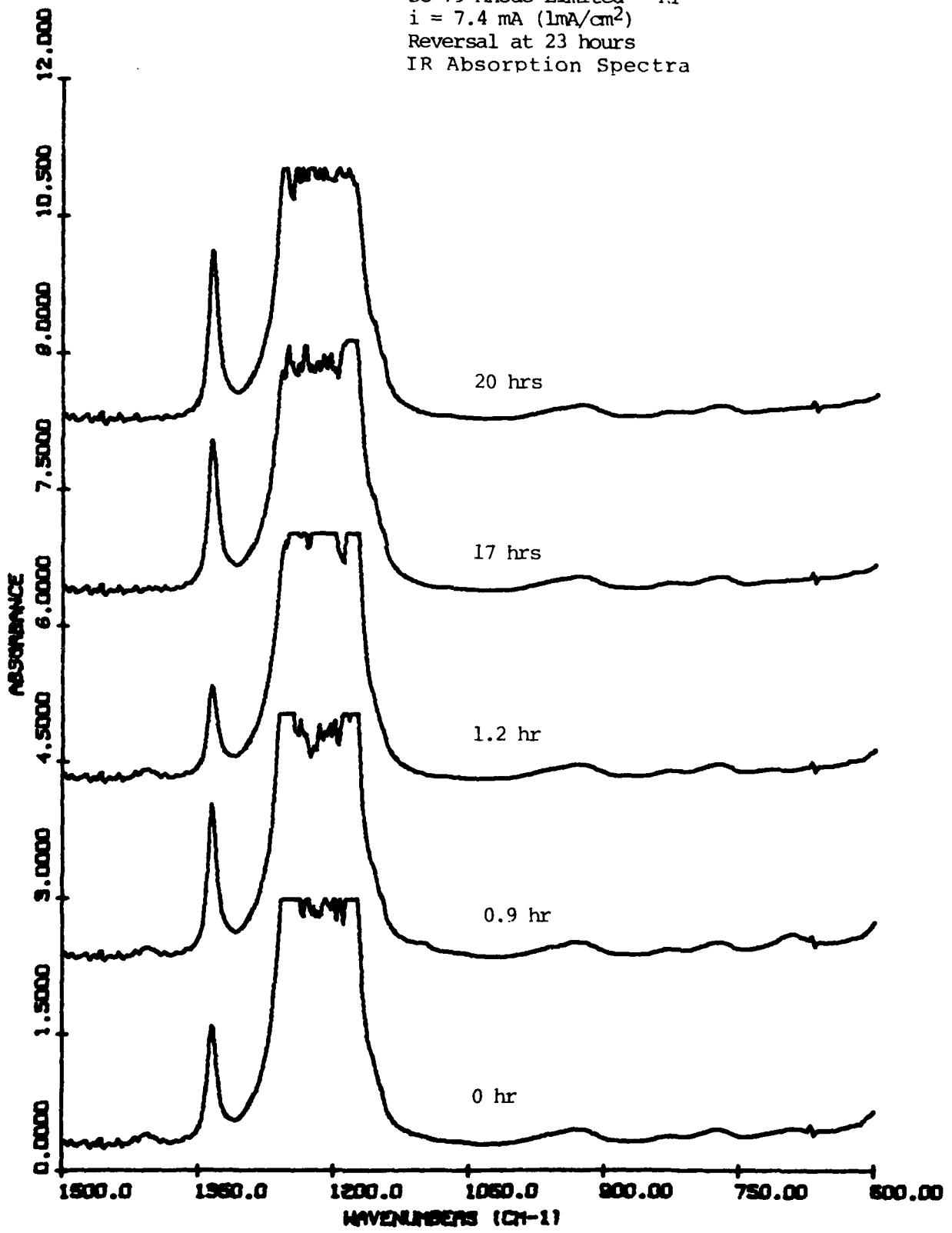

FIGURE 70

SC-79 Anode Limited - RT
i = 7.4 mA (1mA/cm^2)
Reversal at 23 hrs
IR Absorption Spectra

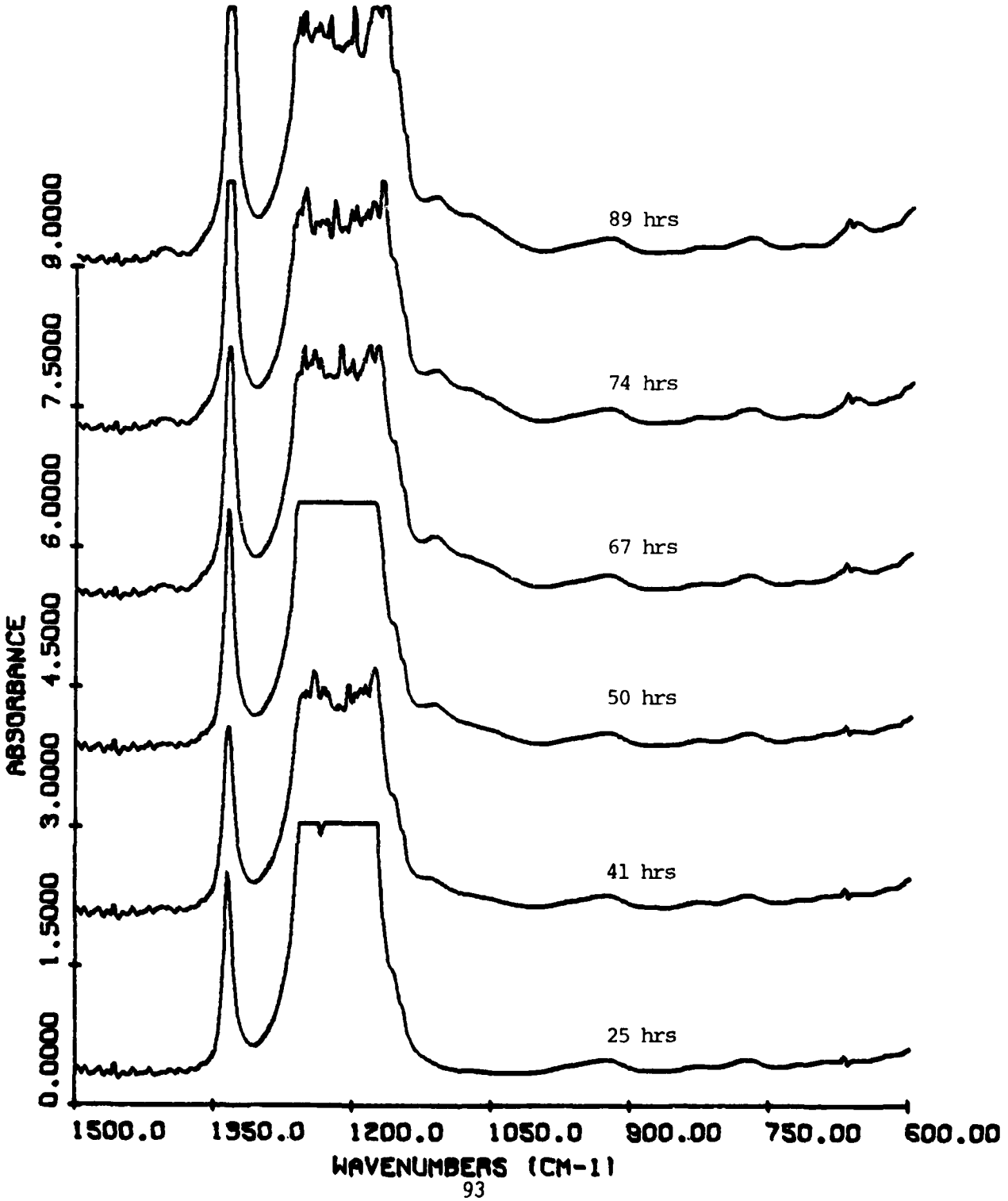

FIGURE 71

SC-79 in Storage after Reversal
i = 0
Storage at 89.2 hrs

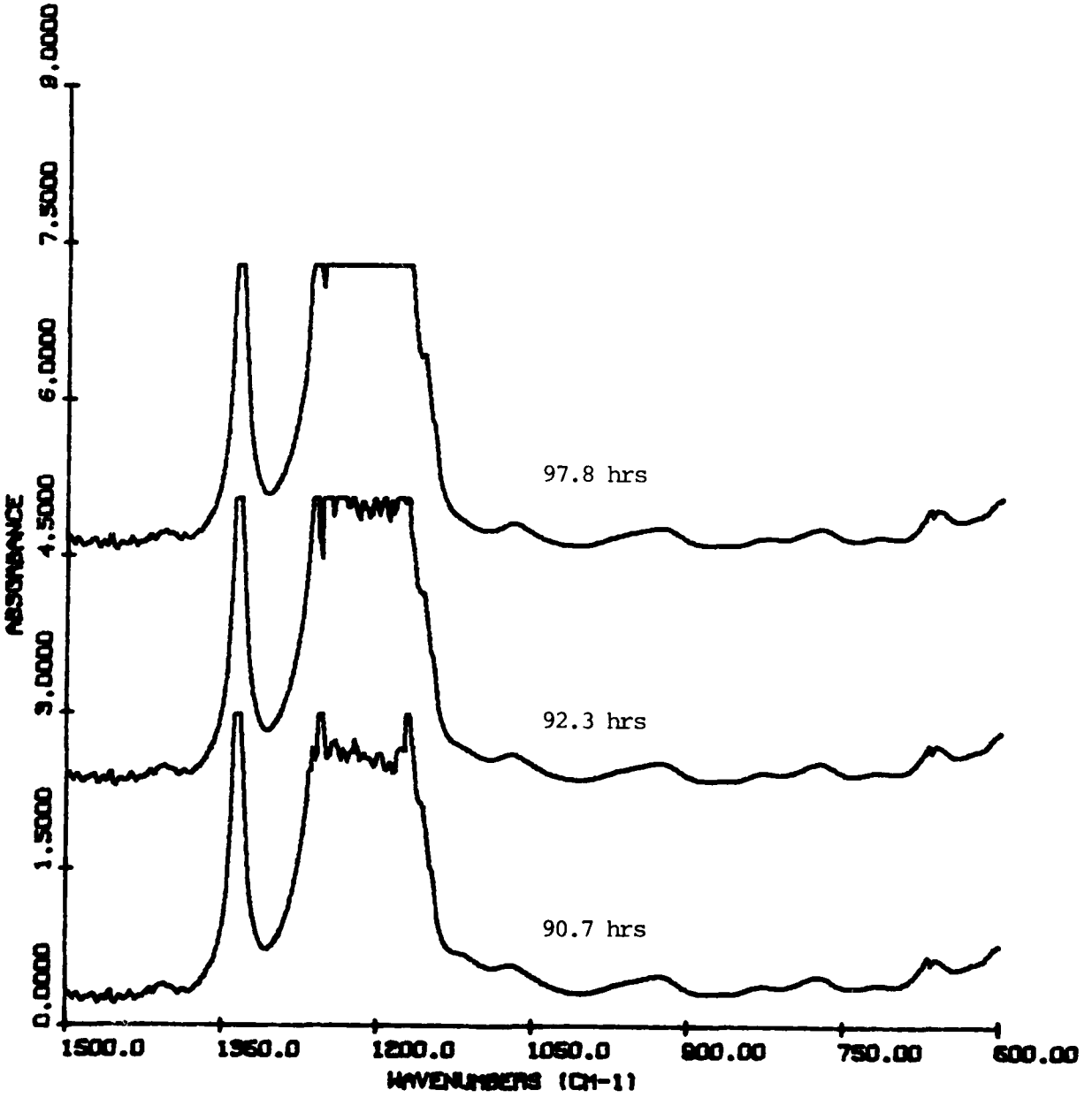

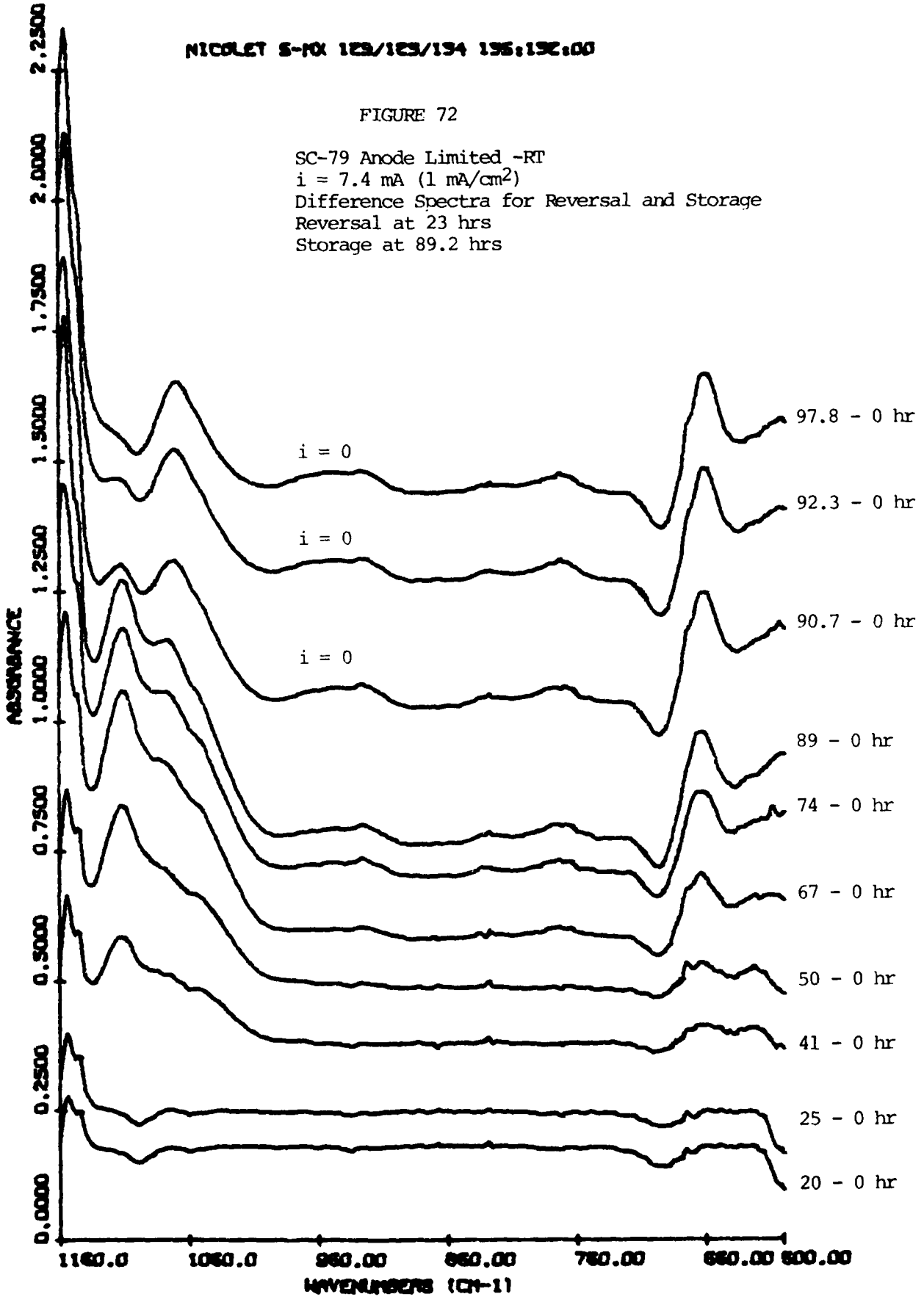

FIGURE 72

SC-79 Anode Limited -RT
i = 7.4 mA (1 mA/cm^2)
Difference Spectra for Reversal and Storage
Reversal at 23 hrs
Storage at 89.2 hrs

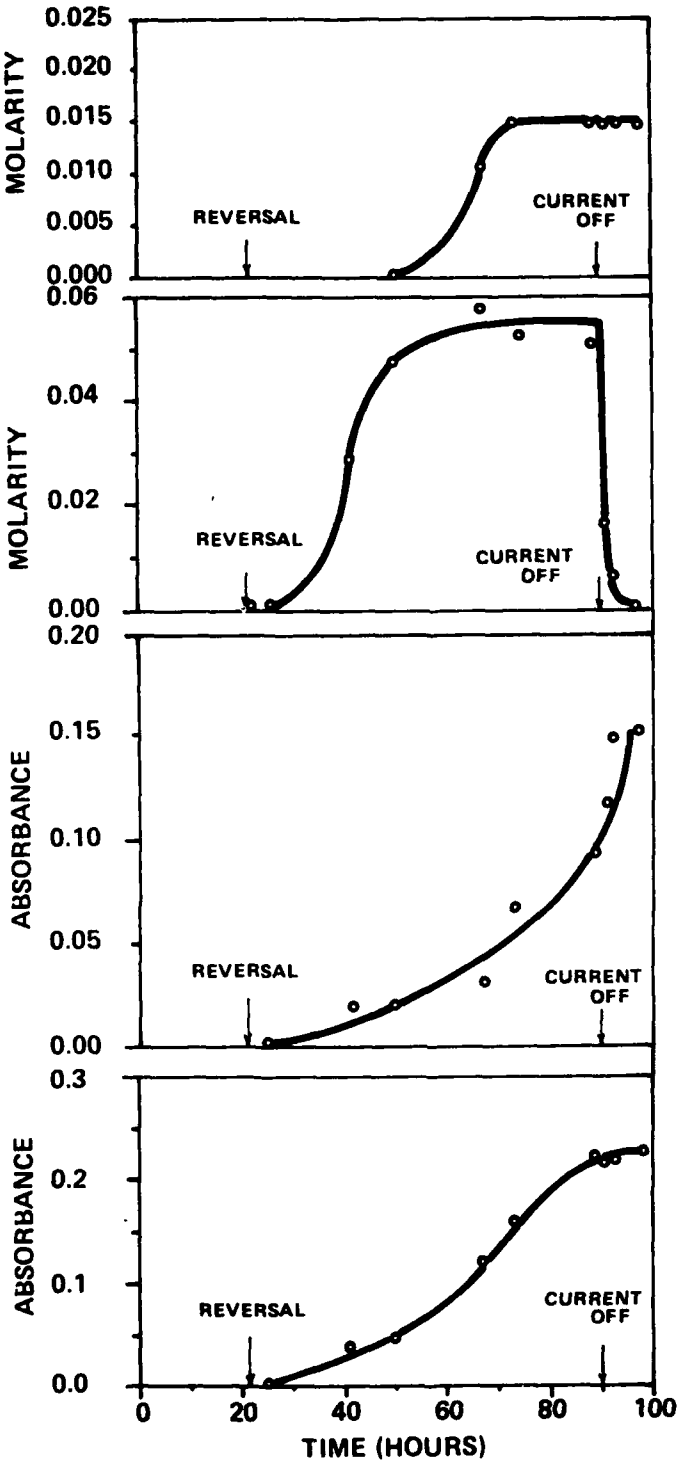

Figure 73 Cell SC-79

Anode Limited: $i = 7.4mA(1mA/cm^2)$

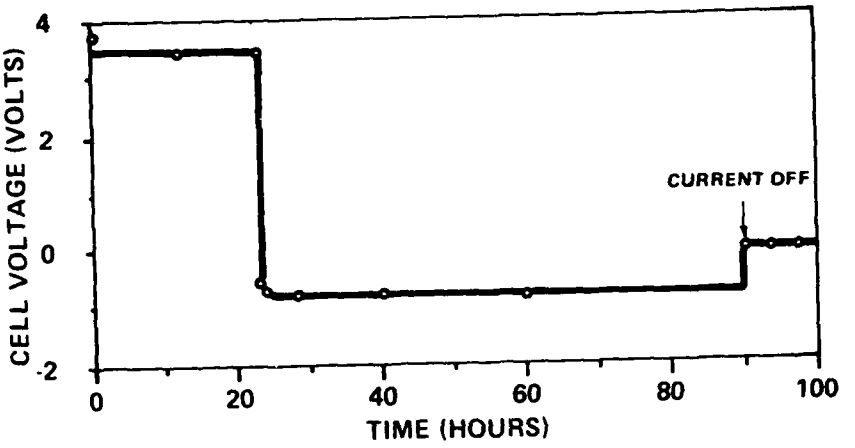

Figure 74 Discharge Curve - Cell SC-79

$i = 7.4mA(1mA/cm^2)$ Anode Limited

Cell SC-81

Cell SC-81 was discharged at -20°C. Cell construction was identical to the preceding ones; however, the cell was placed in a controlled temperature refrigerating bath. The electrolyte was periodically circulated with a peristaltic pump to the spectroscopic cell located in the spectrometer chamber. The length of the tubing leading to the spectroscopic cell and the mass of the latter were sufficient to bring up the sample temperature to ambient. Sampling under those conditions tended to reduce significantly cell polarization (Figure 75). The first 17 hours of discharge were performed at 1 mA/cm^2 (8.14 mA). The current was then brought up to 5 mA/cm^2 (40.70 mA) and the cell went into reversal two hours later. We continued driving the cell into reversal for an additional 22 hours at 5 mA/cm^2. The current was then turned off and the temperature brought up to 20°C over a period of 3 hours. Spectral measurements were taken for another 67 hours. This sequence of events is shown along with the discharge curve in Figure 75. Large voltage fluctuations are observed during reversal; the voltage jumps to more positive values every time we circulate the electrolyte. It is obvious that cell resistance especially during reversal is very high. We have monitored the SO_2 concentration during normal discharge (Figure 76), the $SOCl^+$ concentration during the first six hours of reversal (Figure 77), and the SO_2Cl_2 concentration during the reversal and warming up periods (Figure 78). IR absorption spectra as well as difference spectra illustrating the behavior of these species are shown in Figures 79-84.

The IR absorption bands at 1070cm^{-1} and 665 cm^{-1} exhibit their usual behavior, and some moisture contamination is apparent especially after the onset of reversal (broad band around 694 cm^{-1}). We have plotted in Figure 76 the SO_2 concentration as a function of mAh withdrawn. A slight curvature is noticeable at the beginning of the discharge indicating that SO_2 generation is not linear at this temperature, at least in the early stages of the discharge. The overall stoichiometry, however, corresponds to 7.6 Faradays/mole of SO_2 generated during normal discharge. (Table 2)

One obvious effect of the low temperature is the immediate and sharp increase of $SOCl^+$ concentration during reversal, the increase amounting to about 0.65 mole per Faraday (see Figure 77). At higher temperatures regenerative processes are in effect so that only small amounts of $SOCl^+$ accumulate in the cell.

SO_2Cl_2, however, does not begin to accumulate until at least six hours after the onset of reversal (see Figure 78) and then increases slowly. Turning off the current at -20°C does not seem to affect the SO_2Cl_2 concentration, but a dramatic jump in its concentration occurs as we warm up the cell to 20°C, the concentration at the end of the warm up period being outside the range of our calibration. This behavior points to a chemical reaction between SO_2 and Cl_2 as the source of SO_2Cl_2 in the cell.

Due to the very high intensity of the $SOCl^+$ absorption we were not able to track the absorption at 1070 cm^{-1}. The presence of this peak becomes obvious, however, as the $SOCl^+$ decays after the current is turned off and the cell warmed up.

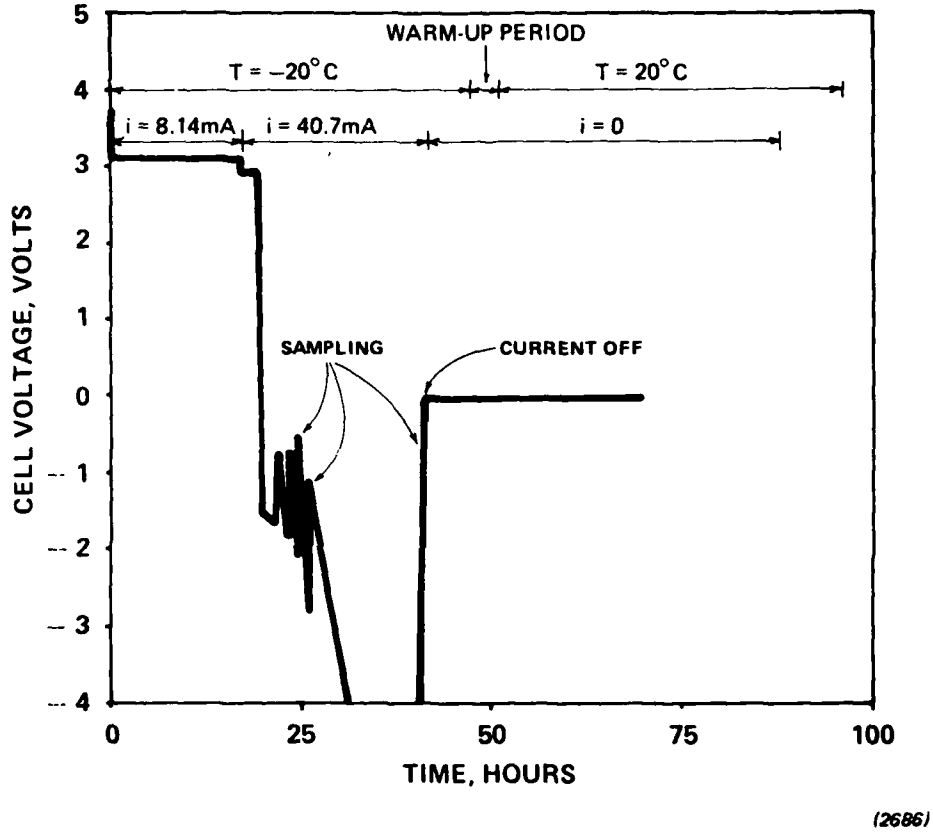

Figure 75 Discharge Curve
Cell SC-81
Anode Limited
–20°C

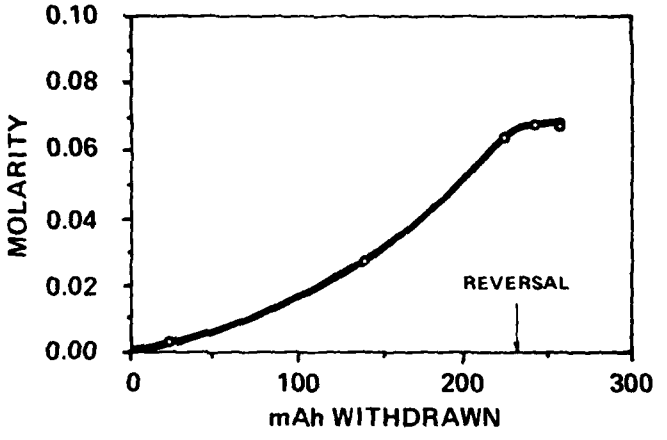

(2687)

Figure 76 Cell SC-81

SO_2 Formation During Discharge -20°C

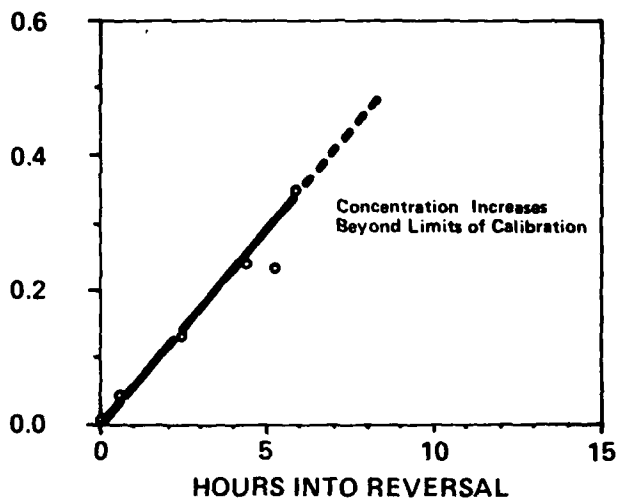

Figure 77 Cell SC-81

SOCl + Formation During Reversal
Anode Limited at -20°C; i = 40.5mA ($5mA/cm^2$)

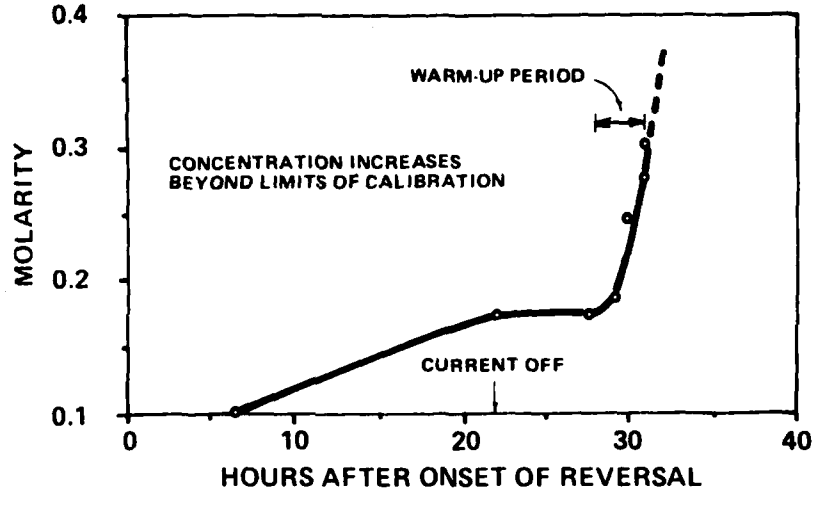

Figure 78 Cell SC-81

SO_2Cl_2 Formation During Reversal and Warm-up Anode Limited i = 40.5mA(5mA/cm^2) T = -20°C

FIGURE 79

SC-81 Anode Limited (-20 C)
Normal Discharge
i = 8.1 mA (1mA/cm^2)
Reversal at 19.75 hrs

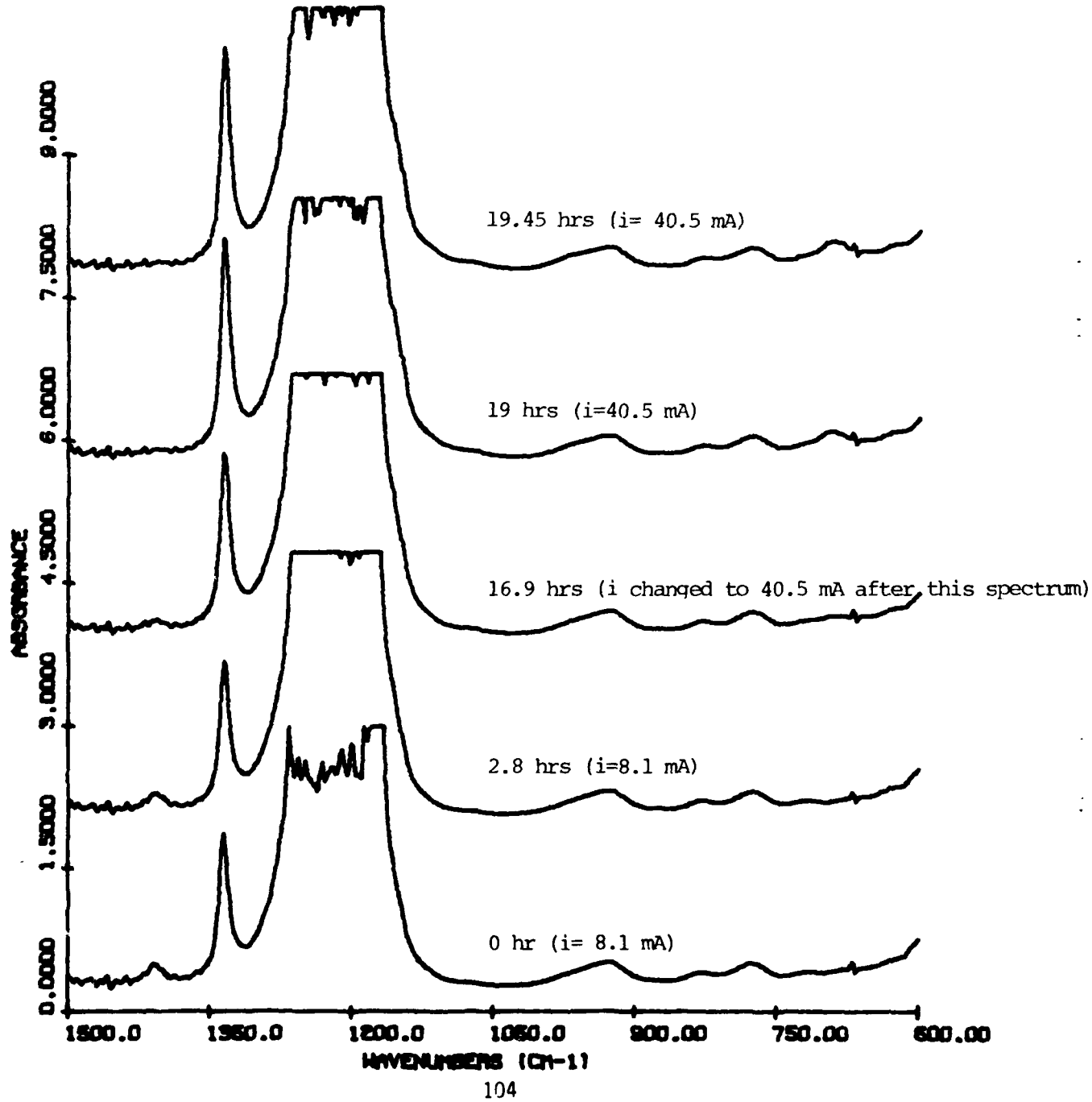

FIGURE 80

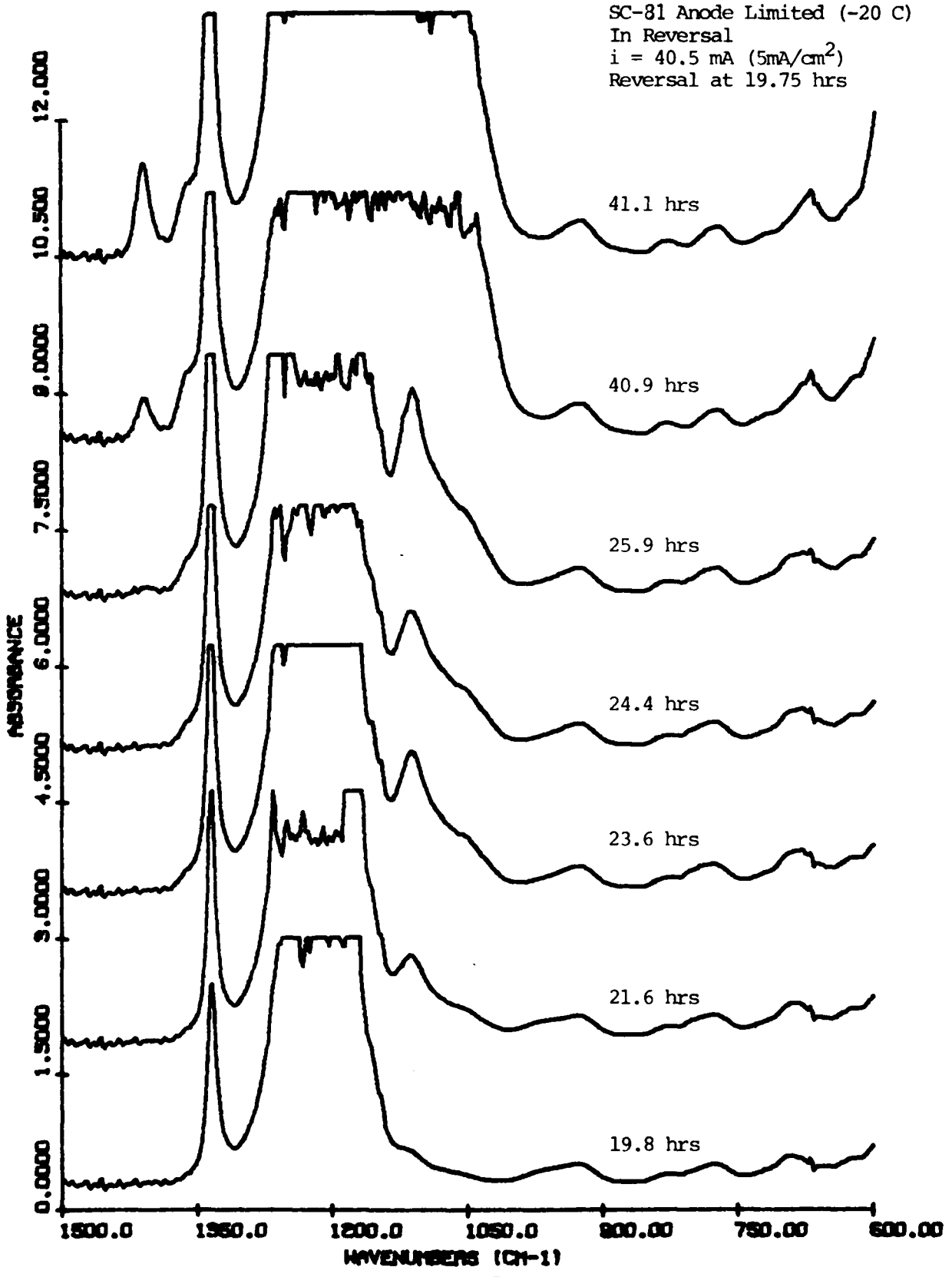
SC-81 Anode Limited (-20 C)
In Reversal
i = 40.5 mA (5mA/cm2)
Reversal at 19.75 hrs
41.1 hrs
40.9 hrs
25.9 hrs
24.4 hrs
23.6 hrs
21.6 hrs
19.8 hrs
ABSORBANCE
12.000
10.500
9.0000
7.5000
6.0000
4.5000
3.0000
1.5000
0.0000
1500.0
1350.0
1200.0
1050.0
900.00
750.00
600.00
WAVENUMBERS (CM-1)

FIGURE 81

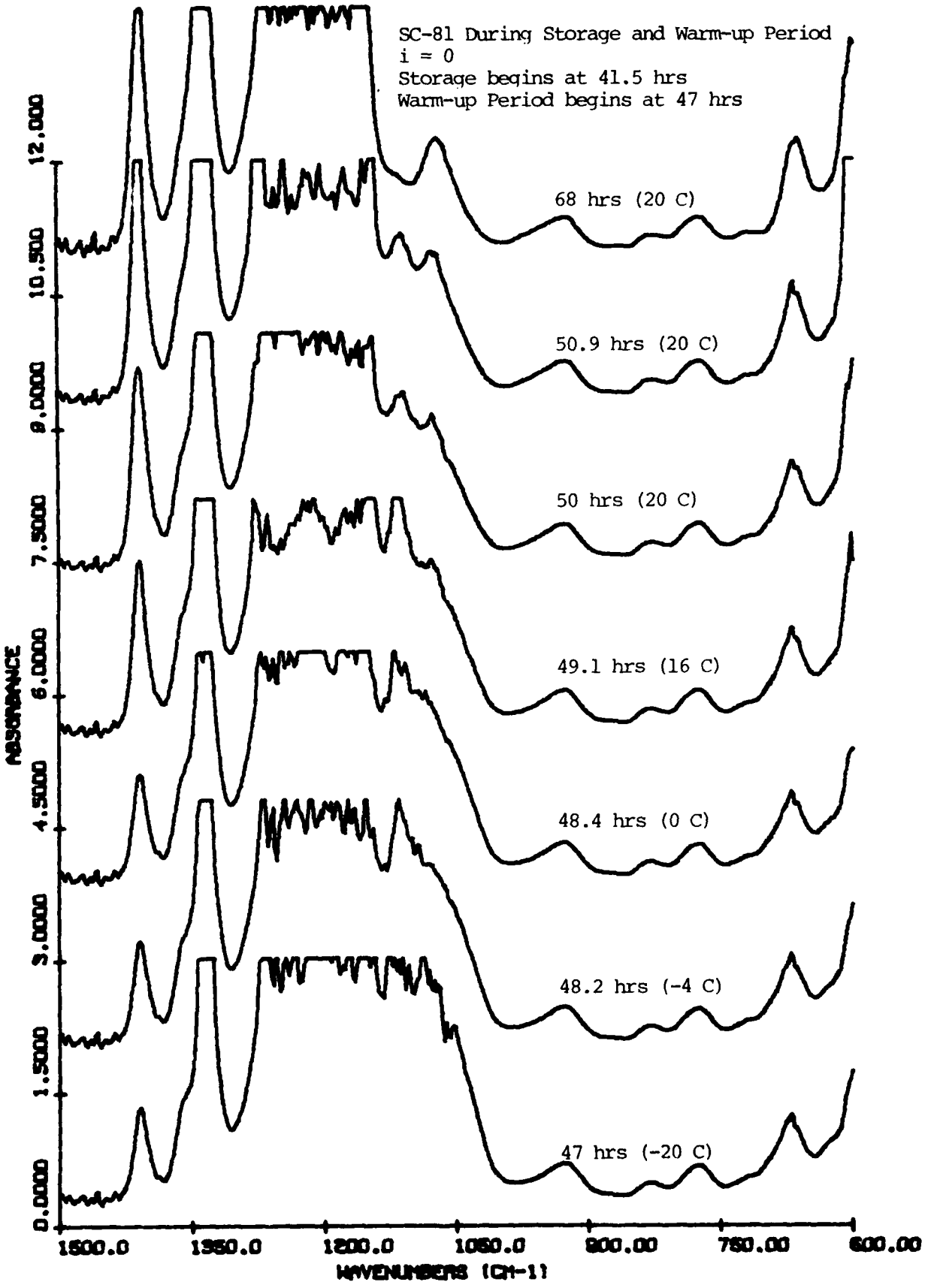
SC-81 During Storage and Warm-up Period
i = 0
Storage begins at 41.5 hrs
Warm-up Period begins at 47 hrs
68 hrs (20 C)
50.9 hrs (20 C)
50 hrs (20 C)
49.1 hrs (16 C)
48.4 hrs (0 C)
48.2 hrs (-4 C)
47 hrs (-20 C)
ABSORBANCE
12.000
10.500
9.0000
7.5000
6.0000
4.5000
3.0000
1.5000
0.0000
1500.0
1350.0
1200.0
1050.0
900.00
750.00
600.00
WAVENUMBERS (CM-1)

FIGURE 82

SC-81 Anode Limited (-20)
Difference Spectra for SO_2 during Normal Discharge
i = 8.1 mA (1mA/cm^2) during the first 16.9 hours
i = 40.5 mA (5mA/cm^2) after 16.9 hrs
Reversal at 19.75 hrs

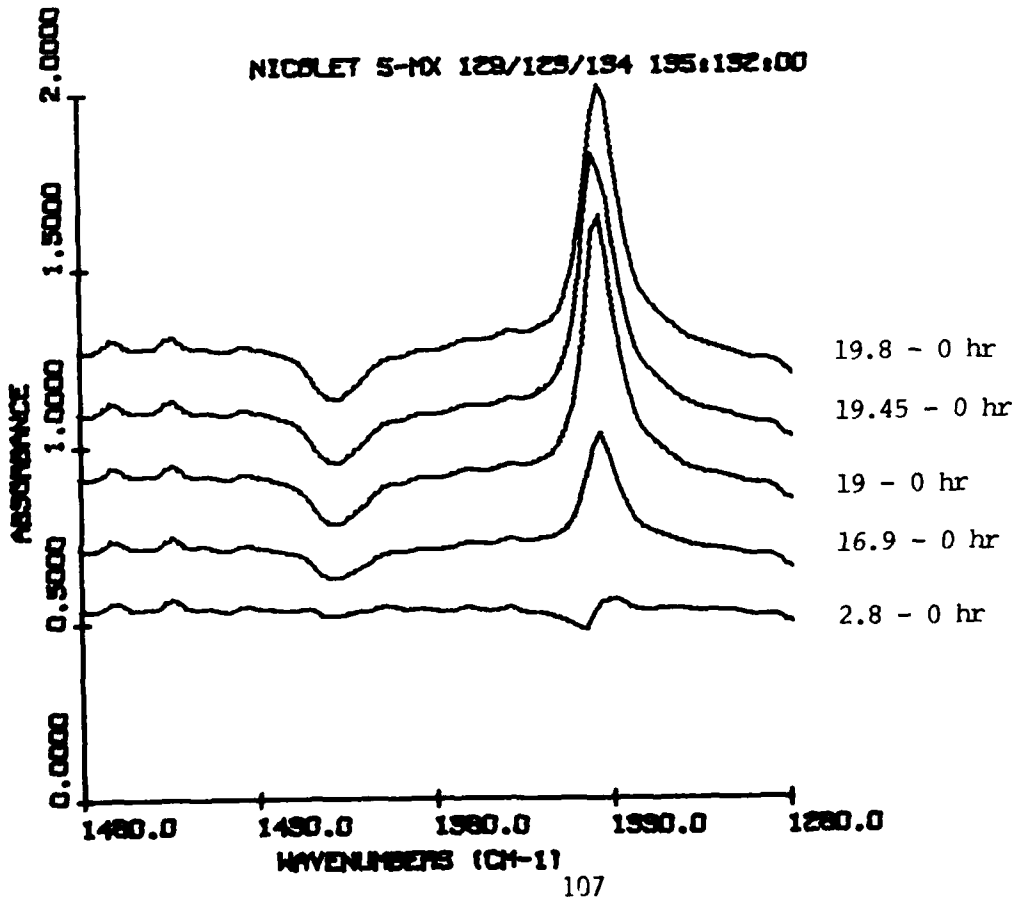

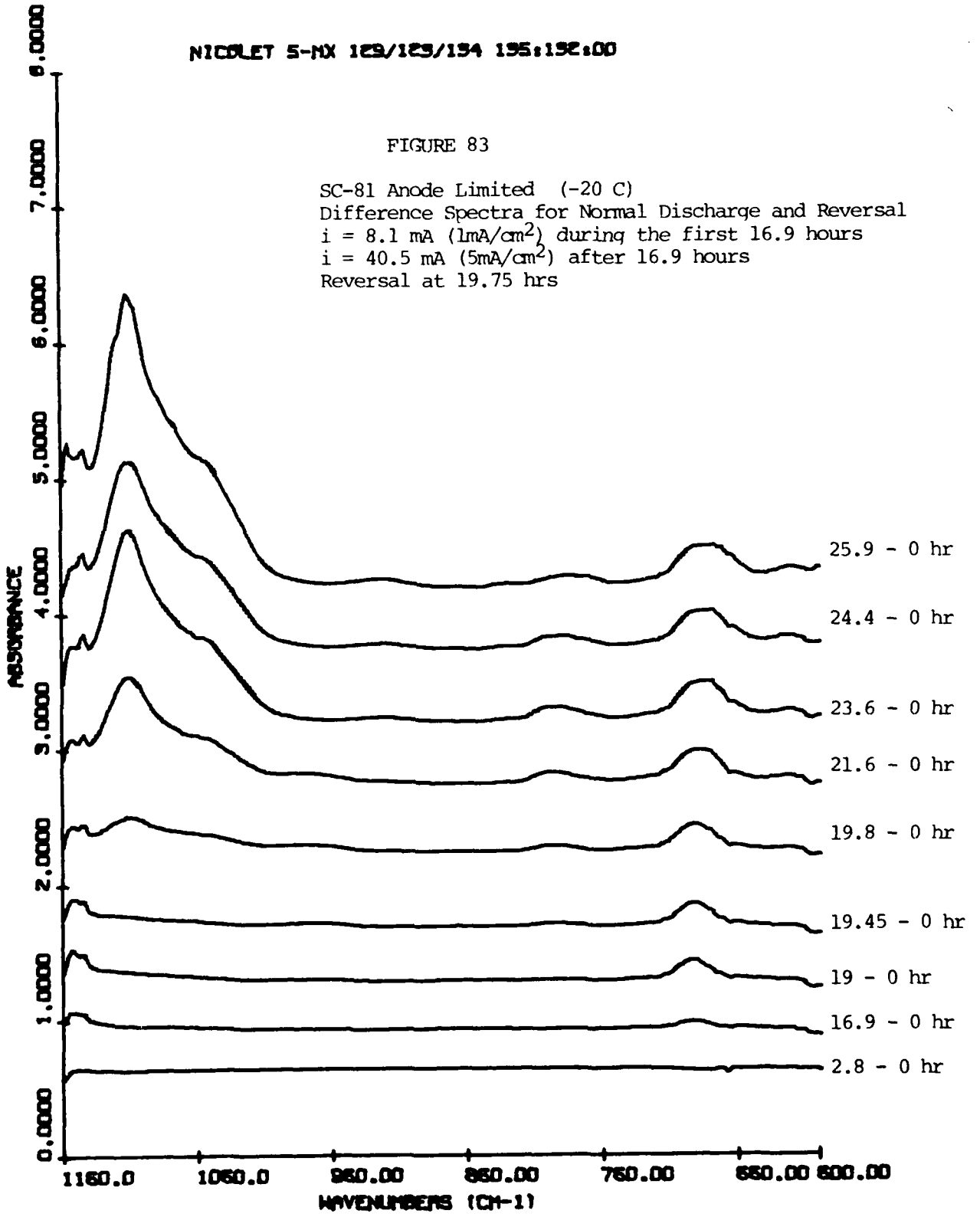

FIGURE 83

SC-81 Anode Limited (-20 C)
Difference Spectra for Normal Discharge and Reversal
i = 8.1 mA (1mA/cm^2) during the first 16.9 hours
i = 40.5 mA (5mA/cm^2) after 16.9 hours
Reversal at 19.75 hrs

FIGURE 84

SC-81 Difference Spectra
SO_2Cl_2 during Reversal, Storage , and warm-up period
i = 40.5 mA (5mA/cm^2)
Reversal at 19.75 hrs
Storage at 41.5 hrs (i=0)
Warm-up period begins at 47 hrs

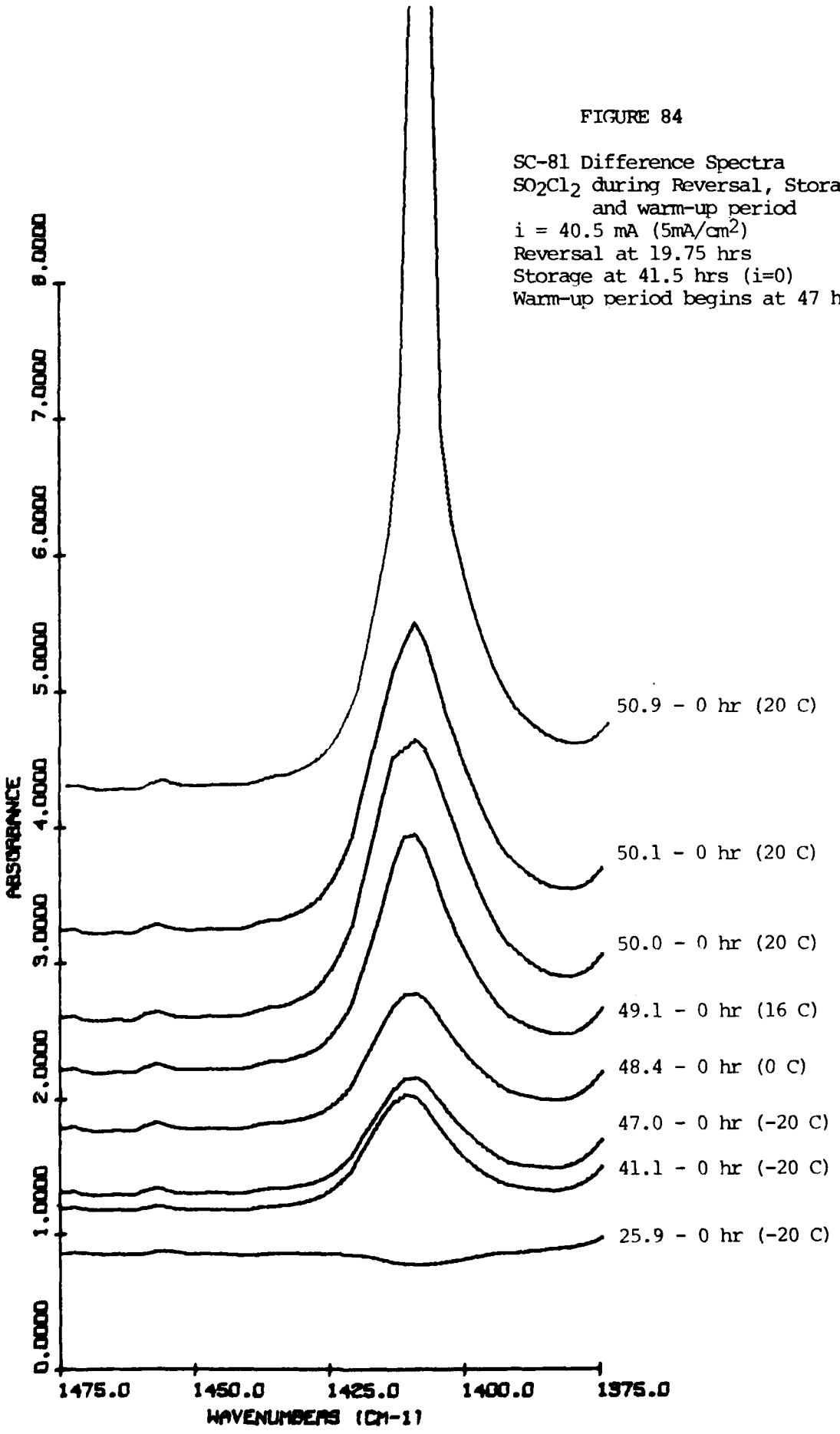

Table 2

SO_2 PRODUCTION DURING NORMAL DISCHARGE

SC-69 (5 mA/cm^2, RT)	0.14 Mole/Faraday
SC-71 (5 mA/cm^2, RT)	0.17 Mole/Faraday
SC-77 (1 mA/cm^2, RT)	0.17 Mole/Faraday
SC-81 (1 mA/cm^2, -20C)	0.13 Mole/Faraday

3.7 Conclusions

The infrared absorption spectrum of lithium-thionyl chloride cells which initially appeared quite complex was greatly simplified as soon as the effects of contaminants such as moisture were understood.

By measuring the spectrum in situ, we were able to limit the interaction of moisture with the electrolyte to an acceptable level. Quantitative and reproducible results have been obtained from run to run for anode limited cells, and definite trends have been demonstrated.

During normal discharge at 25C SO_2 is the only discharge product detected by IR spectroscopy (sulfur and LiCl are also formed but were not measured in this study). The rate of SO_2 formation is linear and appears independent of current density - from 1 to 5 mA/cm^2. At -20C a slightly nonlinear rate of SO_2 production is noticed, and under all conditions, the amount of SO_2 produced was less than what would be predicted by the equation

$$4\ Li + 2\ SO\ Cl_2 = 4\ LiCl + SO_2 + S$$

During reversal the SO_2 concentration continues to rise but at a slower rate. Several other species begin to appear: $SOCl^+$, SO_2Cl_2 and species giving rise to absorptions at 1070 cm^{-1} and 665 cm^{-1}; these last two absorptions are indirectly indicative of Cl_2 or SCl_2 formation on reversal; however, the evidence for Cl_2 is also indirect whereas SCl_2 has been positively identified by mass spectrometry. $SOCl^+$ eventually reaches a steady state concentration which is dependent on both temperature and current density. SO_2Cl_2 is also dependent on both temperature and current density, and its concentration tends to surge upward particularly after disconnecting the cell following reversal. Warming up a cold cell from -20C to +20C results in a disturbingly large increase of SO_2Cl_2 from either an increased rate of reaction between SO_2 and Cl_2 at the higher temperature, or the sudden degradation of an unstable compound.

Formation of SCl_2 during reversal gives rise to compounds absorbing at 1070 cm^{-1} and 665 cm^{-1} whose exact nature is not known; however, complexes such as SCl ($AlCl_4$) have been identified in the reaction of SCl_2 and $AlCl_3$ (19) and may give rise to an absorption around 665 cm^{-1}. The 1070 cm^{-1} absorption reflects the presence of S-O bonds. It is interesting to note that upon addition of SCl_2 to neutral electrolyte SO_2Cl_2 and SO_2 are also formed. The increase in SO_2Cl_2 which is observed after disconnecting the cells may simply arise from this source. The weak absorption at 1070 cm^{-1} observed during cathode limited reversal may also be due to formation of small quantities of SCl_2, and subsequent reactions.

It is quite evident that during anode limited reversal a highly acidic environment is created in the cell. It might be worthwhile to perform calorimetric studies of reactions in $AlCl_3/SOCl_2$ solutions. Several improvements in the experimental approach are also possible to better ascertain the behavior of the lithium-thionyl chloride system. Temperature and pressure measurements would yield additional correlations. Use of shorter optical path lengths for our IR cells would enable us to extend our calibration curves. Extending the FTIR spectrometer's range to 250 cm^{-1} would reveal additional bands in the spectrum. Electrochemical studies in carefully prepared mixtures could help elucidate the mechanism of several electrochemical reactions involving $SOCl_2$. These are just a few of the many additional experiments that need to be performed. It is also obvious that IR spectroscopy alone may not provide all the answers, and that an attempt should be made to identify insoluble products of discharge.

4. A Mass Spectrometric Study of Gases Evolved During Discharge and Reversal of Anode-Limited $Li/SOCl_2$ Cell

In this section we discuss the time-dependent results obtained from a mass spectrometric study of an in-situ anode limited $Li/SOCl_2$ cell, and we report the mass spectra of pure components and their measured appearance potentials.

4.1 Abstract

Species formed during discharge, reversal and storage of a $Li/SOCl_2$ cell were identified and quantitatively measured as a function of time. Mass spectrometric data indicate the existence of molecular HCl, SO_2, CS_2, S_2O, SCl_2, $SOCl_2$ and mass 134 species (mainly SO_2Cl_2). Data also reveal the presence of high levels of chlorine fragments as well as low concentrations of CF_2^+ fragments. Species with molecular weights exceeding nominal mass 140 were also observed. The relative concentrations of the species identified are plotted versus time during discharge and reversal. These plots indicate that the concentrations of HCl, Cl^- and SO_2 remain essentially constant in the gas phase during discharge, but increase after an induction period of approximately five hours during cell reversal. The plots for CS_2 and S_2O show little variation in concentration of these species with time during both discharge and reversal, while the plots for SCl_2 and the mass 134 species clearly indicate that these compounds are formed only after a similar induction period during the reversal mode. Mass spectra for pure SCl_2, $SOCl_2$ and SO_2Cl_2 were obtained. The appearance potential for these pure species as well as for SO_2 and argon were also measured.

4.2 Experimental

A Perkin Elmer (PE 270) mass spectrometer with a home-built all glass gas inlet system was used for the in-situ experiment. A diagram of the experimental sampling system is shown in Figure 85A. This sampling system consists of two (V_1 and V_2) stainless steel shutoff nonrotating stem valves (Circle Seal). The sampling volume contained between V_1 and V_2 is approximately 0.5 cm^3. The glass inlet system is comprised of four teflon stopcocks (V_3-V_6), with V_4 providing access to a roughing pump and V_6 finally leading to the mass spectrometer ion source. V_5 provides access to a perfluorokerosene (PFK) reservoir which is used in the calibration of the mass scale.

The exact mass experiments were performed on an AEI MS-30 double focusing mass spectrometer. Accurate mass measurements were performed with an Anatron peak matching unit. These measurements were carried out with known (20) perfluorkerosene fragments used as the mass reference. The intensity versus time data were obtained with 80 ev electron energy on the PE270 mass spectrometer and with 70 ev electron energy on the MS-30 mass spectrometer. The detailed description of the cell and the method of preparation of these chemicals are given in the previous sections of this report.

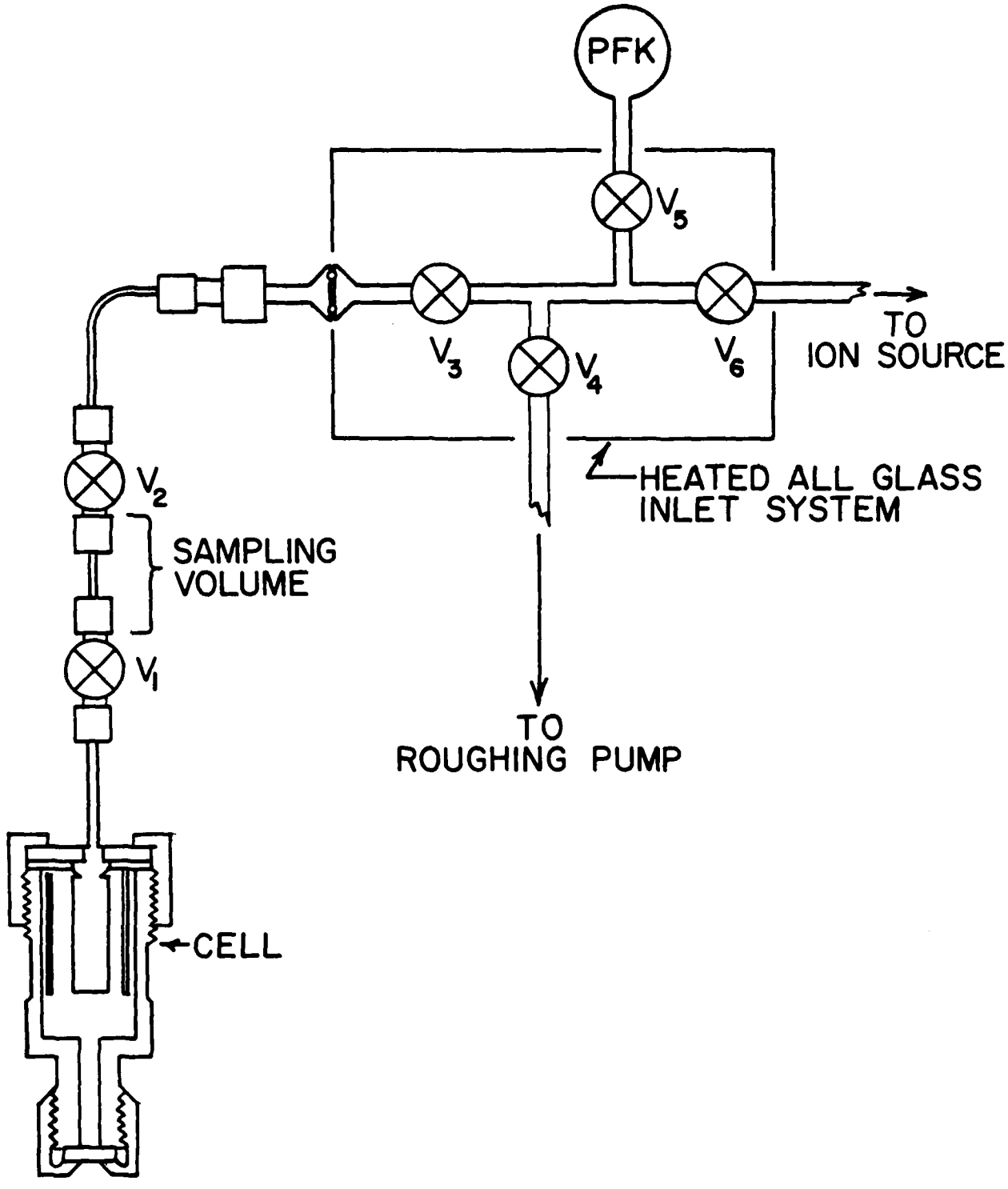

Figure 85A. Mass Spectrometric Sampling System.

4.3 Results

The discharge rate of the anode-limited $Li/SOCl_2$ cell was set at 1 mA/cm^2 of the surface area of the anode. A current level of 6.25 mA/cm^2 was used during reversal. The total surface area of the anode was 8 cm^2. The in-situ experiment spanned 69.25 hours (Figure 85B shows the discharge curve). Fifteen sets of mass spectra were recorded from time zero at the beginning of the discharge through time 69.25 hours. Reversal onset occurred at time t=21 hours, and the reversal process was continued through t=66. The last set of spectra was recorded at time t=69.25 hours. Tabulated intensities for nominal masses appearing between and including masses 35 and 138 are given in Table 3. All intensity data are relative to the intensity of nominal mass 83 ($SOCl^{35+}$) which is set arbitrarily to 100. Plots of intensity versus time for each of these masses are shown in a sequence of figures whose numbers will be given in the discussion section. Data points in each of these graphs are connected to facilitate following the general intensity change with time. The uncertainty in the data shown in Table 3 and the corresponding figures is estimated to be $\pm$ 10%.

Pure samples of SCl_2, $SOCl_2$, SO_2Cl_2 were introduced into the mass spectrometer, their spectra were recorded and the peak intensities were entered in Table 4. Reproduction of these spectra are also shown in figures whose numbers will be given in the discussion. In addition a sample of S_2Cl_2 whose purity is questionable has been admitted into the mass spectrometer and the resulting tentative spectrum is shown. All of these spectra were recorded with electron energy of 80 ev.

The appearance potential of SCl_2, $SOCl_2$, SO_2Cl_2, SO_2, Ar and of slightly impure S_2Cl_2 were measured on the PE270 mass spectrometer. The data obtained for these compounds were then normalized to the appearance potential measured for argon. The appearance potential data are plotted versus electron energy and are shown in subsequent figures.

Three masses were accurately measured in the exact mass experiments. These are masses 50, 76 and 80. Problems arising from the corrosive nature of the species present in the $Li/SOCl_2$ system caused frequent ion source filament burnouts. Further accurate mass measurements should be made in the future in order to positively identify other important species. The results obtained from these measurements were:

Nominal mass 50 exact mass = 49.99597 $\pm$ 30 ppm
Nominal mass 76 exact mass = 75.94528 $\pm$ 20 ppm
Nominal mass 80 exact mass = 79.94057 $\pm$ 20 ppm

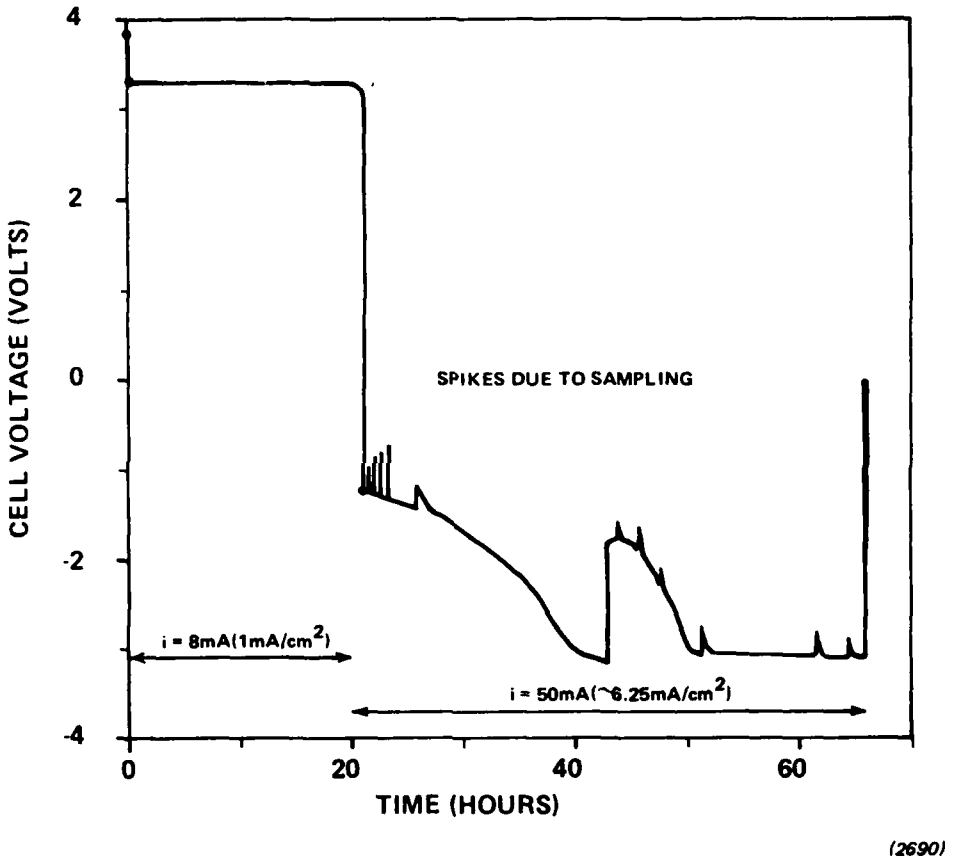

Figure 85B Discharge Curve Cell SC-80 Anode Limited T = 25°C

TABLE 3

Mass intensity vs time data for the in-situ experiment
(a) Time of the onset of reversal
(b) Last data set obtained before conclusion of reversal
(c) All intensities are relative to the intensity of mass 83 which is set arbitrarily to 100.

Mass \ Time, Hrs	0	0.1	1.25	2.33	18.5	20.33	21.00[a]	24.00	26.00	42.33	45.00	48.75	50.25	66.00[b]	69.25
35	18.2	-	25.0	13.2	23.8	16.3	12.2	12.1	20.7	51.3	93	55.9	57.6	52.9	47.4
36	34.7	27.3	37.6	43.3	165	50.5	54.3	40.3	85.5	212	224	385	395	376	357
37	6.5	5.1	8.9	4.8	10.2	5.9	4.1	4.9	6.0	16.7	29.5	17.8	19.2	18.7	17.1
38	27.7	19.1	23.1	14.5	52.5	18.0	18.2	15.6	31.5	69.1	72.1	129	135	120	108
48	92.8	-	68.8	48.1	87.8	-	115	163	170	171	238	256	302	146	128
50	6.9	5.9	8.3	2.4	5.0	11.6	6.5	8.6	12.0	10.5	27.5	12.6	6.1	10.2	9.7
64	93.4	-	62.4	65.2	111	-	145	279	292	307	444	565	648	340	320
67	8.5	9.7	11.6	5.9	5.1	6.6	5.1	7.2	8.5	6.8	28.4	12.5	19.2	11.4	13.2
69	0	4.4	4.9	2.5	3.3	2.8	2.7	2.1	3.7	5.0	12.1	4.8	7.0	9.1	9.1
76	9.7	11.9	27.0	9.6	14.3	25.0	16.3	17.3	14.9	13.7	14.7	15.0	7.9	8.6	8.4
78	0.8	1.1	2.4	0.7	1.2	2.6	1.4	1.5	1.1	1.5	1.0	1.1	0.5	0.6	0.7
80	23.8	27.2	23.7	20.6	16.0	19.9	15.9	19.1	22.2	19.8	28.4	31.9	22.0	19.3	20.0
82	2.0	2.5	2.6	2.0	1.3	1.8	2.0	1.6	1.7	1.7	2.5	2.8	1.8	1.5	1.7
83	100	100	100	100	100	100	100	100	100	100	100	100	100	100	100[c]
85	35.6	37.5	37.5	39.0	35.3	38.9	39.1	39.4	44.4	37.6	42.4	39.5	40.0	42.3	38.9
99	0	0	0	0	0	0	0	0	0	2.11	1.39	1.34	1.10	0.77	0.87
101	0	0	0	0	0	0	0	0	0	1.05	0.70	0.58	0.56	0.32	0.40
102	0	0	0	0	0	0	0	0	0	1.95	9.12	7.21	7.21	6.39	4.15
104	0	0	0	0	0	0	0	0	0	1.26	6.60	5.33	5.00	5.05	2.99
106	0	0	0	0	0	0	0	0	0	0.49	1.12	0.94	0.98	1.24	0.71
118	20.0	18.7	19.1	14.6	14.3	15.9	14.2	14.6	15.0	15.3	16.9	14.8	14.6	12.2	14.7
120	13.8	13.1	14.2	11.6	11.0	12.4	10.6	10.6	9.6	11.4	11.4	11.3	11.0	8.9	10.9
122	2.0	2.1	2.1	2.4	2.2	2.0	2.0	2.0	2.1	2.1	2.7	2.0	2.1	2.0	2.0
134	0	0	0	0	0	0	0	0	0	1.43	1.14	1.17	0.67	0.52	0.64
136	0	0	0	0	0	0	0	0	0	0.78	0.80	0.80	0.37	0.34	0.38
138	0	0	0	0	0	0	0	0	0	0.25	0.22	0.21	0.14	0.07	0.07

TABLE 4

Mass spectral intensities for pure SCl_2, $SOCl_2$ and SO_2Cl_2
*Indicates the most intense peak.

Mass	SCl_2	$SOCl_2$	SO_2Cl_2	Mass	SCl_2	$SOCl_2$	SO_2Cl_2	Mass	SCl_2	$SOCl_2$	SO_2Cl_2
30	0	0	0	67	100*	3.44	0.92	104	43.7	0	0
31	0	0	0	68	0.95	0	0	105	0.96	0	0
32	64.4	100*	36.5	69	36.4	1.32	6.27	106	8.60	0	0
33	0	0	0	70	9.72	0	1.27	107	0.91	0	0
34	1.34	1.13	0.93	71	2.71	0	0	108	0	0	0
35	12.1	17.7	6.67	72	5.56	0	1.17	109	0	0	0
36	75.3	91.4	18.7	73	0	0	0	110	0	0	0
37	4.10	6.55	2.76	74	1.03	0	0	111	0	0	0
38	26.2	27.7	9.41	75	0	0	0	112	0	0	0
39	1.92	0	1.46	76	2.54	2.56	2.16	113	0	0	0
40	4.45	7.25	3.58	77	0	0	0	114	0	0	0
41	4.5	0	0.93	78	0	0	0	115	0	0	0
42	1.86	0	1.46	79	1.05	0	0	116	0	0	0
43	1.95	2.23	2.50	80	0	3.00	0	117	0	0	0
44	1.73	2.80	3.63	81	3.63	0.23	0	118	0	3.6	0
45	0	0	0	82	1.30	0	0	119	0	0	0
46	0	0	0	83	3.5	41.5	0	120	0	2.5	0
47	0	0	0	84	0	0	0	121	0	0	0
48	1.74	49.8	53.5	85	1.79	14.5	0	122	0	0.58	0
49	0	0.92	0.93	86	0	0	0	123	0	0	0
50	0	2.81	4.09	87	0	0.62	0	124	0	0	0
51	2.85	0	0.93	88	0	0	0	125	0	0	0
52	2.21	0	0	89	0	0	0	126	0	0	0
53	0	0	0	90	0	0	0	127	0	0	0
54	0	0	0	91	0.96	0	0	128	0	0	0
55	6.69	0	0.90	92	0	0	0	129	0	0	0
56	2.15	0	0	93	1.09	0	0	130	0	0	0
57	5.24	0	0.98	94	0	0	0	131	0	0	0
58	0	0.75	0.91	95	4.76	0	0	132	0	0	0
59	0	0	0	96	1.11	0	0	133	0	0	0
60	0	0.63	0.78	97	3.70	0	0	134	0	0	6.84
61	0	0	0	98	0	0	0	135	0	0	0
62	0	0	0	99	0	0	35.3	136	0	0	5.08
63	0	0	0	100	0	0	1.17	137	0	0	0
64	4.00	31.1	100*	101	0	0	12.9	138	0	0	1.17
65	0	0	2.28	102	67.8	0	0	139	0	0	0
66	0	2.06	7.54	103	0.83	0	1.17	140	0	0	0

4.4 Discussion

For the purpose of this discussion we will assume that the ratio of peak intensities in a mass spectrum is equal to the partial pressure ratio of the species giving rise to these peaks. We realize that this is not strictly correct since pressure calibration constants are needed in order to convert relative intensities into accurate partial pressures. All times reported in this discussion will be given the symbol t and units of hours.

4.4.1 Cl^+, HCl

Intensity versus time profiles for masses 35 through 38 are shown in Figure 86-89 respectively, and numerical data for these masses are entered in Table 3. The peak intensities of mass 35 (Cl^{35+}) and mass 37 (Cl^{37+}) are seen to be essentially constant (within $\pm$ 10%) at times up to t=26 beyond which a sudden increase in their intensities is observed. With reversal occurring at t=21, there exists an induction period of approximately 5 hours. After this induction period an escalating level of chlorine fragments indicates chemical reactions leading to increased levels of chlorine production. The average concentration of Cl^{35+} between t=o and t=26 is calculated to be 17.7% while that between t=42 and t=66 is calculated to be 62.1%. These values are obtained from averaging intensities of mass 35 between the specified times listed in Table 3. Thus a 3.6 fold increase is seen in the concentration of Cl^{35+} fragments during the reversal process for the anode-limited $Li/SOCl_2$ cell.

Similar observations can be made regarding Cl^{37+} isotope fragments. The ratio just calculated for mass 35 is repeated for mass 37. This is the ratio of the average concentration of Cl^{37+} from t=42 through t=66 and the average concentration of this same species (Cl^{37+}) from t=o through t=26, and is calculated to be 3.2. Comparing these two results, it is seen that Cl^{35+} and Cl^{37+} concentrations have increased between 3.2 and 3.6 fold on or after t=42. The maximum concentration of both of these species occurs at

approximately t=50.25. The ratio of the average intensity of Cl^{35} to Cl^{37} is calculated from our data to be 35.69/11.69 or 3.05 $\pm$ 0.3 while the isotope abundance of Cl^{35}/Cl^{37} is given by 75.53/24.47 or 3.09. Thus our result agrees well with the reported values of chlorine isotope abundance.

For masses 36 and 38 (HCl^{35+} and HCl^{37+}, respectively), the increase in their relative intensities is seen to begin about the same time as does the increase in chlorine fragment intensities, namely at t=26. Thus the induction period for HCl is approximately 5 hours and is similar to the induction period of chlorine fragments. Also the maximum concentration of both of the HCl^{+} species occurs at approximately t=50.25, the same time at which chlorine fragment concentrations are seen to reach their maxima. For HCl^{35+} the ratio of the average concentration on and beyond t=26 to that below t=26 is calculated to be 4.9 while this ratio for HCl^{37+} is found to be 3.9. Thus an increase of HCl^{+} concentration between 3.9 and 4.9 fold is seen during the voltage reversal stage of the anode-limited $Li/SOCl_2$ battery.

Considering the tabulated data (Table 3) we observe a noncharacteristic pulse in both Cl^{+} and HCl^{+} concentrations at time t=18.5 (see Figure 86-89). This pulse can arise from either a true surge of these species in the system or it can be attributed to unresolved experimental variables. Additional experimental work should be performed to resolve this point.

It is interesting to note that the HCl concentration is generally higher than the chlorine concentration in this system. The ratios of the average HCl concentration to the average chlorine concentration before and after an induction period of 5 hours are 3.2 and 5.1 for Cl^{35+} and HCl^{35+} respectively and 3.8 and 5.2 for Cl^{37+} and HCl^{37+} respectively. A few remarks need to be made about these numbers.

First the existence of both HCl^{35+} and HCl^{37+} in higher concentrations than Cl^{+} concentration implies the existence of a substantial source of hydrogen in the $Li/SOCl_2$ system. McDonald (16) observed that hydrogen gas is

one of the sources of pressure generated during normal discharge of $Li/SOCl_2$ batteries. He also postulated that water-contaminated electrolyte can give rise to the source of hydrogen in these batteries. Additional hydrogen sources may include the highly porous carbon cathode. Experiments leading to the characterization of cathode surfaces should be performed in order to reveal the role of these surfaces as gas adsorbers.

Second, although McDonald (15) was unable to detect either Cl^+ or HCl^+ in his mass spectrometric discharge-only study, we believe that this was due to difficulties in detecting these species with indirect sampling procedures. A number of investigators (11, 12) have reported the presence of chlorine species in the $Li/SOCl_2$ system. Our results outlined above clearly show that HCl is formed during both discharge and reversal in this system.

Third, we observe that the ratio of the HCl^{35+} concentration to the HCl^{37+} concentration corresponds within experimental errors to the isotopic abundance ratio of Cl^{35} to Cl^{37}.

Fourth, the increase in HCl concentration is larger (5.1-5.2 fold) during reversal than the concentration rise (3.2-3.8 fold) for Cl^+ species. This last observation indicates that during reversal, hydrogen-chlorine reactions leading to the formation of HCl are more favorable than during normal discharge of the anode-limited $Li/SOCl_2$ cell.

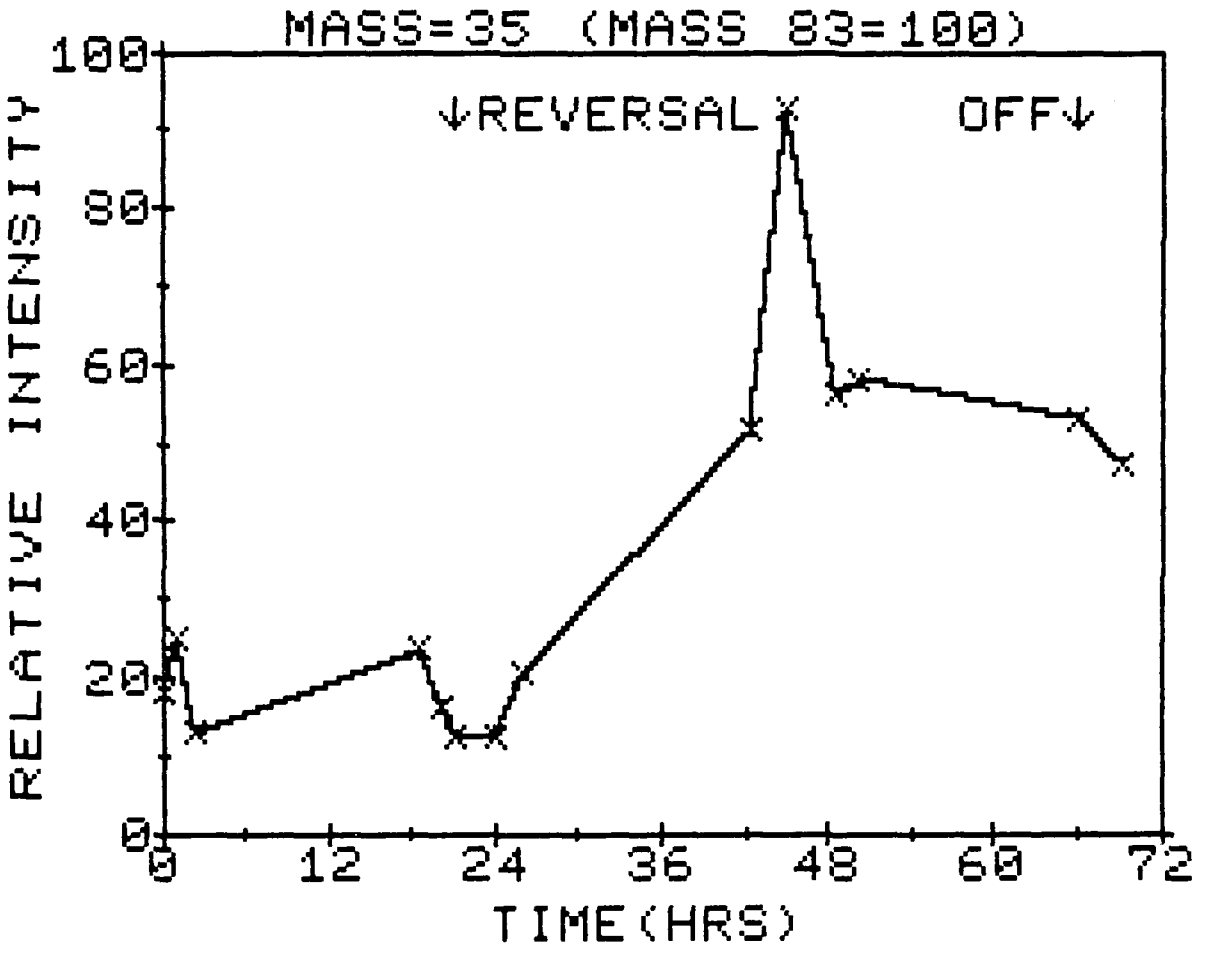

Figure 86. Mass 35 (C_{35}) vs. Time (Hrs.)

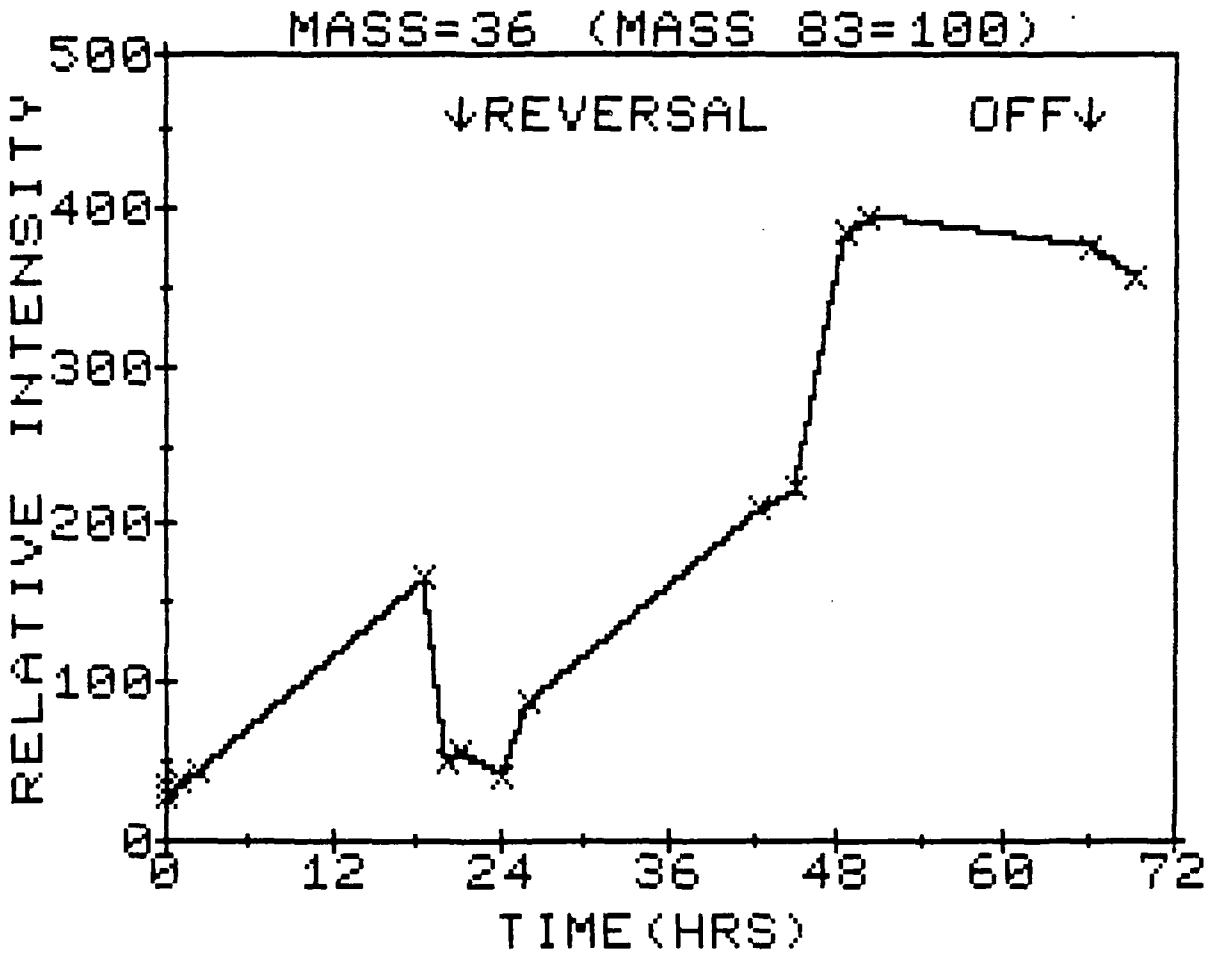

Figure 87. Mass 36 (HCl^{35}) vs. Time (Hrs)

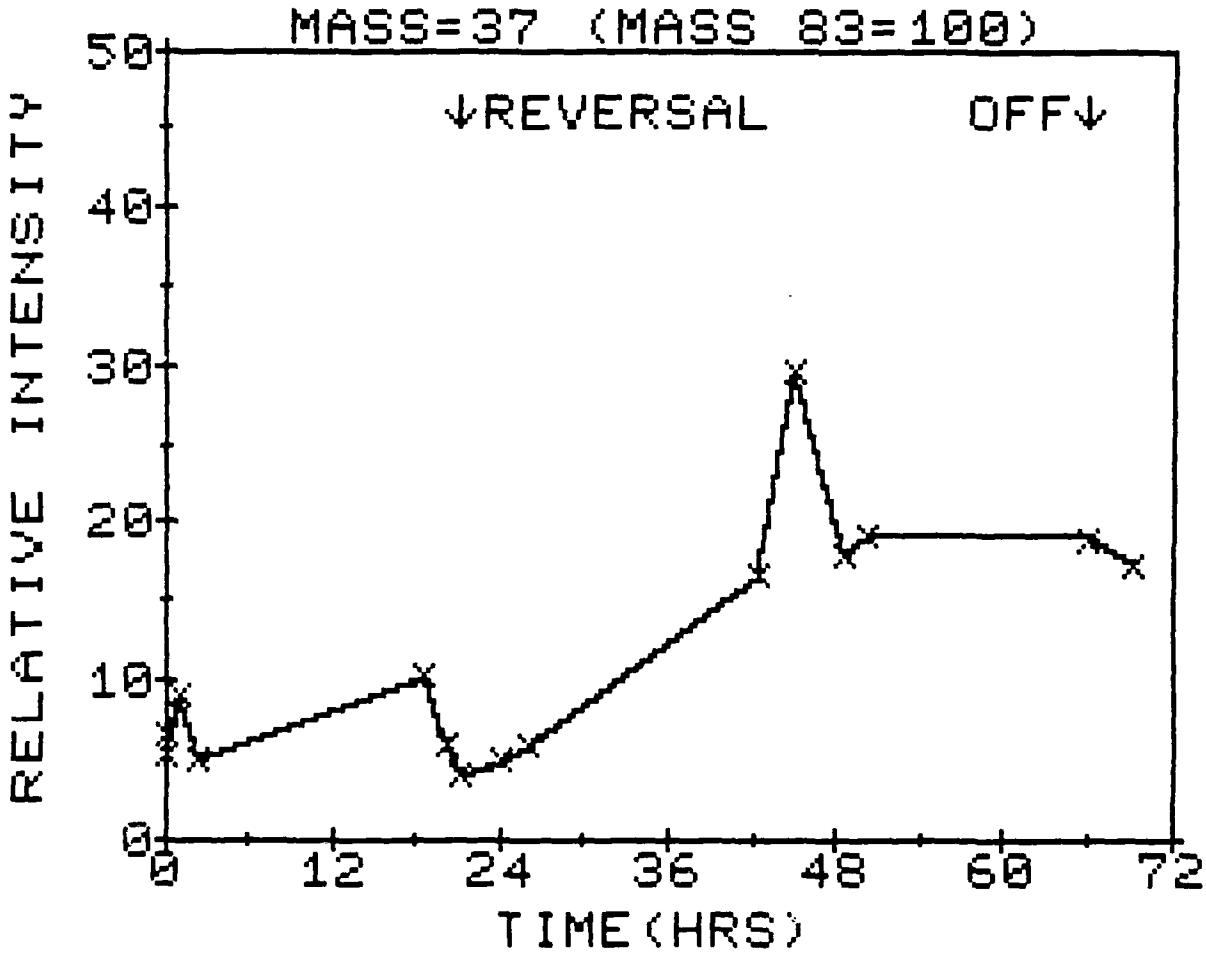

Figure 88. Mass 37 (Cl^{37}) vs. Time (Hrs.)

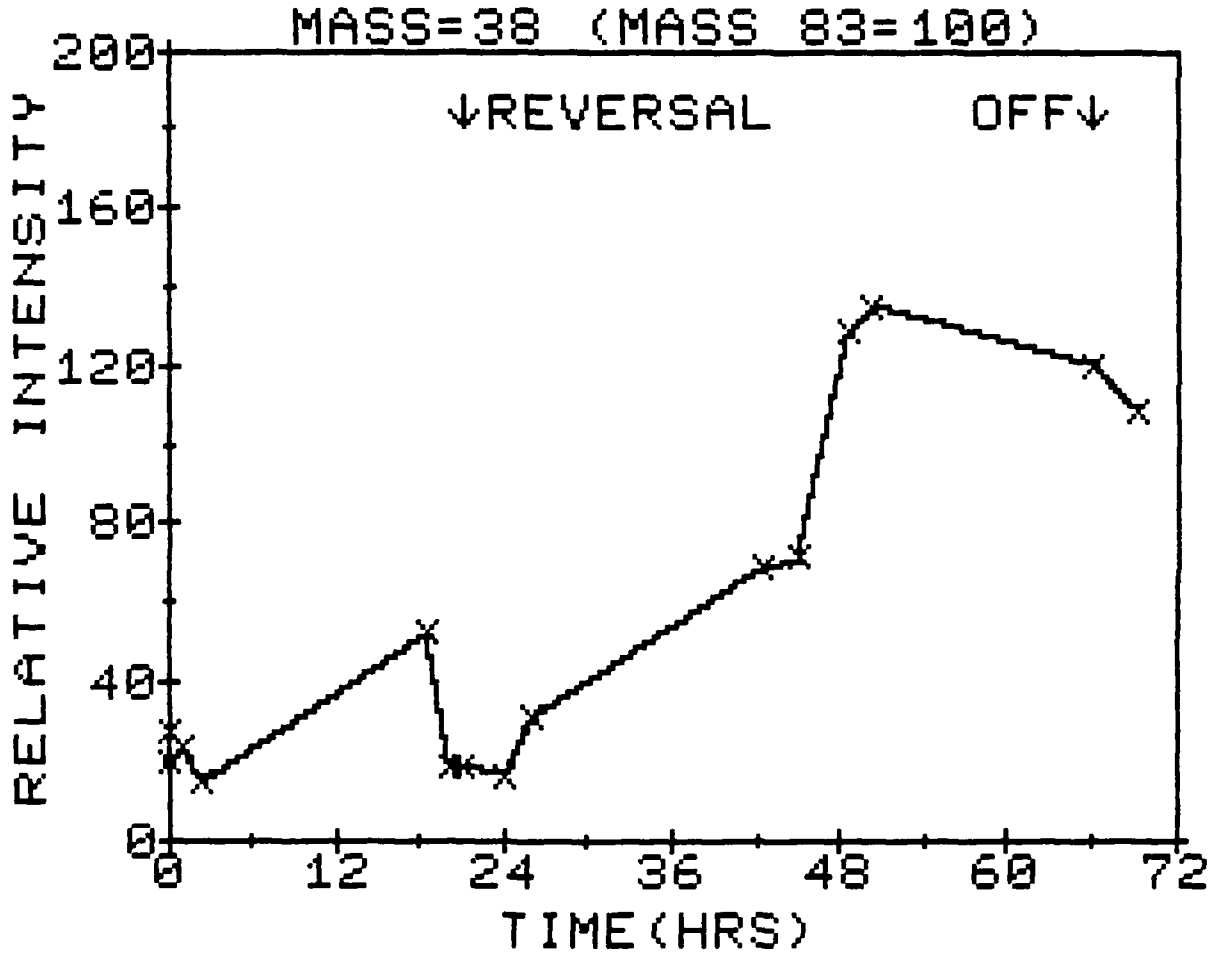

Figure 89. Mass 38 (HCl^{37}) vs. Time (Hrs.)

4.4.2 SO_2, SO^+

Data for the relative intensities of masses 64 and 48 are contained in Table 3 and plots depicting this data are shown in Figure 90 and 91 respectively. Unlike Cl^+ and HCl^+ the intensities of masses 64 (SO^+_2) and 48 (SO^+) begin to increase early in the discharge stage and continue to rise at a faster rate in the reversal mode. The SO^+_2 intensity achieves the highest level of any species during reversal. Our data indicate that the maximum intensity of SO_2^+ occurs at t equal to 50 which is approximately the time at which both Cl^+ and HCl^+ reach their maxima. This is approximately 29 hours after the onset of the voltage reversal in the anode-limited $Li/SOCl_2$ cell.

Examination of the tabulated data for SO_2^+ and for SO^+ yields interesting trends. If the data for these masses are plotted on the same figure and on the same intensity scale, Figure 92 results. This figure clearly shows that the SO^+ intensity-time profile correlates well with the SO_2^+ intensity-time profile. The most interesting feature of this plot is that the SO_2^+ rate of increase is larger than the corresponding rate for the SO^+ fragment intensity.

To illustrate this point we plot the difference in relative intensities of SO_2^+ and SO^+. Let I_{SO2} denote the intensity of SO_2^+ and I_{SO} denote the SO^+ intensity. A plot of $(I_{SO2}-I_{SO})$ versus time is shown in Figure 93. Inspection of this figure shows that the difference in concentration between SO_2^+ and SO^+ fragments increases rapidly after the onset of reversal reaches a maximum and then levels off. Another representation is shown in Figure 94 where the ratio I_{SO}/I_{SO2} is plotted versus time. It is interesting to note that this ratio for pure SO_2 is approximately 0.5. Thus it is seen from Figures 92-94 that the SO^+ intensity in the discharge mode is higher than that accounted for by SO_2 fragmentation alone. Upon reversal the SO^+/SO_2^+ ratio decreases and approaches its limiting value predicted by SO_2 fragmentation alone.

It is clear from the foregoing analysis that during discharge SO^+ intensity results from at least two major contributions. The first is from fragmentations of the SO_2 present in the system, and a second arises from fragmentation of the $SOCl_2$. However, as the cell is brought into reversal, the SO_2 concentration increases and SO_2 fragmentation becomes the major source of SO^+ production in the ion source. It is also worth noting that the average concentration of SO_2 on or after t=26 in the reversal mode is 3.4 times that before t=26.

In summary, our data suggest that mass 48 ions are produced by fragmentation in the electron impact ionization event. There is no strong evidence to postulate that either SO or SO^+ travels from the battery through the sampling system and into the ion source. McDonald's data (16) regarding the SO_2^+, SO^+ pair is puzzling. Although his study spanned only the discharge stage of anode-limited $Li/SOCl_2$ cells, his findings are contradicted by our data. We have clearly shown that SO^+ fragments arise from more than one source, namely SO_2 and $SOCl_2$, during the discharge mode. McDonald suggests however that no SO^+ was detected in his mass spectrometric study. Although SO species in battery electrolytes cannot be detected mass spectrometrically, the role of SO as an intermediate is discussed by a number of investigators including Schlaikjer et al. (10), Bowden and Dey (21) and Salmon and Ramsay (22).

The foregoing analysis of the data obtained here shows that SO^+ is a fragment formed in the ionization of SO_2 (g) and $SOCl_2$ (g) during discharge and to a much greater extent from SO_2 during reversal of the anode-limited $Li/SOCl_2$ cell.

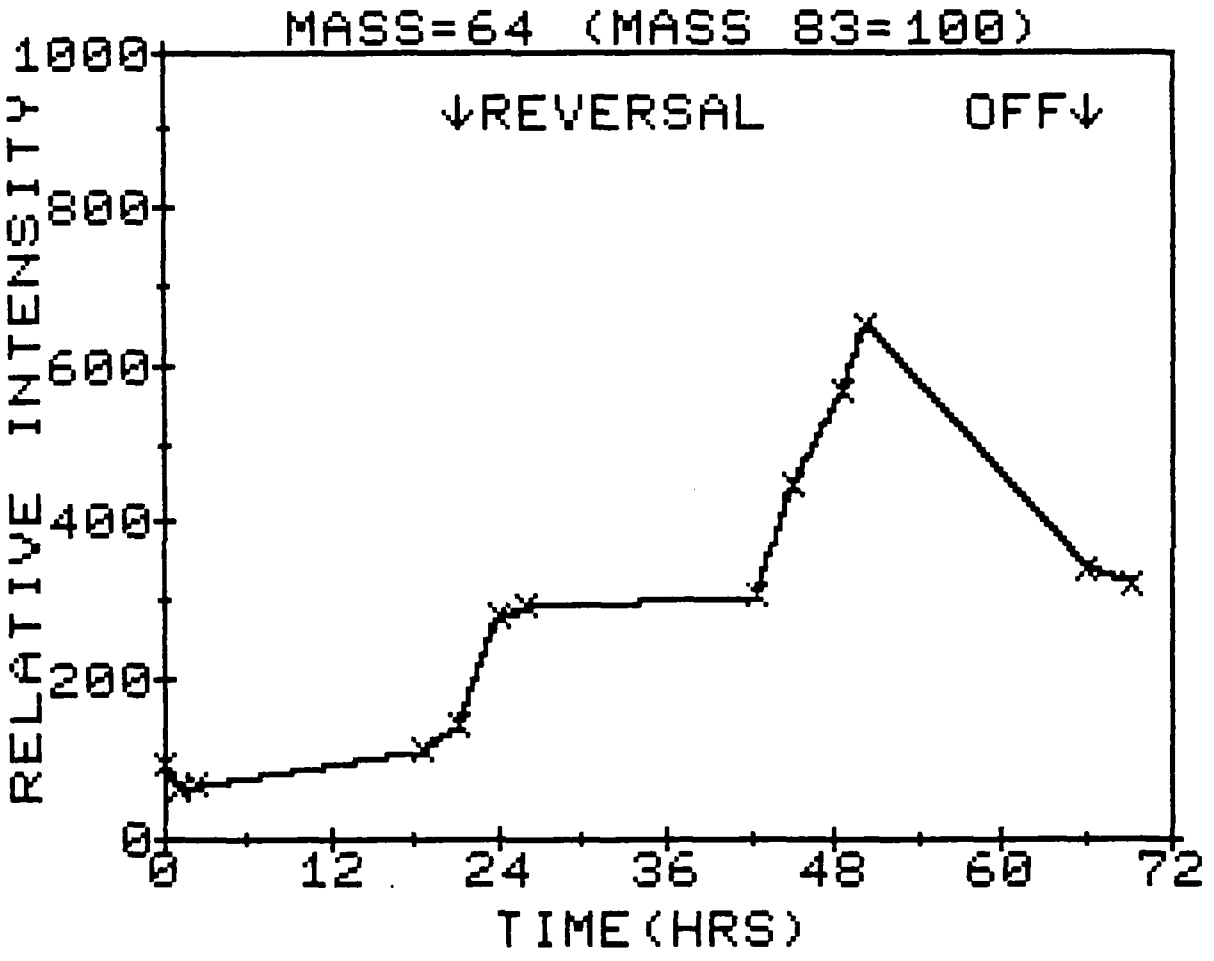

Figure 90. Mass 64 (SO_2) vs. Time (Hrs.)

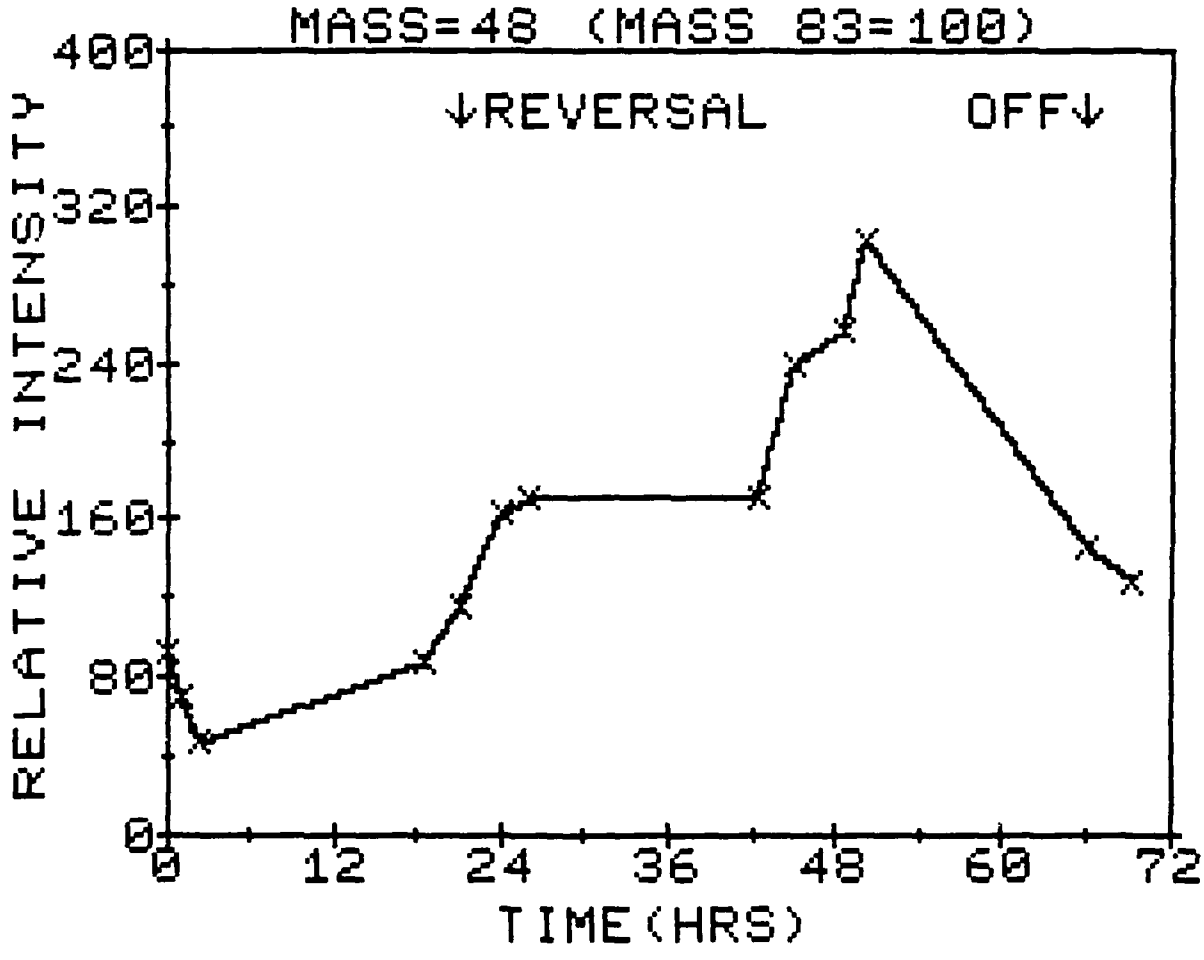

Figure 91. Mass 48 (SO^+) vs. Time (Hrs.)

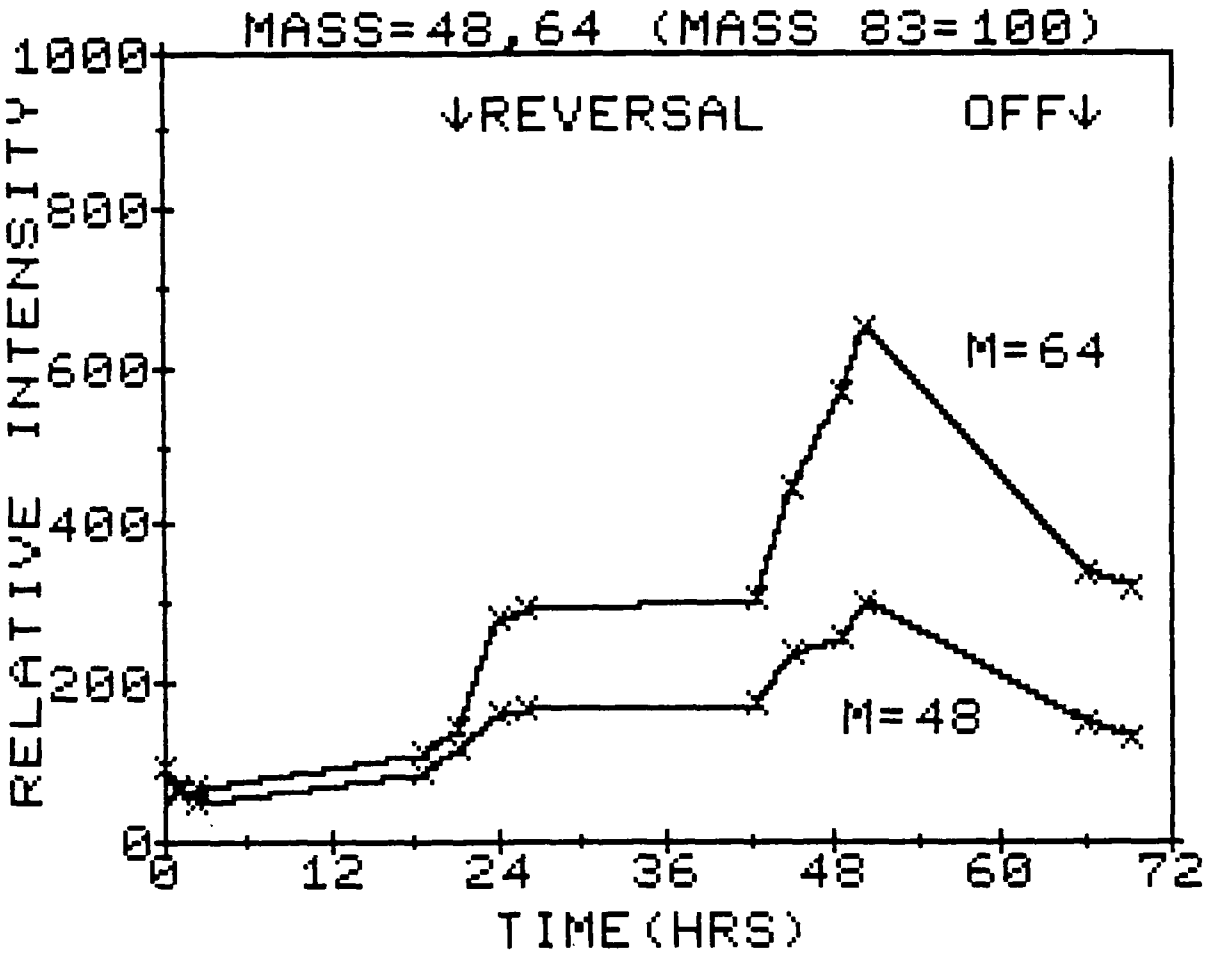

Figure 92. Mass 48 and 64 (SO^+ and SO_2) vs. Time (Hrs.)

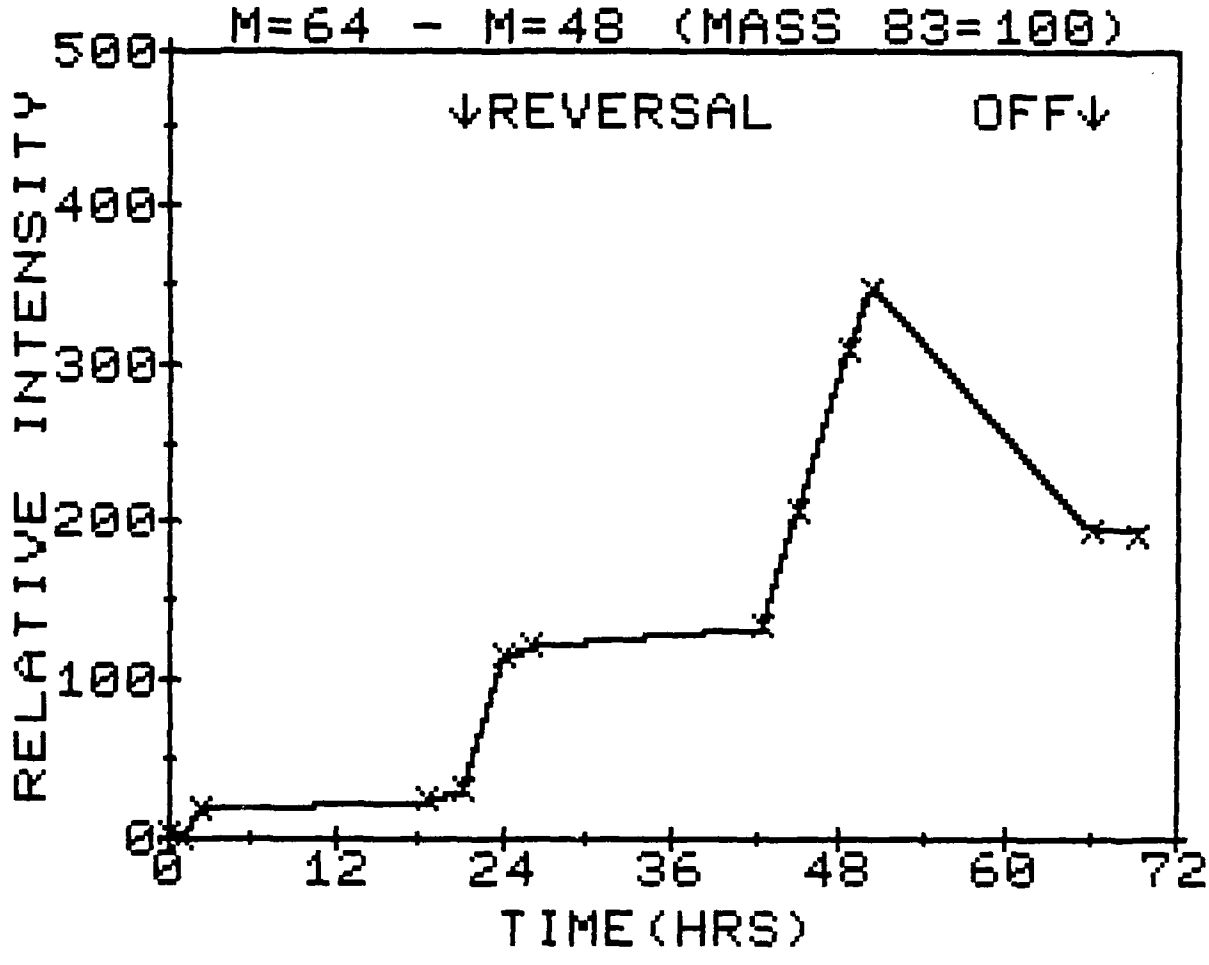

Figure 93. Mass 64 (SO_2) - Mass 48 (SO^+) vs. Time (Hrs.)

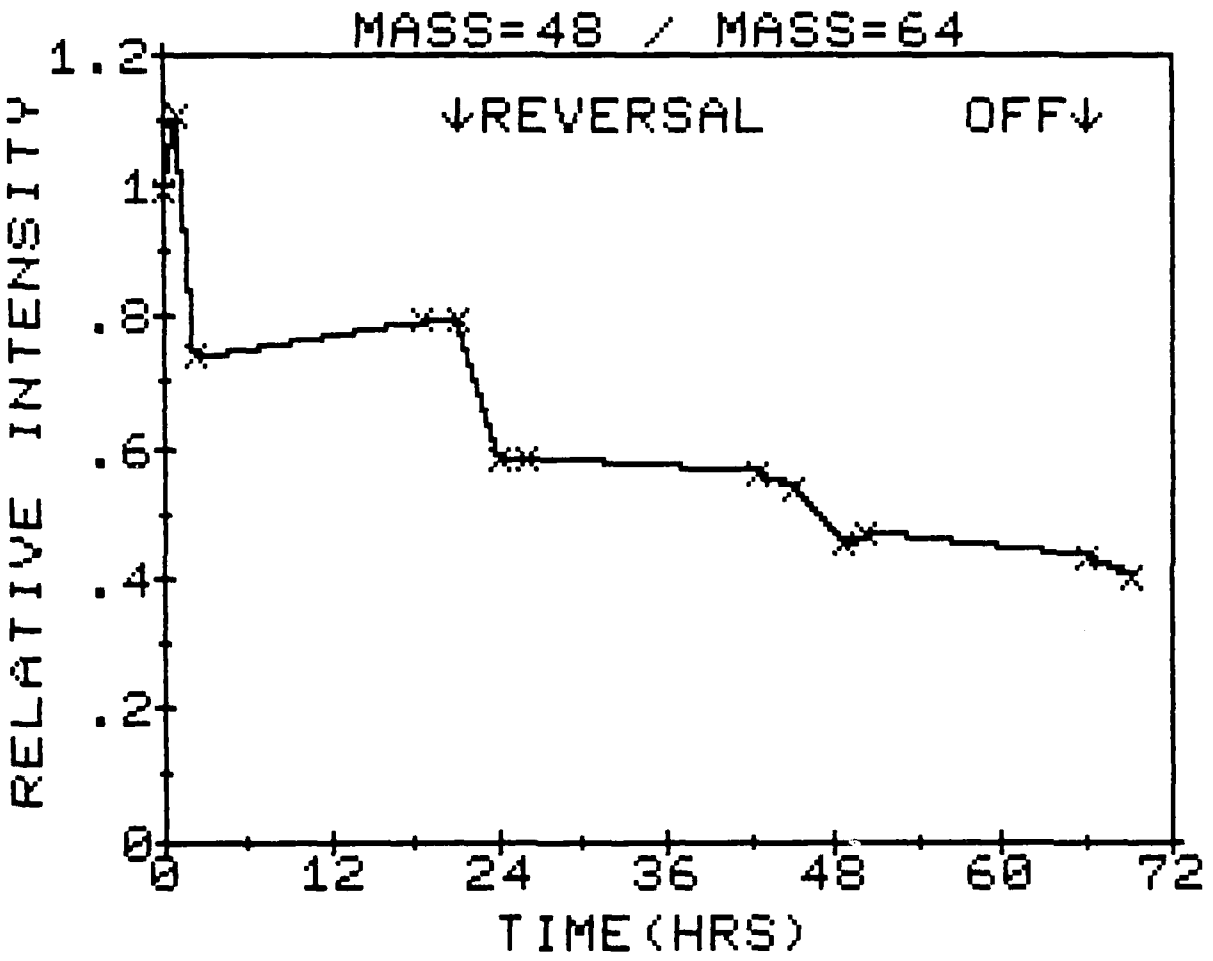

Figure 94. Mass 48 (SO^+)/ Mass 64 (SO_2) vs. Time (Hrs.)

4.4.3 CS_2, S_2O

Mass spectrometric data obtained for nominal masses 76, 78, 80 and 82, and accurate mass measurements for masses 76 and 80 indicate the presence of carbon disulfide and disulfur monoxide in the anode-limited $Li/SOCl_2$ cell tested. Numerical intensity versus time data for these masses are listed in Table 3. Plots for mass pairs 76, 78 and 80, 82 are shown in Figure 95 and Figure 96 respectively. From these graphs it can be seen that the concentrations of both CS_2 and S_2O relative to the $SOCl_2$ concentration show little variation with time. Since the abundance of S^{34} is 4.22%, we expect that the ratio of the peak intensity of mass 78 (CS_2^{34+}) to that of mass 76 (CS_2^{32+}) to be close to 8.88%. (See the attached appendix for the method of calculations.) The same holds true for the ratio of peak intensity of mass 82 ($S_2^{34+}O^+$) to that of mass 80 ($S_2^{32}O^+$). The average intensity of mass 78 is calculated from the data in Table 3 to be 1.21% and that for mass 76 to be 14.29% of nominal mass 83. Thus the ratio of mass 78 intensity expressed in percent of that of mass 76 is 8.5 $\pm$ 0.8%. In addition our accurate mass measurement for nominal mass 76 yielded the mass 75.94528 $\pm$ 20 ppm. With the atomic weights of C^{12} and S^{32} given by 12.00000 and 31.97207 respectively, the theoretical exact mass for CS_2^{32} is 75.94414. This indicates that within the experimental errors nominal mass 76 detected in the anode-limited $Li/SOCl_2$ battery arises from CS_2^{32+}.

Analogous treatments are carried out for masses 80 and 82. The average intensity of mass 82 is calculated from the data presented in Table 3 to be 1.97% and the average intensity of mass 80 is similarily calculated to be 21.99%. Thus the ratio of mass 82 intensity to that of mass 80 equals 8.96 $\pm$ 0.9%. Our accurate mass measurement for nominal mass 80 yielded the mass 79.94057 $\pm$ 20 ppm. With the atomic weight reported for O^{16} of 15.99491, the exact mass of $S_2^{32}O^{16+}$ is 79.93905. These results indicate that within the experimental errors the nominal mass 80 arises from S_2O.

In a mass spectrometric study (23) carried out by Meschi and Myers the

authors identified both S_2O and CS_2 as products of a discharge tube reaction between elemental sulfur and sulfur dioxide. Thermal decomposition of thionyl chloride was shown to yield S_2O as a product. It is worth noting that altnough gaseous sulfur is not detected in our present mass spectrometric study, elemental sulfur was reported to be formed in the condensed phase of the $Li/SOCl_2$ system (10). Since our data clearly show that S_2O is formed in this battery system, we conclude that the conditions for S_2O formation in the $Li/SOCl_2$ battery are favorable.

It is perhaps worth noting that the intensity ratio $CS_2^{32+}/S_2^{32}O^+$ from the Meschi and Myers data is 0.73 whereas our data yield 0.65 $\pm$ 0.07 for this same ratio. It is also interesting to note that both nominal masses 76 and 80 (see Table 4 and Figure 121) appear in the spectrum of pure thionyl chloride. The ratio of intensities of mass 76 to that of mass 80 is 0.85 $\pm$ 0.09. Although accurate mass measurements for these two nominal masses were not obtained in the pure $SOCl_2$ spectrum the data suggest that some S_2O and CS_2 may be present in "pure" samples of thionyl chloride. This question of purity should be investigated more thoroughly.

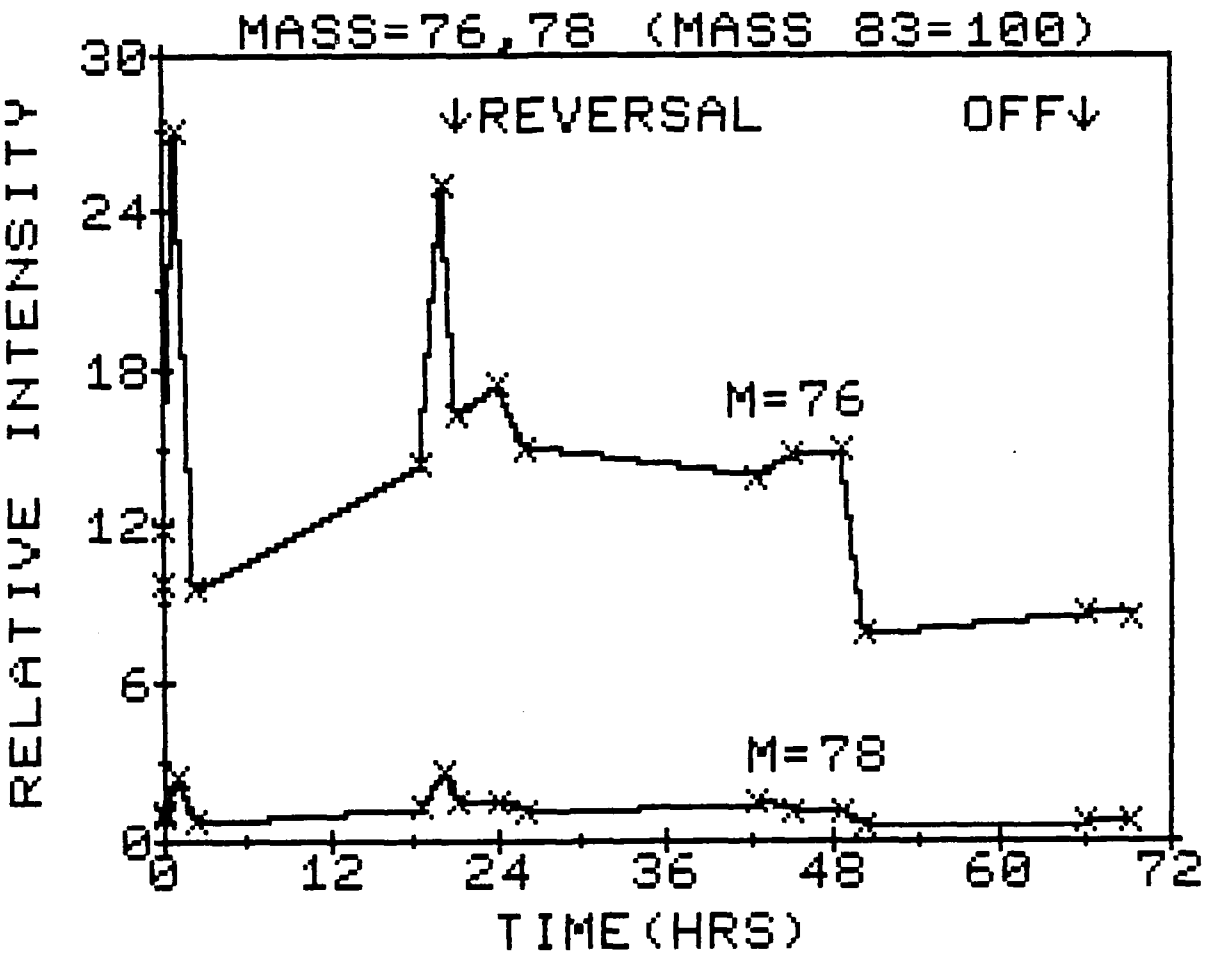

Figure 95. Mass 76 and 78 (CS_2) vs. Time (Hrs.)

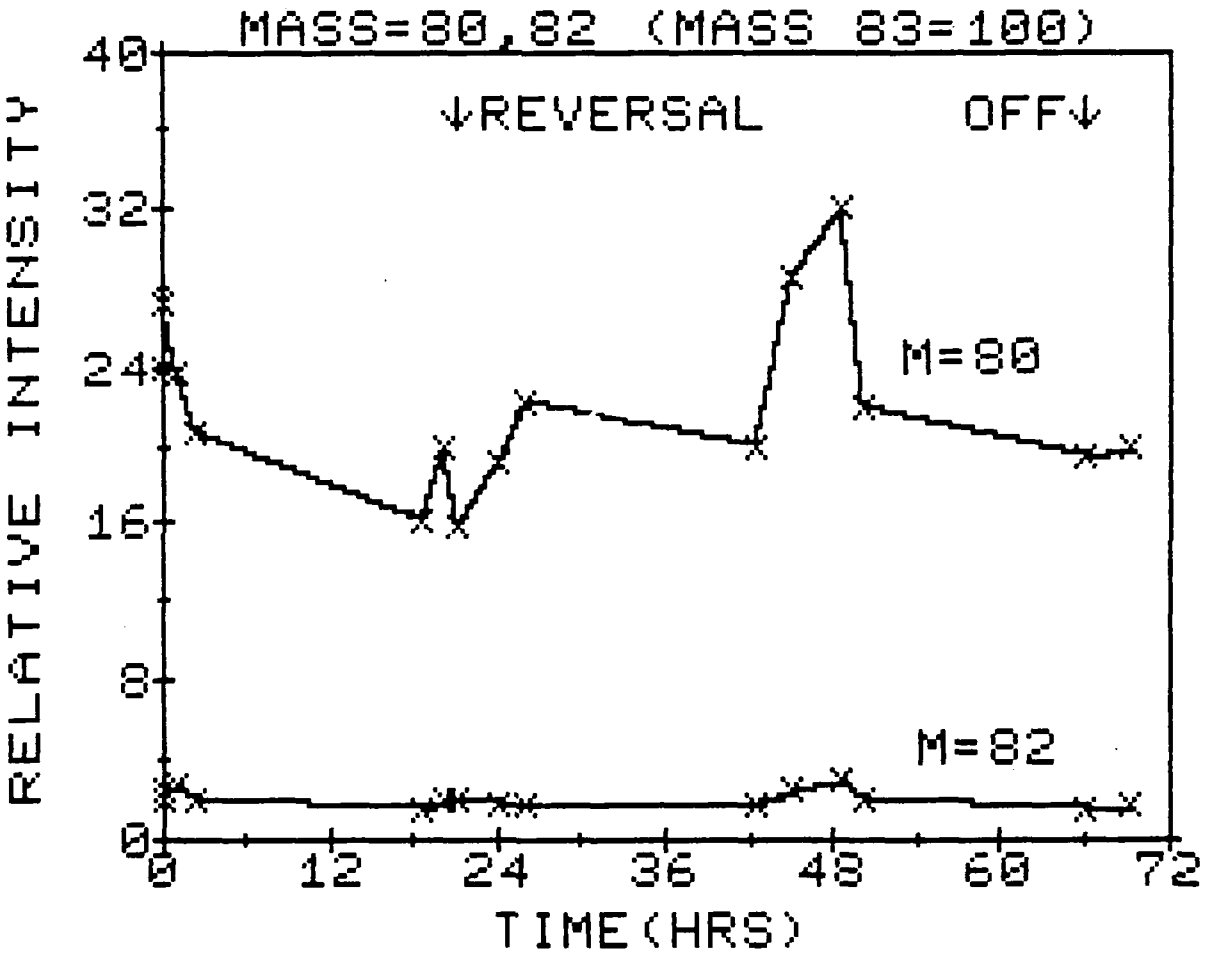

Figure 96. Mass 80 and 82 (S_2O) vs. Time (Hrs.)

4.4.4 $SOCl_2$, $SOCl^+$

The intensity data for the in-situ experiment were normalized to the intensity of mass 83 ($SOCl^{35+}$). The data for $SOCl_2^+$ and $SOCl^{37+}$ are listed in Table 3, and intensity versus time plots for $SOCl_2^+$ (118, 120, 122) and $SOCl^{37+}$ (85) are shown in Figures 97-100, respectively. Figure 101 illustrates the parent peaks of $SOCl_2$ at masses 118, 120 and 122. Now, since $SOCl^{35+}$ was chosen in this present study as a reference peak, and since it ($SOCl^{35+}$) arises from $SOCl_2$ (see pure thionyl chloride spectrum in Figure 121) constant concentrations of both $SOCl_2^+$ and $SOCl^{37+}$ will be expected. We realize that this normalization assumes constant $SOCl_2$ concentration throughout the in-situ experiment. However, the data obtained for $SOCl_2$ and for $SOCl^{37+}$ have been used to calibrate the uncertainty bounds in the intensity data. Since no information is available from this study on the change of $SOCl_2$ concentration with time further experimental modifications are needed in order to normalize subsequent data to a known pressure of an inert species.

With isotopic abundances for Cl^{35} and Cl^{37} of 75.53% and 24.47% respectively and for S^{32} and S^{34} of 95.00% and 4.22% the theoretical $SOCl_2$ intensities for masses 120 and 122 relative to mass 118 are 0.692 and 0.135 respectively (see Appendix for method of calculation).

The experimental results derived from the data in Table 3 yield $SOCl_2$ intensities for masses 120 and 122 relative to mass 118 of 0.731 $\pm$ 0.08 and 0.135 $\pm$ 0.03. These results are consistent with their theoretical counterparts within the experimental errors.

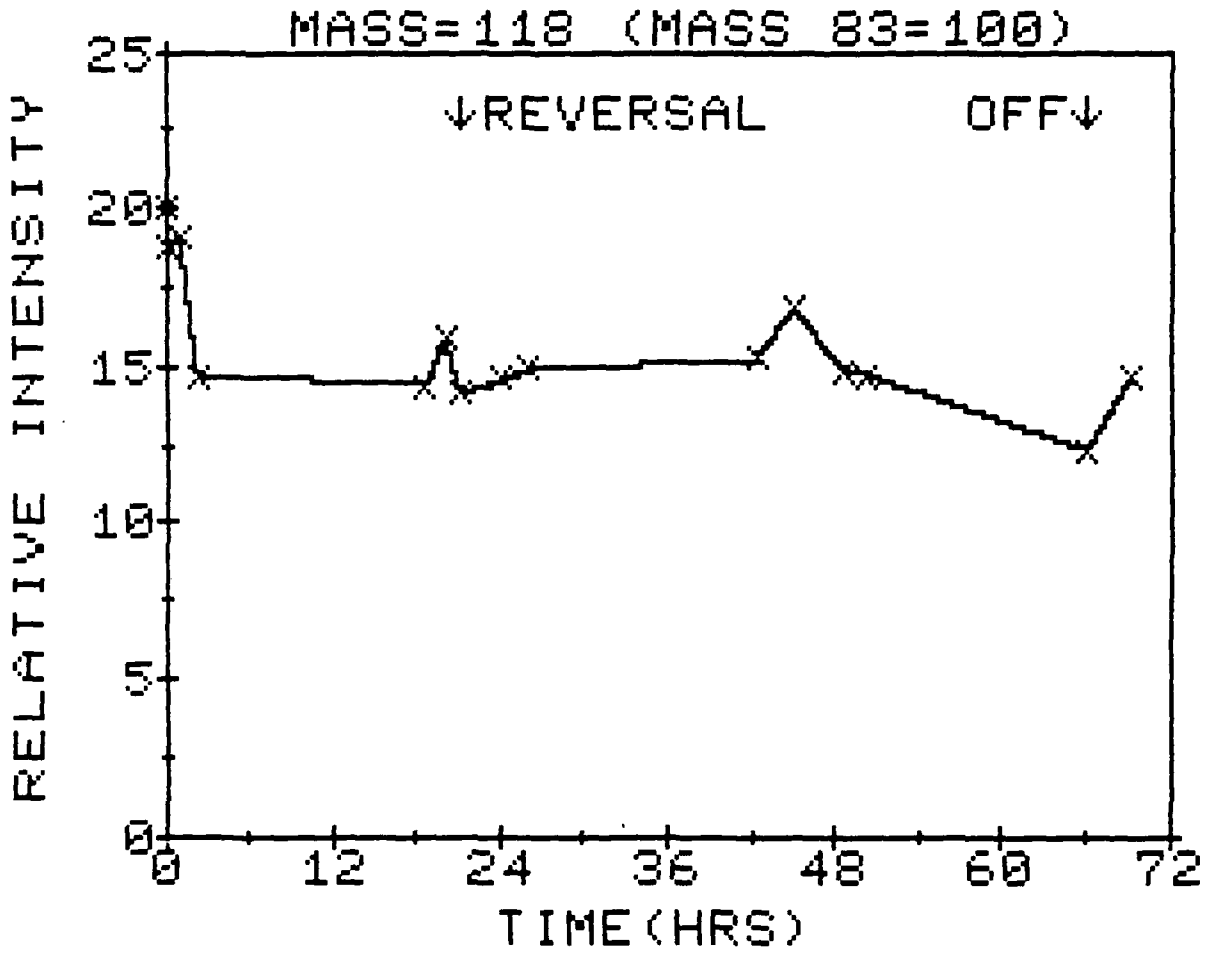

Figure 97. Mass 118 ($SOCl_2$) vs. Time (Hrs)

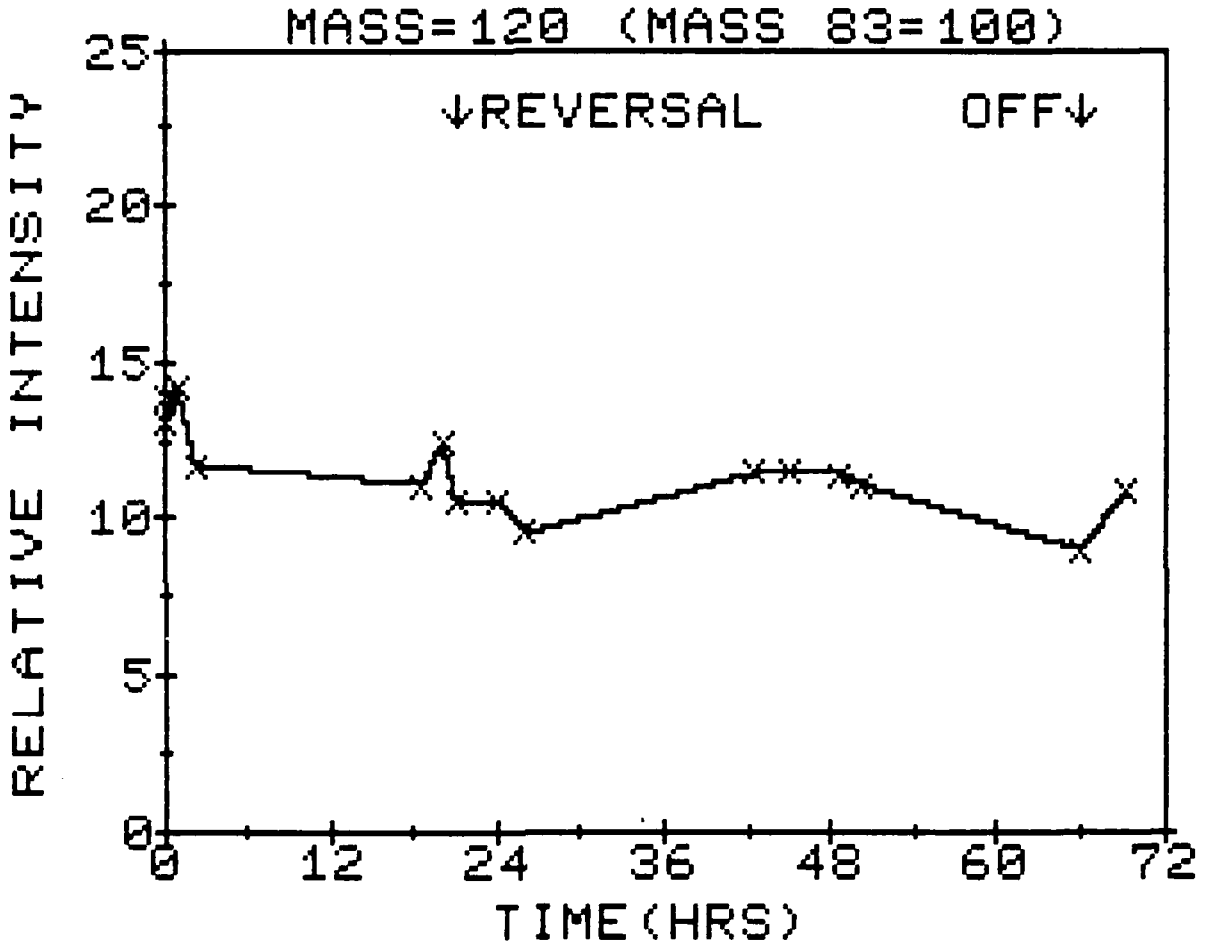

Figure 98. Mass 120 ($SOCl_2$) vs. Time (Hrs.)

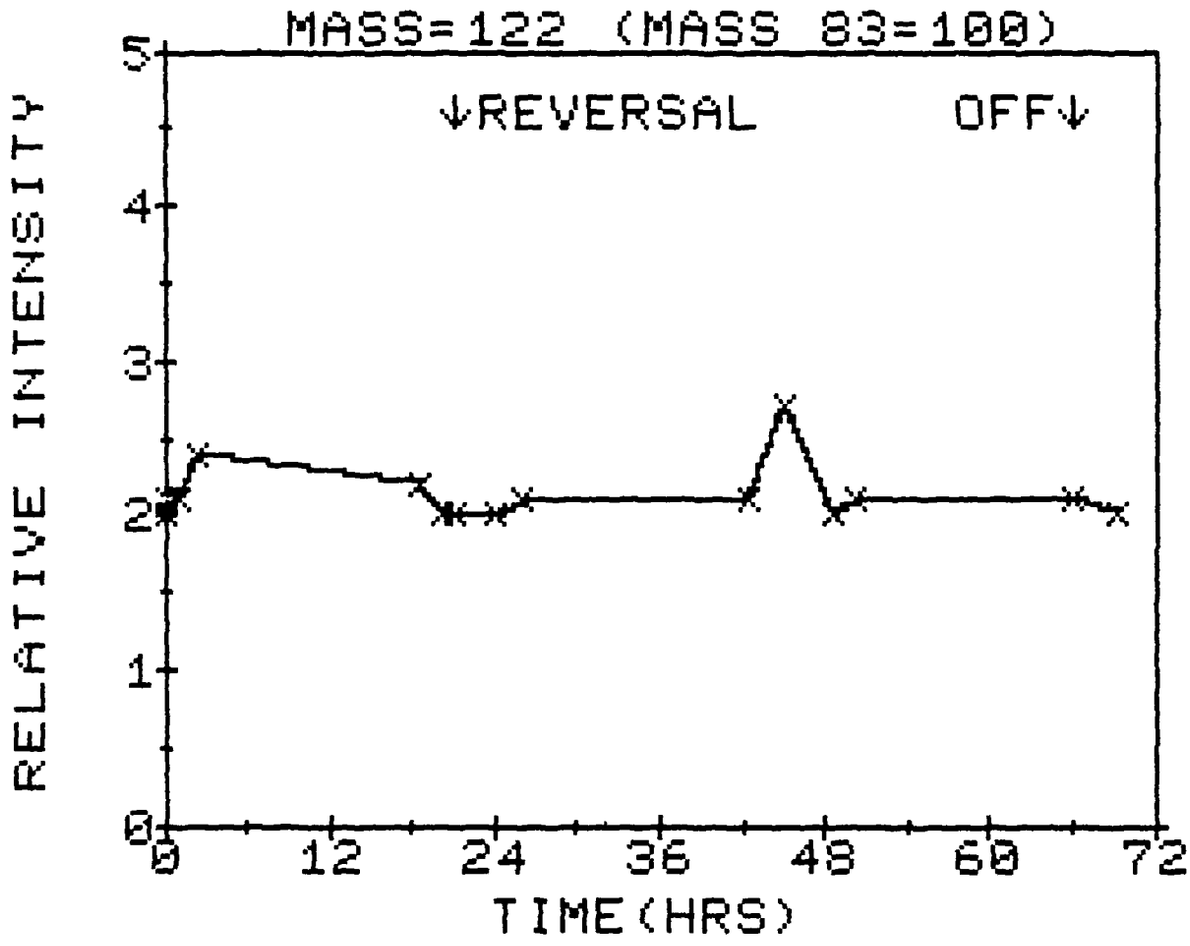

Figure 99. Mass 122 ($SOCl_2$) vs. Time (Hrs.)

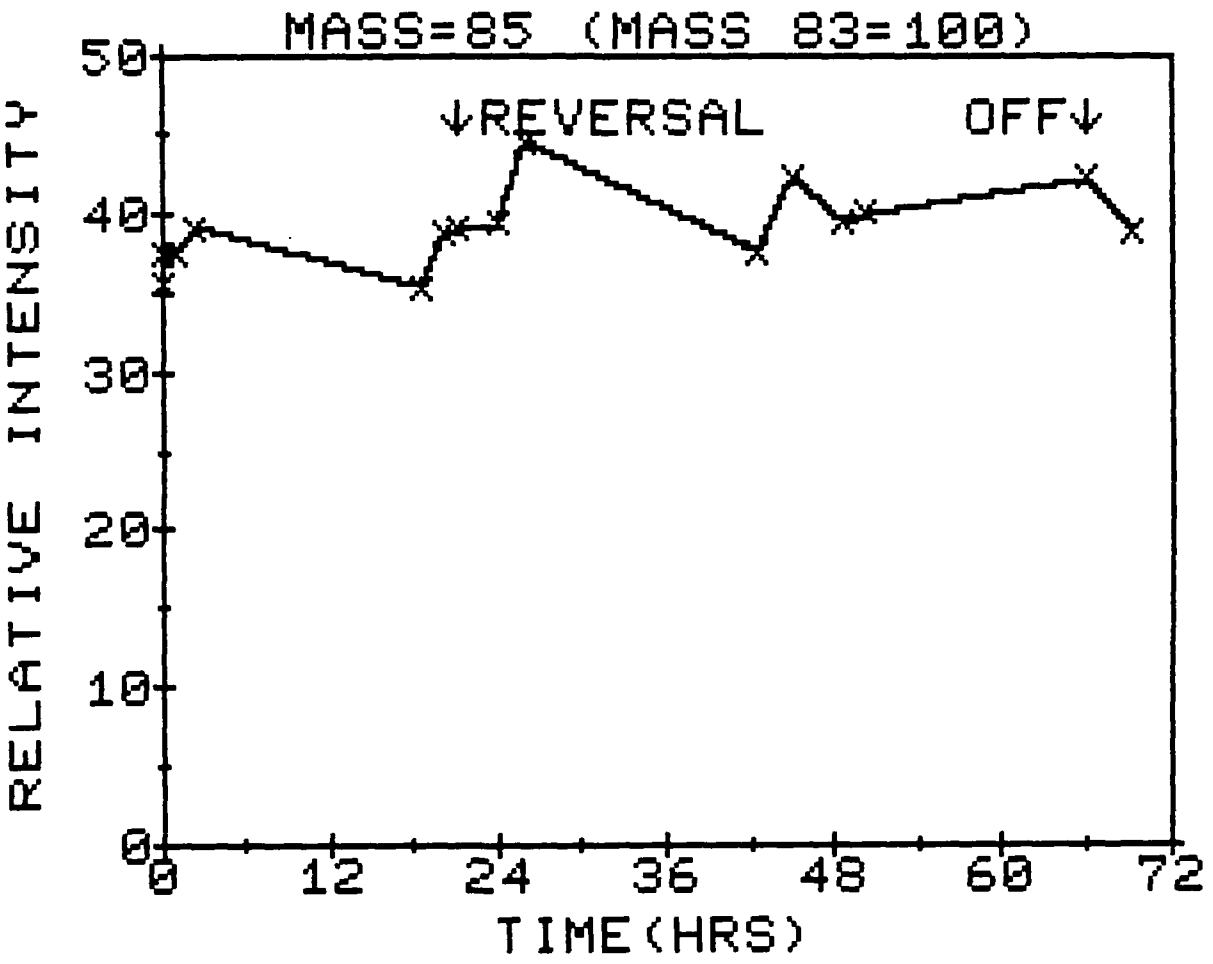

Figure 100. Mass 85 ($SOCl^+$) vs. Time (Hrs.)

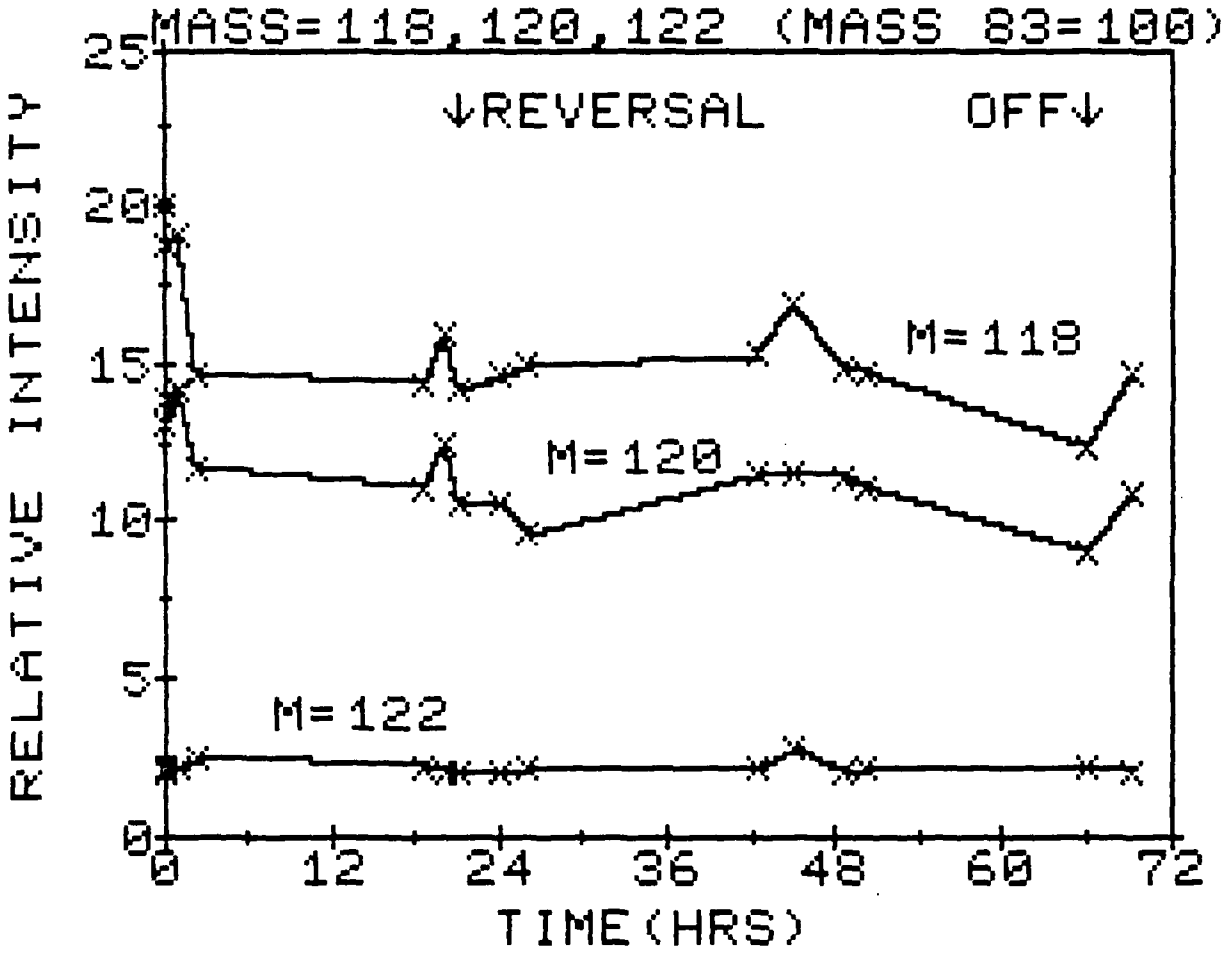

Figure 101. Mass 118, 120 and 122 ($SOCl_2$) vs. Time (Hrs.)

4.4.5 SCl_2, SCl^+

The data for the mass triplet 102, 104, 106 are contained in Table 3 and the intensity versus time data are plotted as shown in Figures 102-105. The most interesting feature about this mass triplet is observed in Figure 105. This figure clearly shows that masses 102, 104 and 106 appear only during the reversal mode. The exact time at which these masses appear in the spectrum cannot be determined from our present data. However, an induction period in the reversal mode of approximately 5 hours precedes the formation and subsequent appearance of these masses. This induction period is found to coincide with the induction periods for Cl^+, HCl^+, discussed earlier in section 4.4.1. The maximum intensity of masses 102, 104 and 106 is reached at approximately t=45, which is about 5 hours earlier than the time at which Cl^+, HCl^+, SO^+ and SO_2^+ reach their maxima during the reversal regime. Beyond t=45 the intensities of these masses gradually decline and then remain at a significant level at the conclusion of our experiment at t=69.25.

The intensities of masses 104 and 106 relative to the intensity of mass 102 are calculated from our data to be 0.728 $\pm$ 0.08 and 0.152 $\pm$ 0.02, respectively. Comparing these results with the theoretical isotopic abundances for the intensities of mass 102, 104 and 106 for pure SCl_2 gives the corresponding values of 0.692 and 0.135. Thus our data show that masses 102, 104 and 106 arise from SCl_2 formed during the reversal mode, beyond t=26.

Next we wish to investigate the species giving rise to masses 67 and 69. Intensity measurements for these masses are contained in Table 3 and plotted in Figure 106 and 107, respectively. As seen from the fragmentation pattern of SCl_2 (Table 4), mass 67 (SCl^{35+}) is the most intense fragment and the intensity of mass 69 (SCl^{37+}) is 0.364 of that of mass 67. Thus both 67 and 69 fragments can arise from SCl_2 fragmentation. However since no SCl_2 is detected at and prior to t=26, then the intensities measured for masses 67 and 69 at and prior to t=26 do not arise from SCl_2 fragments. This result also implies that species other than SCl_2 give rise to masses 67 and 69 in the

anode-limited Li/$SOCl_2$ cell. Although S_2Cl_2 (S_2Cl_2, mass triplet 134, 136, 138, will be discussed in Section 4.4.6) can give rise to fragments of masses 67 (SCl^{37+}), 99 (S_2Cl^{35+}) and 101 (S_2Cl^{37+}), we observe no intensities of any of the masses 134, 136, 138, 99 and 101 at and prior to t=26. Thus as for the case of SCl_2, S_2Cl_2 does not give rise to fragments of masses 67 and 69 at and prior to t=26 for the anode-limited Li/$SOCl_2$ battery tested in the present study. It is important to note that chlorine dioxide (ClO_2, mass 67, 69) can give rise to these masses. Theoretical isotopic abundance considerations yield mass 69/mass 67 ratio of 24.47/75.53 or 0.324. Our data for masses 67 and 69 at and prior to t=26 show that the average mass 69/mass 67 intensity ratio is 0.39 $\pm$ 0.04. This result is seen to neither confirm nor rule out ClO_2 as species giving rise to masses 67 and 69. However since chlorine dioxide is known to be an explosive species (24), and since a study (11) by Salmon et al. indicates that both Cl_2O and ClO_2 are possible products in the anode-limited battery we suggest a careful study to positively identify the species giving rise to the appearance of masses 67 and 69 during both discharge and reversal of this system. It is also noteworthy that the absence of both parent (86, 88, 90) peaks and fragments (51, 53) in the mass spectrum strongly suggests that Cl_2O is not present in measurable concentration in this system.

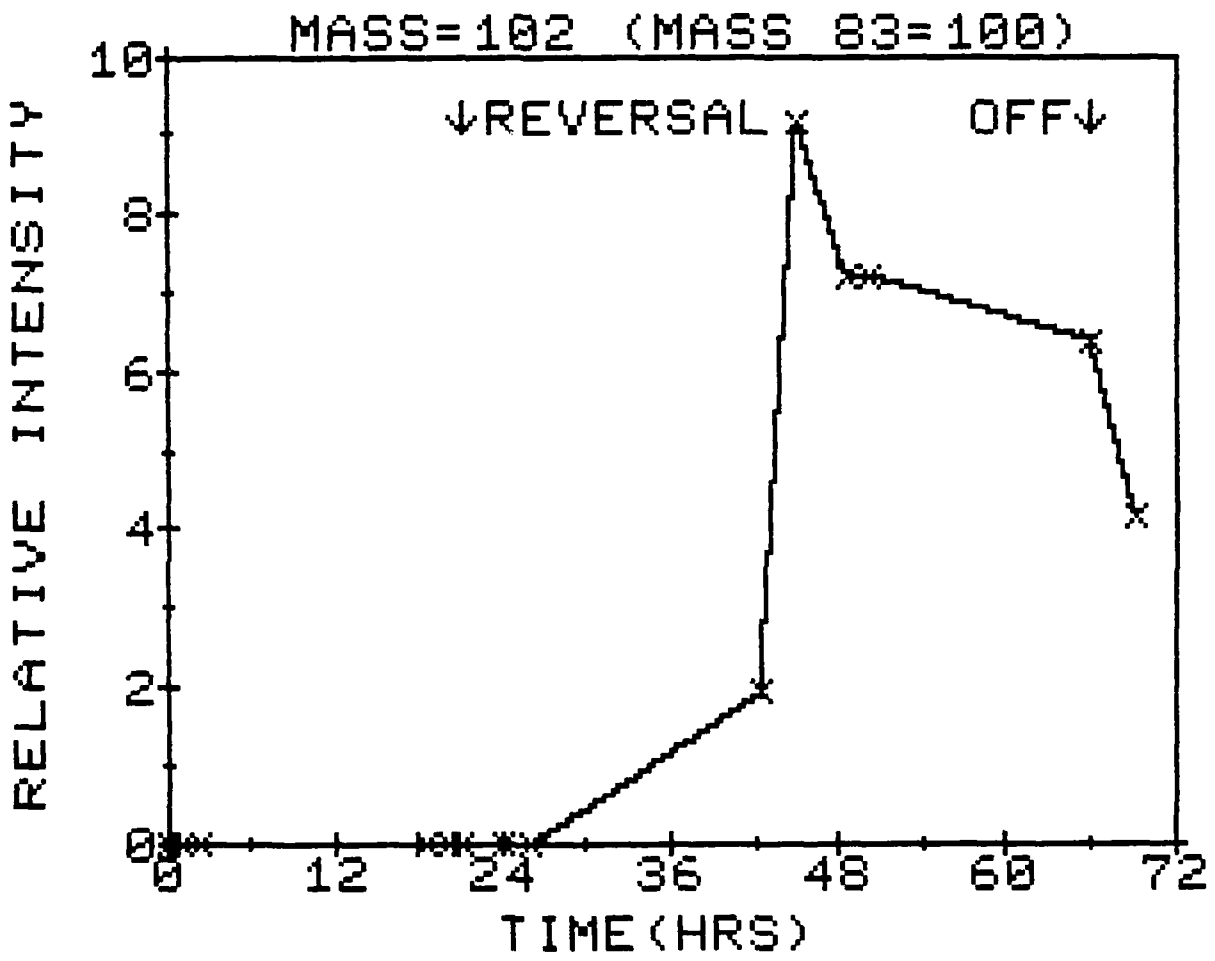

Figure 102. Mass 102 (SCl_2) vs. Time (Hrs.)

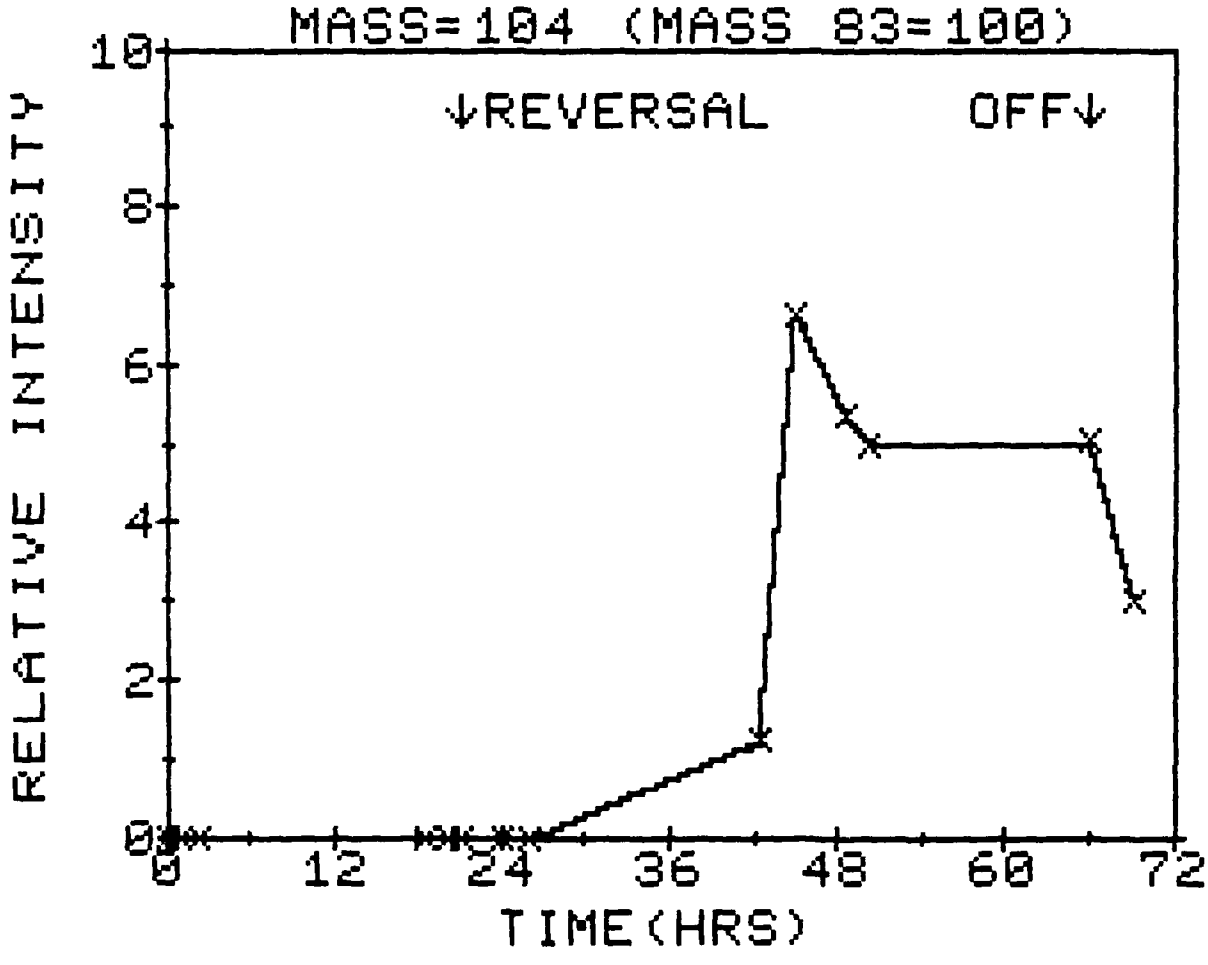

Figure 103. Mass 104 (SCl_2) vs. Time (Hrs.)

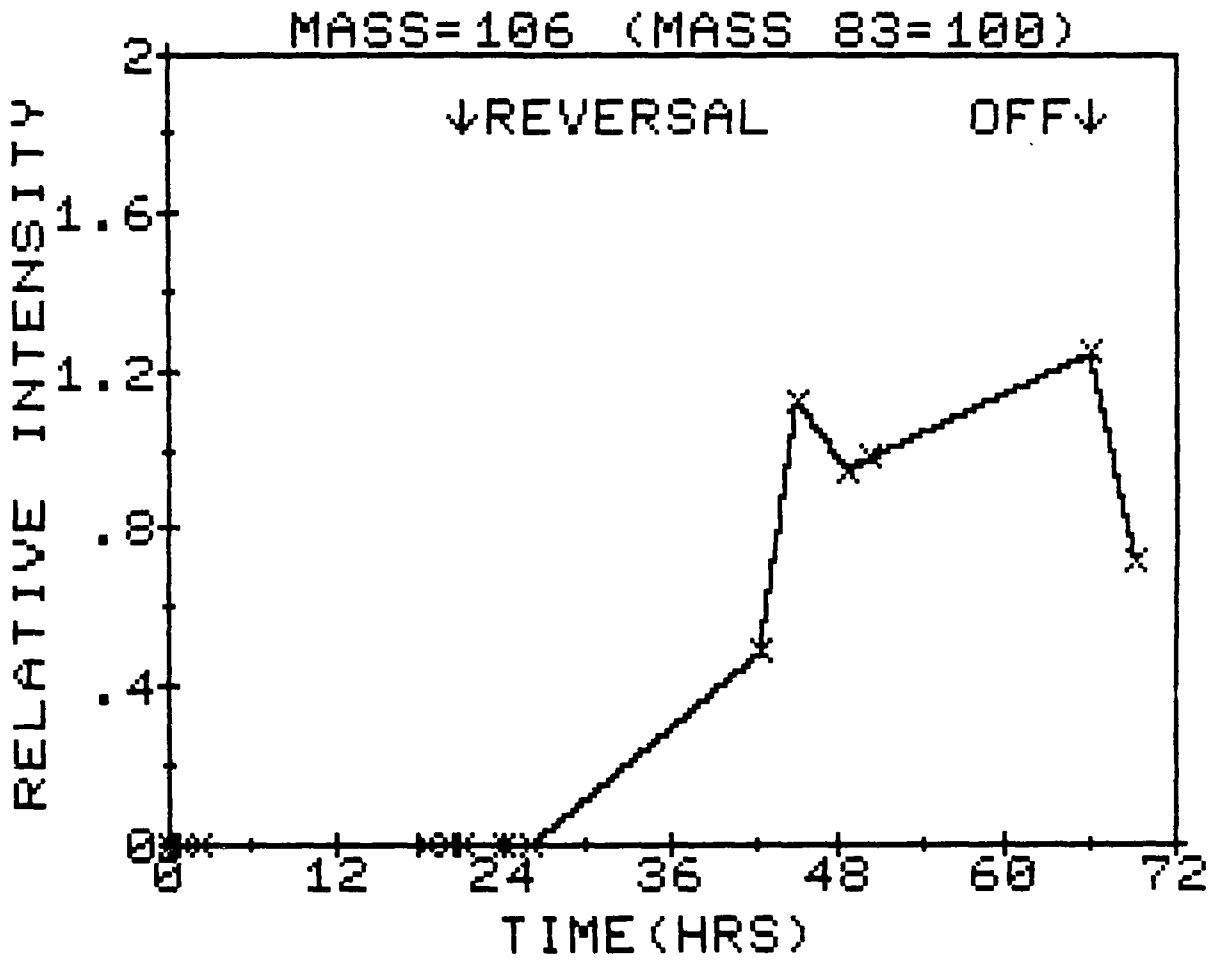

Figure 104. Mass 106 (SCl_2) vs. Time (Hrs.)

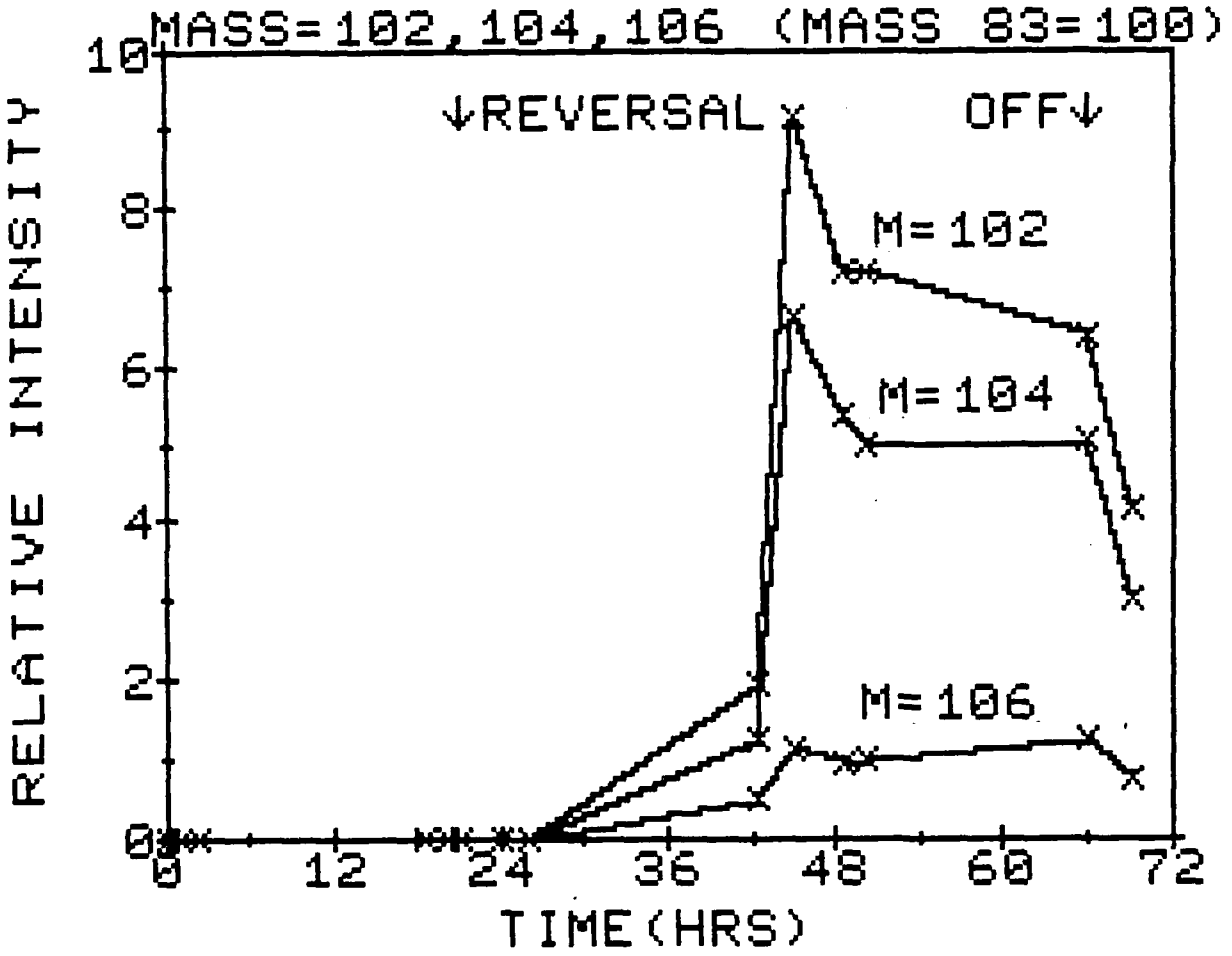

Figure 105. Mass 102, 104 and 106 (SCl_2) vs. Time (Hrs.)

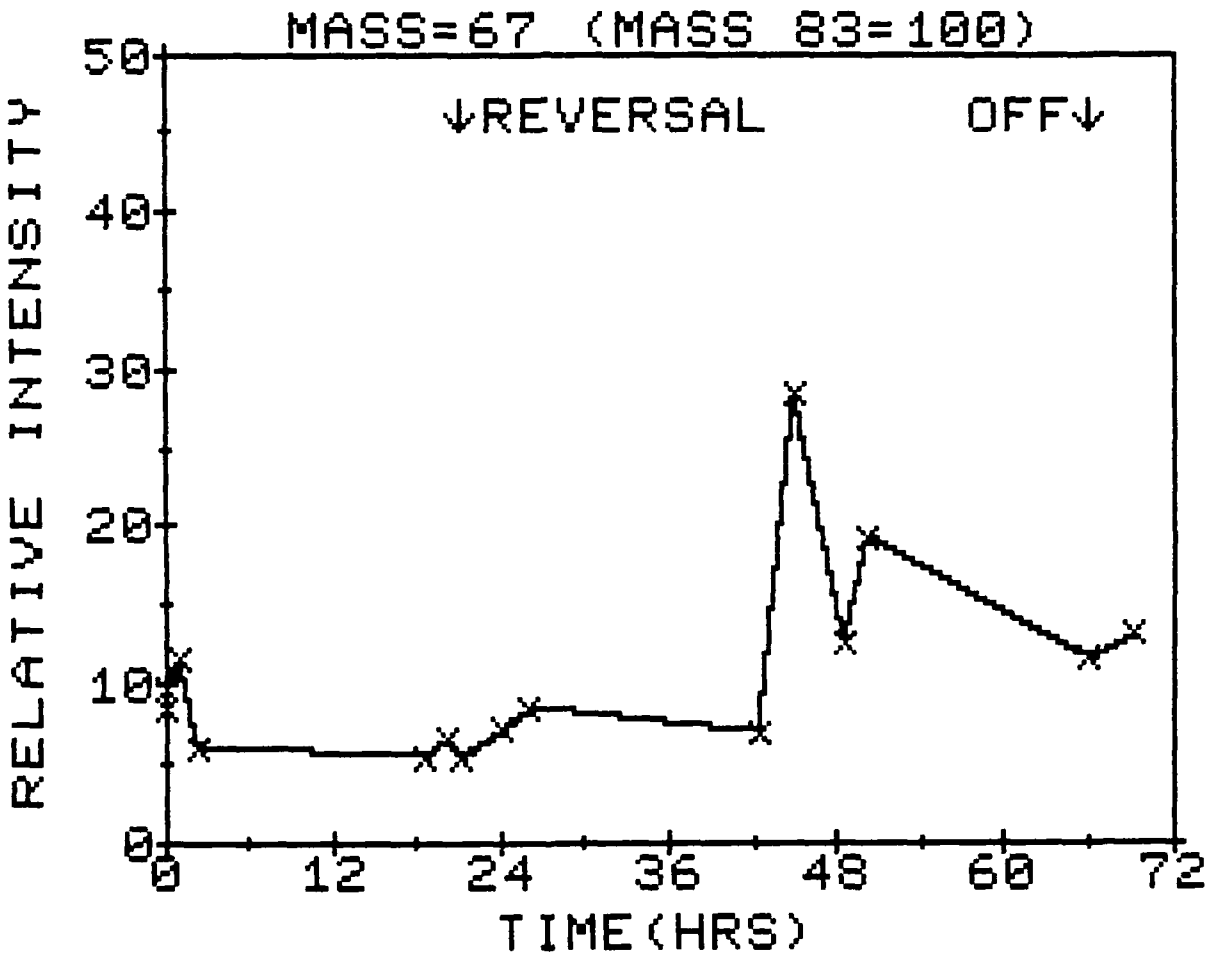

Figure 106. Mass 67 vs. Time (Hrs.)

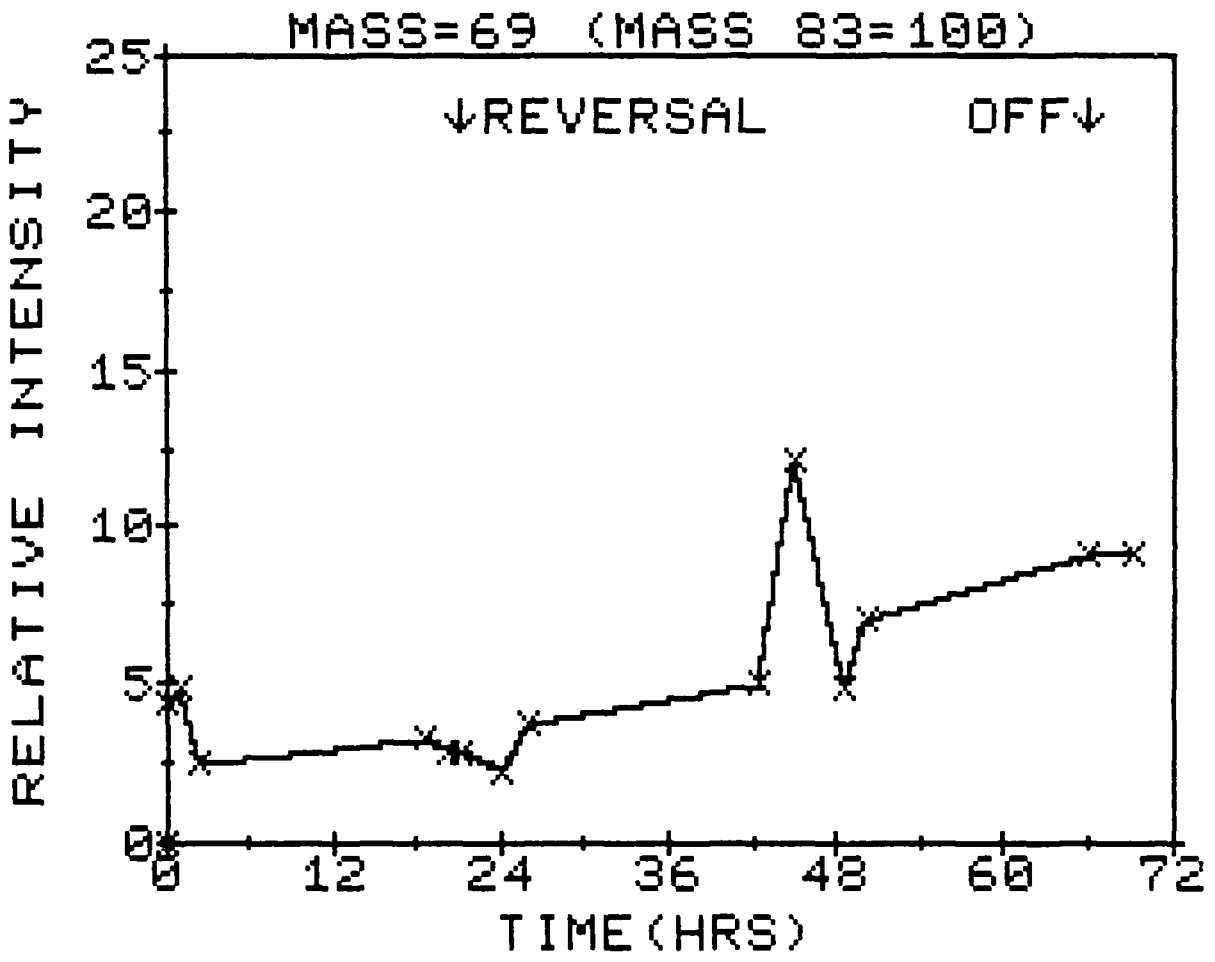

Figure 107. Mass 69 vs. Time (Hrs.)

4.4.6 Mass 134 Species (Mainly SO_2Cl_2)

Intensity measurements for masses 134, 136 and 138 are presented in Table 3 and are plotted in Figure 108, 109, and 110, respectively. Figure 111 shows the combined data for these three masses plotted simultaneously. Examination of these figures reveals that these masses are detected during reversal only. The time at which this triplet appears coincides identically with that time at which SCl_2 first appears, namely t=42.33. However, unlike SCl_2 the maximum concentration of the species giving rise to the intensities at masses 134, 136 and 138 occurs at t=42.33 while the maximum for SCl_2 was seen to occur at t=45. It is also seen from the figures cited above that the former maximum (for 134, 136 and 138) is followed by a slow decline to a stable level at times exceeding t=50.

Identification of the species giving rise to the intensities measured at 134, 136 and 138 will be considered next. The intensity ratios 136/134 and 138/134 indicate that the molecule from which these species arise contains two chlorines. Two likely compounds of molecular weight corresponding to triplet 134, 136 and 138 and each having two chlorines will be discussed. These are SO_2Cl_2 and S_2Cl_2. A number of investigations conducted on the $Li/SOCl_2$ battery system indicate that these species may be products of the reactions taking place in these batteries. Abraham and Mank (12) identified SO_2Cl_2 among other species in an anode-limited $Li/SOCl_2$ cell, while Schlaikjer et al. (10) suggested that S_2Cl_2 may be formed according to the reaction:

$$3S + 2SOCl_2 \longrightarrow SO_2 + 2S_2Cl_2$$

Since both SO_2Cl_2 and S_2Cl_2 are expected to yield the fragments 99 (SO_2Cl^{35+} or S_2Cl^{35+}) and 101 (SO_2Cl^{37+} or S_2Cl^{37+}) in their mass spectra, examination of these peaks will be conducted next. The data for masses 99 and 101 are plotted in Figures 112 and 113, respectively while Figure 114 shows the combined data for these two masses. The mass spectrum for a pure sample of SO_2Cl_2 is shown in Figure 123 and the numerical intensities of masses 134, 136

and 138 relative to mass 99 are 0.194, 0.144 and 0.033, respectively. Now, considering the data obtained from the in-situ experiment for masses 99, 134, 136 and 138 (Table 3), we find that the average intensities of the latter three masses relative to the intensity of mass 99 are 0.748 $\pm$ 0.07, 0.466 $\pm$ 0.05 and 0.129 $\pm$ 0.01, respectively. These results are not consistent with the results obtained for pure SO_2Cl_2. Although no mass spectrum is available for pure S_2Cl_2, a theoretical isotopic abundance calculation is possible for S_2Cl_2 (see Appendix for method of calculation). The theoretical intensity distribution for masses 134, 136 and 138 are given by 0.515, 0.379 and 0.085, respectively for S_2Cl_2 and 0.542, 0.375 and 0.073, respectively for SO_2Cl_2.

We now wish to compare our data for masses 134, 136 and 138 with the theoretical distributions for S_2Cl_2 and SO_2Cl_2. The average intensities for these masses calculated from the in-situ data are 0.928, 0.578 and 0.160 for 134, 136 and 138, respectively. Taking mass 134 as a reference we construct Table 5 in which the theoretical ratios are compared to the experimental mass ratios. From this table it can be seen that the in-situ data is consistent with the mass 136/134 ratio for SO_2Cl_2 and with the mass 138/134 ratio for S_2Cl_2. Thus no clear case exists for either SO_2Cl_2 or S_2Cl_2. It may be pointed out that a mixture of these two species might lead to such results. In any case we feel that accurate mass measurements can easily resolve this dilemma. (Note: the infrared evidence, however, points strongly to formation of SO_2Cl_2 as the major component of that peak.)

Table 5

Calculated Isotopic Mass Ratios Compared

to Experimental Mass Ratios

Molecule	Calculated Mass Ratios		Experimental Mass Ratios	
	136/134	138/134	136/134	138/134
SO_2Cl_2	0.692	0.135	-	-
S_2Cl_2	0.737	0.164	-	-
Mass 134	-	-	0.622 ± 0.06	$0.174 \pm .02$

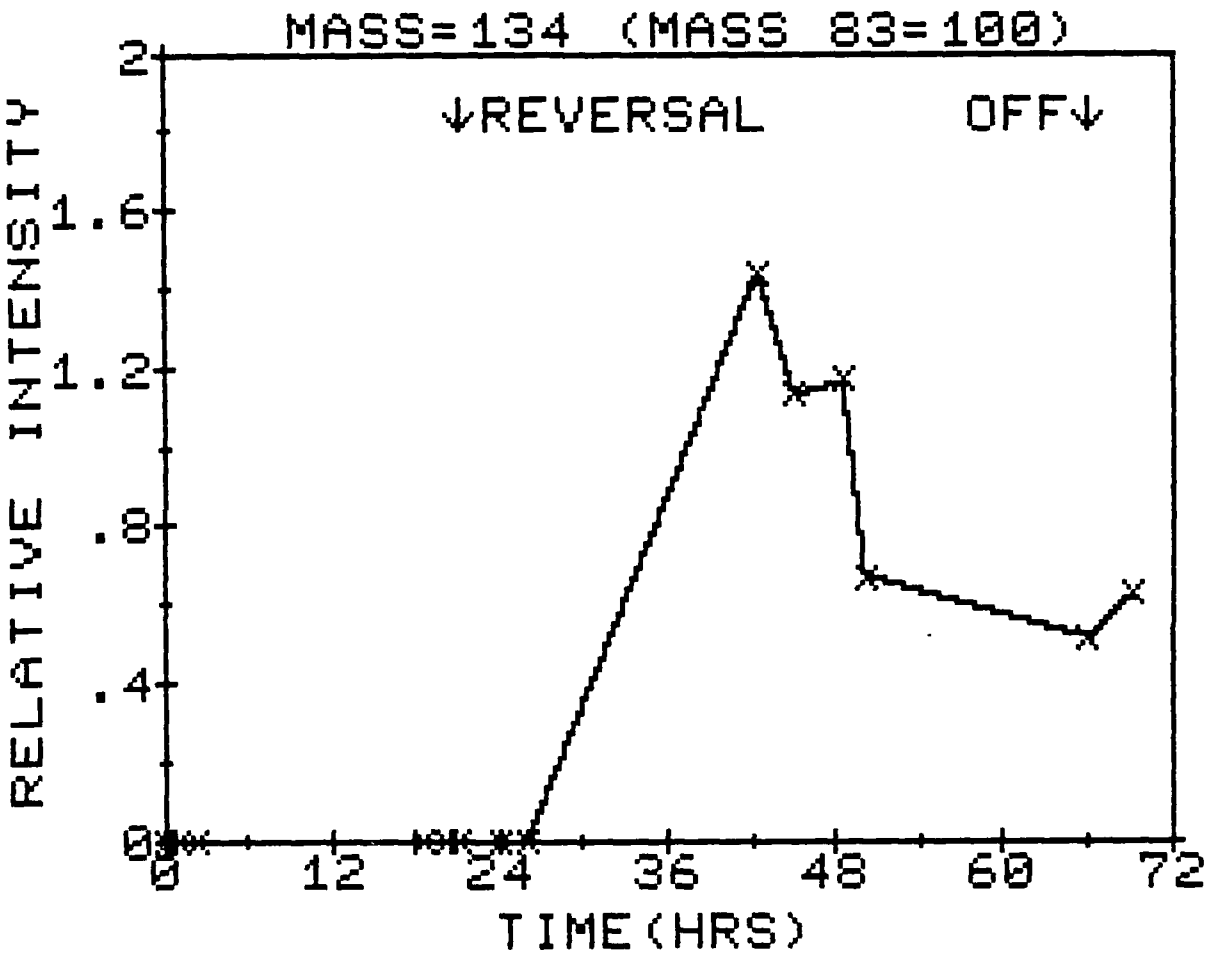

Figure 108. Mass 134 vs. Time (Hrs.)

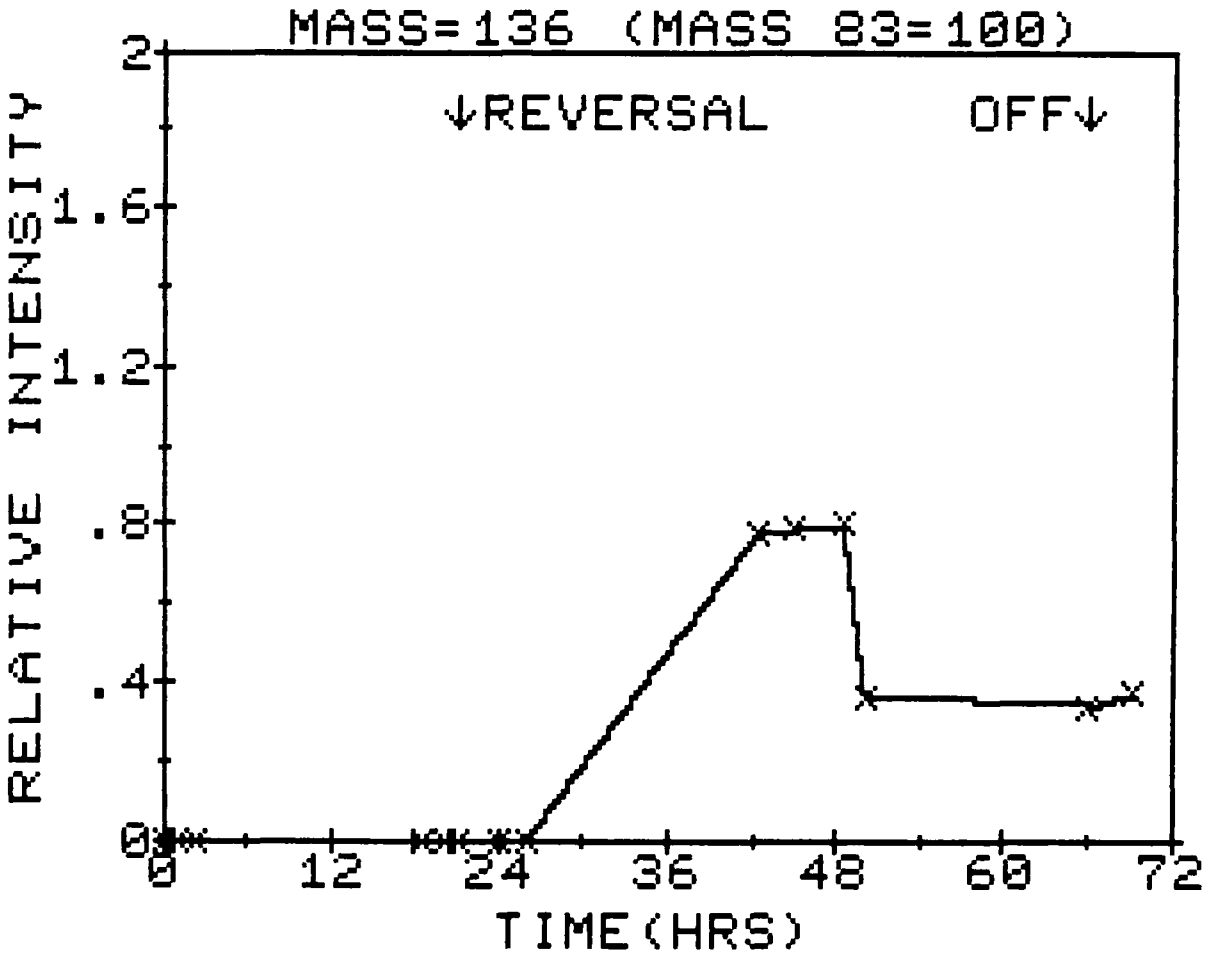

Figure 109. Mass 136 vs. Time (Hrs.)

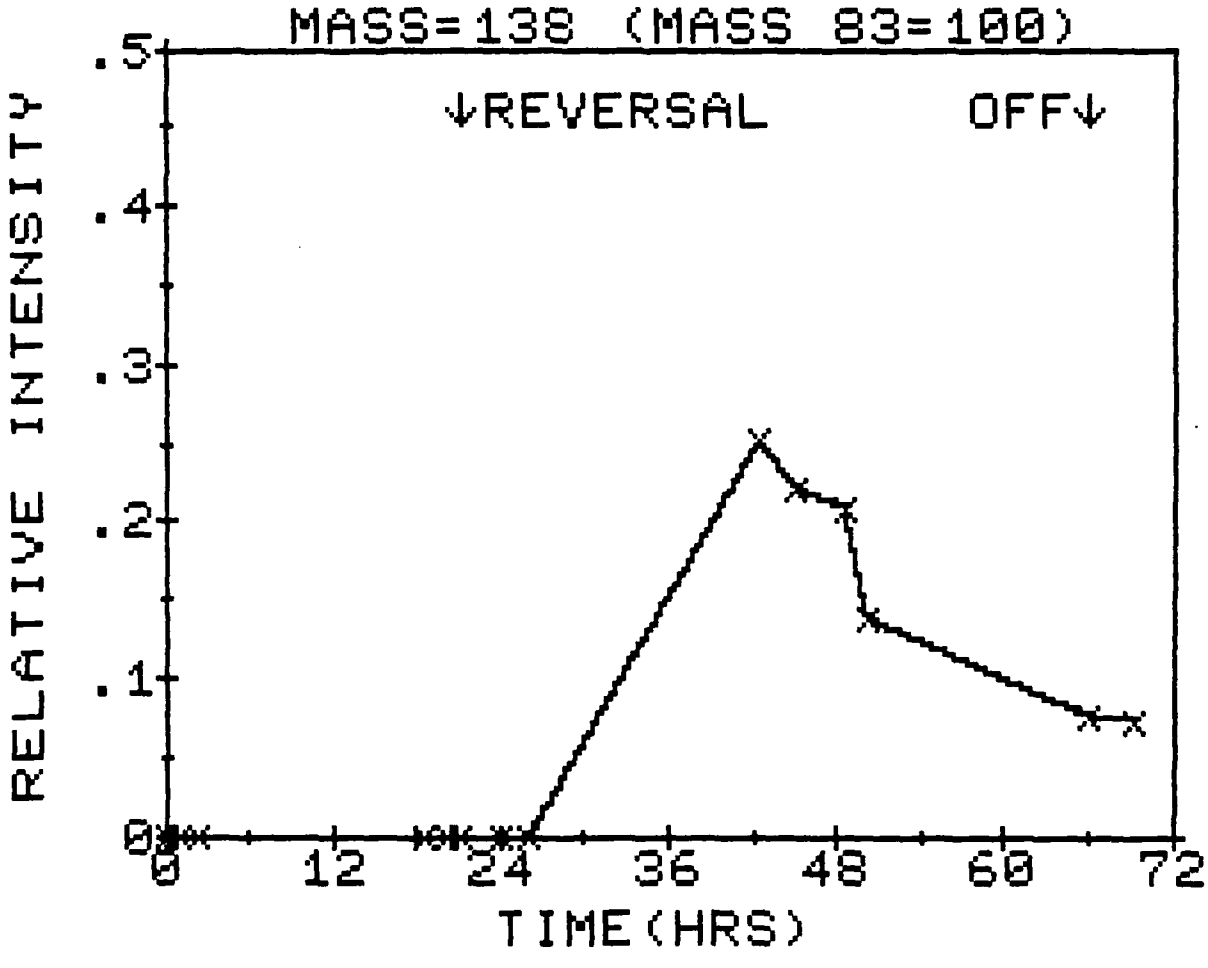

Figure 110. Mass 138 vs. Time (Hrs.)

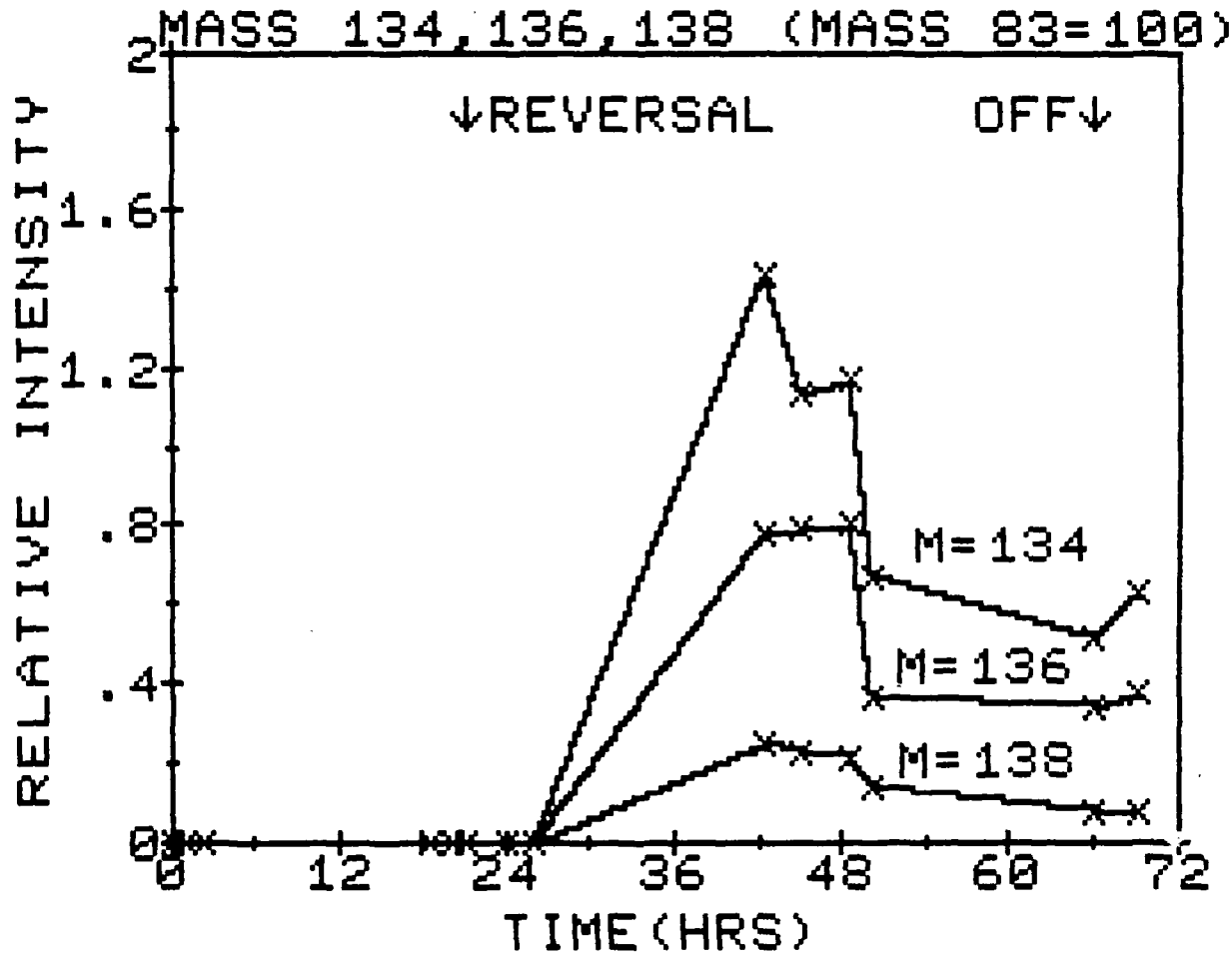

Figure 111. Mass 134, 136 and 138 vs. Time (Hrs.)

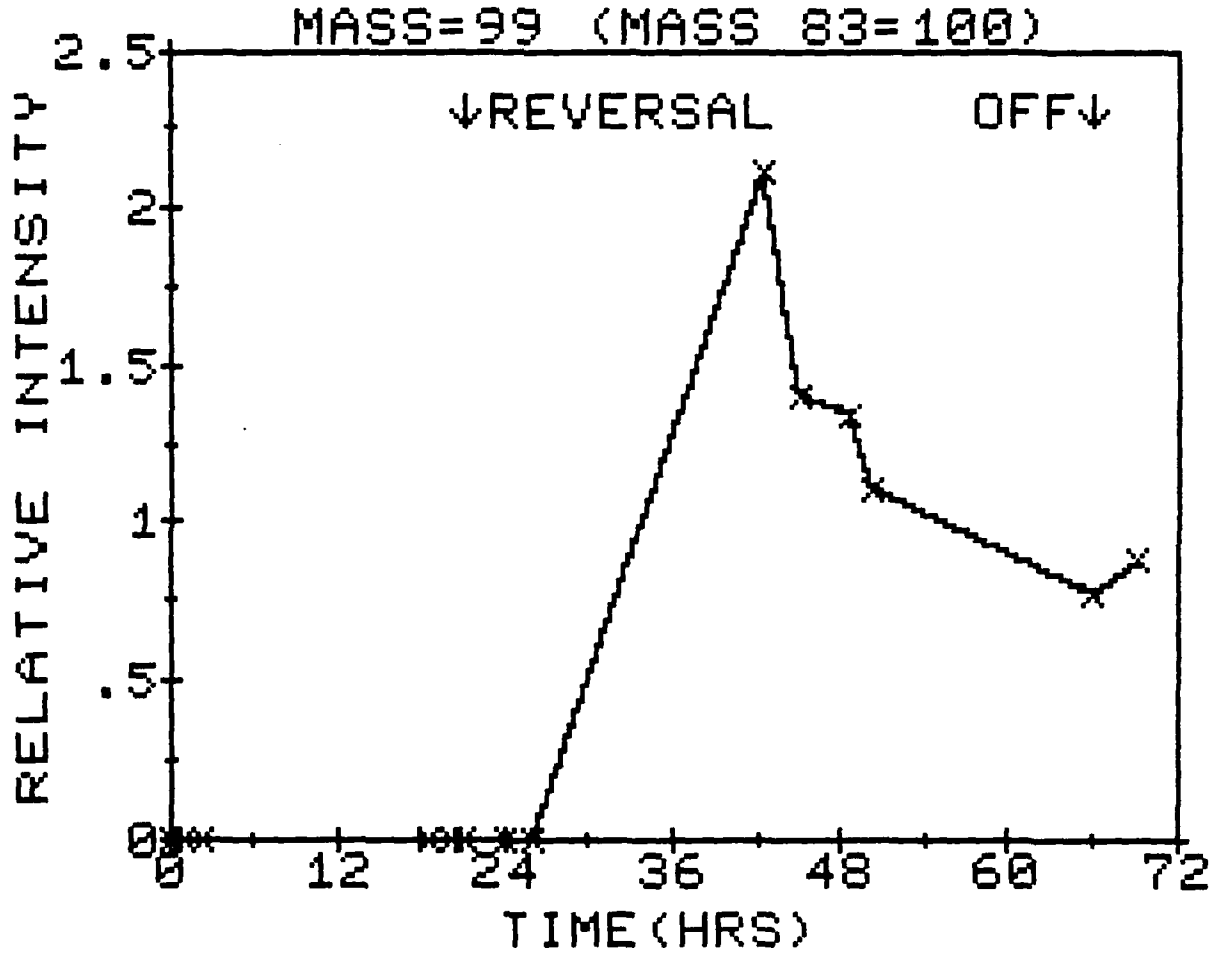

Figure 112. Mass 99 vs. Time (Hrs.)

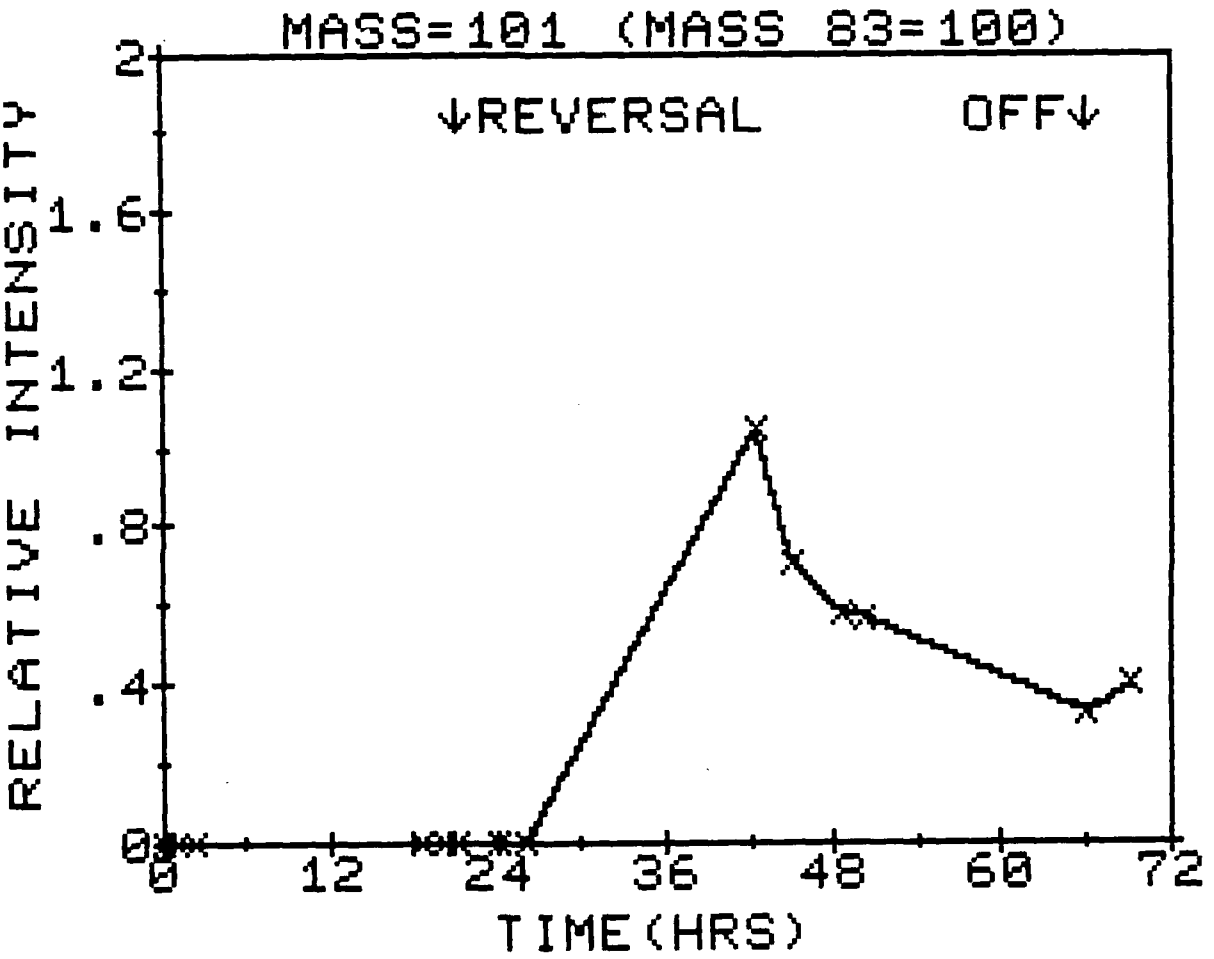

Figure 113. Mass 101 vs. Time (Hrs.)

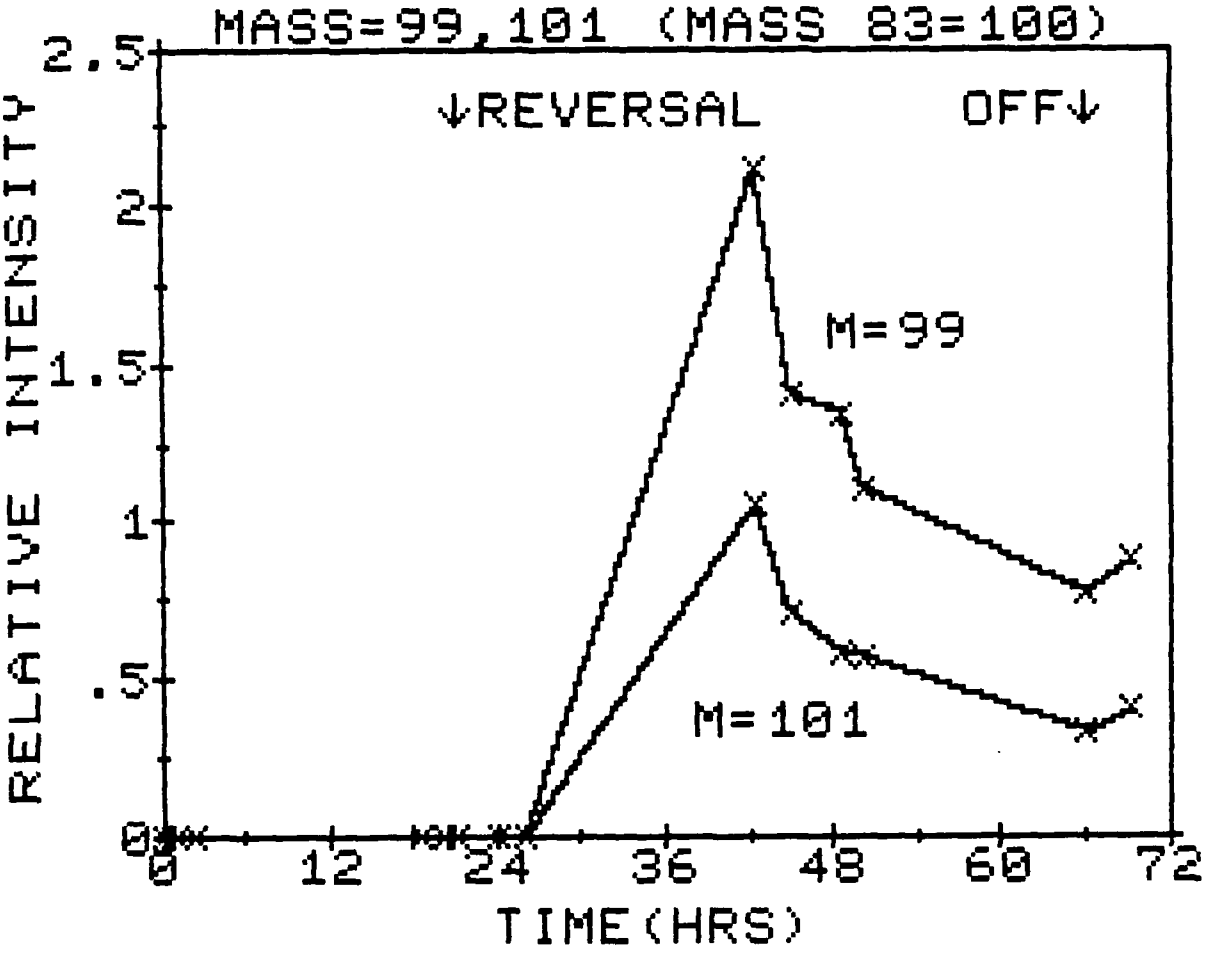

Figure 114. Mass 99 and 101 vs. Time (Hrs)

4.4.7 CF_2^+

The accurate mass of nominal mass 50 appearing in the in-situ experiment was found to be 49.99597 ± 30 ppm. It is interesting to note that the calculated mass for CF_2^+ is 49.99680. The agreement between the theoretical value and the measured value provides strong evidence that CF_2^+ is the correct identity of this mass 50 fragment.

The existence of fluorine-containing fragments is a point worth noting because the only cell component which contains fluorine is the Teflon binder used in the cathode construction. Thus the existence of CF_2^+ implies that the Teflon-impregnated porous carbon electrode is undergoing electrochemical attack during both discharge and reversal (See Figure 125).

We suggest that further work needs to be done in order to characterize the cathode according to:

1. The effect of preparation procedure on the production of CF_2^+ and other fluorinated and/or chlorinated species (e.g., HCl).
2. The effect of preparation procedure on the surface properties of the cathode, both before and after discharge and reversal.

4.4.8 Higher Molecular Weight Species

In the late stages of reversal, the formation of ions with masses 146, 148, 150, 160, 161, 163, 165, 192, 267 and 269 was observed. Further work must be performed in order to identify the precursors of these species.

4.4.9 Mass Spectra and Appearance Potentials for the Pure Compounds

The mass spectra measured at 80 ev for the compounds $SOCl_2$, SCl_2 and SO_2Cl_2 are presented in Figure 121, 122 and 123 respectively. Numerical intensity data for these spectra are presented in Table 4. A tentative mass spectrum for a sample of S_2Cl_2 whose purity is questionable is presented in Figure 124.

The appearance potentials for the compounds SO_2, $SOCl_2$, SCl_2, SO_2Cl_2 and a slightly impure sample of S_2Cl_2 are presented in Figures 115, 116, 117, 118 and 119, respectively. The energy scale was calibrated using argon as a standard (see Figure 120). The measured appearance potentials for SO_2, $SOCl_2$ and SO_2Cl_2 were found to be 12.4 $\pm$ 0.3 ev, 10.8 $\pm$ 0.3 ev and 11.9 $\pm$ 0.5 ev, respectively.

The data for S_2Cl_2 show considerable experimental uncertainty. An appearance potential for S_2Cl_2 is estimated to be 10.4 $\pm$ 0.6 ev. The data for SCl_2 is slightly complicated because of the existence of two linear regions in the appearance potential data. Since the other species containing both sulfur and chlorine have appearance potentials in the range of 10.8 to 11.9 ev, the value of 10.9 $\pm$ 0.4 ev is chosen for the first linear region of the SCl_2 data.

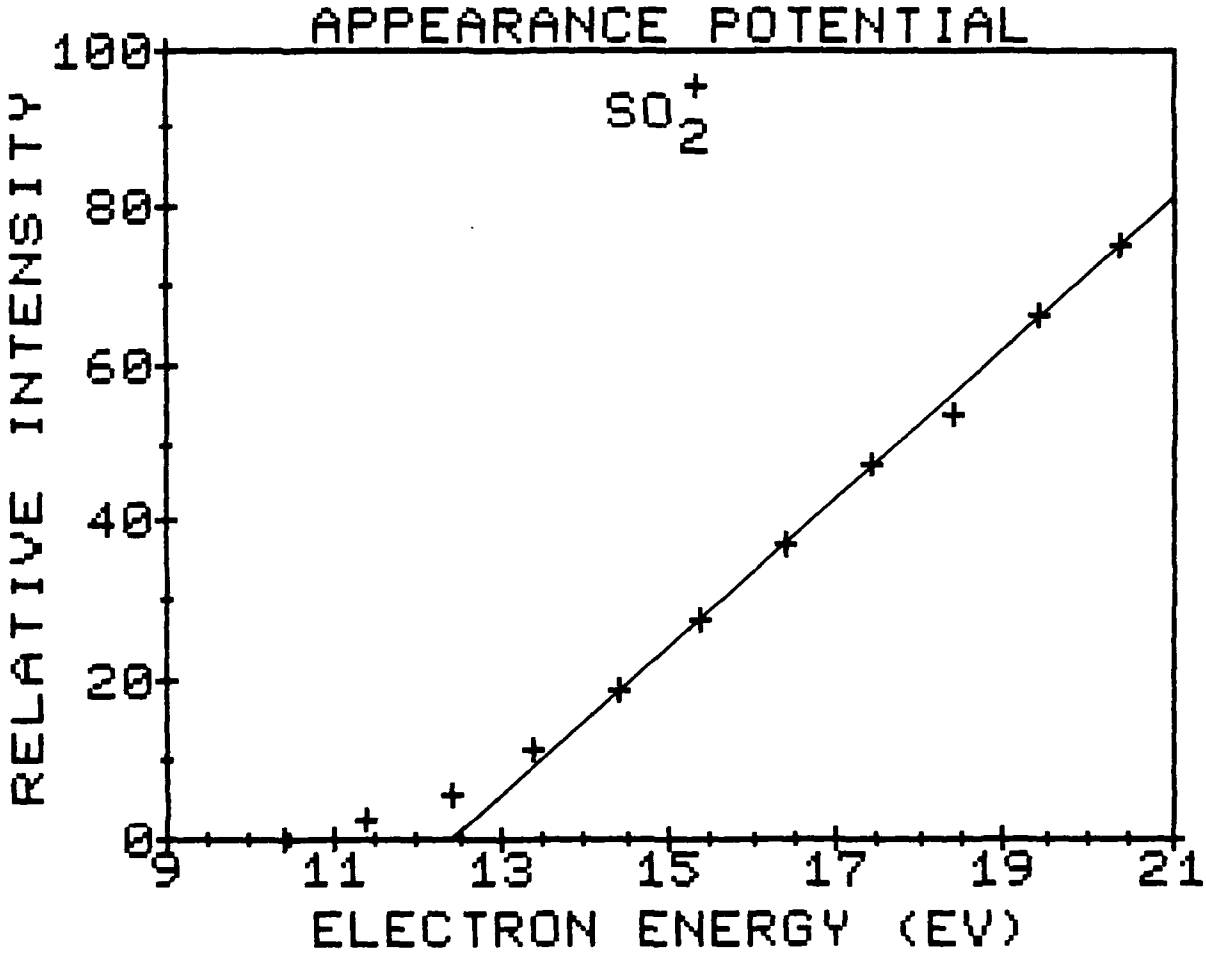

Figure 115. Relative Intensity of SO_2^+ vs. Ionizing Electron Energy

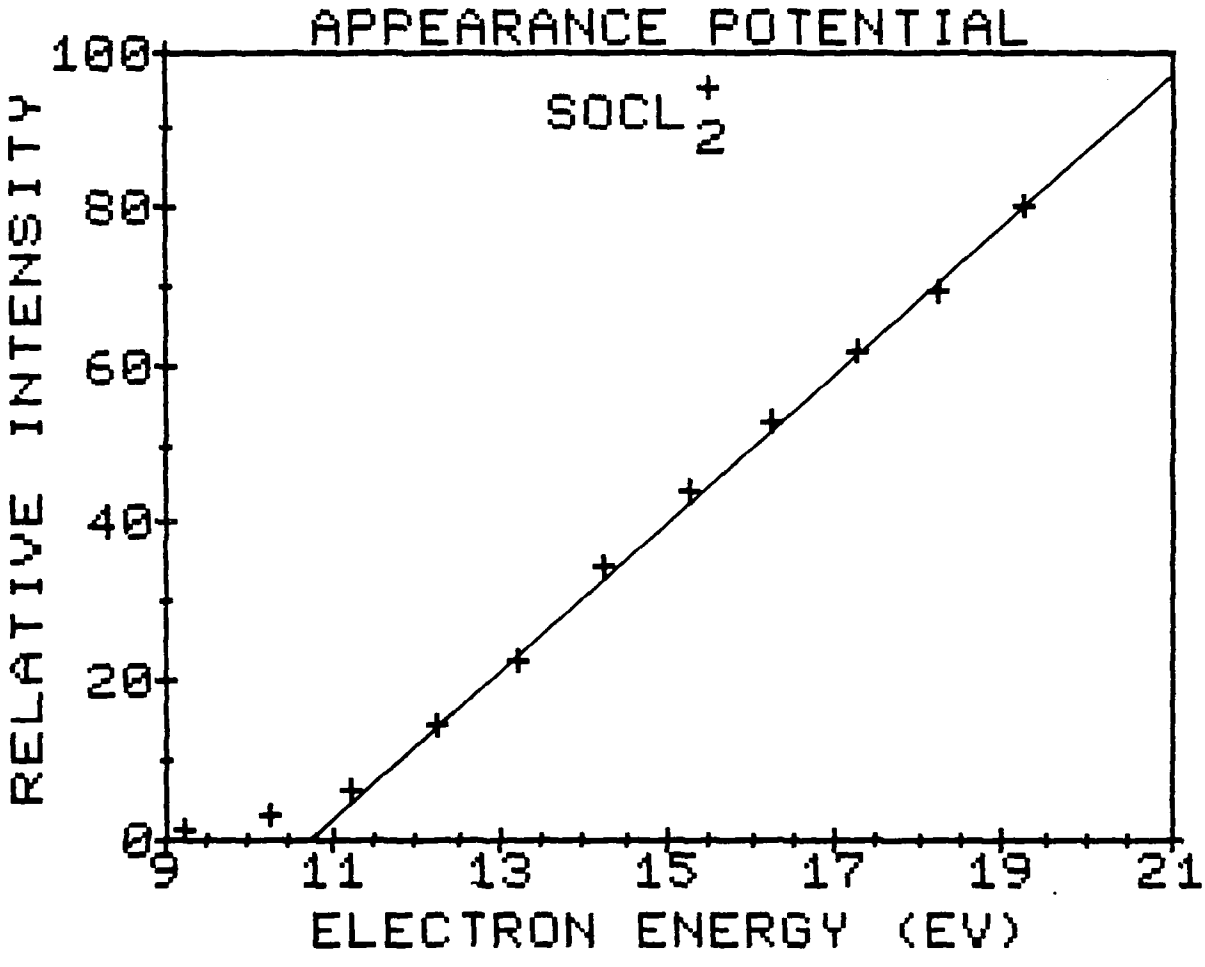

Figure 116. Relative Intensity of $SOCl_2^+$ vs. Ionizing Electron Energy

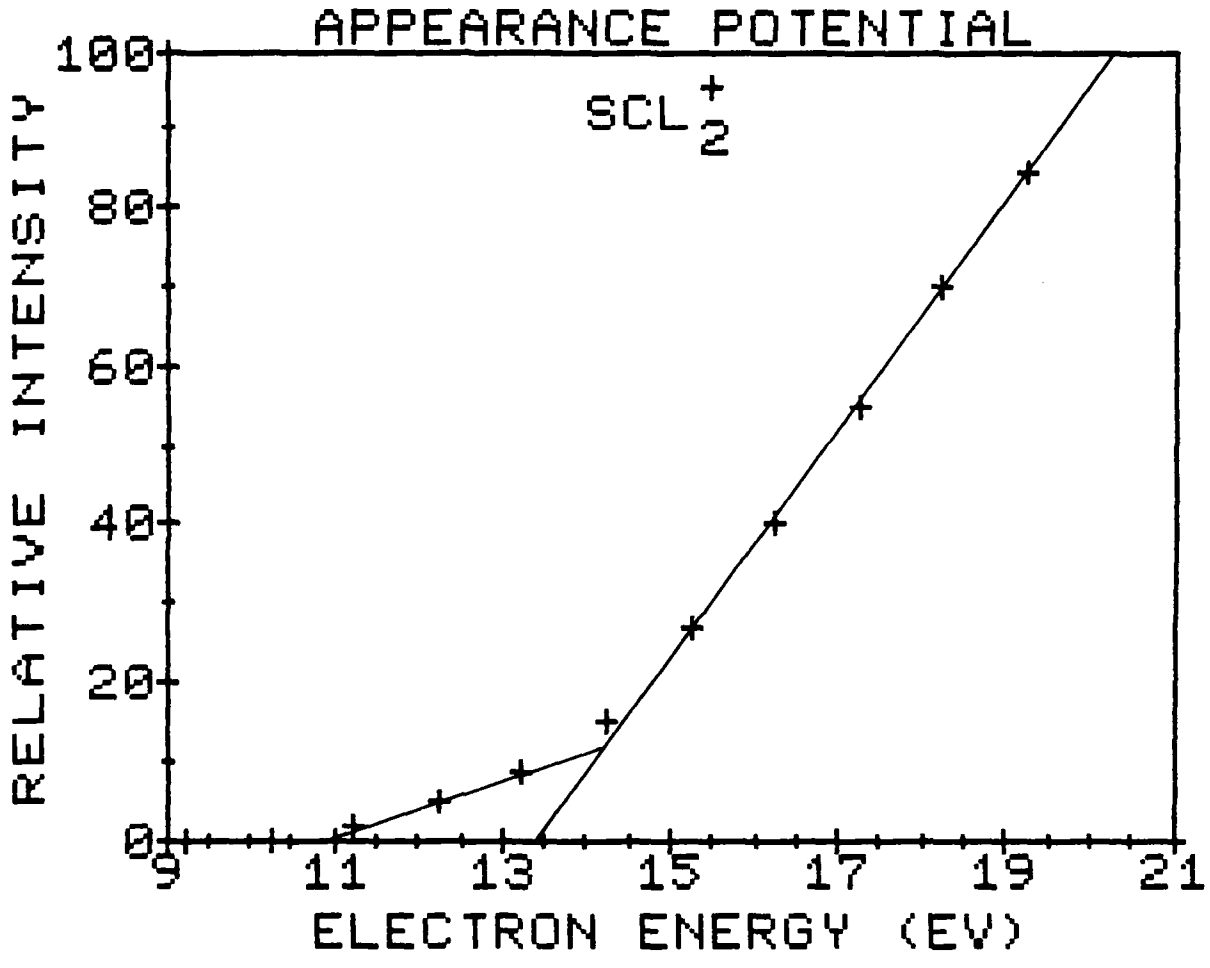

Figure 117. Relative Intensity of SCl_2^+ vs. Ionizing Electron Energy

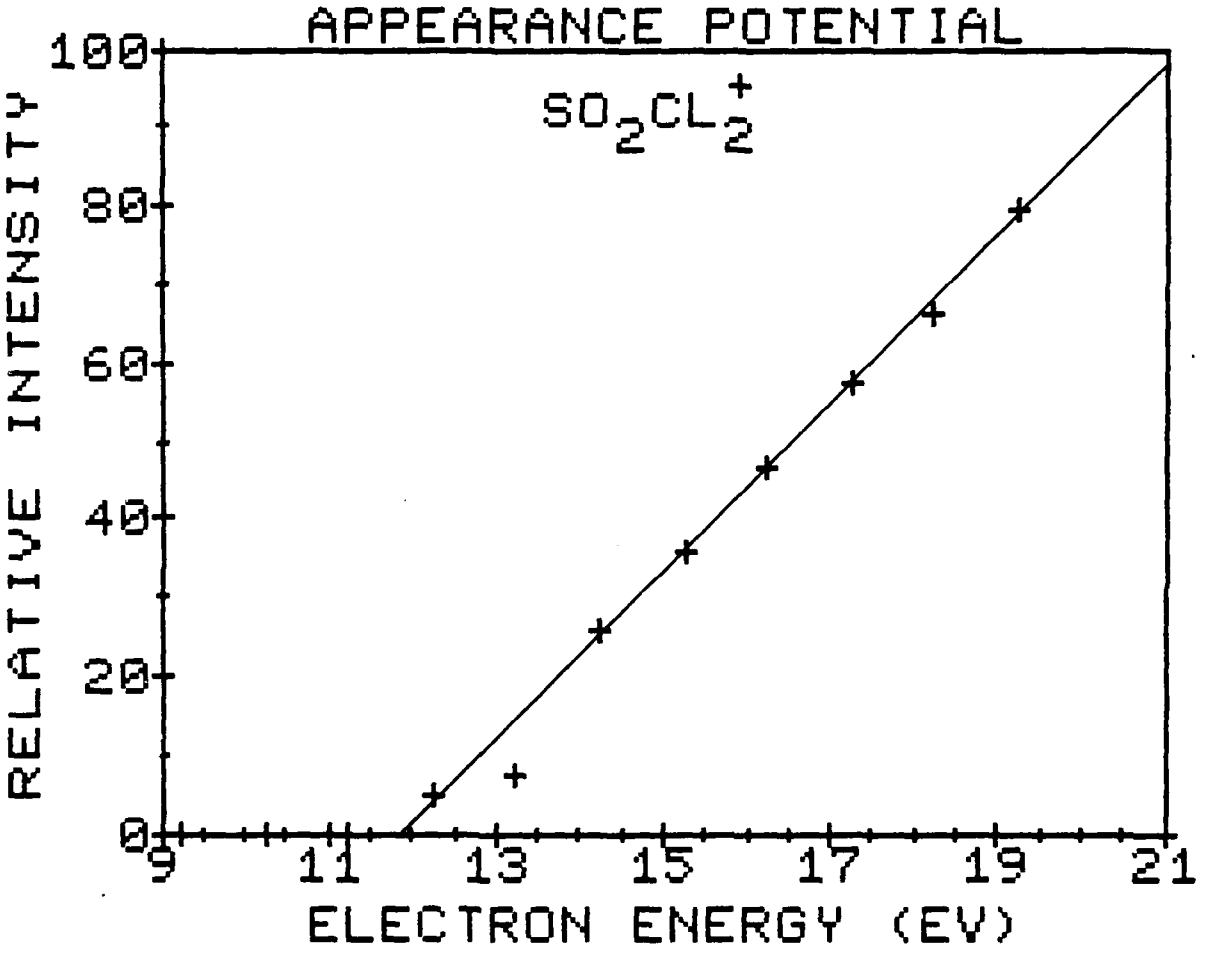

Figure 118. Relative Intensity of $SO_2Cl_2^+$ vs. Ionizing Electron Energy

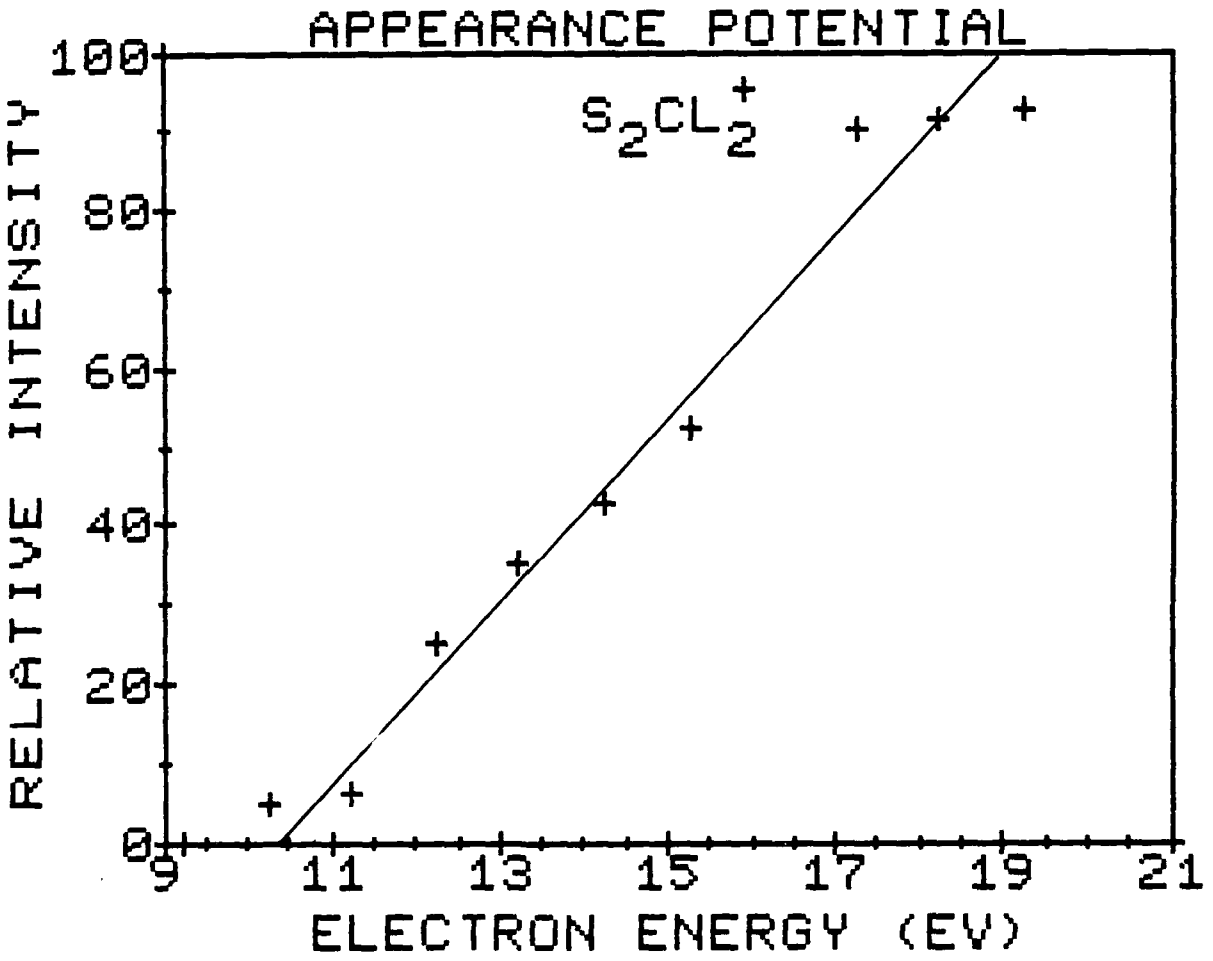

Figure 119. Relative Intensity of $S_2Cl_2^+$ vs. Ionizing Electron Energy

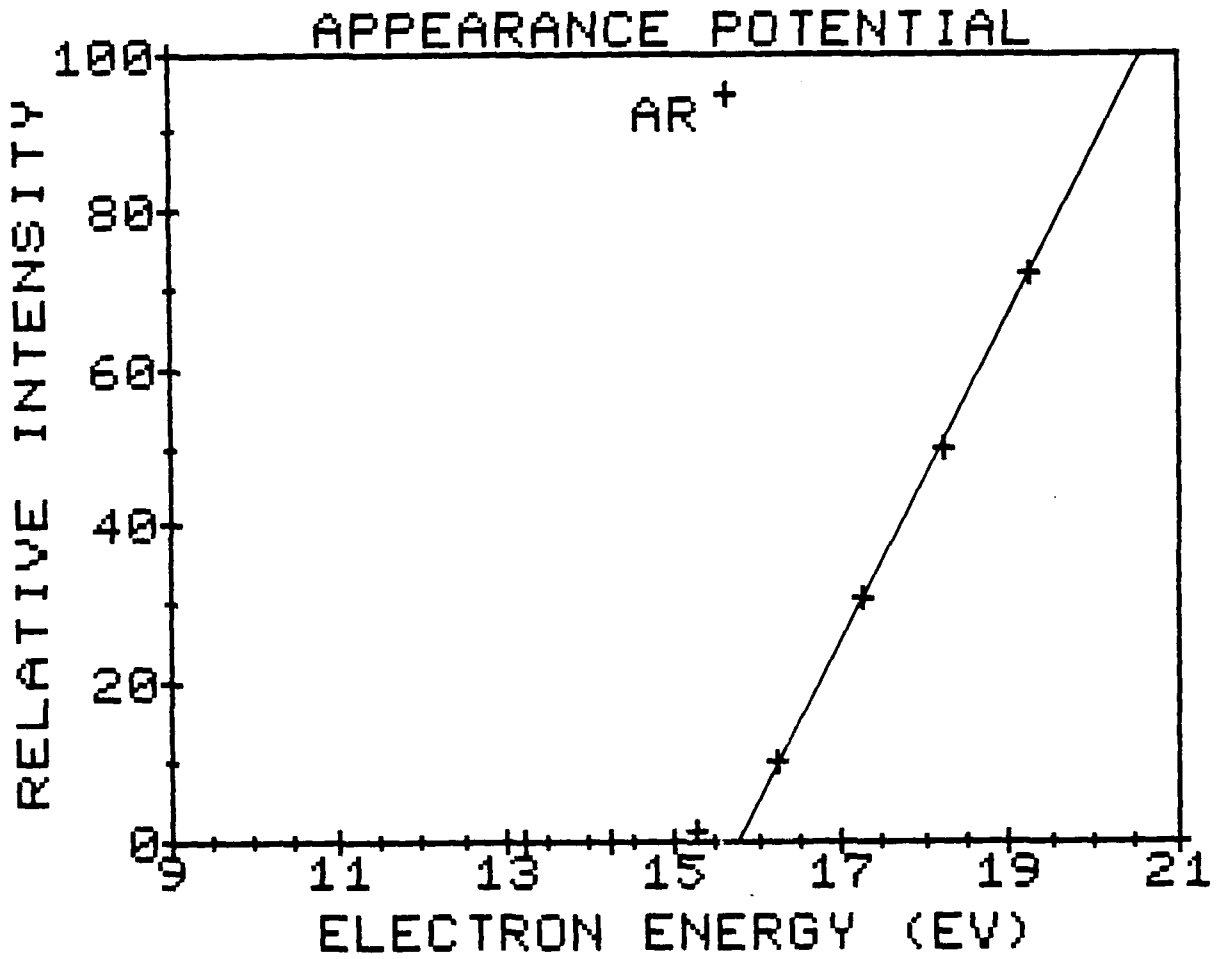

Figure 120. Relative Intensity of Ar^+ vs. Ionizing Electron Energy

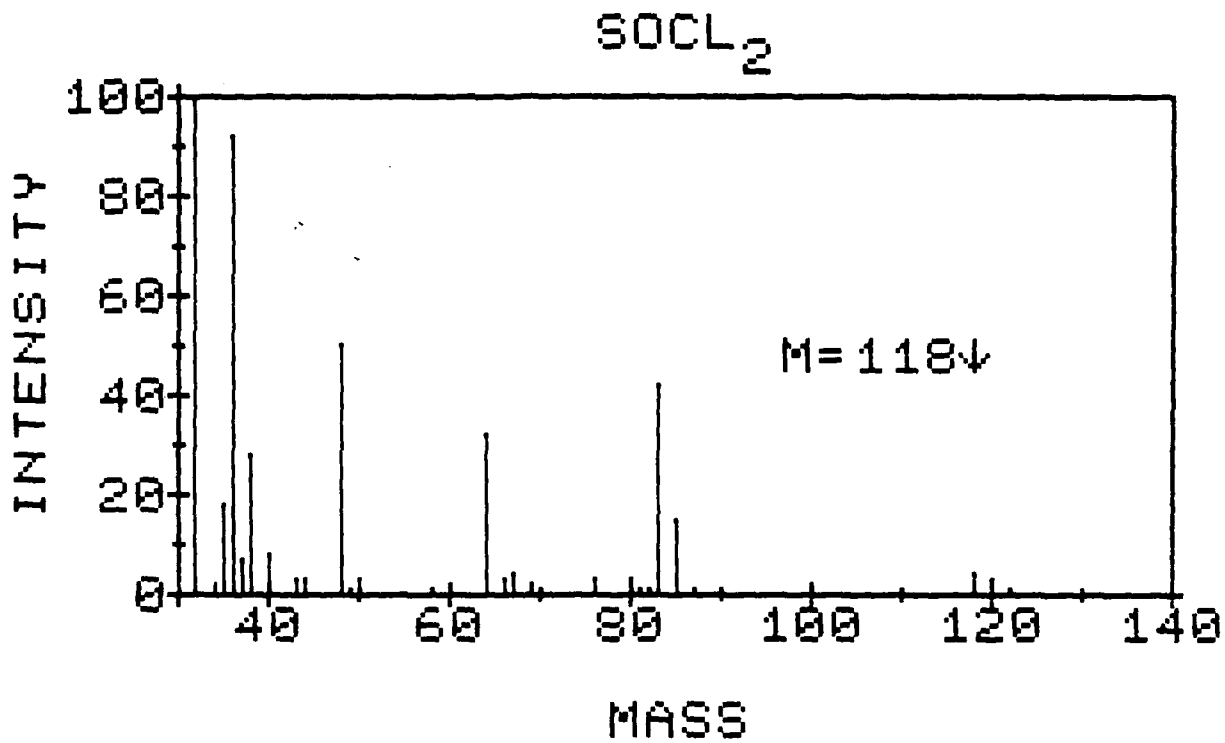

Figure 121. Mass Spectrum of $SOCl_2$ at 80 eV Electron Energy

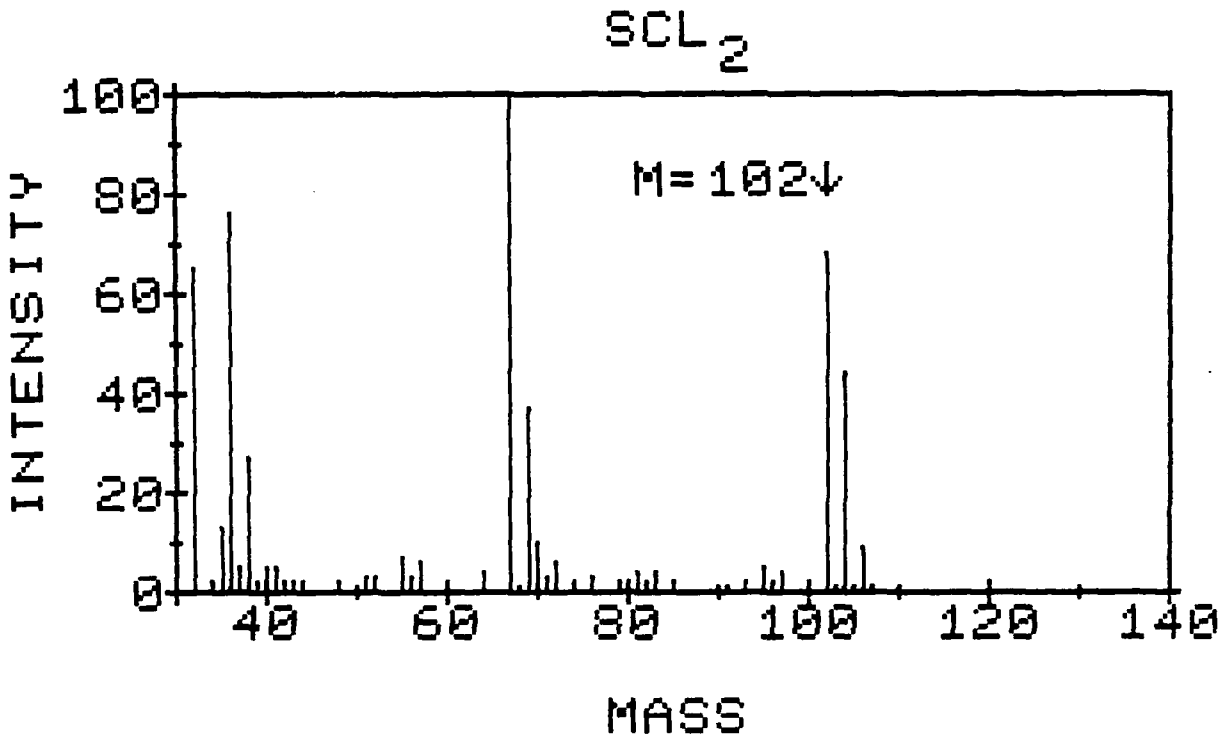

Figure 122. Mass Spectrum of SCl_2 at 80 eV Electron Energy

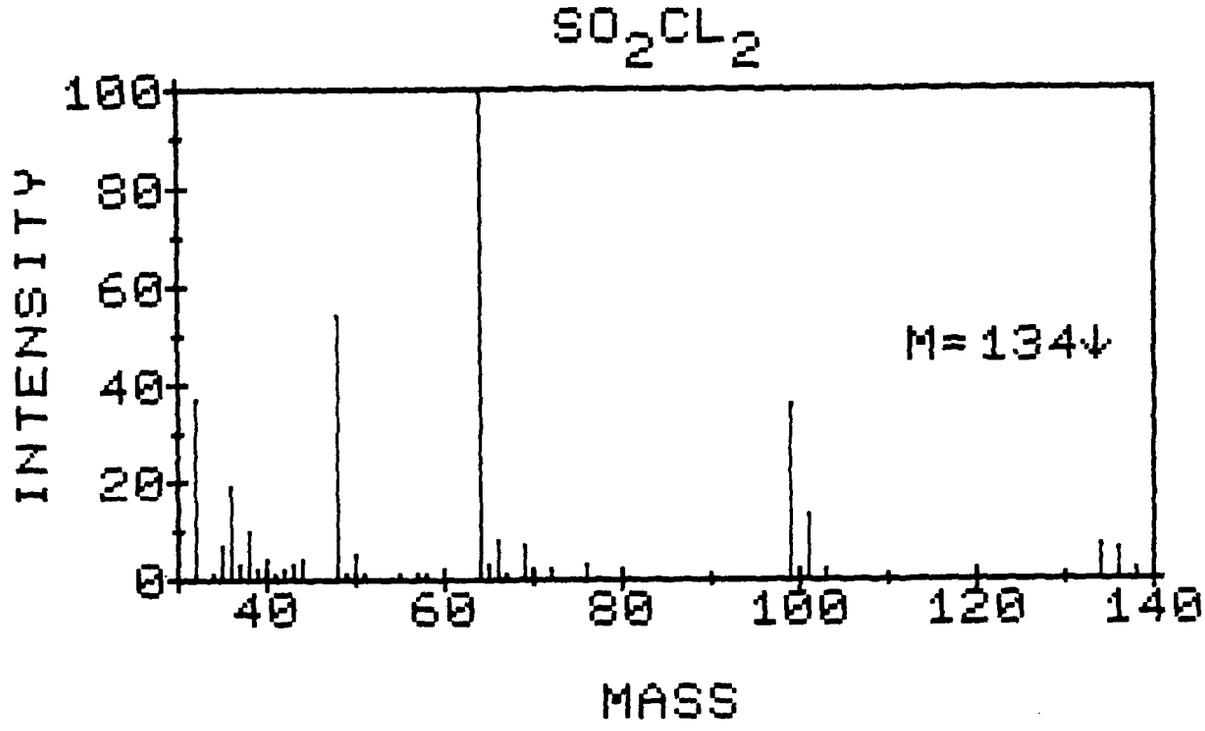

Figure 123. Mass Spectrum of SO_2Cl_2 at 80 eV Electron Energy

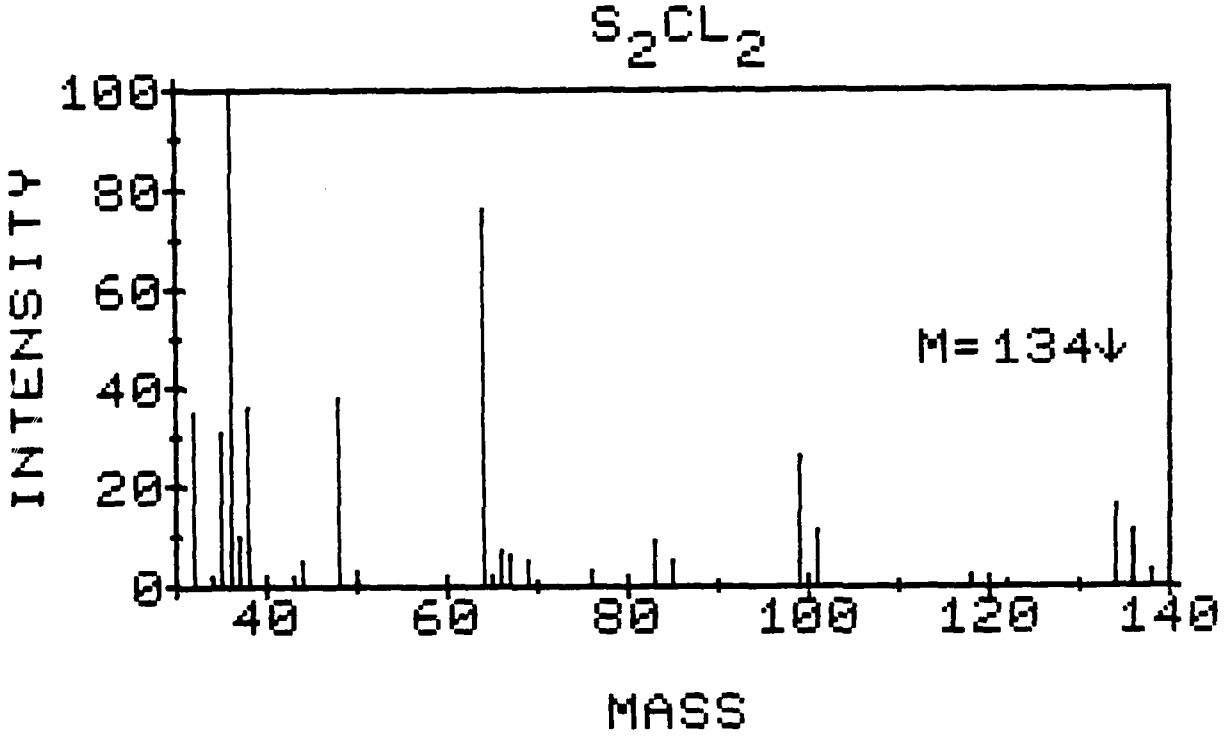

Figure 124. Mass Spectrum of S_2Cl_2 at 80 eV Ionizing Electron Energy

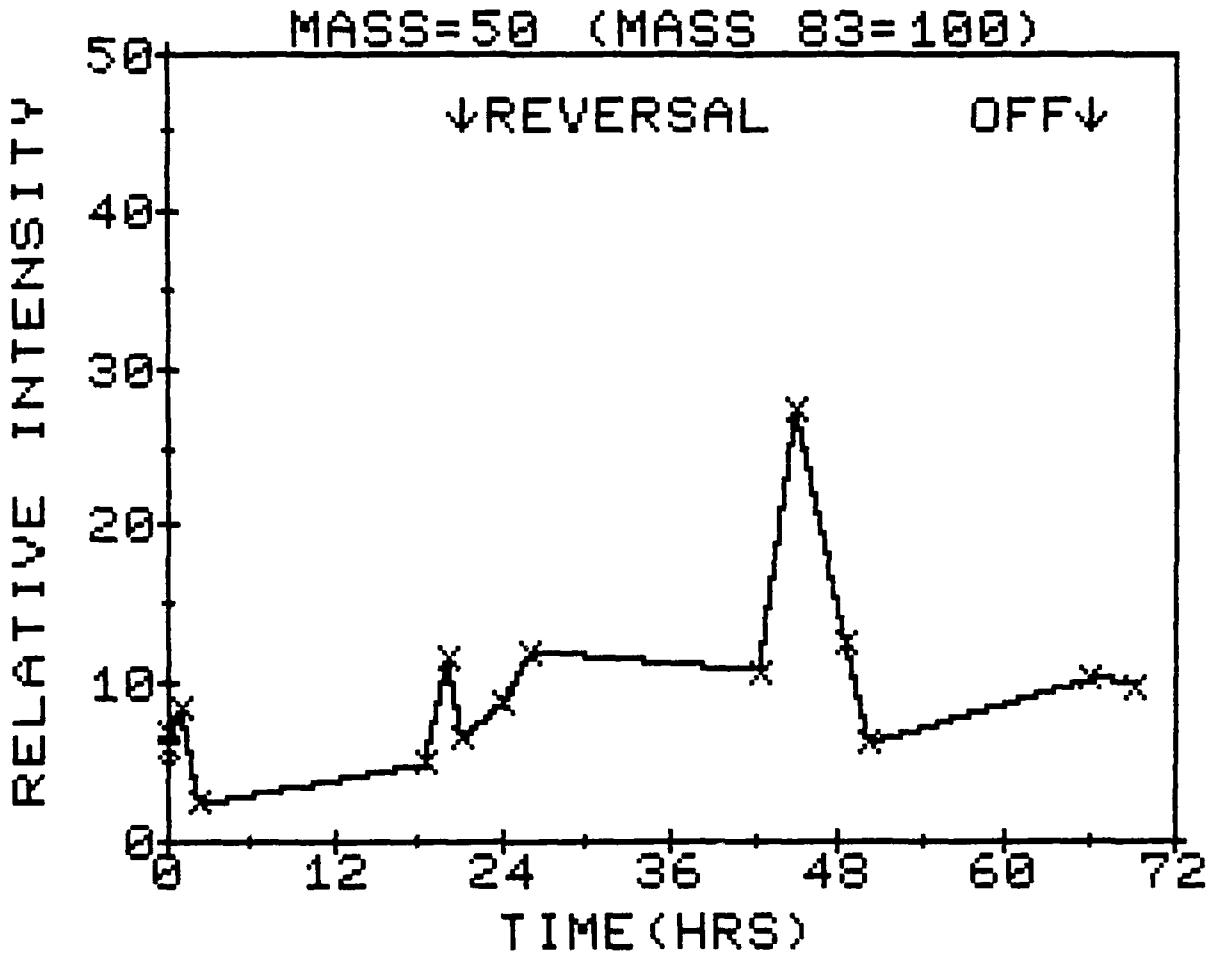

Figure 125. Relative Intensity of Mass 50 (CF_2^+) vs. Time (Hrs.)

4.5 Conclusions

In this study mass spectrometric techniques have been used to investigate the gases present in and evolved from an anode-limited lithium thionyl chloride cell during both discharge and reversal. The species HCl, CS_2, SO_2, S_2O, SCl_2 and $SOCl_2$ were identified as the components present in the vapor over the cell electrolyte. The formation of hydrogen chloride indicates that hydrogen source(s) must exist among the components comprising the cell electrolytes, electrodes and/or the physical structure of the battery.

An induction period of approximately five hours after the onset of reversal is observed beyond which the concentrations of chlorine fragments, HCl and SO_2 increase substantially. The formation of SCl_2 and of species of mass 134 is detected only after a similar induction period after the onset of reversal. The identity of the species appearing at mass 134 is postulated to be either SO_2Cl_2 or S_2Cl_2; the infrared evidence, however, strongly suggests that it is mainly SO_2Cl_2.

HCl is observed to achieve the highest concentration of any species during discharge while SO_2 becomes the most abundant vapor species observed during reversal. The concentration of CS_2 and S_2O were observed to remain essentially constant with time throughout the experiment.

Fragments identified as CF_2^+ were observed in a measurable concentration in t' system. The origin of these fragments is postulated to be the Teflon bind used in the construction of the porous carbon cathode. Other higher molecular weight species give rise to a number of observed fragments detected after lengthy reversal times.

4.6 Recommendation for Future Investigations

The results obtained in this mass spectrometric investigation clearly show that the techniques used can provide valuable insights into the chemistry which takes place not only during normal discharge but also during voltage-reversal. These results were obtained using the simple direct sampling system constructed for this work with the mass spectrometers. Improvements of this system should provide more accurate and reproducible data for further studies. These improvements include the use of an accurate pressure measuring device, modification of the ion sources to minimize corrosion problems, the use of improved hardware to ensure highly reproducible sample size and the use of a simple existing data acquisition system in order to acquire and process the large volume of data generated in these experiments.

The experimental evidence obtained in this work clearly suggests that a better understanding of the chemistry involved in the $Li/SOCl_2$ battery may be reached by conducting the following proposed experiments.

1. Accurate mass experiments will clearly resolve a number of important questions. These include the positive identification of the following masses:

   (a) Mass 67: Presence or absence of ClO_2.
   (b) Mass 69: Presence or absence of CF_3^+.
   (c) Mass 134: S_2Cl_2 or SO_2Cl_2.
   (d) The positive identification of higher molecular weight species generated in the latter stages of battery reversal.

2. Electrode characterization studies. The formation of species such as HCl, CF^+ and other chlorinated and/or fluorinated compounds arising from impurities in this battery system should be studied as a function of the method of electrode preparation. These studies may include electrode surface characterization. We propose simple Auger electron spectroscopy

(AES) experiments and thermal desorption investigations in order to reveal the amount and the identity of species adsorbed on the electrode surfaces. Such investigations have the potential of yielding valuable insights into the mechanism(s) of processes taking place within the cell.

3. Measurements of the total cell pressure as a function of time during discharge and reversal. It is desirable to investigate the relationship between the observed partial pressure fluctuations and possible total pressure variations.

5. EPR Spectroscopy of Lithium Thionyl Chloride Cell

During both discharge and reversal, free radicals are probably generated. For example, a proposed reduction scheme for thionyl chloride involves SOCl as an intermediate

$$SOCl_2 + e = SOCl + Cl^-$$

$$SOCl + e = SO + Cl^-$$

$$2\ SO \longrightarrow SO_2 + S$$

Species such as SOCl are paramagnetic and EPR spectroscopy is an ideal technique for detecting its presence if it accumulates in sufficient concentration. The above reactions may be rate dependent and SOCl may react chemically in low rate cells before any further reduction can occur,

$$SOCl = (k)\ (Products)$$

The possible deactivation of SOCl by a chemical process as a rate related phenomenon may explain the reported effect of discharge rates on the safety of discharged cells.

Samples of electrolyte from discharged cells and from cells driven into either anode or cathode limited reversal were tested for free radical formation and all give strong EPR signals with the same g value. Equally puzzling was the fact that samples of fresh acid electrolyte gave similar signals whereas samples of fresh neutral electrolyte (1.4 M $LiAlCl_4$) gave no signal at all. To resolve the question several in situ experiments were performed.

5.1 In Situ EPR Study

The cell is described in Figure 126. It was assembled in a 3 mm ID quartz tube filled with $SOCl_2$/1.4 M $LiAlCl_4$. The lithium electrode, positioned near the bottom of the tube, consisted of a 5 mil lithium strip pressed on nickel exmet about 2 cm long and 2 mm wide. The cathode was made of our usual 20 mil thick carbon-Teflon formulation pressed on nickel exmet. Insulated nickel wires through the top of the tube were spot welded to the current collectors. The tube was capped then placed in the microwave cavity of an E-4 EPR spectrometer (Varian). Base line measurements before passing any current through the cell showed the presence of a strong signal traceable to the position of the positive electrode in the microwave cavity; this signal obviously due to the carbon did not appear to be affected by the passing of current. The baseline signal disappeared, however, when the carbon electrode was positioned higher up in the tube, just outside of the microwave cavity.

During normal discharge (only the negative electrode was in the cavity) no signal was detected, even at currents as high as 2-3 mA. However, after the onset of anode limited reversal a signal with poorly defined fine structure centered at 3419 gauss (g=1.99) and spread over 20-30 gauss appeared at a relatively high current density.

At 0.5 mA/cm^2 no signal was observed after 30 minutes. At 2.0 mA/cm^2 a signal was noticeable after less than six minutes. The signal increased with time and disappeared slowly when the current was turned off.

Due to instrumental difficulties, we were not able to duplicate these results. In spite of this, we have analyzed the few results obtained keeping in mind that this experiment has to be repeated using a more modern instrument and lower temperatures.

In Figure 127 we have plotted the signal peak height as a function of time. The intensity of the signal appears to increase linearly during

reversal then decay exponentially after the current is cutoff. We have used the following model to analyze the signal decay:

If R. is the free radical generated then

$$R. \xrightarrow{k} R \text{ with } \frac{-d(R)}{dt} = k\,(R.)$$

leading to $(R.) = (R.)_o\, e^{-kt}$

and $\log (R.) = \log (R.)_o - kt$

where k is the deactivation constant and $(R.)_o$ is the initial radical concentration.

Plotting the log of the intensity as a function of time yields a straight line with a slope of -k (see Figure 128)

DEACTIVATION CONSTANT	.07 min^{-1}
HALF-LIFE	7 min.

AD-A128 382 INVESTIGATION OF LITHIUM-THIONYL CHLORIDE BATTERY SAFETY HAZARDS(U) GOULD RESEARCH CENTER ROLLING MEADOWS IL MATERIALS LAB A I ATTIA ET AL. JAN 83 838-012

UNCLASSIFIED N60921-81-C-0363 F/G 10/3 NL

END
DATE FILMED
6-83
DTIC

CONT

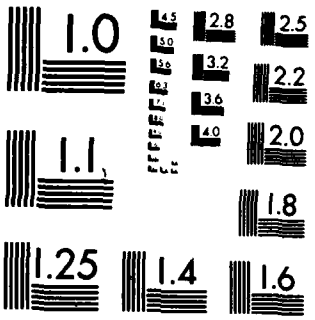

MICROCOPY RESOLUTION TEST CHART
NATIONAL BUREAU OF STANDARDS 1963-A

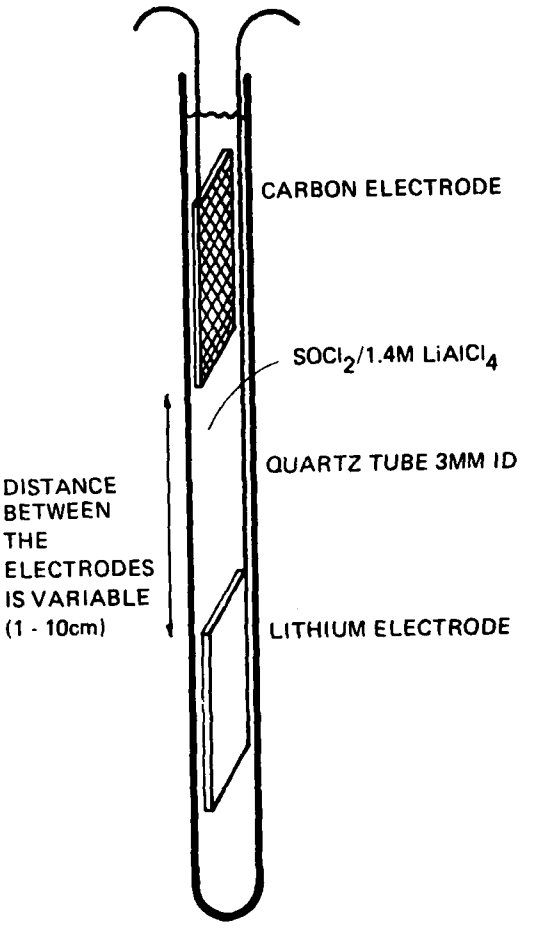

Figure 126 **Spectro-Electrochemical Cell for EPR Measurements**

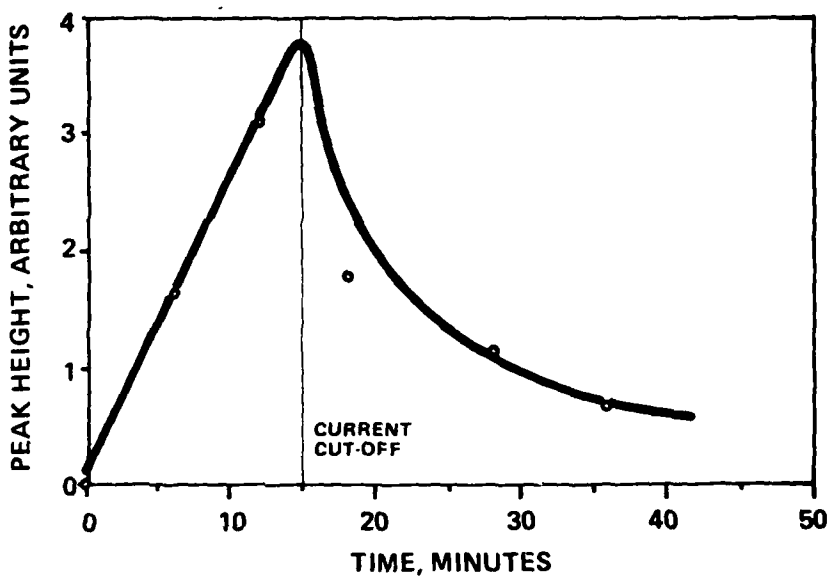

Figure 127 In Situ EPR Spectroscopy
$Li/SOCl_2$ Cell
Anode Limited Reversal
i = 2mA ($2mA/cm^2$)
g = 1.99

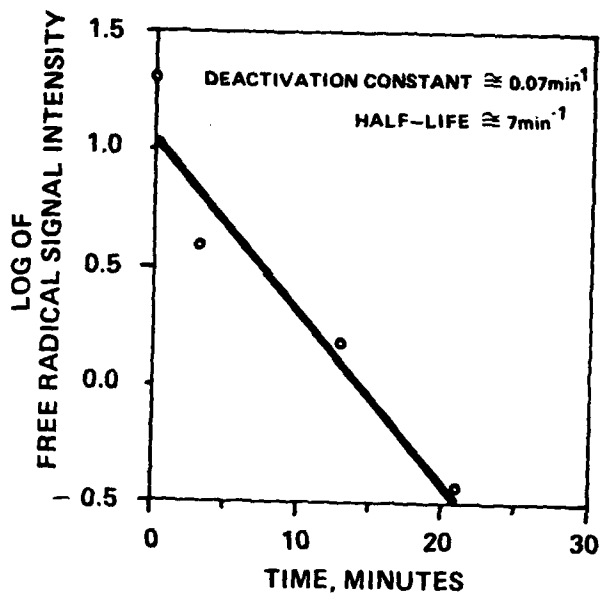

(2692)

Figure 128 Decay of Free Radical Formed during Anode Limited Reversal
T = 25°C

6. Thermal Study of a Lithium-Thionyl Chloride Cell

Microcalorimetric measurements on a small cell during anode limited reversal might detect unusual reactions that could lead to a thermal runaway or other safety hazard in larger cells.

A button type $Li/SOCl_2$ cell about 1 inch in diameter (Figure 129) was introduced in the measuring chamber of a Tronac (Model 351) microcalorimeter and allowed to reach a steady state prior to discharge. A heat flow of 380 μW was measured amounting to a specific heat flow of 75 $\mu W/cm^2$. This translates to a corrosion current of 20 $\mu A/cm^2$ for the lithium electrode.

The cell was then discharged at a constant current of 5 mA (1 mA/cm^2). An average heat evolution of 3 mW was measured during the discharge with a sharp increase at the end of the discharge to 5.1 mW. This higher heat flow remained stable throughout the reversal period.

The voltage was also stable at 3.5 V during discharge and dropped abruptly to -0.7 V then slowly to -1.3 V when reversal occurred.

The results are described in Figure 130. Nothing unusual happened during the discharge except for the nearly doubling of the heat evolved at the end of discharge. This increase may very well be the result of several chemical processes occurring in the cell following oxidation of $SOCl_2$ at the anode

$$2\ SOCl_2 \longrightarrow 2\ SOCl^+ + 2e + Cl_2$$

$$SOCl^+ + AlCl_4^- \longrightarrow SOCl^+\ AlCl_4^-$$

$$LiCl + SOCl^+AlCl_4^- \longrightarrow SOCl_2 + LiAlCl_4$$

The reaction between Cl_2 and SO_2 to form SO_2Cl_2 may also be a factor. Preliminary calculations show that the amount of heat evolved in the formation of SO_2Cl_2 may be as high as 17 kcal/mole.

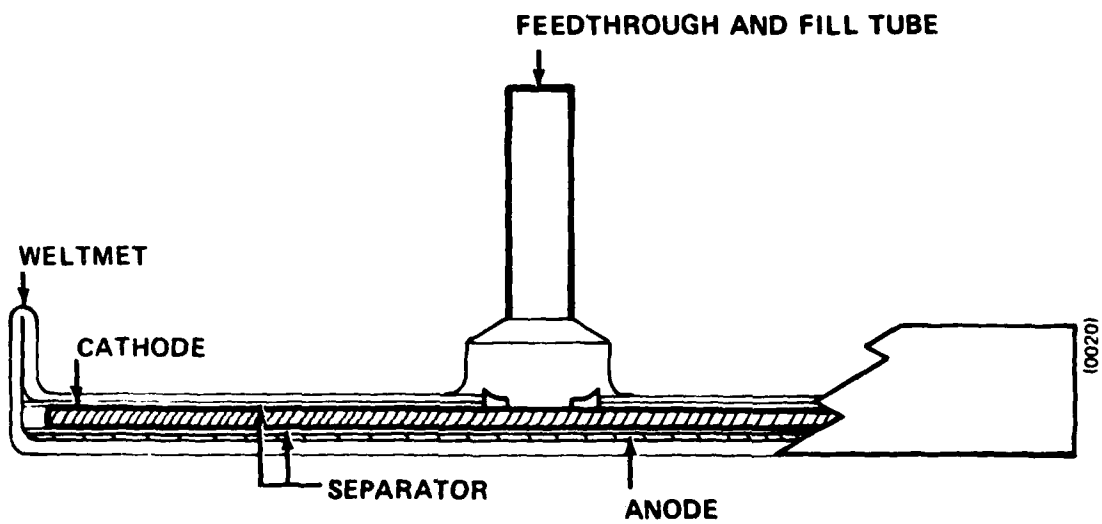

Figure 129 Schematic Cross Section of 25mm Diameter Cell Used for Calorimetric Study

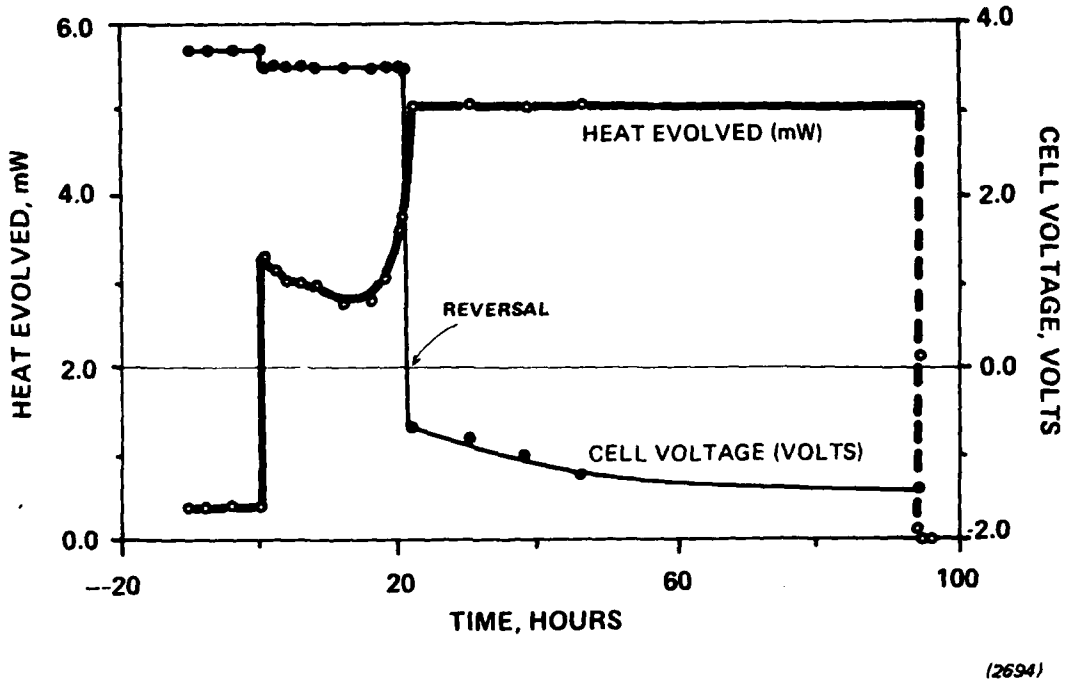

Figure 130 Heat Evolved from a Li/$SOCl_2$ Cell Driven into Reversal
i = 5mA (1mA/cm^2)

References

1. J. Auborn, K. W. French, S. I. Lieberman, U. K. Shan and A. Heller, J. Electrochem Soc., 120, 1613 (1973).

2. D. I. Chua, J. O. Crabb and S. H. Deshpande, "Proceedings of the 28th Power Sources Symposium", Atlantic City, N.J., 28 247 (1978).

3. F. Goebel, R. C. McDonald and N. Marincic "Proceedings of the 15th Intersociety Energy Conversion Engineering Conference", Seattle, WA, 15, 2173 (1980).

4. M. Domeniconi, A. Zolla, R. Waterhouse, D. DeBiccari and G. Griffin, Jr., "Proceedings of the 15th Intersociety Energy Conversion Conference", Seattle, WA, 15 (1980).

5. Private communication, J. C. Hall, Altus.

6. K. M. Abraham et al, "Proceedings of the 28th Power Sources Symposium", Atlantic City, NJ, 28, 255 (1978).

7. A. N. Dey, "Proceedings of the 28th Power Sources Symposium", Atlantic City, NJ 28, 251 (1978).

8. Private Communication from J. C. Hall, Altus.

9. W. K. Istone and R. J. Brodd, J. Electrochem. Society, 129, 1853 (1982).

10. C. R. Schlaikjer, F. Goebel and N. Marincic, J. Electrochem. Society, 126 513 (1979).

11. D. J. Salmon et al, J. Electrochem. Society, 129, 2496 (1982).

12. K. M. Abraham and R. M. Mank, J. Electrochem. Society, 127, 2091 (1980).

13. J. C. Bailey and G. E. Blomgren "Proc. Vol. 82-2, The Electrochemical Society, Pennington, NJ, pg. 485.

14. K. Hedberg, J. Chem Phys. 19 509 (1951).

15. G. Nickless, Inorganic Sulfur Chemistry, Elsevier, Amsterdam, 1978, p. 409.

16. R. C. McDonald, J. Electrochem. Society, 129 2453 (1982).

17. R. J. Gillespie and E. A. Robinson, Can. J. Chem 39 2171 (1961).

18. W. J. Potts, Jr., Chemical Infrared Spectroscopy, John Wiley & Sons, New York, 1963, Vol. 1, p. 155ff.

19. S. Nabi and M. A. Khaleque, J. Chem. Soc. 3626 (1965).

20. Perfluoro kerosene mass spectral Table. PCR Research Chemical, Inc., P.O.B. 1778, Gainesville, Fla 32602.

21. W. L. Bowden and A. N. Dey, Paper 34, presented at the Electrochemical Society Meeting, Los Angeles, Cal. (1979).

22. D. J. Salmon and G. R. Ramsay, paper 35, Presented at the Electrochemical Society Meeting, Los Angeles, Cal. (1979).

23. D. J. Meschi and R. J. Myers, J. Am. Chem. Soc., 78 6220 (1956).

24. W. J. Masschelein, "Chlorine Dioxide. Chemistry and Environmental Impact of Oxychlorine Compounds," Rip G. Rice, Editor, Ann Arbor Science, Pub. (1979).

APPENDIX

The Use of Isotope Ratios in the Mass Spectrometric Identification of Molecular Species

The abundance of the isotopes of many naturally occurring elements can provide characteristic mass spectral patterns. These patterns can be of help in determining molecular composition in certain cases.

In general consider a molecule containing n atoms of the element. Let the fractional natural abundance of the isotopes of this element be given by a, b, c, ... where a+b+c+...=1. The multinomial expansion $(a+b+c+...)^n$ provides a method for expressing the probability of the occurence of the different isotope combinations. As an example consider the element chlorine. Hence:

a = the natural fractional abundance of Cl^{35} = 0.755.

b = the natural fractional abundance of Cl^{37} = 0.245 and assume that the molecule contains two atoms of chlorine, i.e., n=2. Now the expansion becomes

$(a+b)^2 = (0.755)^2 + 2\,(0.775)\,(0.245) + (0.245)^2$ where
$(0.755)^2$ = 0.570 = fractional abundance of a molecule containing $Cl^{35}Cl^{35}$ and $2(0.775)\,(0.245)$ = 0.370 = fractional abundance of a molecule containing $Cl^{35}Cl^{37}$ and $(0.245)^2$ = 0.060 = fractional abundance of a molecule containing $Cl^{37}Cl^{37}$.

Note that the sum of all three fractions (0.570 + 0.370 + 0.060) equals 1.

We can expand this argument to a molecule containing two elements, each of which possess a characteristic isotope distribution as follows:

assume that element M occurs m times in the molecule and has two isotopes a and b, and assume that element N occurs n times in the molecule and has two isotopes c and d. In this case the multinomial expansion becomes:

$(a+b)^m \cdot (c+d)^n$

If m = 2 and n = 2 one writes:

$$(a+b)^2(c+d)^2 = (a^2 + 2ab+b^2)\ (c^2 + 2cd + d^2)$$
$$= a^2c^2 + 2a^2cd + a^2d^2 + 2\ abc^2 + 2abcd + 2\ abd^2$$
$$+ 2b^2c\ + 2b^2cd + b^2d\ .$$

When one collects all terms of the same mass, one obtains the set of fractional abundances predicted for $(a+b)^2(c+d)^2$. If the experimental results agree with the calculated set one has supporting evidence for the postulated number of each atom in the molecular ion.

DISTRIBUTION

	Copies
Defense Documentation Center Cameron Station Alexandria, VA 22314	12
Defense Nuclear Agency Attn: Library Washington, DC 20301	2
Institute for Defense Analyses R&E Support Divison 400 Army-Navy Drive Arlington, VA 22202	1
Naval Material Command Attn: Code 08T223 Washington, DC 20360	1
Office of Naval Research Attn: G. Neece (Code ONR 472) J. Smith 800 N. Quincy Street Arlington, VA 22217	1 1
Naval Research Laboratory Attn: A. Simon (Code NRL 6130) Code NRL 6100 4555 Overlook Avenue, S.W. Chemistry Division Washington, DC 20360	1 1
Naval Postgraduate School Attn: Dr. William M. Tolles (Code 612) Dr. Oscar Biblarz Monterey, CA 93940	1 1
Naval Air Systems Command Attn: Dr. H. Rosenwasser (Code NAVAIR 301C) E. Nebus (Code NAVAIR 5332) Washington, DC 20361	1 1
Naval Electronic Systems Command Attn: A. H. Sobel (Code PME 124-31) Washington, DC 20360	1
Naval Sea Systems Command Attn: F. Romano (Code 63R3) E. Anderson E. Daugherty (Code 06113) J. Pastine (Code 06R) Washington, DC 20	1 1 1 1
Strategic Systems Project Office Attn: K. N. Boley (Code NSP 2721) M. Meserole (Code NSP 2722) Department of the Navy Washington, DC 20360	1 1
Naval Air Development Center Attn: J. Segrest (Code 6012) R. Schwartz (Code 30412) Warminster, PA 18974	1 1
Naval Intelligence Support Center Attn: Dr. H. Ruskie (Code 362) Washington, DC 20390	1
Naval Ocean Systems Center Attn: Dr. S. Szpak (Code 6343) San Diego, CA 92152	1
U. S. Development and Readiness Command Attn: J. W. Crellin (Code DRCDE-L) 5001 Eisenhower Avenue Alexandria, VA 22333	1

	Copies
Union Carbide Battery Products Division Attn: R. A. Powers P.O. Box 6116 Cleveland, OH 44101	1
Wilson Greatbatch LTD. Attn: Library R. M. Carey 1000 Wehrle Drive Clarence NY 14030	1 1
Yardney Electric Corporation Attn: Library 82 Mechanic Street Pawcatuck, CT 02891	1
Naval Surface Weapons Center Attn: W. P. Kilroy (Code R33) New Hampshire Avenue Silver Spring, MD 20910	12
Army Material and Mechanical Research Center Attn: J. J. DeMarco Watertown, MA 01272	1
USA Mobility Equipment R and D Command Attn: J. Sullivan (Code DRXFB) Code DRME-EC Electrochemical Division Fort Belvoir, VA 22060	1
Edgewood Arsenal Attn: Library Aberdeen Proving Ground Aberdeen, MD 21010	1
Picatinny Arsenal Attn: Dr. B. Werbel (Code SAROA-FR-E-L-C) A. E. Magistro (Code SARPA-ND-D-B) U. S. Army Dover, NJ 07801	1 1
Harry Diamond Laboratory Attn: J. T. Nelson (Code DELHD-DE-OP) Department of Army Material Chief, Power Supply Branch 2800 Powder Mill Road Adelphi, MD 20783	1
Headquarters, Department of Transportation Attn: R. Potter (Code GEOE-3/61) U. S. Coast Guard, Ocean Engineering Division Washington, DC 20590	1
NASA Headquarters Attn: Dr. J. H. Ambrus Washington, DC 20546	1
NASA Goddard Space Flight Center Attn: G. Halpert (Code 711) Greenbelt, MD 20771	
NASA Lewis Research Center Attn: J. S. Fordyce (Code MS 309-1) M. Reid 2100 Brookpark Road Cleveland, OH 44135	1 1
Naval Electronic Systems Command Attn: T. Sliwa (Code NAVELEX-01K) Washington, DC 20360	1
Naval Weapons Center Attn: Dr. E. Royce (Code 38) Dr. A. Fletcher China Lake, CA 93555	1 1
Naval Weapons Support Center Attn: M. Robertson (Code 305) D. Mains Electrochemical Power Sources Division Crane, IN 47522	1 1
Naval Coastal Systems Center Attn: Library Panama City, FL 32407	1
Naval Underwater Systems Center Attn: J. Moden (Code SB332) Newport, RI 02840	1
David W. Taylor Naval Ship R & D Center Annapolis Laboratory Annapolis, MD 21402	1

	Copies
Honeywell Corporate Technology Center	
Attn: H. V. Venkatasetty	1
Steven Schafer	1
10701 Lyndale Ave. So.,	
Bloomington, MN 55420	
Honeywell Inc.	
Mat & Process Eng.	
K. Y. Kim MN11-1812	1
600 2nd St. N.E.	
Hopkins, MN 55343	
The Aerospace Corporation	
Attn: Harlan Bittner	1
P.O. Box 92957	
Los Angeles, CA 90009	
Honeywell Power Sources Center	
Attn: Dr. D. L. Chua	1
N. Doddapaneni	1
104 Rock Road	
Horsham, PA 19044	
Air Force Aero Propulsion Laboratory	
Attn: W. S. Bishop	
(Code AFAPL/POE-1)	1
R. Marsh	
(Code AFWAL-POOC-1)	1
Wright-Patterson AFB, OH 45433	
Air Force Rocket Propulsion Laboratory	
Attn: LT. D. Ferguson	
(Code MKPA)	1
Edwards Air Force Base, CA 93523	
Headquarters, Air Force Special Communications Center	
Attn: Library	1
USAFSS	
San Antonio, TX 78243	
Office of Chief of Research and Development	
Department of the Army	
Attn: Dr. S. J. Magram	1
Energy Conversion Branch	
Room 410, Highland Building	
Washington, DC 20315	

	Copies
U. S. Army Research Office	
Attn: B. F. Spielvogel	1
P.O. Box 12211	
Research Triangle Park, NC 27709	
NASA Scientific and Technical Information Facility	
Attn: Library	1
P.O. Box 33	
College Park, MD 20740	
National Bureau of Standards	
Metallurgy Division	
Inorganic Materials Division	
Washington, DC 20234	1
Battelle Memorial Institute	
Defense Metals & Ceramics Information Center	
505 King Avenue	
Columbus, OH 43201	1
Bell Laboratories	
Attn: Dr. J. J. Auborn	1
600 Mountain Avenue	
Murray Hill, NJ 07974	
Brookhaven National Laboratory	
Attn: J. Sutherland	1
Building 815	
Upton, NY 11973	
California Institute of Technology	
Attn: Library	1
B. Carter	1
R. Somoano	1
H. Frank	1
Jet Propulsion Laboratory	
4800 Oak Grove Drive	
Pasadena, CA 91103	
Argonne National Laboratory	
Attn: Dr. E. C. Gay	1
9700 South Cass Avenue	
Argonne, IL 60439	
John Hopkins Applied Physics Laboratory	
Attn: Library	1
Howard County	
Johns Hopkins Road	
Laurel, MD 20810	

	Copies
Oak Ridge National Laboratory Attn: K. Braunstein Oak Ridge, TN 37830	1
Sandia Laboratories Attn: Sam Levy (Mail Services Section 3154-3) P.O. Box 5800 Albuquerque, NM 87715	1
University of Tennesee Attn: G. Mamantov Department of Chemistry Knoxville, TN 37916	1
University of Florida Attn: R. D. Walker Department of Chemical Engineering Gainesville, FL 32611	1
Applied Research Laboratory Attn: Library Penn State University University Park, PA 16802	1
Catalyst Research Corporation Attn: G. Bowser J. Joelson A. Schneider 1421 Clarkview Road Baltimore, MD 21209	1 1 1
ESB Research Center Attn: Library 19 W. College Avenue Yardley, PA 19067	1
EIC Corporation Attn: S. B. Brummer K. M. Abraham 55 Chapel Street Newton, MA 02158	1 1
Eagle-Picher Industries, Inc. Attn: Robert L. Higgins J. Dines L. R. Erisman Electronics Division P.O. Box 47 Joplin, MO 64802	1 1 1
Foote Mineral Company Attn: H. R. Grady Exton, PA 19341	1
Gould, Inc. Attn: S. S. Nielsen A. Attia R. Putt 40 Gould Center Rolling Meadows, IL 60008	1 1 1
GT & E Laboratory Attn: R. McDonald F. Dampier K. Kliendienst W. Clark 520 Winter St. Waltham, MA 02254	1 1 1 1
Hughes Aircraft Company Attn: Dr. L. H. Fentnor Aerospace Groups Missile Systems Group Tucson Engineering Laboratory Tucson, AZ 85734	1
Saft Score, Inc. Attn: L. A. Stein 200 Wight Avenue Cockeysville, MD 21030	1
Lockheed Missiles and Space Company, Inc. Attn: Library Lockheed Palo Alto Research Laboratory 3251 Hanover Street Palo Alto, CA 94304	1
Duracell Int., Inc. Attn: B. McDonald Battery Division South Broadway Tarrytown, NY 10591	1
Duracell Int., Inc. Attn: W. Bowden A. N. Dey H. Taylor Library Laboratory for Physical Science Burlington, MA 01803	1 1 1 1

	Copies
U. S. Army Electronics Command Attn: A. J. Legath (Code DRSEL-TL-P)	1
E. Brooks (Code DRSEL-TL-PD)	1
G. DiMasi Dr. W. K. Behl Dr. Sol Gilman (Code DELET-PR)	1
Fort Monmouth, NJ 07703	
Callery Chemical Company Attn: Library	1
Callery, PA 16024	
Rockwell International Attn: Dr. Samuel J. Yosim	1
Atomics International Division 8900 DeSoto Avenue Canoga Park, CA 91304	
Stanford University Attn: C. John Wen	1
Center for Materials Research Room 249, McCullough Building Stanford, CA 94305	
EDO Corporation Attn: E. P. DiGiannantonio	1
Government Products Division 2001 Jefferson Davis Highway Arlington, VA 22202	
Globe Union Inc. Attn: Dr. K. R. Bullock	1
5757 N. Green Bay Avenue Milwaukee, WI 53201	
University of Missouri, Rolla Attn: Dr. J. M. Marchello	1
210 Parker Hall Rolla, MO 65401	
RAI Research Corporation Attn: Dr. Carl Perini	1
225 Marcus Boulevard Hauppauge, NY 11787	
Battery Engineering Attn: Dr. N. Marincic	1
80 Oak Street Newton, MA 02164	

	Copies
RAY-O-VAC Attn: R. Foster Udell	1
101 East Washington Avenue Madison, WI 53703	
Litton Data Systems Division Attn: Frank Halula, MS 64-61	1
8000 Woodley Avenue Van Nuys, CA 91409	
Lawrence Berkeley Laboratory Attn: F. McLarnon	1
University of California Berkeley, CA 94720	
TRW Systems Attn: I. J. Groce	1
G. L. Juvinal	1
Ed Moon, Rm. 2251, Bldg. 01	3
One Space Park Redondo Beach, CA 90278	
ALTUS Corporation Attn: Dr. Adrian E. Zolla, Library	2
1610 Crane Court San Jose, CA 95112	
Capt. A. S. Alanis BMO/ENBE Norton AFB	1
CA 92409	
Norton AFB Code AFISC/SES	1
CA 92409	
PCI Attn: Thomas Reddy	1
495 Boulevard Elmwook Park, NJ 07407	
Dr. P. Bro Hyde Park Estates	1
Santa Fe, NM 87501	
Old Dominion University Attn: R. L. Ake	1
Dept. of Chemical Sciences Norfold, VA 23508	

	Copies
Scientific Advisor Attn: Code AX Commandant of the Marine Corps Washington, DC 20380	1
Air Force of Scientific Research Attn: R. A. Osteryoung Directorate of Chemical Science 1400 Wilson Boulevard Arlington, VA 22209	1
Frank J. Seiler Research Laboratory, AFSC USAF Academy, CO 80840	1
Dr. R. Burns University of Illinois at Chicago Department of Chemistry Chicago, IL 60680	1
Boeing Aerospace Co. Attn: S. Gross C. Johnson P.O. Box 3999 Seattle, Washington 98124	1 1
Electrochimica Corporation Attn: M. Eisenberg 2485 Charleston Rd. Mt. View, CA 94040	1
Department National Defense Attn: Library Defense Research Establishment Ottowa Ottowa, Ontario K1A0Z4	1
NASA Johnson Space Center Attn: Bob Bragg/EPS Houston, TX 77058	1
Cordis Corporation Attn: W. K. Jones P.O. Box 525700 Miami, FL 33152	1
Tadiran Attn: M. Babai P.O. Box 75 Rehouot, Israel	1
Tel-Aviv University Attn: E. Peled Department of Chemistry Tel Aviv, Israel 69978	1


DA
FILM
6 8
DTIC

AD-A128 382 INVESTIGATION OF LITHIUM-THIONYL CHLORIDE BATTERY SAFETY HAZARDS(U) GOULD RESEARCH CENTER ROLLING MEADOWS IL MATERIALS LAB A I ATTIA ET AL. JAN 83 838-012

UNCLASSIFIED N60921-81-C-0363 F/G 10/3 NL

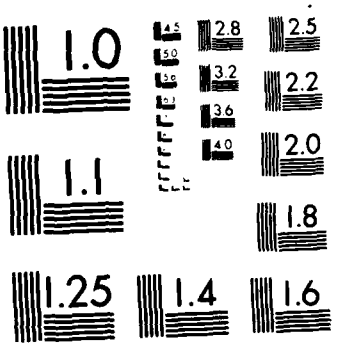

MICROCOPY RESOLUTION TEST CHART
NATIONAL BUREAU OF STANDARDS 1963 A

SUPPLEMENTARY

INFORMATION

Gould Inc., Micro Power Products Division

GOULD
Electronics

AD-A128382

March 6, 1984

Thomas Lin
Defense Logistic Agency
DTIC
Stop #3
Cameron Station
Alexandria, Virginia 22314

REF: Error in Document Abstract AD-A128 382

Dear Mr. Lin:

I am enclosing an abstract of my report "Investigation of Lithium-Thionyl Chloride Battery Safety Hazards" which I believe more closely describes the contents of the report.

This work was performed in 1982, for the Naval Surface Weapons Center, under contract No. : N60921-81-C-0363. The report contains useful information which is not at all evident in the current abstract.

I wish to thank you for your willingness to replace the current abstract with the more accurate version.

Very truly yours,

Alan I. Attia

Alan I. Attia
Project Manager

AIA:rcw

Enclosure

LITHMRPT

ABSTRACT

In-situ Infrared spectroscopy and Mass spectrometry were used to identify the reaction products in Li/$SOCl_2$ batteries during low rate discharge and anode limited reversal.

- The sources of all the absorption bands in the IR absorption spectrum of the electrolyte were identified and quantitated.
- Processes giving rise to free radical formation were detected by in-situ EPR spectroscopy.
- The technique of direct-inlet in-situ mass spectrometry was applied for the first time to the Li/$SOCl_2$ system, to identify without any ambiguity the presence of HCl, SO_2, CS_2, S_2O, SCl_2 and SO_2Cl_2 as well as Cl^+ and CF_2^+ fragments in the gas phase above an operating cell.
- S_2O was not detected in the liquid phase.
- The appearance potentials for SCl_2, $SOCl_2$, SO_2Cl_2 and S_2Cl_2 were measured.
- Evidence for the formation of Cl_2O was refuted.
- Significant effects directly attributable to temperature and current density were identified and quantified.
- No clearly hazardous reactions were identified other than those inherent in the system.

As a result of this work, a much clearer understanding of the chemistry of the Li/$SOCl_2$ system has been achieved. Several analytical techniques have been developed and applied for the first time to the Li/$SOCl_2$ system, which could potentially lead to a more complete explanation of the chemistry of the system.

END

FILMED

3-84

DTIC